LICENSING REPORT FOR STORAGE DENSIFICATION OF D.C. COOK SPENT FUEL POOL

INDIANA MICHIGAN POWER COMPANY

by

Holtec International

AEPSC Contract No. C-7926
Holtec Project 00480

LICENSING REPORT FOR STORAGE DENSIFICATION OF D.C. COOK SPENT FUEL POOL

INDIANA MICHIGAN POWER COMPANY

by

Holtec International

AEPSC Contract No. C-7926
Holtec Project 00480

HOLTEC INTERNATIONAL

REVIEW AND CERTIFICATION LOG

DOCUMENT NAME: LICENSING REPORT FOR STORAGE DENSIFICATION OF D.C. COOK SPENT FUEL POOL

HOLTEC DOCUMENT I.D. NO. HI-90488
HOLTEC PROJECT NO. 00480
CUSTOMER/CLIENT: AMERICAN ELECTRIC POWER (INDIANA MICHICAN POWER CO.)

REVISION BLOCK				
ISSUE NO.	AUTHOR & DATE	REVIEWER & DATE	Q.A. MANAGER & DATE	APPROVED* BY & DATE
ORIGINAL	S.N.C. 6/14/90	Alan Soler 6/16/90	6/18/90	S.N.C. 6/19/90
REVISION 1	Yu Wang WANG 10/2/90	S.N.C. 10/2/90	M Soler 10/2/90	S.N.C. 10/2/90
REVISION 2	Yu Wang YW 3/23/91	Alan Soler 3/28/91	M Soler 3/25/91	Alan Soler for KPS 3/25/91
REVISION 3	Yu Wang YW 5/23/91	Alan Soler A.S. 5/23/91	M Soler 5/23/91	S.N.C. 5/23/91
REVISION 4	Yu Wang YW 6/26/91	Alan Soler A.S. 6/26/91	M Soler 6/26/91	Alan Soler A.S. 6/26/91
REVISION 5	Yu Wang YW 6/31/91	Alan Soler A.S. 6/31/91	M Soler 7/1/91	S.N.C. 6/31/91
REVISION 6	Yu Wang/AES YW 7/10/91	S.N.C. 7/10/91	M Soler 7/10/91	S.N.C. 7/10/91

NOTE: Signatures and printed names are required in the review block.

* Must be Project Manager or his Designee.

This document conforms to the requirement of the design specification and the applicable sections of the governing codes.

This document bears the ink stamp of the professional engineer who is certifying this document.

K P Singh

Professional Engineer

SEAL

SUMMARY OF REVISIONS

Revision 1 contains the following number of pages of text (including tables, but excluding figures):

Title Page	1
Review and Certification Log	1
Summary of Revisions Page	1
Table of Contents	4
List of Figures	3
Section 1	8
Section 2	17
Section 3	8
Section 4	(later)
Section 5	23
Section 6	48
Section 7	5
Section 8	13
Section 9	(later)
Section 10	11

Revision 2 contains the following number of pages of text (including tables and figures):

Title Page	1
Review and Certification Log	1
Summary of Revisions Page	1
Table of Contents	4
List of Figures	3
Section 1	8
Section 2	18
Section 3	14
Section 4	Not included in Revision 2
Section 5	33
Section 6	78
Section 7	5
Section 8	17
Section 9	Not included in Revision 2
Section 10	Not included in Revision 2

SUMMARY OF REVISIONS

Revision 3 contains the following number of pages of text (including tables and figures):

Title Page	1
Review and Certification Log	1
Summary of Revisions Page	2
Table of Contents	4
List of Figures	3
Section 1	9
Section 2	19
Section 3	14
Section 4	34
Appendix A to Section 4	9
Section 5	33
Section 6	76
Section 7	5
Section 8	17
Section 9	11
Section 10	5
Section 11	4

Revision 4 contains the same number of pages as Revision 3 with these exceptions:

List of Tables (added to Rev. 4): 3

Sections revised in Rev. 4 now contain the following number of pages:

Section 1	9
Section 2	18
Section 4	35
Section 5	34
Section 9	11

Individual pages revised and transmitted in Revision 4 are:

Pages 3-1, 3-3, 3-4, 6-6, 6-15, 6-18, 6-28, 6-30, 7-4, 7-5, 7-6, 8,7 and 10-2.

SUMMARY OF REVISIONS

Holtec Report HI-90488

Revision 5

The following is revised in Revision 5:

Pages 4-8 and 4-9
Section 9
Appendix A
Page v of Table of Contents

Revision 6

The following pages are revised in Revision 6:

List of Figures
Table of Contents (page v)

2-1

4-15, 4-16

5-2, 5-3, 5-5, 5-6, 5-8, 5-9, 5-10, 5-12, 5-15, 5-16, 5-17, 5-18, 5-19, 5-20, 5-21, 5-24 through 5-38

6-3, 6-4, 6-35

7-2, 7-4

8-6, 8-7, 8-13

10-4

11-3

TABLE OF CONTENTS

TABLE OF CONTENTS (continued)

TABLE OF CONTENTS (continued)

TABLE OF CONTENTS (continued)

TABLE OF CONTENTS

TABLE OF CONTENTS

LIST OF TABLES

LIST OF TABLES (continued)

LIST OF TABLES (continued)

LIST OF FIGURES

LIST OF FIGURES
(continued)

LIST OF FIGURES (continued)

LIST OF FIGURES
(continued)

1.0 INTRODUCTION

Donald C. Cook is a twin unit pressurized water nuclear power reactor installation owned and operated by Indiana Michigan Power Company. Donald C. Cook received its construction permit from the AEC in March, 1969, and its operating License in October, 1974 for Unit 1 and December 1977 for Unit 2. The two reactors went into commercial operation in August, 1975 (Unit 1) and July, 1978 (Unit 2), respectively. The Donald C. Cook fuel storage system is made up of a fuel pool 58'-3 1/8" long x 39'-1 9/16" wide with an integral cask laydown area. The pool presently contains 1367 spent fuel storage assemblies and 36 miscellaneous hardware items. Thus, out of the total installed storage capacity of 2050 storage cells, 1403 storage cells are presently occupied. Since the full core has 193 fuel assemblies for both Donald C. Cook reactors, maintaining full core offload capability from one reactor implies that 1857 storage cells (2050 minus 193) are available for normal offload storage. Table 1.1.1 provides the data on previous and projected fuel assembly discharge in the Donald C. Cook spent fuel pool. Table 1.1.2, constructed from Table 1.1.1 data, indicates that Donald C. Cook will lose full core discharge capability (for one reactor) in 1995. This projected loss of full core discharge capability prompted the present undertaking to increase spent fuel storage capability in the Donald C. Cook pool.

The purpose of this licensing submittal is to rerack the Donald C. Cook pool and equip it with new poisoned high density storage racks containing 3613 storage cells. The reracking also entails relocation of the thimble plug tool, spent fuel handling tool, Rod Cluster Control Assembly (RCCA) change tool, and Burnable Poison Rod Assembly (BPRA) tool brackets to the South wall adjacent to the cask pit.

Twenty three free-standing poisoned rack modules positioned with a prescribed and geometrically controlled gap between them will contain a total of 3613 storage cells (including 3 triangle cells located at the SW, NW and NE corners of the pool). Out of these cells, the peripheral cells located in each rack module are flux-trap cells*, and the interior ones are of the so-called non-flux trap type. The storage cells suitable for storing fresh fuel (up to 5% enrichment) are uniquely identified (see Section 4.0, Figures 4.1 and 4.2), and are surrounded by non-flux trap cells which have a burnup restriction on the fuel which they can store. Consistent with the concept of two region storage, the placement of fuel with a given burnup in the allowable location is administratively controlled. No credit is taken for soluble boron in normal refueling and full core offload storage conditions.

---

* A flux trap construction implies that there is a water gap between adjacent storage cells such that the neutrons emanating from a fuel assembly are thermalized before reaching an adjacent fuel assembly.

It is noted that the proposed reracking effort will increase the number of licensed storage locations to 3613 and, as indicated in Table 1.1.2, will extend the date of loss of full core discharge capability through the year 2008. Table 1.1.3 presents key comparison data for existing and proposed rack modules for Donald C. Cook.

The new spent fuel storage racks are free-standing and self supporting. The principal construction materials for the new racks are SA240-Type 304 stainless steel sheet and plate stock, and SA564-630 (precipitation hardened stainless steel) for the adjust- able support spindles. The only non-stainless material utilized in the rack is the neutron absorber material which is boron carbide and aluminum-composite sandwich available under the patented product name "Boral".

The new racks are designed and analyzed in accordance with Section III, Division 1, Subsection NF of the ASME Boiler and Pressure Vessel (B&PV) Code. The material procurement, analysis, and fabrication of the rack modules conform to 10CFR 50 Appendix B requirements.

This Licensing Report documents the design and analyses performed to demonstrate that the new spent fuel racks satisfy all governing requirements of the applicable codes and standards, in particular, "OT Position for Review and Acceptance of Spent Fuel Storage and Handling Applications", USNRC (1978) and 1979 Addendum thereto.

The safety assessment of the proposed rack modules involved demonstration of its thermal-hydraulic, criticality and structural adequacy. Hydrothermal adequacy requires that fuel cladding will nct fail due to excessive thermal stress, and that the steady state pool bulk temperature will remain within the limits prescribed for the spent fuel pool to satisfy the pool structural strength constraints. Demonstration of structural adequacy primarily involves analysis showing that the free-standing rack modules will not impact with each other or with the pool walls under the postulated Design Basis Earthquake (DBE) and Operating Basis Earthquake (OBE) events, and that the primary stresses in the rack module structure will remain below the ASME B&PV Code allowables. The structural qualification also includes analytical demonstration that the subcriticality of the stored fuel will be maintained under accident scenarios such as fuel assembly drop, accidental misplacement of fuel outside a rack, etc.

The criticality safety analysis shows that the neutron multiplication factor for the stored fuel array is bounded by the USNRC limit of 0.95 (OT Position Paper) under assumptions of 95% probability and 95% confidence. Consequences of the inadvertent placement of a fuel assembly are also evaluated as part of the criticality analysis. The criticality analysis also sets the requirements on the length of the B-10 screen and the areal B-10 density.

This Licensing Report contains documentation of the analyses performed to demonstrate the large margins of safety with respect to all USNRC specified criteria. This report also contains the results of the analysis performed to demonstrate the integrity of the fuel pool reinforced concrete structure, and an appraisal of

radiological considerations. A cost/benefit analysis demonstrating reracking as the most cost effective approach to increase the on-site storage capacity of the Donald C. Cook Nuclear Plant has also been performed and synopsized in this report.

All computer programs utilized in performing the analyses documented in this licensing report are identified in the appropriate sections. All computer codes are benchmarked and verified in accordance with Holtec International's nuclear Quality Program.

The analyses presented herein clearly demonstrate that the rack module arrays possess wide margins of safety from all three – thermal-hydraulic, criticality, and structural – vantage points. The No Significant Hazard Consideration evaluation submitted to the Commission along with this Licensing Report is based on the descriptions and analyses synopsized in the subsequent sections of this report.

Table 1.1.1

DISCHARGE SCHEDULE

Cycle	Month/ Year	Number of Assemblies Discharged	Cumulative Inventory In the Pool
1A*	12/1976	65	65
2A	4/1978	64	129
3A	4/1979	64	193
1B**	10/1979	80	273
4A	5/1980	65	338
2B	5/1981	92	430
5A	5/1981	64	494
6A	7/1982	64	558
3B	11/1982	72	630
7A	7/1983	80	710
4B	3/1984	92	802
8A	4/1985	80	882
5B	2/1986	88	970
9A	6/1987	80	1050
6B	5/1988	80	1130
10A	3/1989	80	1210
7B	6/1990	77	1282
11A	10/1990	80	1362
8B	11/1991	76	1438
12A	2/1992	80	1518
9B	3/1993	80	1598
13A	6/1993	80	1678
10B	7/1994	80	1758
14A	10/1994	80	1838
11B	11/1995	80	1918
15A	4/1996	80	1998
12B	3/1997	80	2078
16A	8/1997	80	2158
13B	7/1998	80	2238

---

* A - Reactor Unit 1
** B - Reactor Unit 2

Table 1.1.1 (continued)

DISCHARGE SCHEDULE

Cycle	Month/ Year	Number of Assemblies Discharged	Cumulative Inventory In the Pool
17A*	12/1998	80	2318
14B**	1/2001	80	2398
18A	4/2000	80	2478
15B	5/2001	80	2558
19A	8/2001	80	2638
16B	9/2002	80	2718
20A	12/2002	80	2798
17B	1/2004	80	2878
21A	6/2004	80	2958
18B	5/2005	80	3038
22A	10/2005	80	3118
19B	9/2006	80	3198
23A	2/2007	80	3278
20B	1/2008	80	3358
24A	7/2008	80	3438
21B	7/2009	80	3518

---

* A - Reactor Unit 1
** B - Reactor Unit 2

Table 1.1.2

AVAILABLE STORAGE IN THE DONALD C. COOK POOL

NUMBER OF STORAGE LOCATIONS AVAILABLE

Cycle	Month/ Year	With Present Licensed Capacity (2050 Locations)	After Reracking (3616 Locations)
7B	6/1990	768	2334
11A	10/1990	683	2254
8B	11/1991	612	2178
12A	2/1992	532	2098
9B	3/1993	452	2018
13A	6/1993	372	1938
10B	7/1994	292*	1858
14A	10/1994	212	1778
11B	11/1995	132**	1698
15A	4/1996	52***	1618
12B	3/1997		1538
16A	8/1997		1458
13B	7/1998		1378
17A	12/1998		1298
14B	1/2000		1218
18A	4/2000		1138
15B	5/2001		1058
19A	8/2001		978
16B	9/2002		898
20A	12/2002		818
17B	1/2004		738
21A	6/2004		658
18B	5/2005		578
19B	9/2006		418
23A	2/2007		338*
20B	1/2008		258
24A	7/2008		178**
21B	7/2009		98
25A	11/2009		18***

---

* Date of loss of full core offload capability from both reactors.

** Date of loss of full core offload capability for one reactor.

*** Date of loss of normal discharge capability.

Table 1.1.3

RACK MODULE DATA, EXISTING AND PROPOSED RACKS

ITEM	EXISTING RACKS	PROPOSED RACKS
Number of cells	2050	3616*
Number of modules	20	23
Neutron Absorber	Boral	Boral
(Nom.) cell pitch, inch	10.5"	8.97"
(Nom.) cell opening size, inch	8.884 ± 0.124	8.75" ± 0.04

* Include three triangular corner storage cells.

2.0 MODULE DATA

2.1 Synopsis of New Modules

The Donald C. Cook spent fuel pool consists of a 39'-1 9/16" x 58'-3 1/8" rectangular pit with a 10'-4" x 10'-6" space designated for cask handling operations. The pool is connected to the fuel transfer canal through a weir gate on the West wall. This gate is normally closed.

At the present time, the Donald C. Cook pool contains medium density racks with a 10.5" nominal assembly center-to-center pitch. There is a total of 2050 storage cells in the pool. There are two sizes of modules, 10x10 and 10x11. The 10x10 module weighs 33,800 lb. and the 10x11 module weighs 37,200 lb.

Figure 2.1.1 shows the module layout for the Donald C. Cook pool after the proposed reracking campaign. As shown in Figure 2.1.1 and tabulated in Table 2.1.1, there are twenty-three racks containing a total of 3613 storage cells with a 8.97" nominal pitch.

The essential cell data for all storage cells is given in Table 2.1.2. The physical size and weight data on the modules may be found in Table 2.1.3. In summary, the present reracking application will increase the licensed storage capacity of the Donald C. Cook pool from 2050 to 3613 cells.

2.2 Mixed Zone Three Region Storage (MZTR):

The high density spent fuel storage racks in the Donald C. Cook pool will provide storage locations for up to 3613 fuel assemblies and will be designed to maintain the stored fuel, having an initial enrichment of up to 5 wt% U-235, in a safe, coolable, and subcritical configuration during normal discharge and full core offload storages and postulated accident conditions.

All rack modules for Donald C. Cook spent fuel pool are of the so-called "free-standing" type such that the modules are not attached to the pool floor nor do they require any lateral braces or restraints. These rack modules will be placed in the pool in their designated locations using a specifically designed lifting device, and the support legs remotely leveled (using a telescopic removable handling tool) by an operator on the fuel handling bridge. The leveling operations are done when the support legs are lifted off the floor. Except for the crane, no additional lifting equipment is needed while leveling is being performed.

As described in detail in Section 3, all modules in the Donald C. Cook pool are of "non-flux trap" construction. However, the module baseplates extend out by 7/8" (nominal), such that the nominal gap between the adjacent walls of two neighboring racks is 2" (nom.). Thus, although there is a single screen of neutron absorber panel between two fuel assemblies stored in the same rack, there are two poison panels with a water flux trap (2" wide) between them for fuel assemblies located in cells in two facing modules. Out of these flux trap locations, and peripheral cell locations (cells adjacent to pool walls) a certain number of storage cells are designated for storing fresh fuel. In addition, as described in Section 4, a certain number of interior cells in each rack are designated for storing fresh fuel of 5% wt. U-235 (max.) enrichment. In this manner, a sufficient number of locations without any burnup restriction (Region I cells) are identified to enable unrestricted full core offload of the Donald C. Cook reactor in the spent fuel pool. These so-called Region I cells are identified in Section 4 of this report. The remaining storage cells have enrichment/burnup restrictions. Appropriate restrictions on the enrichment/burnup of the stored fuel in Region II and Region III cells are presented in Section 4.

Each rack module is supported by at least four legs which are remotely adjustable. Thus, the racks can be made vertical and the top of the racks can easily be made co-planar with each other. The rack module support legs are engineered to accommodate variations of the pool floor. The support legs also provide an under rack plenum for natural circulation of water through the storage cells. The placement of the racks in the spent fuel pool has been designed to preclude any support legs from being located over existing obstructions on the pool floor.

The Donald C. Cook racks are subjected to mandated seismic loadings per the plant UFSAR. The Design Basis Earthquake (DBE) and Operating Basis Earthquake (OBE) seismic response spectra are provided and synthetic time histories are generated. These acceleration time histories are applied as inertia loads (see Section 6.3).

Under these seismic events, the rack modules have four designated locations of potential impact:

(i) Support leg to bearing pad
(ii) Storage cell to fuel assembly contact surfaces
(iii) Baseplate edges
(iv) Rack top corners

The support leg to pool slab bearing pad impact would occur whenever the rack support foot lifts off the pool floor during a seismic event. The "rattling" of the fuel assemblies in the storage cell is a natural phenomenon associated with seismic conditions. The baseplate and rack top corners impacts would occur if the rack modules tend to slide or tilt towards each other during the postulated DBE or OBE seismic events. Section 6 of this report presents the analysis methodology and results for all three locations of impact, and establishes the structural integrity of the racks under the load combinations specified for plant conditions required by the NRC.

A bearing pad, made of austenitic stainless steel, is interposed between the support foot and the liner such that the loads transmitted to the slab by the rack module under steady state as well as seismic conditions are diffused into the pool slab, and allowable local concrete surface pressures are not exceeded. Section 8 of this report presents the detailed pool structure analysis.

2.3 Material Considerations

2.3.1 Introduction

Safe storage of nuclear fuel in the Donald C. Cook spent fuel pool requires that the materials utilized in the fabrication of racks be of proven durability and be compatible with the pool water environment. This section provides the necessary information on this subject.

2.3.2 Structural Materials

The following structural materials are utilized in the fabrication of the spent fuel racks:

a. ASME SA240-304 for all sheet metal stock.

b. Internally threaded support legs: ASME SA240-304.

c. Externally threaded support spindle: ASME SA564-630 precipitation hardened stainless steel.

d. Weld material - per the following ASME specification: SFA 5.9 ER308.

2.3.3 Poison Material

In addition to the structural and non-structural stainless material, the racks employ Boral, a patented product of AAR Brooks & Perkins, as the thermal neutron absorber material. A brief description of Boral, and its fuel pool experience list follows. Boral is a thermal neutron absorbing material composed of boron carbide and 1100 alloy aluminum. Boron carbide is a compound

having a high boron content in a physically stable and chemical inert form. The 1100 alloy aluminum is a light-weight metal with high tensile strength which is protected from corrosion by a highly resistant oxide film. The two materials, boron carbide and aluminum, are chemically compatible and ideally suited for long-term use in the radiation, thermal and chemical environment of a spent fuel pool.

Boral's use in the spent fuel pool as the neutron absorbing material can be attributed to the following reasons:

(i) The content and placement of boron carbide provides a very high removal cross section for thermal neutrons.

(ii) Boron carbide, in the form of fine particles, is homogenously dispersed throughout the central layer of the Boral.

(iii) The boron carbide and aluminum materials in Boral do not degrade as a result of long-term exposure to gamma radiation.

(iv) The thermal neutron absorbing central layer of Boral is clad with permanently bonded surfaces of aluminum.

(v) Boral is stable, strong, durable, and corrosion resistant.

The passivation process of Boral in an aqueous environment results in the generation of hydrogen gas. If the generation rate of hydrogen is too rapid, then swelling of Boral may occur. Laboratory studies by Boral's supplier indicate that the rate of hydrogen generation is a strong function of the so-called impurities in the chemical composition of the boron carbide powder, namely sodium hydroxide and boron oxide. AAR Brooks & Perkins has instituted a strict program of monitoring of the chemistry of boron carbide used in the manufacturing of Boral to ensure that no swelling of the panels will occur. Furthermore,

randomly selected coupons of Boral panels from production runs are subjected to swelling test checks to preclude any possibility of swelling of Boral.

Boral is manufactured by AAR Brooks & Perkins under the control and surveillance of a computer-aided Quality Assurance/Quality Control Program that conforms to the requirements of 10CFR50 Appendix B, "Quality Assurance Criteria for Nuclear Power Plants and Fuel Reprocessing Plants". As indicated in Table 2.3.1, Boral has been licensed by the USNRC for use in numerous BWR and PWR spent fuel storage racks and has been extensively used in overseas nuclear installations.

Boral Material Characteristics

Aluminum: Aluminum is a silvery-white, ductile metallic element that is abundant in the earth's crust. The 1100 alloy aluminum is used extensively in heat exchangers, pressure and storage tanks, chemical equipment, reflectors and sheet metal work.

It has high resistance to corrosion in industrial and marine atmospheres. Aluminum has atomic number of 13, atomic weight of 26.98, specific gravity of 2.69 and valence of 3. The physical/mechanical properties and chemical composition of the 1100 alloy aluminum are listed in Tables 2.3.2 and 2.3.3.

The excellent corrosion resistance of the 1100 alloy aluminum is provided by the protective oxide film that develops on its surface from exposure to the atmosphere or water. This film prevents the loss of metal from general corrosion or pitting corrosion and the film remains stable between a pH range of 4.5 to 8.5.

Boron Carbide: The boron carbide contained in Boral is a fine granulated powder that conforms to ASTM C-750-80 nuclear grade Type III. The particles range in size between 60 and 200 mesh and the material conforms to the chemical composition and properties listed in Table 2.3.4.

2.3.4 Compatibility with Coolant

All materials used in the construction of the Donald C. Cook racks have an established history of in-pool usage. Their physical, chemical and radiological compatibility with the pool environment is an established fact at this time. As noted in Table 2.3.1, Boral has been used in both vented and unvented configurations in fuel pools with equal success. Consistent with the recent practice, the Donald C. Cook rack construction allows full venting of the Boral space. Austenitic stainless steel (304) is widely used in nuclear power plants.

2.4 Existing Rack Modules and Proposed Reracking Operation

The Donald C. Cook fuel pool currently has medium density rack modules containing a total of 2050 storage cells in twenty modules. At the time of the proposed reracking operation, approximately 1678 cells (between 6/1993 and 7/1994) out of 2050 locations will be occupied with spent fuel. There is sufficient number of open (unoccupied) cells in the pool to permit relocation of all fuel such that the existing modules can be emptied and removed from the pool, and new modules installed in a programmed manner.

A remotely engagable lift rig, which is designed to meet the criteria of NUREG-0612 "Control of Heavy Loads of Nuclear Power Plants", will be used to lift the empty modules. Auxiliary Building Cranes will be used for this purpose. A module change-out

scheme and procedure will be developed which ensures that all modules being handled are empty when the module is moving at a height which is more than 12" above the pool floor.

The Auxiliary Building has two overhead cranes which ride on rails that traverse the entire fuel handling area of the building. Each crane has a main hook rated at 150 tons. These hooks are single failure proof (SFP) (up to 60 tons). In addition there is an auxiliary hoist on the East Crane rated at 20 tons.

Pursuant to the defense-in-depth approach of NUREG-0612, the following additional measures of safety will be undertaken for the reracking operation.

(i) The crane and hoist will be given a preventive maintenance checkup and inspection within 3 months of the beginning of the reracking operation.

(ii) The crane hook will be used to lift no more than 50% of its single failure proof capacity of 60 tons at any time during the reracking operation. (The maximum weight of any module and its associated handling tool is 24 tons).

(iii) The old fuel racks will be lifted no more than 6" above the pool floor and held in that elevation for approximately 10 minutes before beginning the vertical lift.

(iv) The rate of vertical lift will not exceed 6' per minute.

(v) The rate of horizontal movement will not exceed 6' per minute.

(vi) Preliminary safe load paths have been developed. The "old" or "new" racks will not be carried over any region of the pool containing fuel.

(vii) The rack upending or laying down will be carried out in an area which is not overlapping to any safety related component.

(viii) All crew members involved in the reracking operation will be given training in the use of the lifting and upending equipment. The training

seminar will utilize videotapes of the actual lifting and upending rigs on typical modules to be installed in the pool. Every crew member will be required to pass a written examination in the use of lifting and upending apparatus administered by the rack designer.

(ix) Referring to Figure 2.1.1, it is noted that the fuel handling bridge crane cannot access storage cells facing the east wall and several locations in the southwest corner. Therefore, it will be necessary to load the inaccessible cells with fuel when the rack is staged a certain distance (approximately 20 inches) from the pool wall. Having loaded these cells, the module will be lifted approximately 4 inches above the pool liner, and laterally transported to its final designated locations. A fuel shuffling and rack installation sequence has been developed to ensure that all heavy load handling criteria of NUREG-0612 are satisfied. The rack handling rig is designed with consideration of the rack module weight along with the contained fuel assembly mass.

The fuel racks will be brought directly into the Auxiliary Building through the access door which is at ground level (609' elevation). This direct access to the building greatly facilitates the rack removal and installation effort.

The "old" racks will be decontaminated to the extent practical on-site and approved for shipping per the requirements of 10 CFR71 and 49 CFR 171-178, be housed in shipping containers, and transported to a processing facility for volume reduction. Non-decontaminatable portions of the racks will be shipped to a licensed radioactive waste burial site or returned to site for storage if disposal access is unavailable. The volume reduction is expected to reduce the overall volume of the racks to about 1/10th of their original value.

All phases of the reracking activity will be conducted in accordance with written procedures which will be reviewed and approved by I&M.

Table 2.1.1

MODULE DATA

Module I.D.	Quantity	Array Cell Size	Total Cell Count for this Module Type
A**	5	13x14	910
B	4	12x14	672
C	4	13x12	624
D	2	12x12	288
E	4	13x11	572
F	2	12x11	264
G	1	12x10	120
H*	1	13x14 - (8x2)	166
Total	23		3616

---

* Non-rectangular module.

** Three of the A modules have one triangle cell to accommodate pool corner curvature.

Table 2.1.2

COMMON MODULE DATA

Storage cell inside dimension:	8.75" ± 0.04"
Storage cell height (above the baseplate):	168 ± 1/16"
Baseplate thickness:	0.75" (nominal)
Support leg height:	5.25" (nominal)
Support leg type:	Remotely adjustable legs
Number of support legs:	4 (minimum)
Remote lifting and handling provision:	Yes
Poison material:	Boral
Poison length:	144"
Poison width:	7.5"
Cell Pitch:	8.97" (nominal)

Table 2.1.3

MODULE DATA

Module I.D.	Dimensions (inch)* East-West	North-South	Shipping Weight (kips)
A	117-3/16	126-3/16	25.7
B	108-1/8	126-3/16	23.7
C	117-3/16	108-1/8	22.5
D	108-1/8	108-1/8	20.9
E	117-3/16	99-1/16	20.8
F	108-1/8	99-1/16	19.3
G	108-1/8	90-1/8	17.7
H	117-3/16	126-3/16	23.9

* All dimensions are bounding rectangular envelopes rounded to the nearest one sixteenth of an inch.

Table 2.3.1

BORAL EXPERIENCE LIST (Domestic and Foreign)

Pressurized Water Reactors

Plant	Utility	Vented Construction	Mfg. Year
Bellefont 1, 2	Tennessee Valley Authority	No	1981
Donald C. Cook 1, 2	Indiana & Michigan Electric	No	1979
Indian Point 3	NY Power Authority	Yes	1987
Maine Yankee	Maine Yankee Atomic Power	Yes	1977
Salem 1, 2	Public Service Elec & Gas	No	1980
Seabrook	New Hampshire Yankee	No	---
Sequoyah 1,2	Tennessee Valley Authority	No	1979
Yankee Rowe	Yankee Atomic Power	Yes	1964/1983
Zion 1,2	Commonwealth Edison Co.	Yes	1980
Byron 1,2	Commonwealth Edison Co.	Yes	1988
Braidwood 1,2	Commonwealth Edison Co.	Yes	1988
Yankee Rowe	Yankee Atomic Electric	Yes	1988
Three Mile Island I	GPU Nuclear	Yes	1990

Boiling Water Reactors

Browns Ferry 1,2,3	Tennessee Valley Authority	Yes	1980
Brunswick 1,2	Carolina Power & Light	Yes	1981
Clinton	Illinois Power	Yes	1981
Cooper	Nebraska Public Power	Yes	1979
Dresden 2,3	Commonwealth Edison Co.	Yes	1981
Duane Arnold	Iowa Elec. Light & Power	No	1979
J.A. Fitzpatrick	NY Power Authority	No	1978
E.I. Hatch 1,2	Georgia Power	Yes	1981
Hope Creek	Public Service Elec & Gas	Yes	1985
Humboldt Bay	Pacific Gas & Electric	Yes	1986
LaCrosse	Dairyland Power	Yes	1976
Limerick 1,2	Philadelphia Electric	No	1980
Monticello	Northern States Power	Yes	1978
Peachbottom 2,3	Philadelphia Electric	No	1980
Perry, 1,2	Cleveland Elec. Illuminating	No	1979
Pilgrim	Boston Edison	No	1978
Shoreham	Long Island Lighting	Yes	---
Susquehanna 1,2	Pennsylvania Power & Light	No	1979
Vermont Yankee	Vermont Yankee Atomic Power	Yes	1978/1986
Hope Creek	Public Service Elec & Gas	Yes	1989

Table 2.3.1 (continued)

Foreign Installations Using Boral

France

12 PWR Plants	Electricite de France

South Africa

Koeberg 1,2	ESCOM

Switzerland

Beznau 1,2	Nordostschweizerische Kraftwerke AG
Gosgen	Kernkraftwerk Gosgen-Daniken AG

Taiwan

Chin-Shan 1,2	Taiwan Power Company
Kuosheng 1,2	Taiwan Power Company

Table 2.3.2

1100 ALLOY ALUMINUM PHYSICAL AND MECHANICAL PROPERTIES

Density	0.098 lb/cu. in. 2.713 gm/cc
Melting Range	1190-1215 deg. F 643-657 deg. C
Thermal Conductivity (77 deg. F)	128 BTU/hr/sq ft/deg. F/ft 0.53 cal/sec/sq cm/deg. C/cm
Coef. of Thermal Expansion (68-212 deg. F)	13.1×10^{-6}/deg. F 23.6×10^{-6}/deg. C
Specific heat (221 deg. F)	0.22 BTU/lb/deg. F 0.23 cal/gm/deg. C
Modulus of Elasticity	10×10^{6} psi
Tensile Strength (75 deg. F)	13,000 psi annealed 18,000 psi as rolled
Yield Strength (75 deg. F)	5,000 psi annealed 17,000 psi as rolled
Elongation (75 deg. F)	35-45% annealed 9-20% as rolled
Hardness (Brinell)	23 annealed 32 as rolled
Annealing Temperature	650 deg. F 343 deg. C

Table 2.3.3

CHEMICAL COMPOSITION (by weight) - ALUMINUM (1100 Alloy)

99.00% min.	Aluminum
1.00% max.	Silicone and Iron
0.05-0.20% max.	Copper
.05% max.	Manganese
.10% max.	Zinc
.15% max.	others each

Table 2.3.4

BORON CARBIDE CHEMICAL COMPOSITION, Weight %

Total boron	70.0 min.
B^{10} isotopic content in natural boron	18.0
Boric oxide	3.0 max.
Iron	2.0 max.
Total boron plus total carbon	94.0 min.

BORON CARBIDE PHYSICAL PROPERTIES

Chemical formula	B_4C
Boron content (weight)	78.28%
Carbon content (weight)	21.72%
Crystal Structure	rombohedral
Density	2.51 gm./cc-0.0907 lb/cu. in.
Melting Point	2450^0C (4442^0F)
Boiling Point	3500^0C (6332^0F)
Microscopic thermal-neutron cross-section	600 barn

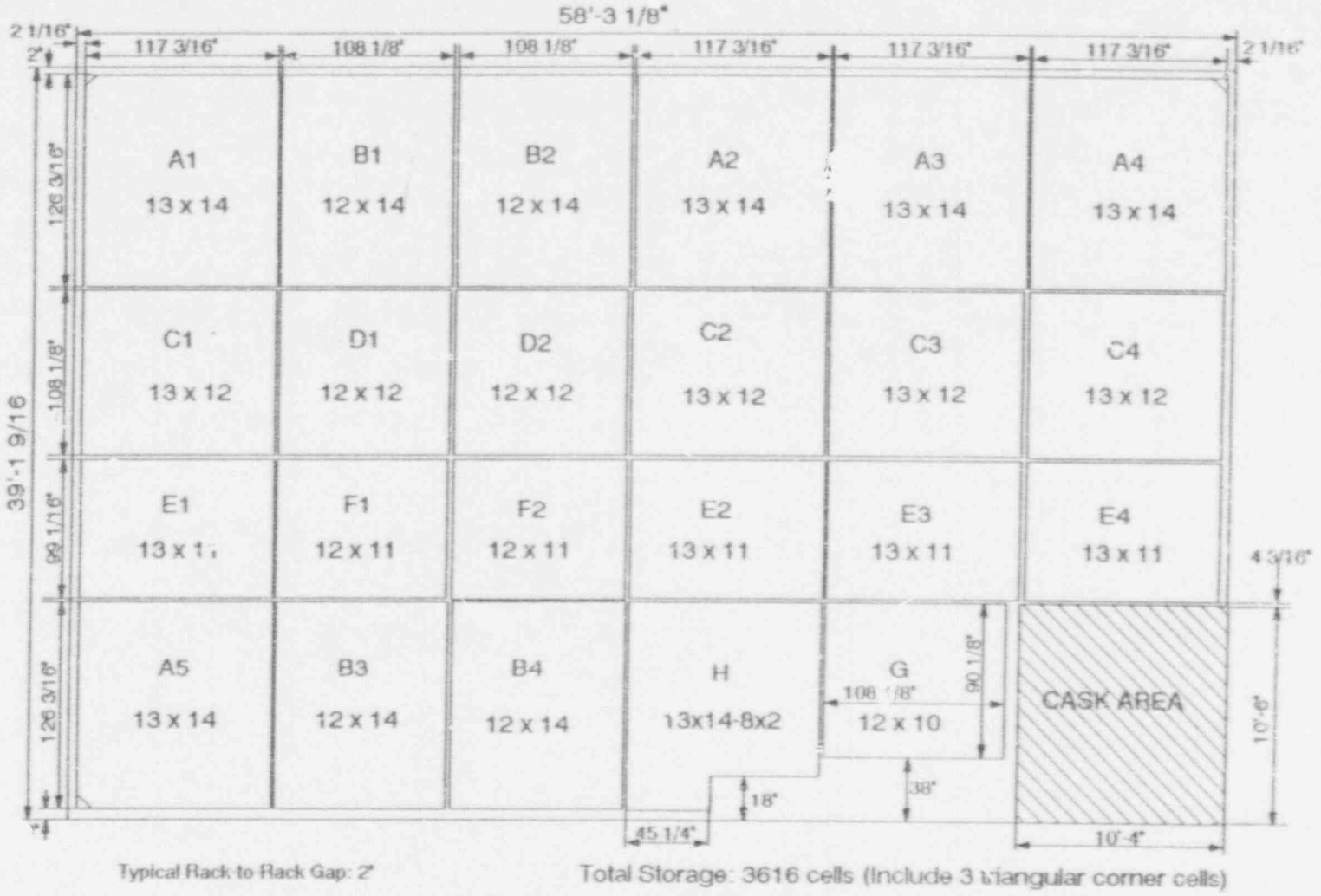

Typical Rack to Rack Gap: 2"

Total Storage: 3616 cells (Include 3 triangular corner cells)

FIGURE 2.1.1 COOK SPENT FUEL POOL LAYOUT

3.0 CONSTRUCTION OF RACK MODULES

The object of this section is to provide a description of rack module construction for the Donald C. Cook spent fuel pool to enable an independent appraisal of the adequacy of the design. Similar rack structure designs have recently been used in previous licensing efforts for Kuosheng Units 1 & 2 (Taiwan Power Company); J.A. FitzPatrick (New York Power Authority); Indian Point 2 (Consolidated Edison Company of New York, Inc.); Three Mile Island Unit 1 (GPU Nuclear); and Hope Creek 1 (Public Service Electric & Gas Company). A list of applicable codes and standards is also presented.

3.1 Fabrication Objective

The requirements in manufacturing the high density storage racks for the Donald C. Cook fuel pool may be stated in four interrelated points:

(1) The rack module will be fabricated in such a manner that there is no weld splatter on the storage cell surfaces which would come in contact with the fuel assembly.

(2) The storage locations will be constructed so that redundant flow paths for the coolant are available.

(3) The fabrication process involves operational sequences which permit immediate verification by the inspection staff.

(4) The storage cells are connected to each other by austenitic stainless steel corner welds which leads to a honeycomb lattice construction. The extent of welding is selected to "detune" the racks from the seismic input motion of the Operating Basis Earthquake (OBE) and Design Basis Earthquake (DBE).

3.2 Mixed Zone Two Region Storage

All rack modules designed and fabricated for the Donald C. Cook spent fuel pool are of the so-called "non-flux trap" type. In the non-flux trap modules, a single screen of the poison panel is interposed between two fuel assemblies. The poison material utilized in this project is Boral, which does not require lateral support to prevent slumping due to the inherent stiffness. However, accurate dimensional control of the poison location is essential for nuclear criticality and thermal-hydraulic considerations. The design and fabrication approach to realize this objective is presented in the next sub-section.

3.3 Anatomy of Rack Modules

As stated earlier, the storage cell locations have a single poison panel between adjacent austenitic stainless steel surfaces. The significant components of the rack module are: (1) the storage box subassembly (2) the baseplate, (3) the thermal neutron absorber material, (4) picture frame sheathing, and (5) support legs.

(1) The rack module manufacturing begins with fabrication of the box. The "boxes" are fabricated from two precision formed channels by seam welding in a machine equipped with copper chill bars and pneumatic clamps to minimize distortion due to welding heat input. Figure 3.3.1 shows the box.

The minimum weld penetration will be 80% of the box metal gage which is 0.075" (14 gage). The boxes are manufactured to 8.75" I.D. (nominal irside dimension).

The design objective calls for installing Boral with minimal surface loading. This is accomplished by die forming a "picture frame sheathing" as shown in Figure

3.3.2. This sheathing is 0.035" thick and is made to precise dimensions such that the offset is .010" to .005" greater than the poison material thickness.

As shown in Figure 3.3.1, each box has four lateral 1" diameter holes punched near its bottom edge to provide auxiliary flow holes. The edges of the sheathing and the box are welded together to form a smooth edge. The box, with integrally connected sheathing, is referred to as the "composite box".

The "composite boxes" are arranged in a checkerboard array to form an assemblage of storage cell locations (Figure 3.3.3). The inter-box welding and pitch adjustment are accomplished by small longitudinal connectors. Further details are given later in this section.

This assemblage of box assemblies is welded edge-to-edge as shown in Figure 3.3.3, resulting in a honeycomb structure with axial, flexural and torsional rigidity depending on the extent of intercell welding provided. It can be seen from Figure 3.3.3 that the edges of each interior box are connected to the contiguous boxes resulting in a well defined path to resist shear.

(2) Baseplate: The baseplate provides a continuous horizontal surface for supporting the fuel assemblies.

The baseplate is attached to the cell assemblage by fillet welds. The baseplate in each storage cell has a 5" diameter flow hole. The baseplate is 3/4" thick to withstand accident fuel assembly drop loads postulated and discussed in Section 7 of this report.

(3) thermal neutron absorber material: As mentioned in the preceding section, Boral is used as the thermal neutron absorber material.

(4) Picture Frame Sheathing: As described earlier, the sheathing serves as the locator and retainer of the poison material. Figure 3.3.2 shows a schematic of the sheathing.

The poison material is placed in the customized flat depression region of the sheathing, which is next laid on a side of the "box". The precision of the shape of the sheathing obtained by die forming guarantees that the poison sheet installed in it will not be subject to surface compression. The flanges of the sheathing (on all four sides) are attached to the box using skip welds. The sheathing serves to locate and position the poison sheet accurately, and to preclude its movement under seismic conditions.

(5) Support Legs: All support legs are the adjustable type (Figure 3.3.4). The top portion is made of austenitic steel material. The bottom part is made of SA564-630 stainless steel to avoid galling problems.

Each support leg is equipped with a readily accessible socket to enable remote leveling of the rack after its placement in the pool. Lateral holes in the support leg provide the requisite coolant flow path.

An elevation cross-section of the rack module shown in Figure 3.3.5 shows two box cells, and a developed cell in elevation. The Boral panels and their location are also indicated in this figure. The boral panels are positioned such that the entire enriched fuel portion of the fuel assembly is enveloped by the thermal neutron absorber material.

The joint between the composite box arrays and the baseplate is made by single fillet welds which provide a minimum of 7" of connectivity between each cell wall and the baseplate surface.

As shown in Figure 3.3.4, the support leg is gusseted to provide an increased section for load transfer between the support legs and the cellular structure above the baseplate. Use of the gussets also minimizes heat input induced distortions of the support/baseplate contact region.

3.4 Codes, Standards, and Practices for the Donald C. Cook Spent Fuel Pool Racks

The fabrication of the rack modules for the Donald C. Cook spent fuel pool is performed under a strict quality assurance system suitable for manufacturing and complying with the provisions of 10CFR50 Appendix B.

The following codes, standards and practices will be used as applicable for the design, construction, and assembly of the spent fuel storage racks. Additional specific references related to detailed analyses are given in each section.

a. Codes and Standards for Design and Testing

(1) AISC Manual of Steel Construction, 8th Edition, 1980.

(2) ANSI N210-1976, "Design Objectives for Light Water Reactor Spent Fuel Storage Facilities at Nuclear Power Stations".

(3) American Society of Mechanical Engineers (ASME), Boiler and Pressure Vessel Code, Section III, Subsection NF, 1989.

(4) ASNT-TC-1A, June, 1980 American Society for Nondestructive Testing (Recommended Practice for Personnel Qualifications).

(5) ASME Section V - Nondestructive Examination

(6) ASME Section IX - Welding and Brazing Qualifications

(7) Building Code Requirements for Reinforced Concrete, ACI318-89/ACI318R-89.

(8) Code Requirements for Nuclear Safety Related Concrete Structures, ACI 349-85 and Commentary ACI 349R-85

(9) Reinforced Concrete Design for Thermal Effects on Nuclear Power Plant Structures, ACI 349.1R-80 .

(10) ACI Detailing Manual - 1980

(11) ASME NQA-2, Part 2.7 "Quality Assurance Requirements of Computer Software for Nuclear Facility Applications (draft).

(12) ANSI/ASME, Qualification and Duties of Personnel Engaged in ASME Boiler and Pressure Vessel Code Section III, Div. 1, Certifying Activities, N626-3-1977.

b. Material Codes

(1) American Society for Testing and Materials (ASTM) Standards - A-240.

(2) American Society of Mechanical Engineers (ASME), Boiler and Pressure Vessel Code, Section II - Parts A and C, 1989.

c. Welding Codes

ASME Boiler and Pressure Vessel Code, Section IX-Welding and Brazing Qualifications (1986) or later issue accepted by USNRC.

d. Quality Assurance, Cleanliness, Packaging, Shipping, Receiving, Storage, and Handling Requirements

(1) ANSI N45.2.2 - Packaging, Shipping, Receiving, Storage and Handling of Items for Nuclear Power Plants.

(2) ANSI 45.2.1 - Cleaning of Fluid Systems and Associated Components during Construction Phase of Nuclear Power Plants.

(3) ASME Boiler and Pressure Vessel, Section V, Nondestructive Examination, 1983 Edition, including Summer and Winter Addenda, 1983.

(4) ANSI - N16.1-75 Nuclear Criticality Safety Operations with Fissionable Materials Outside Reactors.

(5) ANSI - N16.9-75 Validation of Calculation Methods for Nuclear Criticality Safety.

(6) ANSI - N45.2.11, 1974 Quality Assurance Requirements for the Design of Nuclear Power Plants.

(7) ANSI 14.6-1978, "Special Lifting Devices for Shipping Containers weighing 10,000 lbs. or more for Nuclear Materials".

(8) ANSI N45.2.6, Qualification of Inspection and Testing Personnel.

(9) ANSI N45.2.8, Installation, Inspection.

(10) ANSI N45.2.9, Records.

(11) ANSI N45.2.10, Definitions.

(12) ANSI N45.2.12, QA Audits.

(13) ANSI N45.2.13, Procurement.

(14) ANSI 45.2.23, QA Audit Personnel.

e. Other References
(In the references below, RG is NRC Regulatory Guide)

(1) RG 1.13 - Spent Fuel Storage Facility Design Basis, Rev. 2 (proposed).

(2) RG 1.123 - (endorses ANSI N45.2.13) Quality Assurance Requirements for Control of Procurement of Items and Services for Nuclear Power Plants.

(3) RG 1.124 - Service Limits and Loading Combinations for Class 1 Linear Type Component Supports, Rev. 1.

(4) RG 1.25 - Assumptions Used for Evaluating the Potential Radiological Consequences of a Fuel Handling Accident in the Fuel Handling and Storage Facility of Boiling and Pressurized Water Reactors.

(5) RG 1.28 - (endorses ANSI N45.2) - Quality Assurance Program Requirements, June, 1972.

(6) RG 1.29 - Seismic Design Classification, Rev. 3.

(7) RG 1.31 - Control of Ferrite Content in Stainless Steel Weld Metal, Rev. 3.

(8) RG 1.38 - (endorses ANSI N45.2.2) Quality Assurance Requirements for Packaging, Shipping, Receiving, Storage and Handling of Items for Water-Cooled Nuclear Power Plants, March, 1973.

(9) RG 1.44 - Control of the Use of Sensitized Stainless Steel.

(10) RG 1.58 - (endorses ANSI N45.2.2) Qualification of Nuclear Power Plant Inspection, Examination, and Testing Personnel, Rev. 1, September, 1980.

(11) RG 1.64 - (endorses ANSI N45.2.11) Quality Assurance Requirements for the Design of Nuclear Power Plants, October, 1973.

(12) RG 1.71 - Welder Qualifications for Areas of Limited Accessibility.

(13) RG 1.74 - (endorses ANSI N45.2.10) Quality Assurance Terms and Definitions, February, 1974.

(14) RG 1.85 - Materials Code Case Acceptability ASME Section III, Division 1.

(15) RG 1.88 - (endorses ANSI N45.2.9) Collection, Storage and Maintenance of Nuclear Power Plant Quality Assurance Records, Rev. 2, October, 1976.

(16) RG 1.92 - Combining Modal Responses and Spatial Components in Seismic Response Analysis.

(17) RG 3.41 - Validation of Calculation Methods for Nuclear Criticality Safety.

(18) General Design Criteria for Nuclear Power Plants, Code of Federal Regulations, Title 10, Part 50, Appendix A (GDC Nos. 1, 2, 61, 62, and 63).

(19) NUREG-0800, Standard Review Plan, Sections 3.2.1, 3.2.2, 3.7.1, 3.7.2, 3.7.3, 3.8.4.

(20) "OT Position for Review and Acceptance of Spent Fuel Storage and Handling Applications," dated April 14, 1978, and the modifications to this document of January 18, 1979. (Note: OT stands for Office of Technology).

(21) NUREG-0612, "Control of Heavy Loads at Nuclear Power Plants".

(22) Regulatory Guide 8.8, "Information Relative to Ensuring that Occupational Radiation Exposure at Nuclear Power Plants will be as Low as Reasonably Achievable (ALARA).

(23) 10CFR50 Appendix B, Quality Assurance Criteria for Nuclear Power Plants and Fuel Reprocessing Plants

(24) 10CFR21 - Reporting of Defects and Non-Compliance

3.5 Materials of Construction

Storage Cell:	ASME SA240-304
Baseplate:	ASME SA240-304
Support Leg (female):	ASME SA240-304
Support Leg (male):	Ferritic stainless steel (anti-galling material) ASME SA564-630
Poison:	Boral

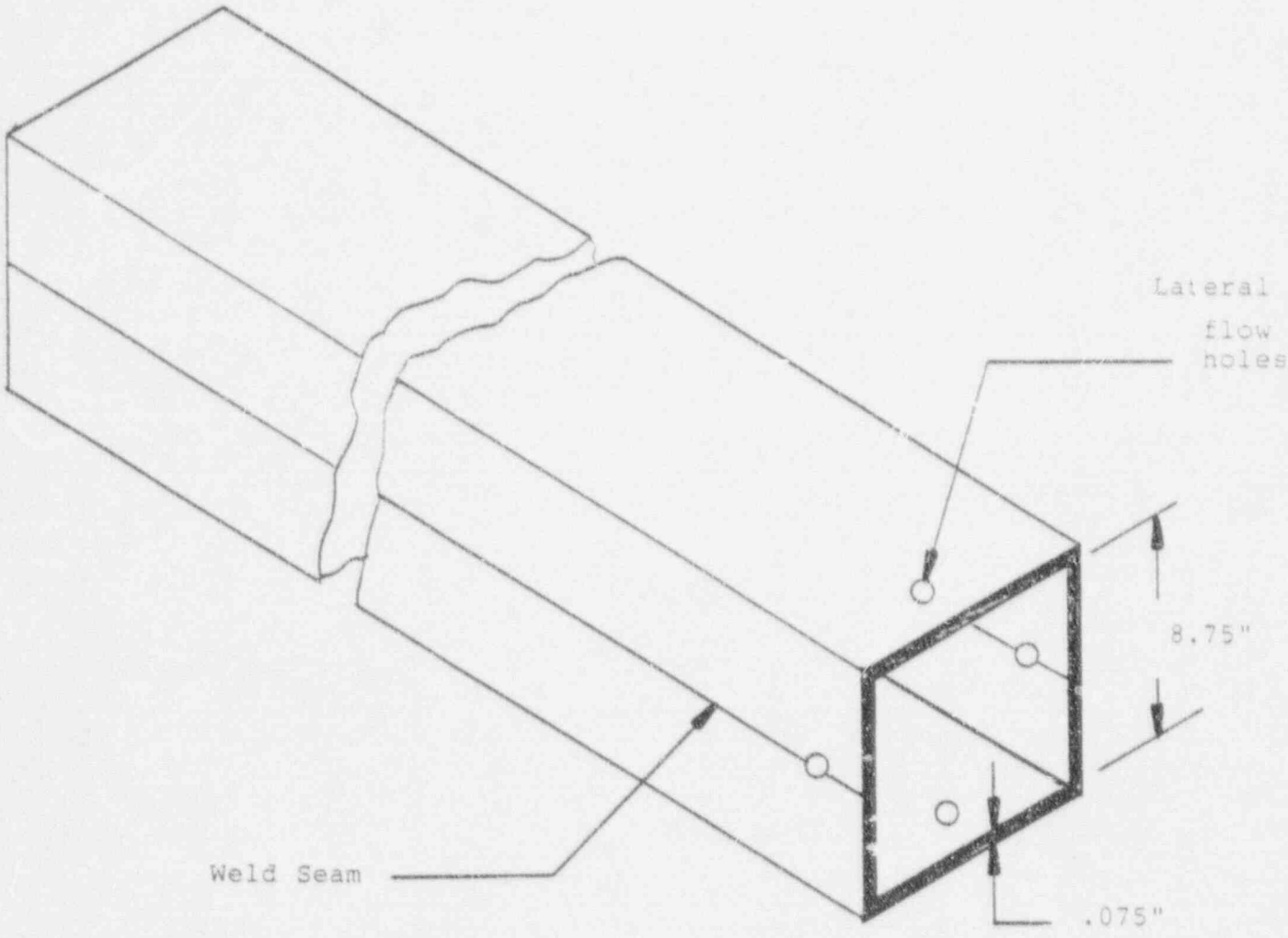

Figure 3.3.1 SEAM WELDING PRECISION FORMED CHANNELS

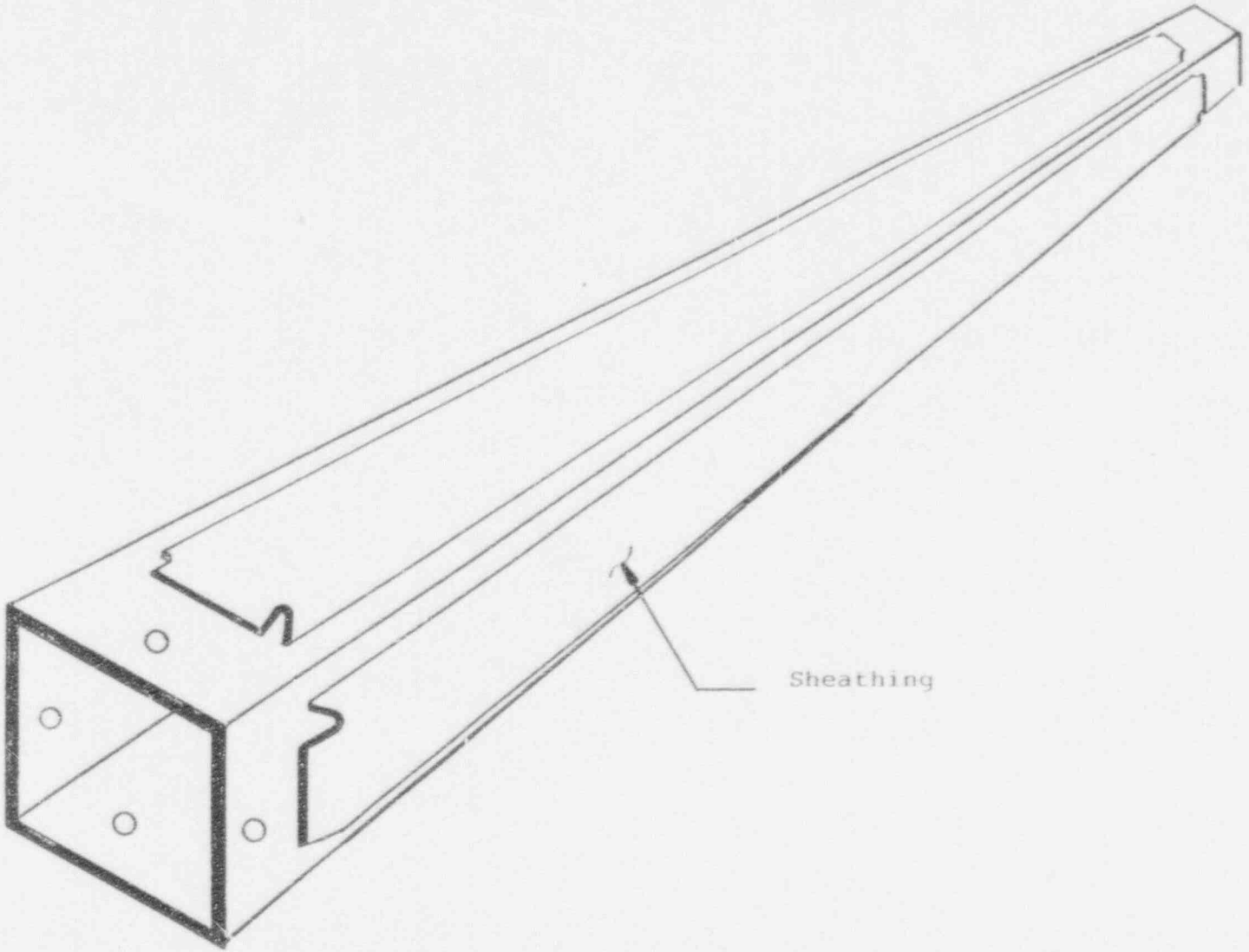

Figure 3.3.2 COMPOSITE BOX ASSEMBLY

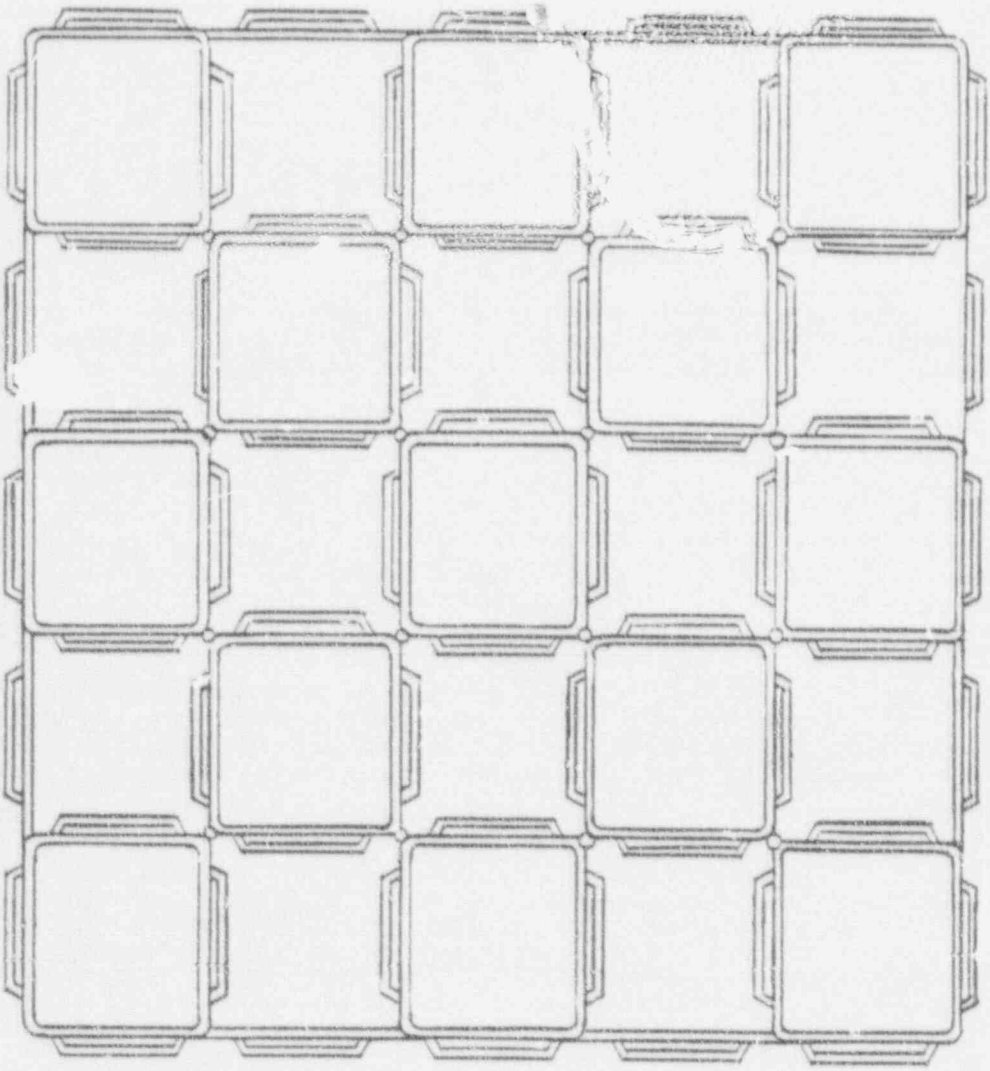

Figure 3.3.3 ARRAY OF CELLS FOR NON-FLUX TRAP MODULES

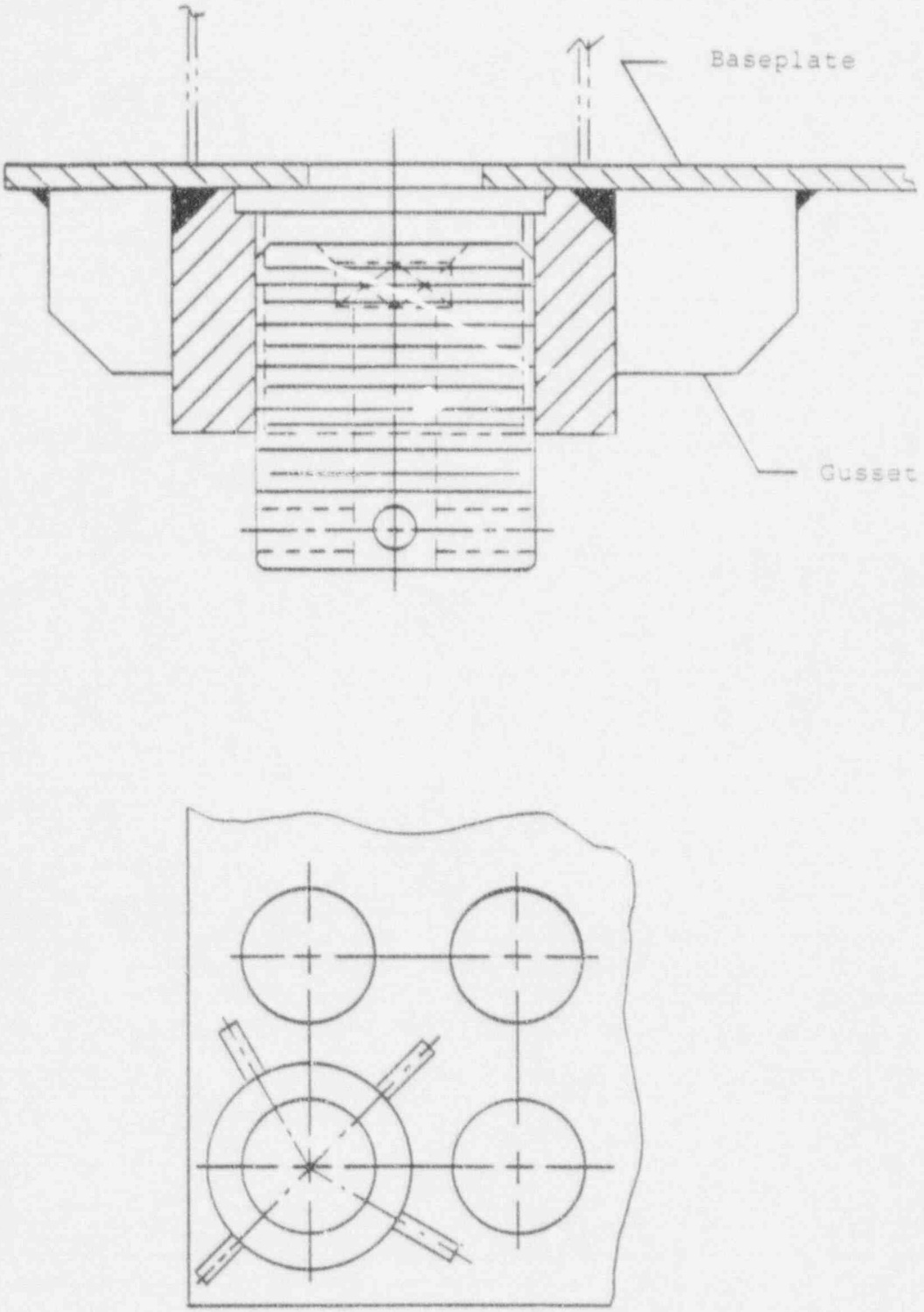

Figure 3.3.4 ADJUSTABLE SUPPORT LEG

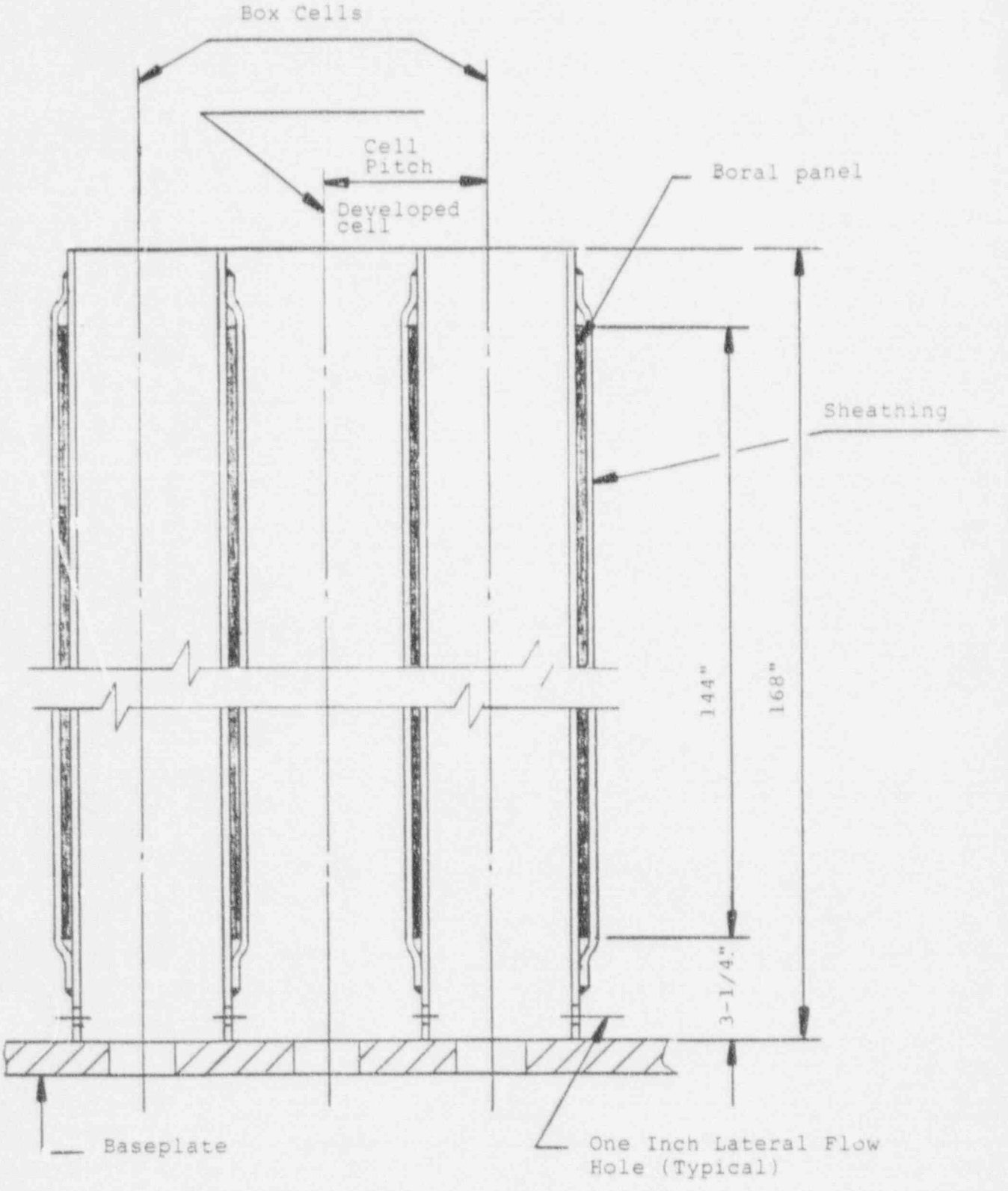

Figure 3.3.5 ELEVATION VIEW OF RACK MODULE

4.0 CRITICALITY SAFETY ANALYSES

4.1 Design Basis

The high density spent fuel storage racks for Donald C. Cook Nuclear Plant are designed to assure that the effective neutron multiplication factor (k_{eff}) is equal to or less than 0.95 with the racks fully loaded with fuel of the highest anticipated reactivity, and flooded with unborated water at the temperature within the operating range corresponding to the highest reactivity. The maximum calculated reactivity includes a margin for uncertainty in reactivity calculations including mechanical tolerances. All uncertainties are statistically combined, such that the final k_{eff} will be equal to or less than 0.95 with a 95% probability at a 95% confidence level.

Applicable codes, standards, and regulations or pertinent sections thereof, include the following:

- General Design Criteria 62, Prevention of Criticality in Fuel Storage and Handling.
- USNRC Standard Review Plan, NUREG-0800, Section 9.1.2, Spent Fuel Storage, Rev. 3 - July 1981
- USNRC letter of April 14, 1978, to all Power Reactor Licensees - OT Position for Review and Acceptance of Spent Fuel Storage and Handling Applications, including modification letter dated January 18, 1979.
- USNRC Regulatory Guide 1.13, Spent Fuel Storage Facility Design Basis, Rev. 2 (proposed), December 1981.
- ANSI ANS-8.17-1984, Criticality Safety Criteria for the Handling, Storage and Transportation of LWR Fuel Outside Reactors.

To assure the true reactivity will always be less than the calculated reactivity, the following conservative assumptions were made:

- Moderator is assumed to be unborated water at a temperature within the operating range that results in the highest reactivity (determined to be 20 °C).
- The effective multiplication factor of an infinite radial array of fuel assemblies was used (see section 4.4.1) except for the boundary storage cells where leakage is inherent.
- Neutron absorption in minor structural members is neglected, i.e., spacer grids are analytically replaced by water.

The design basis fuel assembly is a 15 x 15 (Standard) Westinghouse containing UO_2 at a maximum initial enrichment of 4.95 ± 0.05 wt% U-235 by weight. For fuel assemblies with natural UO_2 blankets, the enrichment is that of the central enriched zone. Calculations confirmed that this reference design fuel assembly was the most reactive of the assembly types expected to be stored in the racks. Three separate storage regions are provided in the spent fuel storage pool, with independent criteria defining the highest potential reactivity in each of the two regions as follows:

- Region 1 is designed to accommodate new fuel with a maximum enrichment of 4.95 ± 0.05 wt% U-235, or spent fuel regardless of the discharge fuel burnup.
- Region 2 is designed to accommodate fuel of 4.95% initial enrichment burned to at least 50,000 MWD/MtU (assembly average), or fuel of other enrichments with a burnup yielding an equivalent reactivity.
- Region 3 is designed to accommodate fuel of 4.95% initial enrichment burned to at least 38,000 MWD/MtU (assembly average), or fuel of other enrichments with a burnup yielding an equivalent reactivity.

The water in the spent fuel storage pool normally contains soluble boron which would result in large subcriticality margins under actual operating conditions. However, the NRC guidelines, based upon the accident condition in which all soluble poison is assumed to have been lost, specify that the limiting K_{eff} of 0.95 for normal storage be evaluated in the absence of soluble boron. The double contingency principle of ANSI N-16.1-1975 and of the April 1978 NRC letter allows credit for soluble boron under other abnormal or accident conditions since only a single independent accident need be considered at one time. Consequences of abnormal and accident conditions have also been evaluated, where "abnormal" refers to conditions which may reasonably be expected to occur during the lifetime of the plant and "accident" refers to conditions which are not expected to occur but nevertheless must be protected against.

4.2 Summary of Criticality Analyses

4.2.1 Normal Operating Conditions

The design basis layout of storage cells for the three regions is shown in Figure 4.1. In this configuration, the fresh fuel cells (Region 1) are located alternately along the rack periphery (where neutron leakage reduces reactivity) or along the boundary between two storage modules (where the water gap provides a flux-trap which reduces reactivity). High burnup fuel in Region 2 affords a low-reactivity barrier between fresh fuel assemblies and Region 3 fuel of intermediate burnup. There are at the present time, an adequate number of spent fuel assemblies to nearly fill and "block off" the Region 2 barrier locations (see Section 4.7). Thus, the administrative controls required are comparable to a conventional two-region storage rack design.

Prior to approaching the reactor end-of-life, not all storage cells are needed for spent fuel. Therefore, an alternative configuration may be used in which the internal cells are loaded in a checkerboard pattern of fresh fuel (or fuel of any burnup) with empty cells, as indicated in Figure 4.2. This configuration is intended primarily to facilitate a full core unload when needed, prior to the time the racks are beginning to fill up.

Figure 4.3 define the acceptable burnup domains and illustrates the limiting burnup for fuel of various initial enrichments for both Region 2 (upper curve) or Region 3 (lower curve), both of which assume that the fresh fuel (Region 1) is enriched to 4.95% U-235. Criticality analyses show that the most reactive configuration occurs along the boundary between modules with the reactivity of

the edge configuration being slightly lower*. The bounding criticality analyses are summarized in Table 4.1 for the design basis storage condition (which assumes the single accident condition of the loss of all soluble boron) and in Table 4.2 for the interim checkerboard loading arrangement. The calculated maximum reactivity of 0.940 (same for both the normal storage condition and the interim checkerboard arrangement) is within the regulatory limit of a k_{eff} of 0.95. This maximum reactivity includes calculational uncertainties and manufacturing tolerances (95% probability at the 95% confidence level), an allowance for uncertainty in depletion calculations and the evaluated effect of the axial distribution in burnup. Fresh fuel of less than 4.95% enrichment would result in lower reactivities. As cooling time increases in long-term storage, decay of Pu-241 results in a continuous decrease in reactivity, which provides an increasing subcriticality margin with time. No credit is taken for this decrease in reactivity other than to indicate conservatism in the calculations.

The burnup criteria identified above (Figure 4-3) for acceptable storage in Region 2 and Region 3 can be implemented in appropriate administrative procedures to assure verified burnup as specified in the proposed Regulatory Guide 1.13, Revision 2. Administrative procedures will also be employed to confirm and assure the presence of soluble poison in the pool water during fuel handling operations, as a further margin of safety and as a precaution in the event of fuel misplacement during fuel handling operations.

---

* The thick base-plate on the rack modules extend beyond the storage cells and provide assurance that the necessary water-gap between modules is maintained.

For convenience, the minimum (limiting) burnup data in Figure 4.3 for unrestricted storage may be described as a function of the initial enrichment, E, in weight percent U-235 by fitted polynomial expressions as follows;

For Region 2 Storage

Minimum Burnup in MWD/MTU =

$$- 22{,}670 + 22{,}220\ E - 2{,}260\ E^2 + 149\ E^3$$

For Region 3 Storage

Minimum Burnup in MWD/MTU =

$$- 26{,}745 + 18{,}746\ E - 1{,}631\ E^2 + 98.4\ E^3$$

4.2.2 Abnormal and Accident Conditions

Although credit for the soluble poison normally present in the spent fuel pool water is permitted under abnormal or accident conditions, most abnormal or accident conditions will not result in exceeding the limiting reactivity (k_{eff} of 0.95) even in the absence of soluble poison. The effects on reactivity of credible abnormal and accident conditions are discussed in Section 4.7 and summarized in Table 4.3. Of these abnormal or accident conditions, only one has the potential for a more than negligible positive reactivity effect.

The inadvertent misplacement of a fresh fuel assembly has the potential for exceeding the limiting reactivity, should there be a concurrent and independent accident condition resulting in the loss of all soluble poison. Administrative procedures to assure the presence of soluble poison during fuel handling operations will preclude the possibility of the simultaneous occurrence of the two independent accident conditions. The largest reactivity increase (+ 0.065 δk) would occur if a new fuel assembly of 4.95% enrichment were to be positioned in a Region 2 location with the remainder of the rack fully loaded with fuel of the highest permissible reactivity. Under this accident condition, credit for the presence of soluble poison is permitted by NRC guidelines*, and calculations indicate that 550 ppm soluble boron would be adequate to reduce the k_{eff} to the calculated k_{eff} (0.940) and approximately 450 ppm would be sufficient to assure that the limiting k_{eff} of 0.95 is not exceeded.

---

*Double contingency principle of ANSI N16.1-1975, as specified in the April 14, 1978 NRC letter (Section 1.2) and implied in the proposed revision to Reg. Guide 1.13 (Section 1.4, Appendix A).

4.3 Reference Fuel Storage Cells

4.3.1 Reference Fuel Assembly

The design basis fuel assembly, described in Figure 4.4, is a 15 x 15 array of fuel rods with 21 rods replaced by 20 control rod guide tubes and 1 instrument thimble. Table 4.4 summarizes the fuel assembly design specifications and the expected range of significant manufacturing tolerances. As shown below, initial cell calculations with CASMO-3 indicated that the W 15 x 15 fuel exhibited a slightly higher reactivity in the storage rack cell than either the W 17 x 17 standard or optimized (OFA) fuel or the ANF fuel assembly designs.

Fuel type	Enrichment	Burnup MWD/KgU	Cell K_{eff}
W 15 x 15	2.5	0	1.0261 *
W 15 x 15	2.5	10	0.9210 *
W 17 x 17 OFA	2.5	0	1.0205
W 17 x 17 OFA	2.5	10	0.9144
W 17 x 17 Stnd	2.5	0	1.0217
W 17 x 17 Stnd	2.5	10	0.9188
ANF 15 x 15	2.5	0	1.0148
ANF 17 x 17	2.5	0	1.0126
W 15 x 15	4.95	0	1.1941 *
W 15 x 15	4.95	40	0.9204 *
W 17 x 17 OFA	4.95	0	1.1933
W 17 x 17 OFA	4.95	40	0.9149
W 17 x 17 Stnd	4.95	0	1.1880
ANF 15 x 15	4.95	0	1.1857
ANF 17 x 17	4.95	0	1.1883

* Highest values

Based upon the calculations listed above, the Westinghouse 15 x 15 rod design was used as the basis for the criticality calculations.

4.3.2 High Density Fuel Storage Cells

The nominal spent fuel storage cell used for the criticality analyses of the Donald C. Cook spent fuel storage cells is shown in Figure 4.4. Each storage cell is composed of Boral absorber panels positioned between a 8.75-inch I.D., 0.075-inch thick inner stainless steel box, and a 0.035-inch outer stainless steel sheath which forms the wall of the adjacent cell. The fuel assemblies are normally located in the center of each storage cell on a nominal lattice spacing of 8.97 ± 0.04 inches. The Boral absorber has a thickness of 0.101 ± 0.005 inch and a nominal B-10 areal density of 0.0345 g/cm^2.

4.4 Analytical Methodology

4.4.1 Reference Design Calculations

In the fuel rack analyses, the primary criticality analyses of the high density spent fuel storage racks were performed with the KENO-5a computer code package[1], using the 27-group SCALE* cross-section library[2] and the NITAWL subroutine for U-238 resonance shielding effects (Nordheim integral treatment). Depletion analyses and determination of equivalent enrichments were made with the two-dimensional transport theory code, CASMO-3[3]. Benchmark calculations, presented in Appendix A, indicate a bias of 0.0000 with an uncertainty of ± 0.0024 for CASMO-3 and 0.0090 ± 0.0021 (95%/95%) for NITAWL-KENO-5a. In tracking long-term (30-year) reactivity effects of spent fuel stored in Region 2 of the fuel storage rack, previous CASMO calculations confirmed a continuous reduction in reactivity with time (after Xe decay) due primarily to Pu-241 decay and Am-241 growth.

KENO-5a Monte Carlo calculations inherently include a statistical uncertainty due to the random nature of neutron tracking. To minimize the statistical uncertainty of the KENO-calculated reactivity, a minimum of 500,000 neutron histories in 1000 generations of 500 neutrons each, are accumulated in each calculation. For the design calculation for the racks, 1,250,000 histories were used to confirm convergence of the KENO-5a calculation.

Figure 4.5 represents the basic geometric model used in the KENO-5a calculations. This model effectively describes a repeating array of 10 storage cells in the X-direction separated by a 2-inch water

---

*"SCALE" is an acronym for Standardized Computer Analysis for Licensing Evaluation, a standard cross-section set developed by ORNL for the USNRC.

gap between modules and an infinite array of cells in the Y-direction (periodic boundary conditions). In the axial (Z) direction, the full length 144-inch fuel assembly was described with a 30-cm water reflector. A similiar model was used for calculations of the rack peripheral cells where the calculations were made with both water and concrete reflectors (a concrete reflector gave a slightly higher reactivity by 0.004 δk).

Larger models, encompassing an entire storage module (half of an 11 x 11 array, run for 1,250,000 neutron histories to assure convergence) confirmed results obtained with the smaller infinite array model. The larger model was also used to confirm the reactivity calculation for the checkerboard arrangement with fresh fuel and empty cells in Region 3 and in the investigation of the consequences of potential accident conditions with a misplaced fresh fuel assembly. In addition, the corner intersection was explicitly modeled and, as expected, gave a lower reactivity than the reference design calculation.

In the CASMO-3 geometric model (cell), each fuel rod and its cladding were described explicitly and reflecting boundary conditions (zero neutron current) were used in the axial direction and at the centerline of the Boral and steel plates between storage cells. These boundary conditions have the effect of creating an infinite array of storage cells in all directions and provide a conservative estimate of the uncertainties in reactivity attributed to manufacturing tolerances.

Because NITAWL-KENO-5a does not have burnup capability, burned fuel was represented by fuel of equivalent enrichment as determined by CASMO-3 calculations in the storage cell (i.e. an enrichment which yields the same reactivity <u>in the storage cell</u> as the burned fuel).

Figure 4.6 shows this equivalent enrichment for fuel of 4.95% initial enrichment at various discharge burnups, evaluated in the storage cell.

4.4.2 Fuel Burnup Calculations and Uncertainties

CASMO-3 was used for burnup calculations in the hot operating condition. CASMO-3 has been extensively benchmarked (Appendix A and Refs. 2 and 7) against critical experiments (including plutonium-bearing fuel). In addition to burnup calculations, CASMO-3 was used for evaluating the small reactivity increments (by differential calculations) associated with manufacturing tolerances.

Since there are no critical experiment data with spent fuel for determining the uncertainty in burnup-dependent reactivity calculations, an allowance for uncertainty in reactivity* was assigned based upon the assumption of 5% uncertainty in burnup. This is approximately equivalent to 5% of the total reactivity decrement. At the design basis burnups of 38 and 50 MWD/KgU, the uncertainties in burnup are ± 1.9 and ± 2.5 MWD/KgU respectively. To evaluate the reactivity consequences of the uncertainties in burnup, independent calculations were made with fuel of 36,100 and 47,500 MWD/MtU burnup in Regions 2 and 3, and the incremental change from the reference burnups assumed to represent the net uncertainties in reactivity. These calculations resulted in an incremental reactivity uncertainty of ± 0.0047 δk in Region 2 (isolation barrier at 50 MWD/KgU burnup) and ± 0.0019 for Region 3 (at 38 MWD/KgU burnup). In the racks, the fresh unburned fuel in Region 1 strongly dominate the reactivity which tends to minimize the reactivity consequences of uncertainties in burnup. The

---

*Only that portion of the uncertainty due to burnup. Other uncertainties are accounted for elsewhere.

allowance for uncertainty in burnup calculations is a conservative estimate, particularly in view of the substantial reactivity decrease with time as the spent fuel ages.

4.4.3 Effect of Axial Burnup Distribution

Initially, fuel loaded into the reactor will burn with a slightly skewed cosine power distribution. As burnup progresses, the burn distribution will tend to flatten, becoming more highly burned in the central regions than in the upper and lower ends, as may be seen in the curves compiled in Ref. 4. At high burnup, the more reactive fuel near the ends of the fuel assembly (less than average burnup) occurs in regions of lower reactivity worth due to neutron leakage. Consequently, it would be expected that over most of the burnup history, distributed burnup fuel assemblies would exhibit a slightly lower reactivity than that calculated for the average burnup. As burnup progresses, the distribution, to some extent, tends to be self-regulating as controlled by the axial power distribution, precluding the existence of large regions of significantly reduced burnup. Among others, Turner[5] has provided generic analytic results of the axial burnup effect based upon calculated and measured axial burnup distributions. These analyses confirm the minor and generally negative reactivity effect of the axially distributed burnup. The trends observed, however, suggest the possibility of a small positive reactivity effect at high burnup.

Calculations were made with KENO-5a in three dimensions, based upon the typical axial burnup distribution of spent fuel (that observed at the Surrey plant was taken as representative). In these calculations, the axial height of the burned fuel was divided into a number of axial zones (6-inch intervals near the more significant top of the fuel), each with an enrichment equivalent to the burnup

of that zone. These calculations resulted in an incremental reactivity increase of 0.0037 δk for the reference design case. Fuel of lower initial enrichments (and lower burnup) would have a smaller (or negative) reactivity effect as a result of the axial variation in burnup. These estimates are conservative since smaller axial increments in the calculations have been shown to result in lower incremental reactivities[5].

4.5 Criticality Analyses and Tolerances

4.5.1 Nominal Design

For the nominal storage cell design, the NITAWL-KENO-5a calculation resulted in a bias-corrected k_∞ of 0.9250 ± 0.0012 (95%/95%), which, when combined with all known uncertainties and the axial burnup effect, results in a k_∞ of 0.929 ± 0.011 or a maximum k_∞ of 0.940 with a 95% probability at the 95% confidence level[6].

For the interim loading pattern of checkerboarded fuel and empty cells in Region 3, calculations resulted in essentially the same reactivity as the reference design within the normal KENO-5a statistics (maximum k_∞ of 0.940, including all allowances and uncertainties, see Table 4.2).

4.5.2 Uncertainties Due to Manufacturing Tolerances

The uncertainties due to manufacturing tolerances are summarized in Table 4-5 and discussed below.

4.5.2.1 Boron Loading Tolerances

The Boral absorber panels used in the storage cells are nominally 0.101 inch thick, 7.50-inch wide and 144-inch long, with a nominal B-10 areal density of 0.0345 g/cm^2. The vendors manufacturing tolerance limit is ± 0.0045 g/cm^2 in B-10 content which assures that at any point, the minimum B-10 areal density will not be less than 0.030 g/cm^2. Differential KENO-5a calculations for the reference design with the minimum tolerance B-10 loading results in an incremental reactivity of + 0.00614 δk uncertainty.

4.5.2.2 Boral Width Tolerance

The reference storage cell design uses a Boral panel with an initial width of 7.50 ± 0.06 inches. For the maximum tolerance of 0.06 inch, the differential CASMO-3 calculated reactivity uncertainty is ± 0.0009 δk.

4.5.2.3 Tolerances in Cell Lattice Spacing

The manufacturing tolerance on the inner box dimension, which directly affects the storage cell lattice spacing between fuel assemblies, is ± 0.06 inches. This corresponds to an uncertainty in reactivity of ± 0.0015 δk determined by differential CASMO-3 calculations.

4.5.2.4 Stainless Steel Thickness Tolerances

The nominal stainless steel thickness is 0.075 ± 0.005 inch for the inner stainless steel box and 0.035 ± 0.003 inch for the Boral cover plate. The maximum positive reactivity effect of the expected stainless steel thickness tolerances was calculated (CASMO-3) to be + 0.0009 δk.

4.5.2.5 Fuel Enrichment and Density Tolerances

The design maximum enrichment is 4.95 ± 0.05 wt% U-235. Separate CASMO-3 burnup calculations were made for fuel of the maximum enrichment (5.00%) and for the maximum UO_2 density (10.50 g/cc). Reactivities in the storage cell were then calculated using the restart capability in CASMO-3 and equivalent enrichments determined for the reference fuel burnups of 38 and 50 MWD/KgU. The incremental reactivities between these calculations and the reference CASMO-3 cases, were conservatively taken as the

sensitivity to small enrichment and density variations. For the tolerance on U-235 enrichment, the uncertainty in k_∞ is ± 0.0034 δk and for fuel density is ± 0.0035.

4.5.3 Water-gap Spacing Between Modules

The water-gap between modules constitute a neutron flux-trap for the outer (peripheral) row of storage cells. Calculations with KENO-5a were made for various water-gap spacings (Figure 4.7). From these data, it was determined that the incremental reactivity consequence (uncertainty) for the minimum water-gap tolerance of ± 1/4 inch is ± 0.0045 δk. The racks are constructed with the base plate extending beyond the edge of the cells. This assures that a minimum spacing of 1.75 inch between storage modules is maintained under all credible conditions.

4.5.4 Eccentric Fuel Positioning

The fuel assembly is assumed to be normally located in the center of the storage rack cell. Infinite array calculations were made using KENO-5a for a single cell with the fuel assemblies centered and with the assemblies assumed to be in the corner of the storage rack cell (four-assembly cluster at closest approach). These calculations indicated that the reactivity uncertainty could be as much as ± 0.0019 δk.

4.6 Abnormal and Accident Conditions

4.6.1 Temperature and Water Density Effects

The moderator temperature coefficient of reactivity is negative; a moderator temperature of 20°C (68°F) was assumed for the reference designs, which assures that the true reactivity will always be lower over the expected range of water temperatures. Temperature

effects on reactivity have been calculated and the results are shown in Table 4.6. With soluble poison present, the temperature coefficients of reactivity would differ from those inferred from the data in Table 4.6. However, the reactivities would also be substantially lower at all temperatures with soluble boron present, and the data in Table 4.6 is pertinent to the higher-reactivity unborated case.

4.6.2 Dropped Fuel Assembly

For a drop on top of the rack, the fuel assembly will come to rest horizontally on top of the rack with a minimum separation distance from the fuel in the rack of more than 12 inches, including the potential deformation under seismic or accident conditions. At this separation distance, the effect on reactivity is insignificant (<0.0001 δk). Furthermore, soluble boron in the pool water would substantially reduce the reactivity and assure that the true reactivity is always less than the limiting value for any conceivable dropped fuel accident.

4.6.3 Lateral Rack Movement

Lateral motion of the rack modules under seismic conditions could potentially alter the spacing between rack modules. However, the maximum rack movement has been determined to be less than the tolerance on the water-gap spacing. Furthermore, soluble poison would assure that a reactivity less than the design limitation is maintained under all accident or abnormal conditions.

4.6.4 Abnormal Location of a Fuel Assembly

The abnormal location of a fresh unirradiated fuel assembly of 4.95 wt% enrichment could, in the absence of soluble poison, result in exceeding the design reactivity limitation (k_∞ of 0.95). This could occur if a fresh fuel assembly of the highest permissible enrichment were to be either positioned outside and adjacent to a storage rack module or inadvertently loaded into either a Region 2 or Region 3 storage cell. Calculations (KENO-5a) showed that the highest reactivity, including uncertainties, for the worst case postulated accident condition (fresh fuel assembly in Region 2) would exceed the limit on reactivity in the absence of soluble boron. Soluble boron in the spent fuel pool water, for which credit is permitted under these accident conditions, would assure that the reactivity is maintained substantially less than the design limitation. It is estimated that a soluble poison concentration of 550 ppm boron would be sufficient to maintain k_∞ at the reference design value of 0.940 under the maximum postulated accident condition. Approximately 450 ppm boron would be required to limit the maximum reactivity to a k_{eff} of 0.95.

4.7 Existing Spent Fuel

As of May 1990, there were 1596 spent fuel assemblies in storage at the Donald C. Cook plant, including those now in the reactor and their projected burnups at discharge. Figure 4.8 superimposes the enrichment-burnup combination of these fuel assemblies on the curves defining the acceptable burnup domains. As may be seen in this figure, most of the spent fuel now in storage falls well into the acceptable domain for the barrier fuel (Region 2). The number of fuel assemblies meeting the enrichment-burnup criteria for storage in Region 2 is 1390 which will nearly fill the 1447 Region 2 storage locations. Twelve fuel assemblies (discharged

prematurely for various reasons) will need to be kept in a Region 1 storage location, and the remaining 194 assemblies may be stored in Region 3 locations. Future discharge batches may reasonably be expected to have a preponderance of highly burned fuel capable of being stored in Region 2 (or in Region 3 once Region 2 is filled). An appreciable number of spent fuel assemblies have enrichment-burnup combinations well in excess of the design basis and this provides further conservatism in the criticality safety of the spent fuel storage rack design.

4.8 References

1. Green, Lucious, Petrie, Ford, White, and Wright, "PSR-63-/NITAWL-1 (code package) NITAWL Modular Code System For Generating Coupled Multigroup Neutron-Gamma Libraries from ENDF/B", ORNL-TM-3706, Oak Ridge National Laboratory, November 1975.

2. R.M. Westfall et. al., "SCALE: A Modular System for Performing Standardized Computer Analysis for Licensing Evaluation", NUREG/CR-0200, 1979. Volume 2, Section F11, "KENO-5a An Improved Monte Carlo Criticality Program with Supergrouping".

3. A. Ahlin, M. Edenius, and H. Haggblom, "CASMO - A Fuel Assembly Burnup Program", AE-RF-76-4158, Studsvik report.

   A. Ahlin and M. Edenius, "CASMO - A Fast Transport Theory Depletion Code for LWR Analysis", ANS Transactions, Vol. 26, p. 604, 1977.

   "CASMO-3 A Fuel Assembly Burnup Program, Users Manual", Studsvik/NFA-87/7, Studsvik Energitechnik AB, November 1986

4. H. Richings, Some Notes on PWR (W) Power Distribution Probabilities for LOCA Probabilistic Analyses, NRC Memorandum to P.S. Check, dated July 5, 1977.

5. S. E. Turner, "Uncertainty Analysis - Burnup Distributions", presented at the DOE/SANDIA Technical Meeting on Fuel Burnup Credit, Special Session, ANS/ENS Conference, Washington, D.C.,November 2, 1988

6. M.G. Natrella, Experimental Statistics National Bureau of Standards, Handbook 91, August 1963

Table 4.1

SUMMARY OF CRITICALITY SAFETY ANALYSES
NORMAL STORAGE CONFIGURATION

Design Basis Burnups at 4.95% ± 0.05% initial enrichment		0 in Region 1 50 in Region 2 38 in Region 3
Temperature for analysis		20°C (68°F)
Reference k_∞ (KENO-5a)		0.9160
Calculational bias, δk[1]		0.0090
Uncertainties		
Bias statistics (95%/95%)	± 0.0021	
KENO-5a statistics (95%/95%)	± 0.0013	
Manufacturing Tolerances	± 0.0064	
Water-gap	± 0.0045	
Fuel enrichment	± 0.0034	
Fuel density	± 0.0035	
Burnup (38 MWD/KgU)	± 0.0019	
Burnup (50 MWD/KgU)	± 0.0047	
Eccentricity in position	± 0.0019	
Statistical combination of uncertainties[2]	± 0.0110	
Axial Burnup Effect		0.0037
Total		0.9287 ± 0.0110
Maximum Reactivity (k_∞)		0.940

(1) See Appendix A
(2) Square root of sum of squares.

Table 4.2

SUMMARY OF CRITICALITY SAFETY ANALYSES
INTERIM CHECKERBOARD LOADING

Design Basis burnups at 4.95% ± 0.05% initial enrichment		0 in Region 1 50 in Region 2 Region 3 -CHECKERBOARD (FRESH FUEL AND EMPTY)
Temperature for analysis		20°C (68°F)
Reference k_∞ (KENO-5a)		0.9168
Calculational bias, δk[1]		0.0090
Uncertainties (Assumed same as the reference case)		
Bias statistics (95%/95%)	± 0.0021	
KENO-5a statistics (95%/95%)	± 0.0012	
Manufacturing Tolerances	± 0.0064	
Water-gap	± 0.0045	
Fuel enrichment	± 0.0034	
Fuel density	± 0.0035	
Burnup (38 MWD/KgU)	NA	
Burnup (50 MWD/KgU)	± 0.0047	
Eccentricity	± 0.0019	
Statistical combination of uncertainties[2]	± 0.0108	
Axial Burnup Effect		0.0037
Total		0.9295 ± 0.0108
Maximum Reactivity (k_∞)		0.940

(1) See Appendix A
(2) Square root of sum of squares.

Table 4.3

REACTIVITY EFFECTS OF ABNORMAL AND ACCIDENT CONDITIONS

Accident/Abnormal Conditions	Reactivity Effect
Temperature increase (above 68°F)	Negative (Table 4.6)
Void (boiling)	Negative (Table 4.6)
Assembly dropped on top of rack	Negligible (<0.0001 δk)
Lateral rack module movement	(Included in Tolerances)
Misplacement of a fuel assembly	Positive (0.065 Max δk) (controlled by soluble poison)

Table 4.4

DESIGN BASIS FUEL ASSEMBLY SPECIFICATIONS

FUEL ROD DATA	
Outside diameter, in.	0.422
Cladding thickness, in.	0.0241
Cladding inside diameter, in.	0.3734
Cladding material	Zr-4
Pellet density, % T.D.	95.0
Stack density, g UO_2/cc	10.29 ± 0.20
Pellet diameter, in.	0.3659
Maximum enrichment, wt % U-235	4.95 ± 0.05
FUEL ASSEMBLY DATA	
Fuel rod array	15 x 15
Number of fuel rods	204
Fuel rod pitch, in.	0.563
Number of control rod guide and instrument thimbles	21
Thimble O.D., in. (nominal)	0.533
Thimble I.D., in. (nominal)	0.499

Table 4.5

Reactivity Effects of Manufacturing Tolerances

Tolerance	Incremental Reactivity, δk
Boron-10 loading (± 0.0045 g/cm^2)	± 0.0061
Boral Width (± 1/16 inch)	± 0.0009
Lattice spacing (± 0.04 inch)	± 0.0015
Stainless Thickness (± 0.005 incn)	± 0.0009
Total (statistical sum)	± 0.0064

Table 4.6

EFFECT OF TEMPERATURE AND VOID ON CALCULATED REACTIVITY OF STORAGE RACK

Case	Incremental Reactivity Change, δk	
	Region 1	Region 2
20°C (68°F)	Reference	Reference
40°C (104°F)	-0.003	-0.002
66°C (150°F)	-0.009	-0.005
90°C (194°F)	-0.013	-0.010
122°C (252°F)	-0.024	-0.015
122°C (252°F) + 20% void	-0.071	-0.061

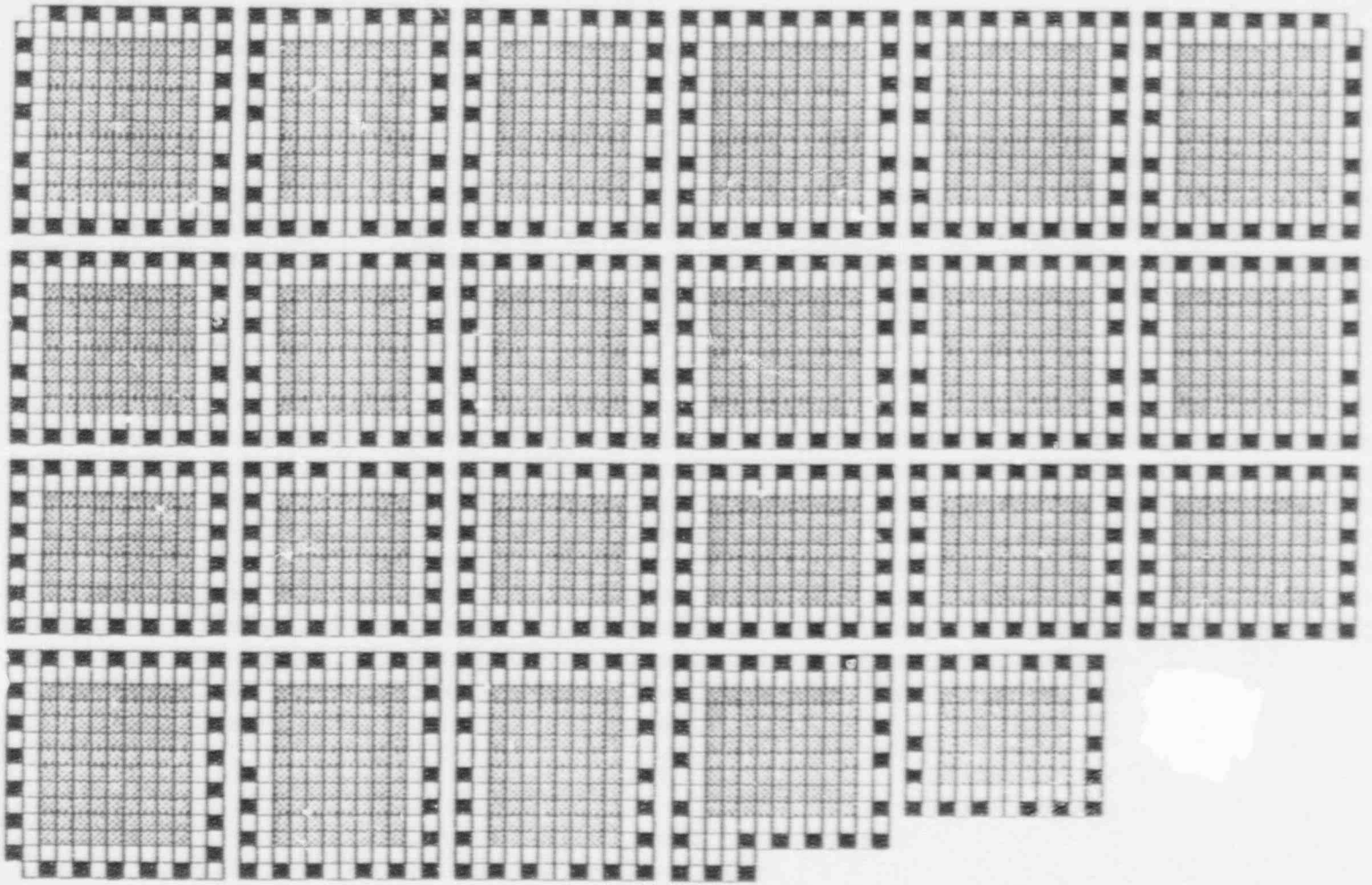

Fig. 4-1 NORMAL STORAGE PATTERN (MIXED THREE ZONE)

504 REGION 1 CELLS 1415 REGION 2 CELLS 1694 REGION 3 CELLS

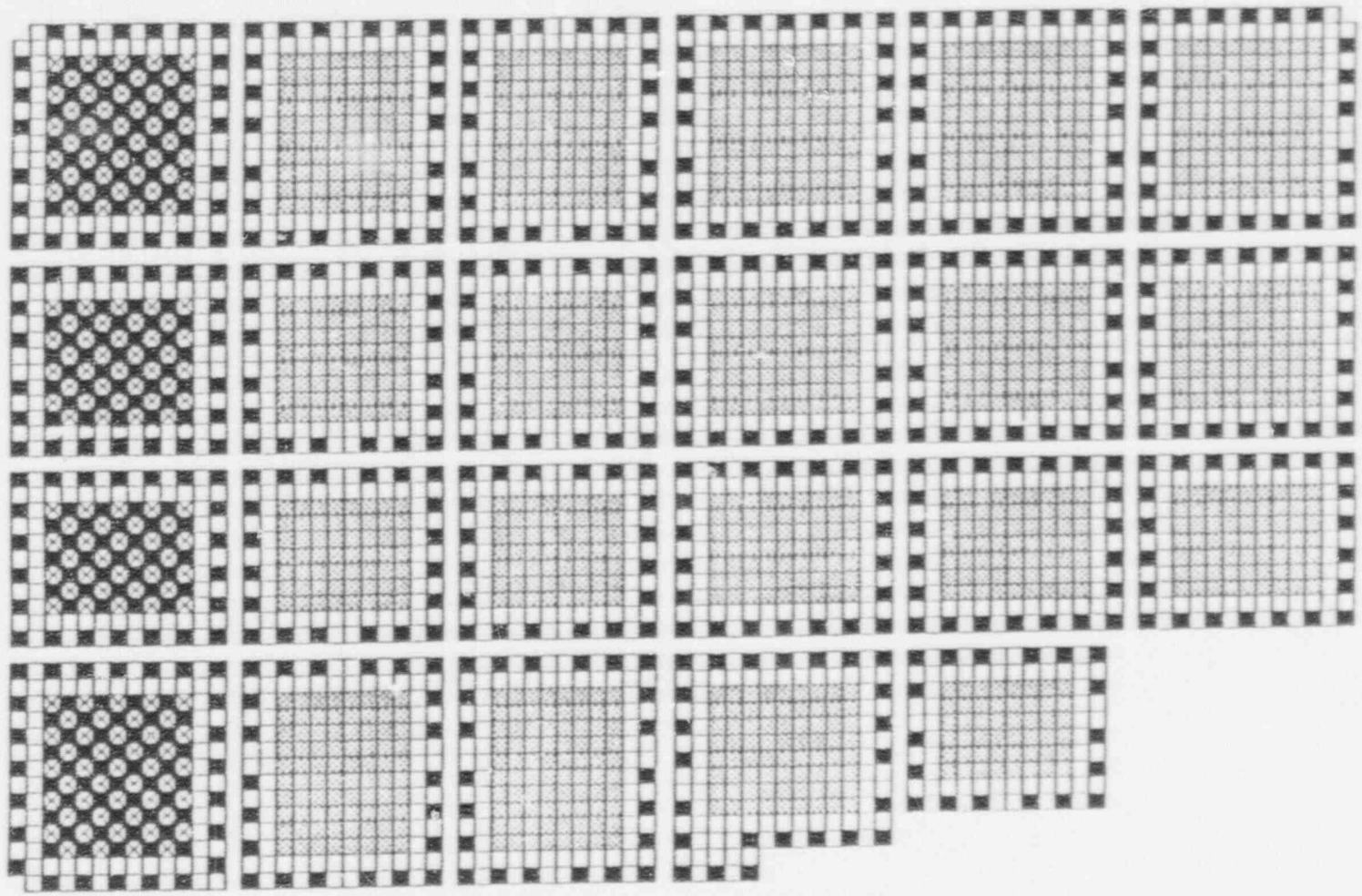

Fig. 4-2 INTERIM STORAGE PATTERN (CHECKERBOARD)

158 EMPTY LOCATIONS 661 REGION 1 CELLS 1415 REGION 2 CELLS 1379 REGION 3 CELLS

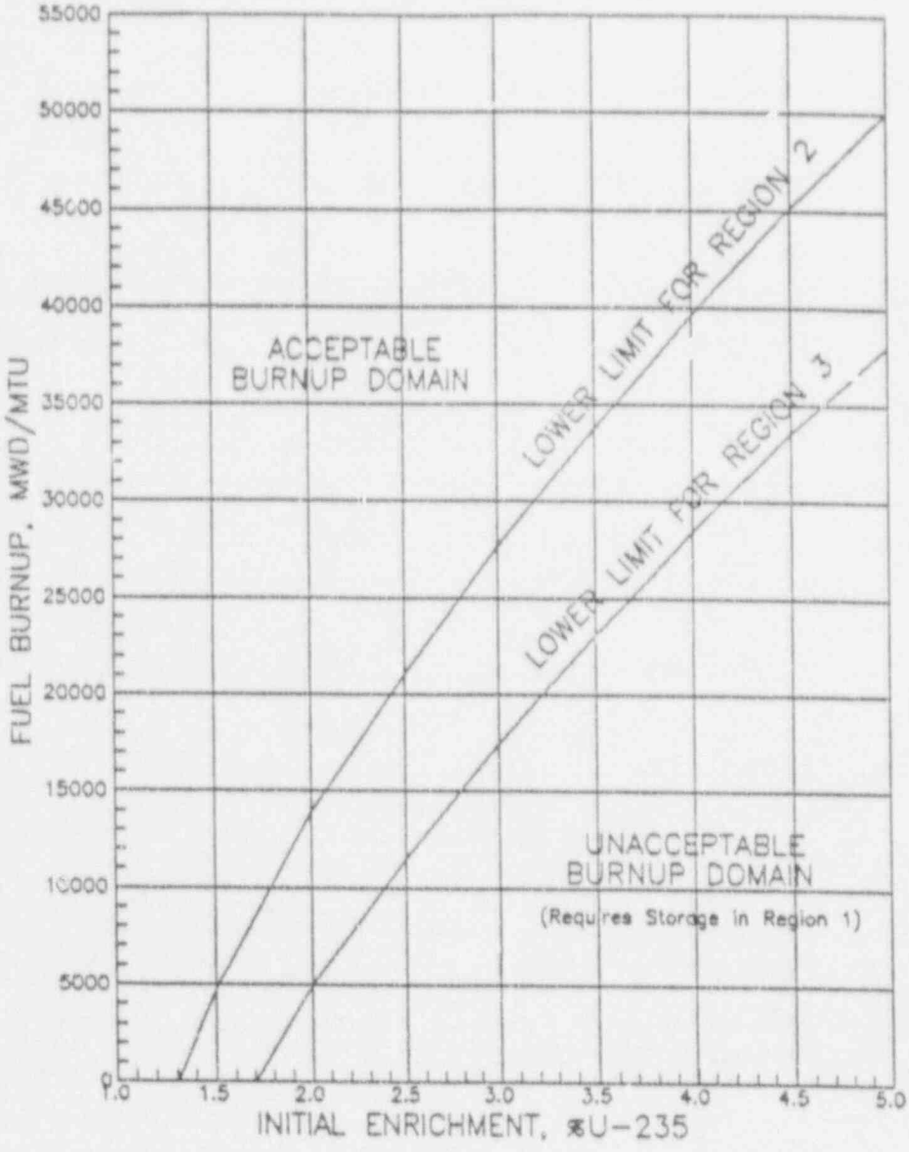

Fig. 4-3 ACCEPTABLE BURNUP DOMAIN IN REGIONS 2 & 3

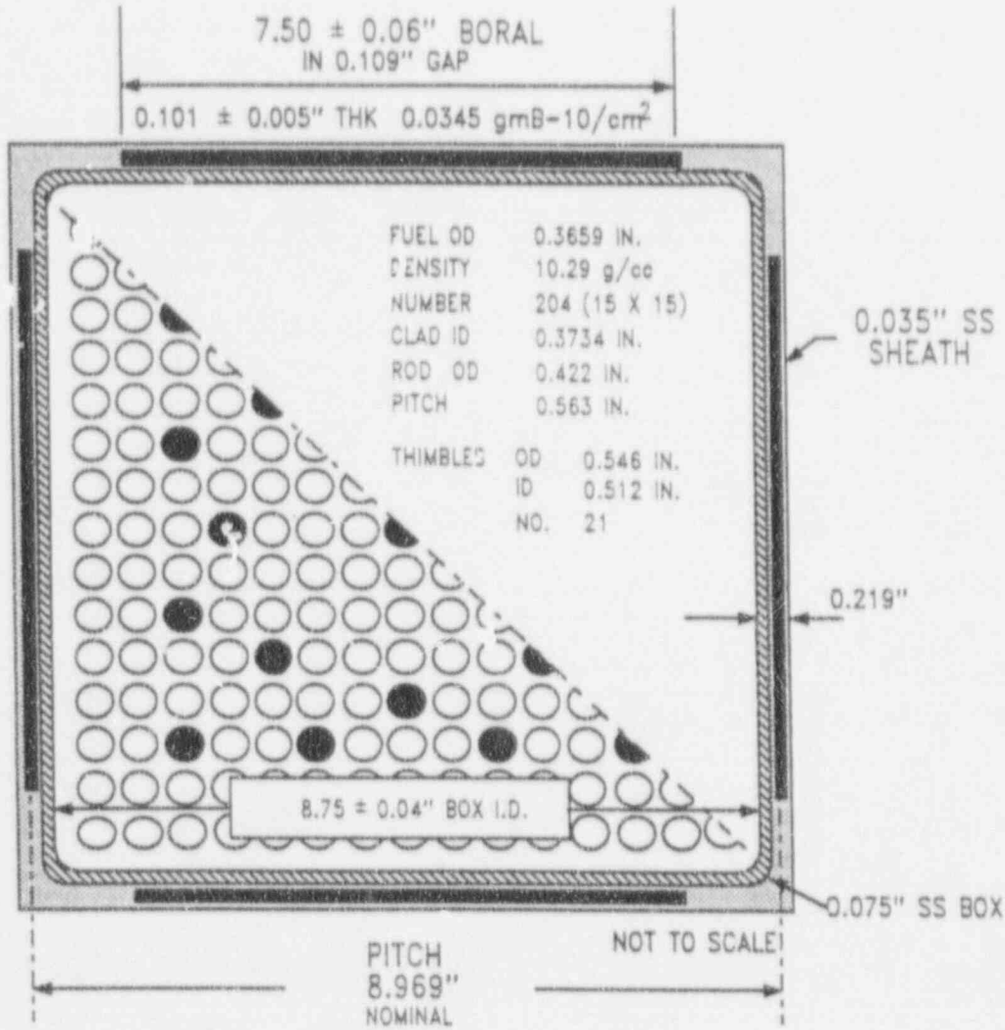

FIG. 4-4 FUEL STORAGE CELL CROSS SECTION

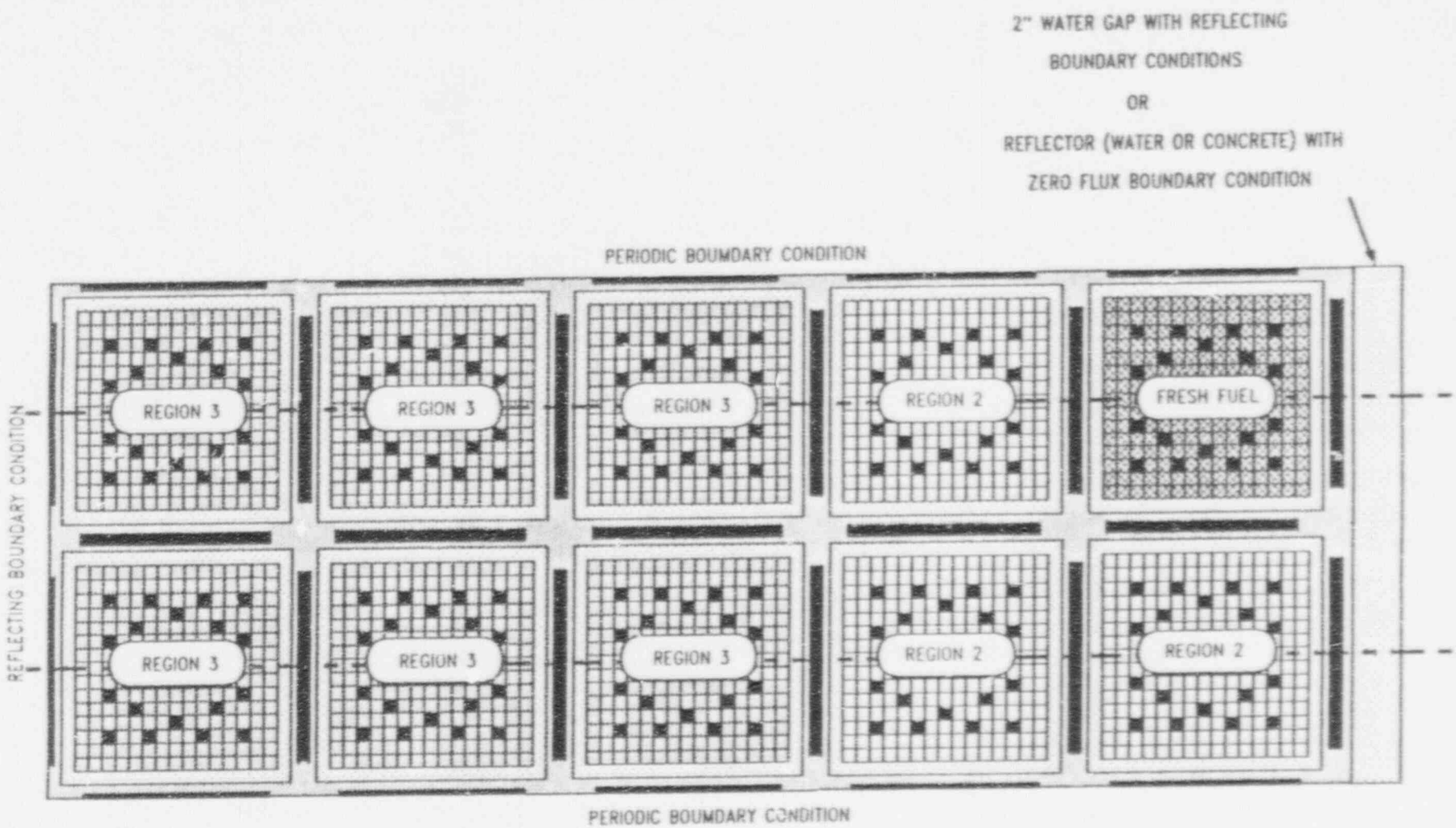

FIG. 4-5 KENO CALCULATIONAL MODEL

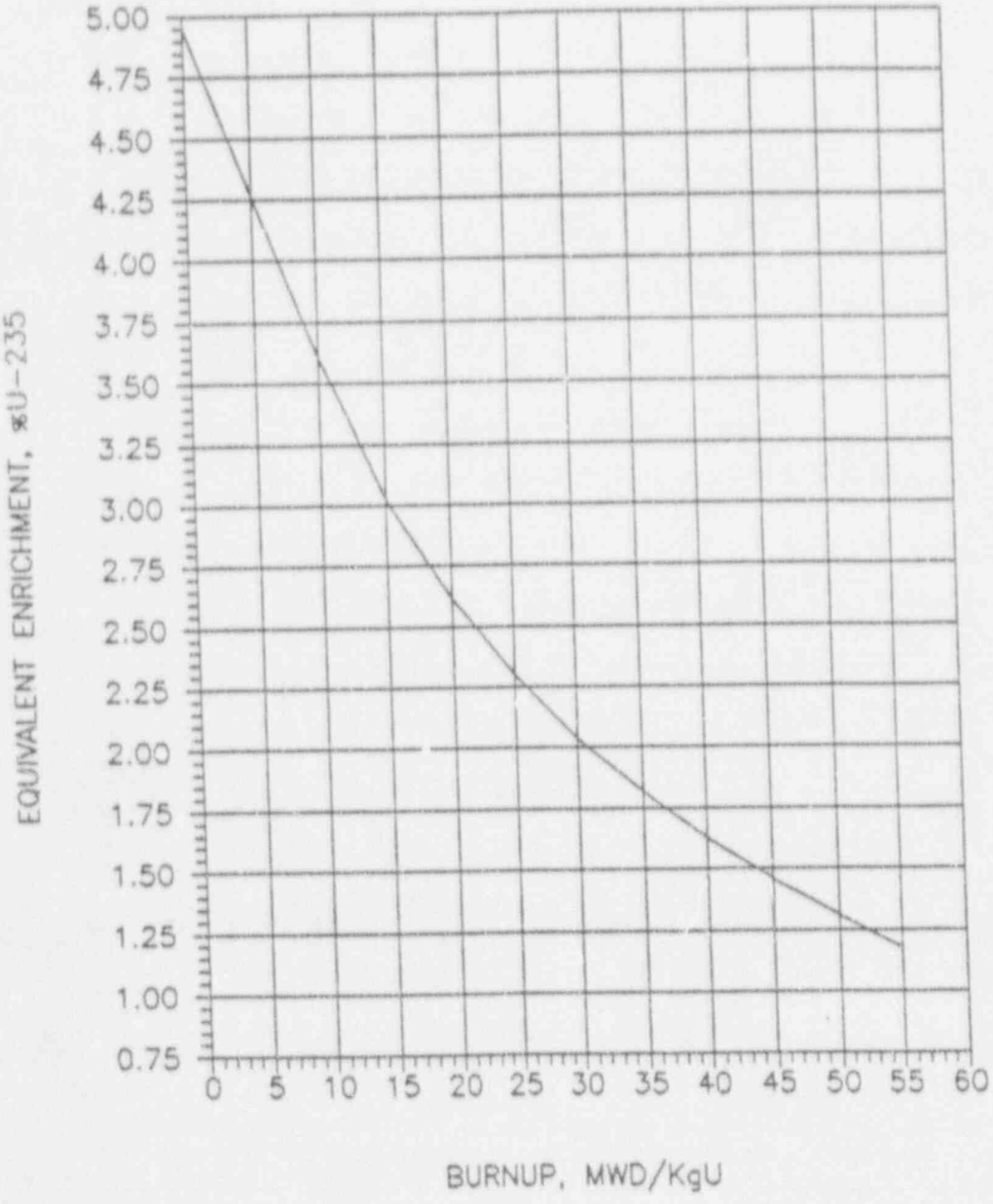

Fig. 4-6 EQUIVALENT ENRICHMENT FOR SPENT FUEL AT VARIOUS BURNUPS FOR INITIAL ENRICHMENT OF 4.95%

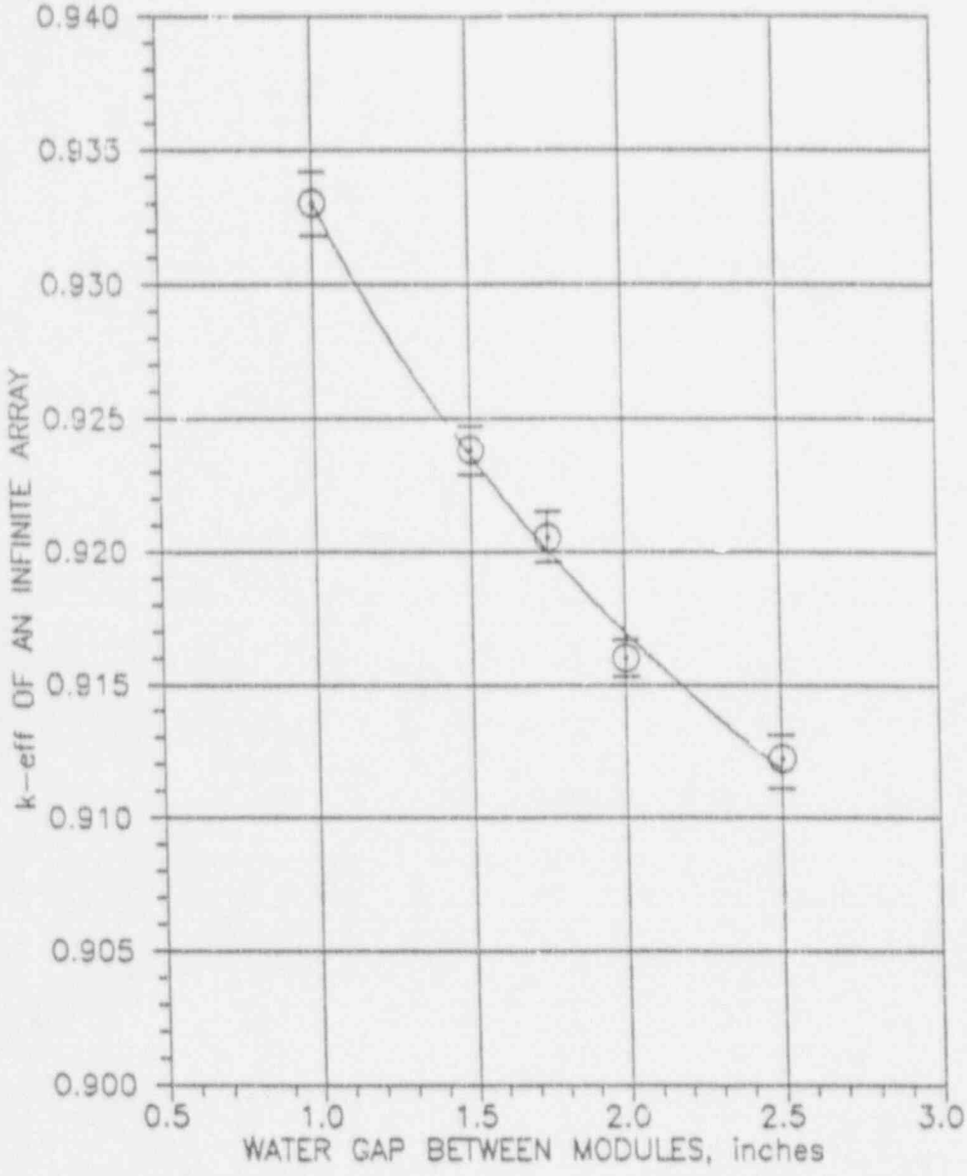

Fig. 4-7 EFFECT OF WATER-GAP SPACING BETWEEN MODULES ON SYSTEM REACTIVITY

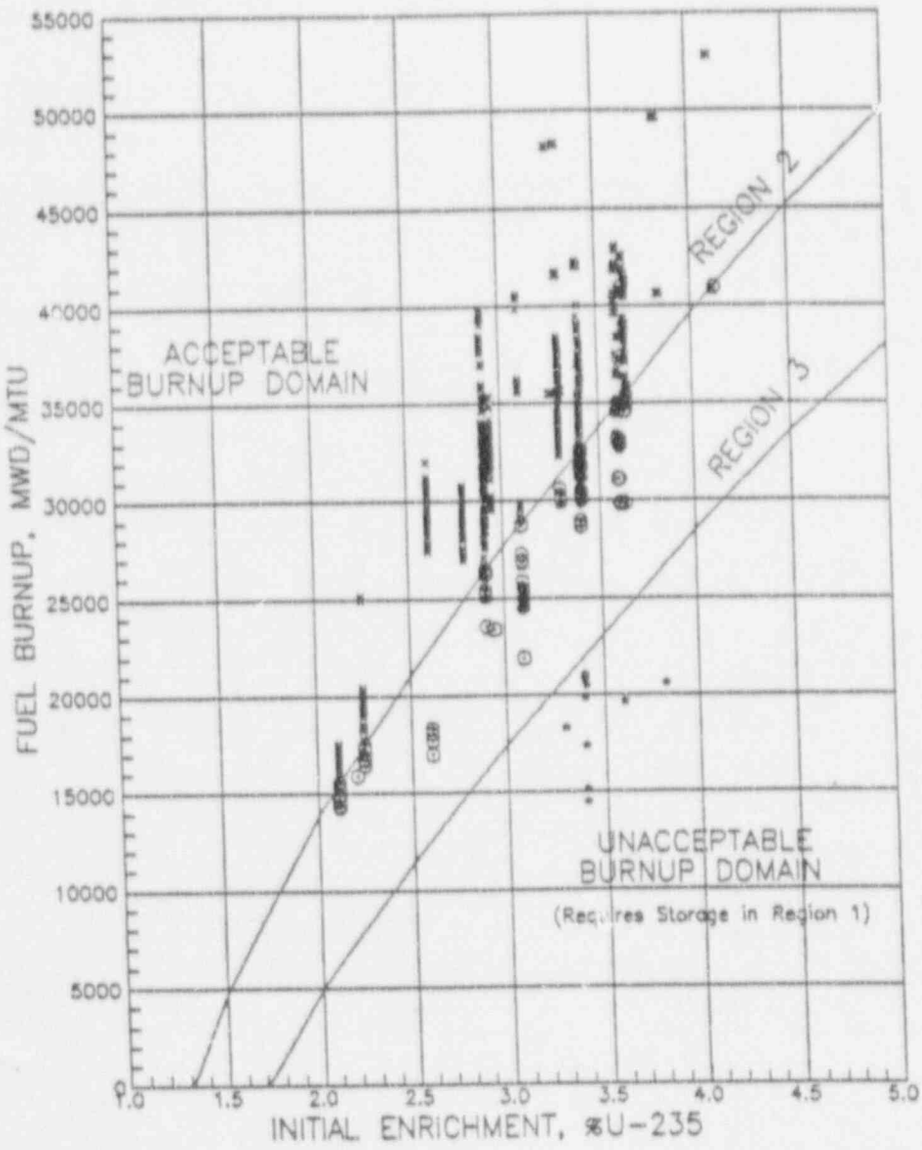

Fig. 4-8 ACCEPTABLE BURNUP DOMAIN IN REGIONS 2 & 3 SHOWING EXISTING SPENT FUEL ASSEMBLIES

APPENDIX A

BENCHMARK CALCULATIONS

by

Stanley E. Turner, PhD, PE

HOLTEC INTERNATIONAL

January 1991

1.0 INTRODUCTION AND SUMMARY

The objective of this benchmarking study is to verify both the NITAWL-KENO-5a[1,2] methodology with the 27-group SCALE cross-section library and the CASMO-3 code[3] for use in criticality safety calculations of high density spent fuel storage racks. Both calculational methods are based upon transport theory and have been benchmarked against critical experiments that simulate typical spent fuel storage rack designs as realistically as possible. Results of these benchmark calculations with both methodologies are consistent with corresponding calculations reported in the literature.

Results of the benchmark calculations show that the 27-group (SCALE) NITAWL-KENO-5a calculations consistently underpredict the critical eigenvalue by 0.0090 ± 0.0021 δk (with a 95% probability at a 95% confidence level) for critical experiments[4] that are as representative as possible of realistic spent fuel storage rack configurations and poison worths.

Extensive benchmarking calculations of critical experiments with CASMO-3 have also been reported[5], giving a mean k_{eff} of 1.0004 ± 0.0011 for 37 cases. With a K-factor of 2.14[6] for 95% probability at a 95% confidence level, and conservatively neglecting the small overprediction, the CASMO-3 bias then becomes 0.0000 ± 0.0024. CASMO-3 and NITAWL-KENO-5a intercomparison calculations of infinite arrays of poisoned cell configurations (representative of typical spent fuel storage rack designs) show very good agreement, confirming that 0.0000 ± 0.0024 is a reasonable bias and uncertainty for CASMO-3 calculations. Reference 5 also documents good agreement of heavy nuclide concentrations for the Yankee core isotopics, agreeing with the measured values within experimental error.

The benchmark calculations reported here confirm that either the 27-group (SCALE) NITAWL-KENO or CASMO-3 calculations are acceptable for criticality analysis of high-density spent fuel storage racks. Reference calculations for the rack designs should be performed with both code packages to provide independent verification.

2.0 NITAWL-KENO 5a BENCHMARK CALCULATIONS

Analysis of a series of Babcock & Wilcox critical experiments[4], including some with absorber panels typical of a poisoned spent fuel rack, is summarized in Table 1, as calculated with NITAWL-KENO-5a using the 27-group SCALE cross-section library and the Nordheim resonance integral treatment in NITAWL. Dancoff factors for input to NITAWL were calculated with the Oak Ridge SUPERDAN routine (from the SCALE[2] system of codes). The mean for these calculations is 0.9910 ± 0.0033 (1 σ standard deviation of the population). With a one-sided tolerance factor corresponding to 95% probability at a 95% confidence level[6], the calculational bias is + 0.0090 with an uncertainty of ± 0.0021 for the sixteen critical experiments analyzed.

Similar calculational deviations have been reported by ORNL[7] for some 54 critical experiments (mostly clean critical without strong absorbers), obtaining a mean bias of 0.0100 ± 0.0013 (95%/95%). These published results are in good agreement with the results obtained in the present analysis and lend further credence to the validity of the 27-group NITAWL-KENO-5a calculational model for use in criticality analysis of high density spent fuel storage racks. No trends in k_{eff} with intra-assembly water gap, with absorber panel reactivity worth, with enrichment or with poison concentration were identified.

Additional benchmarking calculations were also made for a series of French critical experiments[9] at 4.75% enrichment and for several of the BNWL criticals with 4.26% enriched fuel. Analysis of the French criticals (Table 2) showed a tendency to overpredict the reactivity, a result also obtained by ORNL[10]. The calculated k_{eff} values showed a trend toward higher values with decreasing core size. In the absence of a significant enrichment effect (see Section 3 below), this trend and the overprediction is attributed to a small inadequacy in NITAWL-KENO-5a in calculating neutron leakage from very small assemblies.

Similar overprediction was also observed for the BNWL series of critical experiments[11], which also are small assemblies (although significantly larger than the French criticals). In this case (Table 2), the overprediction appears to be small, giving a mean k_{eff} of 0.9990 ± 0.0037 (1 σ population standard deviation). Because of the small size of the BNWL critical experiments and the absence of any significant enrichment effect, the overprediction is also attributed to the failure of NITAWL-KENO-5a to adequately treat neutron leakage in very small assemblies.

Since the analysis of high-density spent fuel storage racks generally does not entail neutron leakage, the observed inadequacy of NITAWL-KENO-5a is not significant. Furthermore, omitting results of the French and BNWL critical experiment analyses from the determination of bias is conservative since any leakage that might enter into the analysis would tend to result in overprediction of the reactivity.

3. CASMO-3 BENCHMARK CALCULATIONS

The CASMO-3 code is a multigroup transport theory code utilizing transmission probabilities to accomplish two-dimensional calculations of reactivity and depletion for BWR and PWR fuel assemblies. As such, CASMO-3 is well-suited to the criticality analysis of spent fuel storage racks, since general practice is to treat the racks as an infinite medium of storage cells, neglecting leakage effects.

CASMO-3 is a modification of the CASMO-2E code and has been extensively benchmarked against both mixed oxide and hot and cold critical experiments by Studsvik Energiteknik[5]. Reported analyses[5] of 37 critical experiments indicate a mean k_{eff} of 1.0004 ± 0.0011 (1σ). To independently confirm the validity of CASMO-3 (and to investigate any effect of enrichment), a series of calculations were made with CASMO-3 and with NITAWL-KENO-5a on identical poisoned storage cells representative of high-density spent fuel storage racks. Results of these intercomparison calculations* (shown in Table 3) are within the normal statistical variation of KENO calculations and confirm the bias of 0.0000 ± 0.0024 (95%/95%) for CASMO-3.

Since two independent methods of analysis would not be expected to have the same error function with enrichment, results of the intercomparison analyses (Table 3) indicate that there is no significant effect of fuel enrichment over the range of enrichments involved in power reactor fuel. Furthermore, neglecting the French and BNWL critical benchmarking in the determination of bias is a conservative approach.

---

*Intercomparison between analytical methods is a technique endorsed by Reg. Guide 5.14, "Validation of Calculational Methods for Nuclear Criticality Safety".

REFERENCES TO APPENDIX A

1. Green, Lucious, Petrie, Ford, White, and Wright, "PSR-63-/NITAWL-1 (code package) NITAWL Modular Code System For Generating Coupled Multigroup Neutron-GAmma Libraries from ENDF/B", ORNL-TM-3706, Oak Ridge National Laboratory, November 1975.

2. R.M. Westfall et. al., "SCALE: A Modular System for Performing Standardized Computer Analysis for Licensing Evaluation", NUREG/CR-0200, 1979.

3. A. Ahlin, M. Edenius, and H. Haggblom, "CASMO - A Fuel Assembly Burnup Program", AE-RF-76-4158, Studsvik report.

   A. Ahlin and M. Edenius, "CASMO - A Fast Transport Theory Depletion Code for LWR Analysis", ANS Transactions, Vol. 26, p. 604, 1977.

   "CASMO-3 A Fuel Assembly Burnup Program, Users Manual", Studsvik/NFA-87/7, Studsvik Energitechnik AB, November 1986

4. M.N. Baldwin et al., "Critical Experiments Supporting Close Proximity Water Storage of Power Reactor Fuel", BAW-1484-7, The Babcock & Wilcox Co., July 1979.

5. M. Edenius and A. Ahlin, "CASMO-3: New Features, Benchmarking, and Advanced Applications", Nuclear Science and Engineering, 100, 342-351, (1988)

6. M.G. Natrella, Experimental Statistics, National Bureau of Standards, Handbook 91, August 1963.

7. R.W. Westfall and J. H. Knight, "SCALE System Cross-section Validation with Shipping-cask Critical Experiments", ANS Transactions, Vol. 33, p. 368, November 1979

8. S.E. Turner and M.K. Gurley, "Evaluation of NITAWL-KENO Benchmark Calculations for High Density Spent Fuel Storage Racks", Nuclear Science and Engineering, 80(2):230-237, February 1982.

9. J.C. Manaranche, et. al., "Dissolution and Storage Experiment with 4.75% U-235 Enriched UO_2 Rods", Nuclear Technology, Vol. 50, pp 148, September 1980

10. S.R. Bierman, et. al., "Critical Separation between Subcritical Clusters of 4.29 Wt. % ^{235}U Enriched UO_2 Rods in Water with Fixed Neutron Poisons", Batelle Pacific Northwest Laboratories, NUREG/CR/0073, May 1978 (with August 1979 errata).

11. A.M. Hathout, et. al., "Validation of Three Cross-section Libraries Used with the SCALE System for Criticality Analysis", Oak Ridge National Laboratory, NUREG/CR-1917, 1981.

Table 1

RESULTS OF 27-GROUP (SCALE) NITAWL-KENO-5a CALCULATIONS OF B&W CRITICAL EXPERIMENTS

Experiment Number	Calculated k_{eff}	σ
I	0.9932	± 0.0016
II	0.9915	± 0.0015
III	0.9916	± 0.0013
IX	0.9918	± 0.0014
X	0.9923	± 0.0015
XI	0.9919	± 0.0014
XII	0.9961	± 0.0015
XIII	0.9960	± 0.0015
XIV	0.9817	± 0.0015
XV	0.9843	± 0.0014
XVI	0.9912	± 0.0015
XVII	0.9866	± 0.0013
XVIII	0.9904	± 0.0014
XIX	0.9861	± 0.0013
XX	0.9934	± 0.0013
XXI	0.9874	± 0.0014
Mean	0.9910	± 0.0014[1]
Bias	0.0090	± 0.0003[2]
Bias (95%/95%)	0.0090	± 0.0021

(1) Calculated from individual standard deviations.
(2) Calculated from k_{eff} values and used as reference.

Table 2

RESULTS OF 27-GROUP (SCALE) NITAWL-KENO-5a CALCULATIONS OF FRENCH and BNWL CRITICAL EXPERIMENTS

French Experiments		
Separation Distance, cm	Critical Height, cm	Calculated k_{eff}
0	23.8	1.0231 ± 0.0036
2.5	24.48	1.0252 ± 0.0043
5.0	31.47	1.0073 ± 0.0013
10.0	64.34	0.9944 ± 0.0014

BNWL Experiments		
Case	Expt. No.	Calculated k_{eff}
No Absorber	004/032	0.9964 ± 0.0034
SS Plates (1.05 B)	009	0.9988 ± 0.0038
SS Plates (1.62 B)	011	1.0032 ± 0.0033
SS Plates (1.62 B)	012	0.9986 ± 0.0036
SS Plates	013	0.9980 ± 0.0038
SS Plates	014	0.9936 ± 0.0036
Zr Plates	030	1.0044 ± 0.0035
Mean		0.9990 ± 0.0037

Table 3

RESULTS OF CASMO-3 AND NITAWL-KENO-5a
BENCHMARK (INTERCOMPARISON) CALCULATIONS

Enrichment[1] Wt. % U-235	NITAWL-KENO-5a[2] k_∞[1]	CASMO-3	$\lvert\delta k\rvert$
2.5	0.8385 ± 0.0016	0.8379	0.0006
3.0	0.8808 ± 0.0016	0.8776	0.0032
3.5	0.9074 ± 0.0016	0.9090	0.0016
4.0	0.9311 ± 0.0016	0.9346	0.0035
4.5	0.9546 ± 0.0018	0.9559	0.0013
5.0	0.9743 ± 0.0018	0.9741	0.0002
		Mean	0.0017

(1) Infinite array of assemblies typical of high-density spent fuel storage racks.

(2) k_∞ from NITAWL-KENO-5a corrected for bias of 0.0090 δk.

5.0 THERMAL-HYDRAULIC CONSIDERATIONS

5.1 Introduction

A primary objective in the design of the high density spent fuel storage racks for the Donald C. Cook spent fuel pool is to ensure adequate cooling of the fuel assembly cladding. In the following section a brief synopsis of the design basis, the method of analysis, and the numerical results is provided.

Similar methods of thermal-hydraulic analysis have been used in previous licensing efforts on high density spent fuel racks for Fermi 2 (Docket 50-341), Quad Cities 1 and 2 (Dockets 50-254 and 50-265), Rancho Seco (Docket 50-312), Grand Gulf Unit 1 (Docket 50-416), Oyster Creek (Docket 50-219), Virgil C. Summer (Docket 50-395), Diablo Canyon 1 and 2 (Docket Nos. 50-275 and 50-323), Byron Units 1 and 2 (Docket 50-454, 455), St. Lucie Unit One (Docket 50-335), Millstone Point I (50-245), Vogtle Unit 2 (50-425), Kuosheng Units 1 & 2 (Taiwan Power Company), Ulchin Unit 2 (Korea Electric Power Company), J.A. FitzPatrick (New York Power Authority) and TMI Unit 1 (GPU Nuclear).

The analyses to be carried out for the thermal-hydraulic qualification of the rack array may be broken down into the following categories:

(i) Pool decay heat evaluation and pool bulk temperature variation with time.

(ii) Determination of the maximum pool local temperature at the instant when the bulk temperature reaches its maximum value.

(iii) Evaluation of the maximum fuel cladding temperature to establish that bulk nucleate boiling at any location resulting in two phase conditions environment around the fuel does not occur.

(iv) Evaluation of the time-to-boil if all heat rejection paths through the cooling and cleanup are lost.

(v) Compute the effect of a blocked fuel cell opening on the local water and maximum cladding temperature.

The following sections present a synopsis of the methods employed to perform such analyses and a final summary of the results.

5.2 Spent Fuel Cooling System Description

The principal functions of the Spent Fuel Cooling System are the removal of decay heat from the spent fuel stored in the pool it serves and maintaining the clarity of, and a low activity level in, the water of the pool. Cleanup of pool water is accomplished by diverting part of the flow, maintained for removal of decay heat, through filters and/or demineralizers as described in Section 9.4 of UFSAR.

5.2.1 System Functions

The Spent Fuel Pool Cooling System is designed to remove from the spent fuel pool the heat generated by stored spent fuel elements. The system serves the spent fuel pool which is shared between the two units.

The system design incorporates two separate cooling trains. System piping is arranged so that failure of any pipeline does not drain the spent fuel pool below the top of the stored fuel elements.

5.2.2 System Description

Each of the two cooling loops in the Spent Fuel Pool Cooling System consists of a pump, heat exchanger, strainer, piping, associated valves and instrumentation. The pump draws water from the pool, circulates it through the heat exchanger and returns it to the pool. Component cooling water cools the heat exchanger.

The clarity and purity of the spent fuel pool water is maintained by passing approximately 100 gpm of the cooling flow through a filter and demineralizer. Skimmers are provided to prevent dust and debris from accumulating on the surface of the water.

The refueling water purification pump and filter can be used separately or in conjunction with the spent fuel pool demineralizer to regain refueling water clarity after a crud burst in either unit. This can prevent loss of time during refueling due to poor visibility. The system is also used to maintain water quality in the Refueling Water Storage Tanks of both units.

The spent fuel pool filter/demineralizer is downstream of the spent fuel pool cooler. As a result, the pool purification components are subjected to water temperatures which correspond to the cooler outlets (less than 140°F). All elements of the purification system, including the resins, are qualified for 200°F design temperature.

The spent fuel pool pump suction lines penetrate the spent fuel pool wall above the fuel assemblies stored in the pool to prevent loss of water as a result of a suction line rupture. The pool is initially filled with water at the same boron concentration (2400 ppm) as in the refueling water storage tank.

The spent fuel pool is located outside the reactor containment. During refueling the water in the pool can be isolated from that in the re-fueling canal by a weir gate so that there is only a very small amount of interchange of water as fuel assemblies are transferred.

5.2.3 Performance Requirements

The first design basis of the system is based on the normal refueling operation with a normal batch of 80 assemblies being removed from the unit each time.

The second design basis for the system considers that it is possible to unload the reactor vessel (193 fuel assemblies) for maintenance or inspection at a time when a maximum of 3518 spent fuel assemblies are assumed already stored in the spent fuel pool.

5.3 Decay Heat Load Calculations

The decay heat load calculation is performed in accordance with the provisions of USNRC Branch Technical Position ASB9-2, "Residual Decay Energy for Light Water Reactors for Long Term Cooling", Rev. 2, July, 1981. For purposes of this licensing

application, it is assumed that the pool contains an inventory accumulated through scheduled discharges from 1975 to 2009 (Table 1.1.1). Further, since the decay heat load increases monotonically with reactor exposure time, an upper bound of 1260 full power operation days (approximately 3.5 years) is assumed for all stored fuel. The cumulative decay heat load is computed for the instance of hypothetical normal discharge (21B in Table 1.1.1) in the year 2009. As shown in Table 5.4.1, the ratio of this decay heat load due to the inventory of previously stored fuel to the average assembly operating power β is 0.3303.

This decay heat load is assumed to remain invariant for the duration of the pool temperature evaluations performed in the wake of normal and full core offloads discussed below.

5.4 Discharge Scenarios

The following discharge scenarios are examined:

Case 1: Normal discharge

A normal batch of 80 assemblies with 1260 days of reactor exposure time at full power is discharged in the pool at the end of a normal 18 month operating cycle. There are 43 previously discharged batches in the pool. As described later, the normal discharge is assumed to occur at the rate of approximately 4 assemblies per hour after 168 hours of decay in the reactor. One fuel pool cooling train is active and running. One cooling train contains one heat exchanger and one fuel pool pump.

This case is run with the design fuel pool water flow rate (2300 gpm) and actual available flow rate (2800 gpm). These two cases are labelled as Case 1a and Case 1b, respectively.

Case 2: Normal discharge

Same as Case 1 except two fuel pool cooling trains are operating.

Case 3: Back-to-Back Full core offload

The full core offload condition corresponds to the emergency reactor offload condition wherein the shutdown of a reactor occurs 30 days after the other reactor shutdown for a normal refueling. Two cooling trains are assumed to be operating in parallel after the shutdown. The decay time of the core in the reactor and the rate of discharge to the pool are the same as in Case 1.

Case 4:

Same as Case 3 except only one cooling train is in operation. This case is listed for reference only; it is not a design basis case by the Donald C. Cook Technical Specification or the USNRC guidelines (NUREG-0800).

Detailed data on the three cases are given in Table 5.4.1 to 5.4.3.

5.5 Bulk Pool Temperature

In order to perform the analysis conservatively, the heat exchangers are assumed to be fouled to their design maximum. Thus, the temperature effectiveness, p, for the heat exchanger utilized in the analysis is the lowest postulated value calculated from heat exchanger thermal hydraulic codes. p is assumed constant in the calculation.

The mathematical formulation can be explained with reference to the simplified heat exchanger alignment of Figure 5.5.1.

Referring to the spent fuel pool/cooler system, the governing differential equation can be written by utilizing conservation of energy:

$$C \frac{dT}{d\tau} = Q_L - Q_{HX} \qquad (5\text{-}1)$$

$$Q_L = P_{cons} + Q(\tau) - Q_{EV}(T, t_a)$$

where:

C:	Thermal capacitance of the pool (net water volume times water density and times heat capacity), Btu/°F.
Q_L:	Heat load to the heat exchanger, Btu/hr.
$Q(\tau)$:	Heat generation rate from recently discharged fuel, which is a specified function of time, τ, Btu/hr.
$P_{cons} = \beta P_o$:	Heat generation rate from "old" fuel, Btu/hr. (P_o = average assembly operating power, Btu/hr.)
Q_{HX}:	Heat removal rate by the heat exchanger, Btu/hr.
$Q_{EV}(T, t_a)$:	Heat loss to the surroundings, which is a function of pool temperature T and ambient temperature t_a, Btu/hr.

Q_{HX} is a non-linear function of time if we assume the temperature effectiveness p is constant during the calculation. Q_{HX} can, however, be written in terms of effectiveness p as follows:

$$Q_{HX} = W_t C_t p (T - t_i) \qquad (5\text{-}2)$$

$$p = \frac{t_o - t_i}{T - t_i}$$

where:

W_t: Coolant flow rate, lb./hr.

C_t: Coolant specific heat, Btu/lb.°F.

p: Temperature effectiveness of heat exchanger.

T: Pool water temperature, °F

t_i: Coolant inlet temperature, °F

t_o: Coolant outlet temperature, °F

p is obtained by rating the heat exchanger on a Holtec proprietary thermal/hydraulic computer code. $Q(\tau)$ is specified according to the provisions of "USNRC Branch Technical Position ASB9-2, "Residual Decay Energy for Light Water Reactors for Long Term Cooling", Rev. 2, July, 1981. $Q(\tau)$ is a function of decay time, number of assemblies, and in-core exposure time. During the fuel transfer, the heat load in the pool will increase with respect to the rate of fuel transfer and equals to $Q(\tau)$ after the fuel transfer.

Q_{EV} is a non-linear function of pool temperature and ambient temperature. Q_{EV} contains the heat evaporation loss through the pool surface, natural convection from the pool surface and heat conduction through the pool walls and slab. Experiments show that the heat conduction takes only about 4% of the total heat loss [5.5.1], therefore, can be neglected. The evaporation heat and nature convection heat loss can be expressed as:

$$Q_{EV} = m \Gamma A_s + h_C A_s \theta \qquad (5\text{-}3)$$

where:

m: Mass evaporation rate, lb./hr. ft.^{2}

Γ: Latent heat of pool water, Btu/lb.

A_s: Pool surface area, ft.^{2}

h_C: Convection heat transfer coefficient at pool surface, Btu/ft.^{2} hr. °F

$\theta = T - t_a$: The temperature difference between pool water and ambient air, °F

The mass evaporation rate m can be obtained as a non-linear function of θ. We, therefore, have

$$m = h_D(\theta)\,(W_{ps} - W_{as}) \qquad (5\text{-}4)$$

where:

W_{ps}: Humidity ratio of saturated moist air at pool water surface temperature T.

W_{as}: Humidity ratio of saturated moist air at ambient temperature t_a

$h_D(\theta)$: Diffusion coefficient at pool water surface. h_D is a non-linear function of θ, lb./hr. ft.^{2} °F

The non-linear single order differential equation (5-1) is solved using Holtec's Q.A. validated numerical integration code "ONEPOOL".

Figures 5.5.2 through 5.5.6 provide the bulk pool temperature profiles for the normal discharge, and full core offload scenarios respectively. Table 5.5.1 gives the peak water temperature, coincident time, and coincident heat load to the cooler and coincident heat loss to the ambient for three cases.

The next step in the analysis is to determine the temperature rise profile of the pool water if all forced indirect cooling modes are suddenly lost. Make-up water is provided with a fire hose.

Clearly, the most critical instant of loss-of-cooling is when pool water has reached its maximum value. It is assumed that cooling water is added through a fire hose at the rate of G lb./hr. The

cooling water is at temperature, t_{cool}. The governing enthalpy balance equation for this condition can be written as

$$[C + G(C_t)(\tau - t_o)] \frac{dT}{d\tau} = P_{cons} + Q(\tau + t_{ins}) + G\,(C_t)\,(t_{cool} - T) - Q_{EV}$$

where water is assumed to have specific heat of unity, and the time coordinate τ is measured from the instant maximum pool water temperature is reached. t_o is the time coordinate when the direct addition (fire hose) cooling water application is begun. t_{ins} is the time coordinate measured from the instant of reactor shutdown to when maximum pool water temperature is reached. T is the dependent variable (pool water temperature). For conservatism, Q_{EV} is assumed to remain constant after pool water temperature reaches and rises above 170°F.

A Q.A. validated numerical quadrature code is used to integrate the foregoing equation. The pool water heat up rate, time-to-boil, and subsequent water evaporation-time profile are generated and compiled for safety evaluation.

Assuming no make-up water (G = 0), the time-to-boil output results are presented in Table 5.5.2. Figures 5.5.6 through 5.5.10 show the plot of the inventory of water in the pool after loss-of-coolant-to-the-pool condition begins.

It is seen from Table 5.5.2 that sufficient time to introduce manual cooling measures exists and the available time is consistent with other PWR reactor installations.

5.6 Local Pool Water Temperature

In this section, a summary of the methodology, calculations and results for local pool water temperature is presented.

5.6.1 Basis

In order to determine an upper bound on the maximum fuel cladding temperature, a series of conservative assumptions are made. The most important assumptions are listed below:

- The fuel pool will contain spent fuel with varying time-after-shutdown (τ_s). Since the heat emission falls off rapidly with increasing τ_s, it is conservative to assume that all fuel assemblies are from the latest batch discharged simultaneously in the shortest possible time and they all have had the maximum postulated years of operating time in the reactor. The heat emission rate of each fuel assembly is assumed to be equal and maximum.

- As shown in the pool layout drawings, the modules occupy an irregular floor space in the pool. For the hydrothermal analysis, a circle circumscribing the actual rack floor space is drawn (Fig. 5.6.1). It is further assumed that the cylinder with this circle as its base is packed with fuel assemblies at the nominal layout pitch.

- The actual downcomer space around the rack module group varies. The nominal downcomer gap available in the pool is assumed to be the total gap available around the idealized cylindrical rack; thus, the maximum resistance to downward flow is incorporated into the analysis (Figs. 5.6.2 and 5.6.3) (i.e. minimum gap between the pool wall and rack module, including seismic kinematic effect).

- No downcomer flow is assumed to exist between the rack modules.

- O The ANF 17x17 fuel assembly has been used in the analysis which, from the thermal-hydraulic standpoint, bounds all types of fuel bundles utilized in the Donald C. Cook reactor.

- O No heat transfer is assumed to occur between pool water and the surroundings (wall, etc.)

5.6.2 Model Description

In this manner, a conservative idealized model for the rack assemblage is obtained. The water flow is axisymmetric about the vertical axis of the circular rack assemblage, and thus, the flow is two-dimensional (axisymmetric three-dimensional). Fig. 5.6.2 shows a typical "flow chimney" rendering of the thermal hydraulics model. The governing equation to characterize the flow field in the pool can now be written. The resulting integral equation can be solved for the lower plenum velocity field (in the radial direction) and axial velocity (in-cell velocity field), by using the method of collocation. The hydrodynamic loss coefficients which enter into the formulation of the integral equation are also taken from well-recognized sources (Ref. 5.6.1) and wherever discrepancies in reported values exist, the conservative values are consistently used. Reference 5.6.2 gives the details of mathematical analysis used in this solution process.

After the axial velocity field is evaluated, it is a straightforward matter to compute the fuel assembly cladding temperature. The knowledge of the overall flow field enables pinpointing of the storage location with the minimum axial flow (i.e, maximum water outlet temperatures). This is called the most "choked" location. In order to find an upper bound on the temperature in a typical cell, it is assumed that it is located at the most choked location. Knowing the global plenum velocity field, the revised

axial flow through this choked cell can be calculated by solving the Bernoulli's equation for the flow circuit through this cell. Thus, an absolute upper bound on the water exit temperature and maximum fuel cladding temperature is obtained. In view of these aforementioned assumptions, the temperatures calculated in this manner overestimate the temperature rise that will actually occur in the pool. Holtec's computer code THERPOOL*, based on the theory of Ref. 5.6.2, automates this calculation. The analysis procedure embodied in THERPOOL has been accepted by the Nuclear Regulatory Commission on several dockets. The Code THERPOOL for local temperature analyses includes the calculation of void generations. The effect of void on the conservation equation, crud layer in the clad, flux trap temperature due to gamma heating, and the clad stress calculation when a void exists, are all incorporated in THERPOOL. The peaking factors are given in Table 5.6.1.

5.7 Cladding Temperature

The maximum specific power of a fuel array q_A can be given by:

$$q_A = q\ F_{xy} \qquad (1)$$

where:

F_{xy} = radial peaking factor
q = average fuel assembly specific power

---

* THERPOOL has been used in qualifying the spent fuel pools for Enrico Fermi Unit 2 (1980), Quad Cities I and II (1981), Oyster Creek (1984), V.C. Summer (1984), Rancho Seco (1983), Grand Gulf I (1985), Diablo Canyon I and II (1986), among others.

The maximum temperature rise of pool water in the most disadvantageously placed fuel assembly is computed for all loading cases. Having determined the maximum local water temperature in the pool, it is now possible to determine the maximum fuel cladding temperature. A fuel rod can produce F_z times the average heat emission rate over a small length, where F_z is the axial rod peaking factor. The axial heat distribution in a rod is generally a maximum in the central region, and tapers off at its two extremities.

It can be shown that the power distribution corresponding to the chopped cosine power emission rate is given by

$$q(x) = q_A \sin \frac{\pi (a + x)}{h + 2a}$$

where:

h: active fuel length

a: chopped length at both extremities in the power curve

x: axial coordinate with origin at the bottom of the active fuel region

The value of a is given by

$$a = \frac{h z}{1 - 2z}$$

where:

$$z = \frac{1}{\pi F_z} - \left[\frac{1}{\pi^2 F_z^2} - \frac{1}{\pi F_z} + \frac{2}{\pi^2} \right]^{1/2}$$

where F_z is the axial peaking factor.

The cladding temperature T_c is governed by a third order differential equation which has the form of

$$\frac{d^3 T}{d x^3} + \alpha_1 \frac{d^2 T}{d x^2} - \alpha_2 \frac{dT}{dx} = f(x)$$

where α_1, α_2 and $f(x)$ are functions of x, and fuel assembly geometric properties. The solution of this differential equation with appropriate boundary conditions provides the fuel cladding temperature and local water temperature profile.

In order to introduce some additional conservatism in the analysis, we assume that the fuel cladding has a crud deposit which results in .005 ^{0}F-sq.ft.-hr/Btu of crud resistance, which covers the entire surface.

Table 5.6.2 provides the key input data for local temperature analysis. The results of maximum local pool water temperature and minimum local fuel cladding temperature are presented in Table 5.7.1.

The local boiling temperature of water is approximately 242°F at 26' below the free water surface and higher at lower elevations.

The location where the local water temperature reaches its maximum value is deeper than 26' below the free water surface, where the coincident boiling temperature of water is greater than 242°F. It is shown that the local pool water temperature is lower than the local boiling point and therefore, nucleate boiling will not occur.

Finally, it is noted that the fuel cladding temperature is considerably lower than the temperatures to which the cladding is subjected inside the reactor. Therefore, it is concluded that there is sufficient margin against fuel cladding failure in the spent fuel pool.

5.8 Blocked Cell Analysis

Calculations are also performed assuming that 50% of the top opening in the thermally limiting storage cell is blocked due to a horizontally placed (misplaced) fuel assembly. The corresponding maximum local pool water temperature and local fuel cladding temperature data are also presented in Table 5.7.1.

There is also no incidence of localized nucleate boiling of the pool water or potential for fuel cladding damage.

5.9 References for Section 5

5.6.1 General Electric Corporation, R&D Data Books, "Heat Transfer and Fluid Flow", 1974 and updates.

5.6.2 Singh, K.P. et al., "Method for Computing the Maximum Water Temperature in a Fuel Pool Containing Spent Nuclear Fuel", Heat Transfer Engineering, Vol. 7, No. 1-2, pp. 72-82 (1986).

Table 5.4.1

FUEL SPECIFIC POWER AND POOL CAPACITY DATA

Total water volume of Pool:	635645 gallons
Specific Operating Power of a Fuel Assembly:	60.3E+06 Btu/hr.
Dimensionless decay power of "old" discharges:	0.3303

Table 5.4.2

DATA FOR SCENARIOS 1 through 4

CASE NO.	1a	1b	2	3	4
Pool thermal capacity C x 10^{-6}, Btu/^{0}F	4.241	4.241	4.241	4.241	4.241
No. of Cooling Trains	1	1	2	2	1
No. of Discharges Considered for the Analysis	1	1	1	2	2
Time between Shutdowns, hr.	---	---	---	720	720
Cooler Inlet Temp., 0F	108.4	108.4	103.9	101.4	104.7
Coolant Flow Rate/ Cooler, 10^6 lb./hr.	1.49	1.49	1.49	1.49	1.49
Fuel Pool Water Flow Rate, 10^6 lb./hr.	1.14	1.40	1.14	1.14	1.14
Temperature Effectiveness/ cooler, p	0.3970	0.43	0.3975	0.3979	0.3987

Table 5.4.3

DATA FOR SCENARIOS 1 THROUGH 4

Case No.	Discharge ID	No. of Assemblies	Time After Shutdown when Transfer Begins (hrs)	Offload Time (hrs)	Expo. Time (hrs)
1a or 1b	Discharge 1	80	168	19.07	30240
2	Discharge 1	80	168	19.07	30240
3 or 4	Discharge 1	80	168	19.07	30240
	Discharge 2 (Full Core)	80 113	168	46.00	10080 30240

Table 5.5.1

POOL BULK TEMPERATURE AND HEAT LOAD DATA

Case No.	Coincident Cooler Duty 10^6 Btu/hr.	T_{max} Max. Pool Bulk Temp., °F	Time Coincident to T_{max} (after reactor shutdown)	Coincident Evaporation Heat Loss, 10^6 Btu/hr.
1a	30.241	159.54	207	3.00
1b	30.69	156.31	206	2.578
2	32.787	131.57	198	0.689
3	50.690	143.84	222	1.395
4	45.04	176.91	225	6.887

Table 5.5.2

TIME-TO-BOIL FOR VARIOUS DISCHARGE SCENARIOS

Case Number	Time-to-Boil (hours) G = 0 GPM
1a	7.82
1b	8.27
2	11.52
3	5.74
4	3.02

Table 5.6.1

PEAKING FACTOR DATA

Radial Bundle Peaking Factor	1.65
Total peaking factor	2.40

Table 5.6.2

DATA FOR LOCAL TEMPERATURE

Type of Fuel Assembly	PWR
Fuel Cladding Outer Diameter, inches	0.36
Fuel Cladding Inside Diameter, inches	0.31
Storage Cell inside Dimension, inches	8.75
Active fuel length, inches	144
No. of Fuel Rods/Assembly	264
Operating Power per Fuel Assembly P_o x -6, Btu/hr	60.3
Cell pitch, inches	8.97
Cell height, inches	168
Plenum radius, feet	29.3
Min. Bottom height, inches	4.75
Min. gap between pool wall and outer rack periphery, inches	1.5

Table 5.7.1

LOCAL AND CLADDING TEMPERATURE OUTPUT DATA FOR THE MAXIMUM POOL WATER CONDITION (Case a)

Condition	Water Temp., °F	Temp., °F
No blockage	168.0	212.9
50% blockage	219.2	246.9

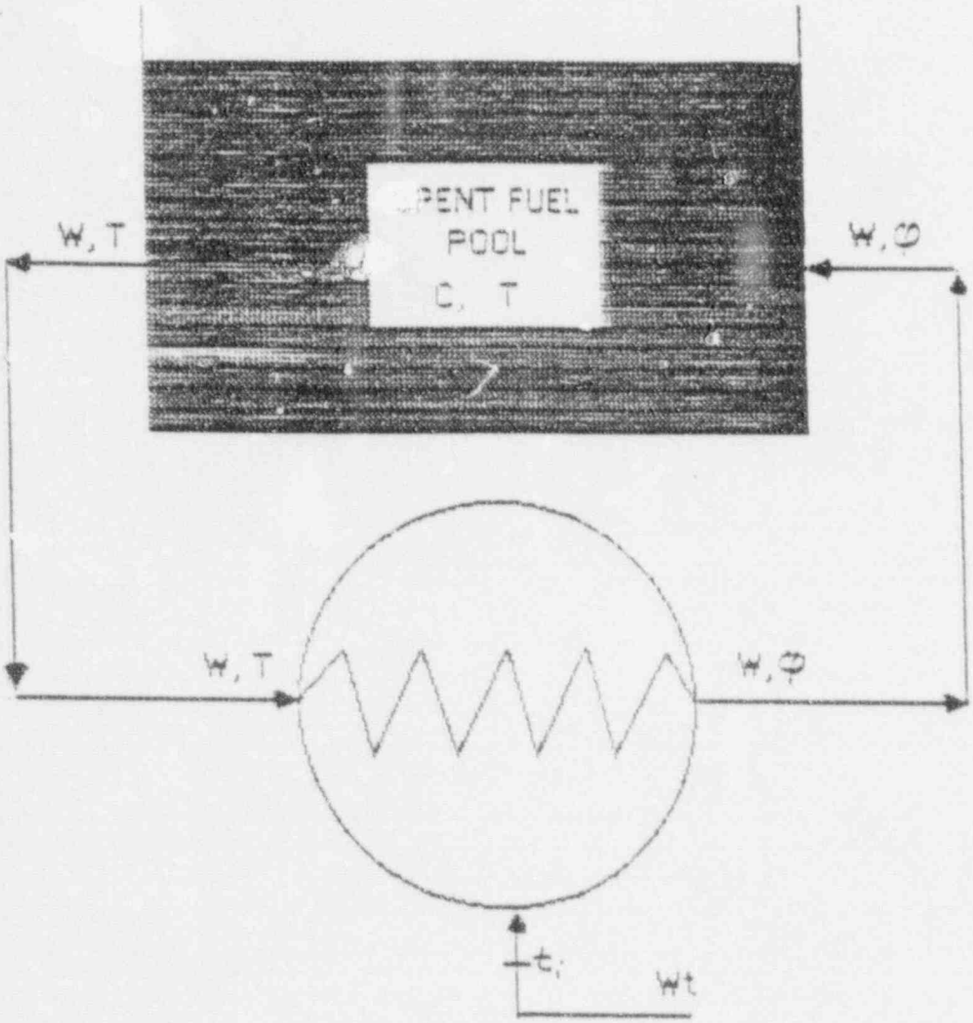

FIGURE 5.5.1 Pool Bulk Temperature Model

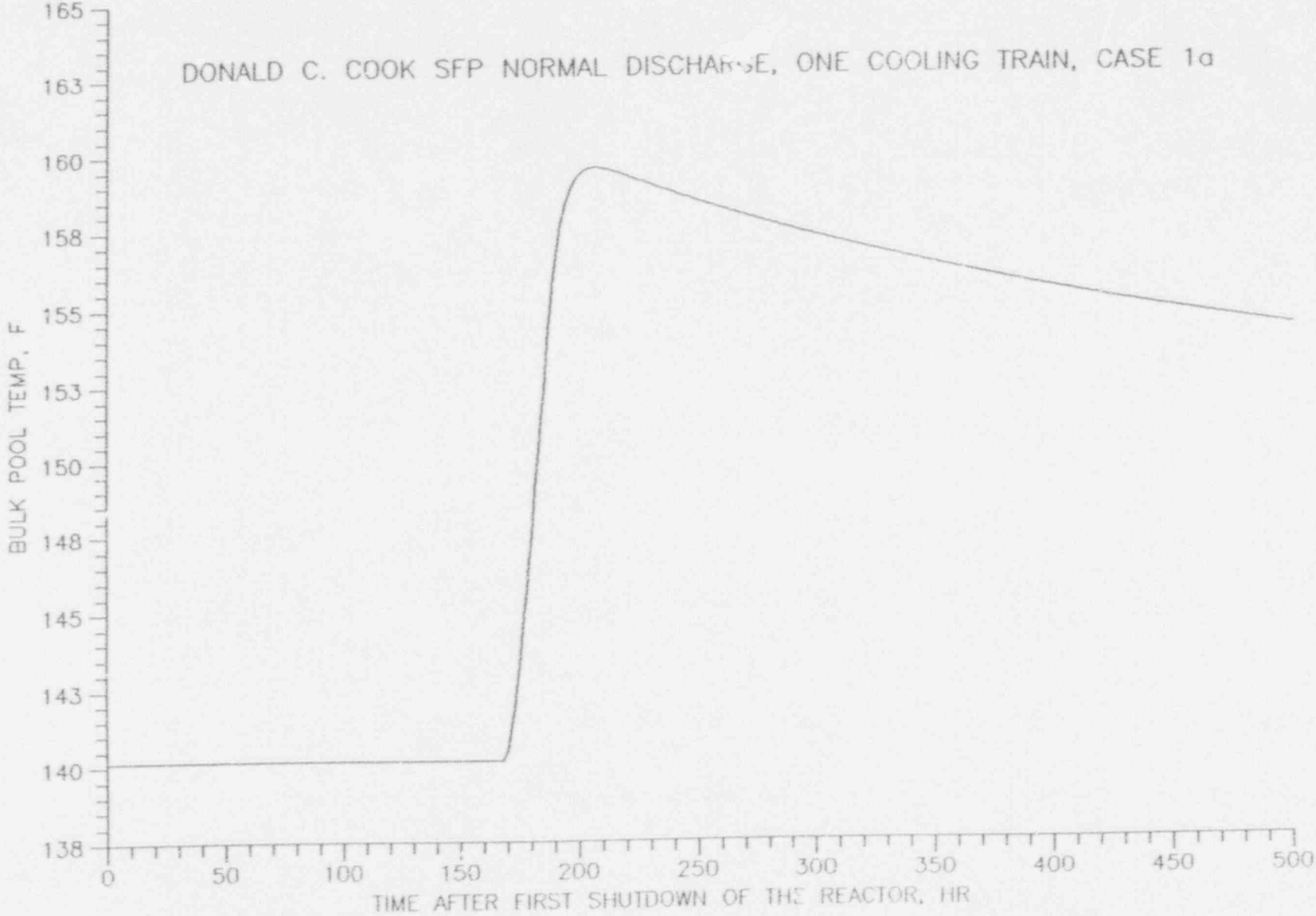
DONALD C. COOK SFP NORMAL DISCHARGE, ONE COOLING TRAIN, CASE 1a
BULK POOL TEMP, F
165
163
160
158
155
153
150
148
145
143
140
138
0
50
100
150
200
250
300
350
400
450
500
TIME AFTER FIRST SHUTDOWN OF THE REACTOR, HR

FIGURE 5.5.2

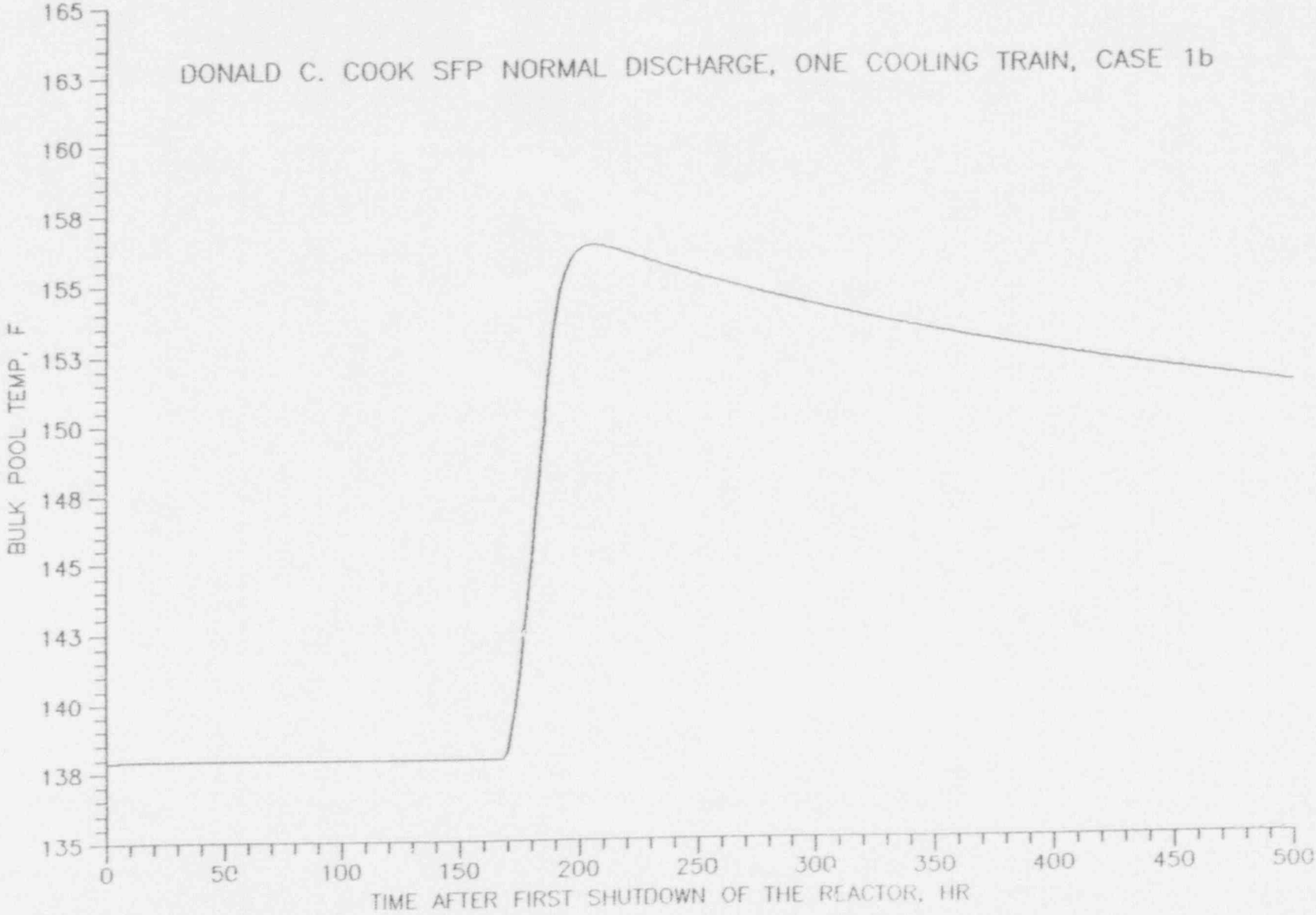
DONALD C. COOK SFP NORMAL DISCHARGE, ONE COOLING TRAIN, CASE 1b
BULK POOL TEMP, F
165
163
160
158
155
153
150
148
145
143
140
138
135
0
50
100
150
200
250
300
350
400
450
500
TIME AFTER FIRST SHUTDOWN OF THE REACTOR, HR

FIGURE 5.5.3

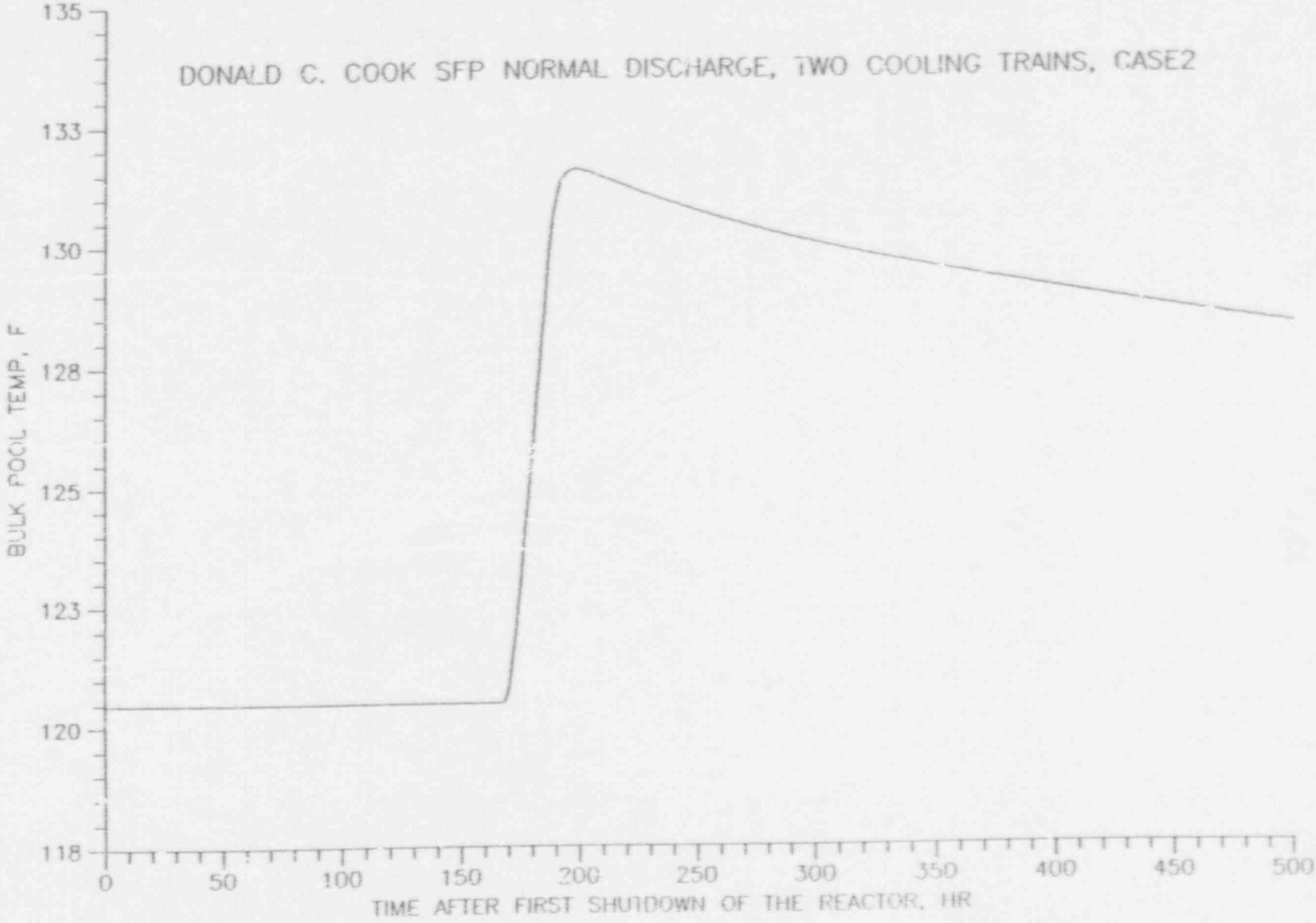
DONALD C. COOK SFP NORMAL DISCHARGE, TWO COOLING TRAINS, CASE2
BULK POOL TEMP, F
135
133
130
128
125
123
120
118
0
50
100
150
200
250
300
350
400
450
500
TIME AFTER FIRST SHUTDOWN OF THE REACTOR, HR

FIGURE 5.5.4

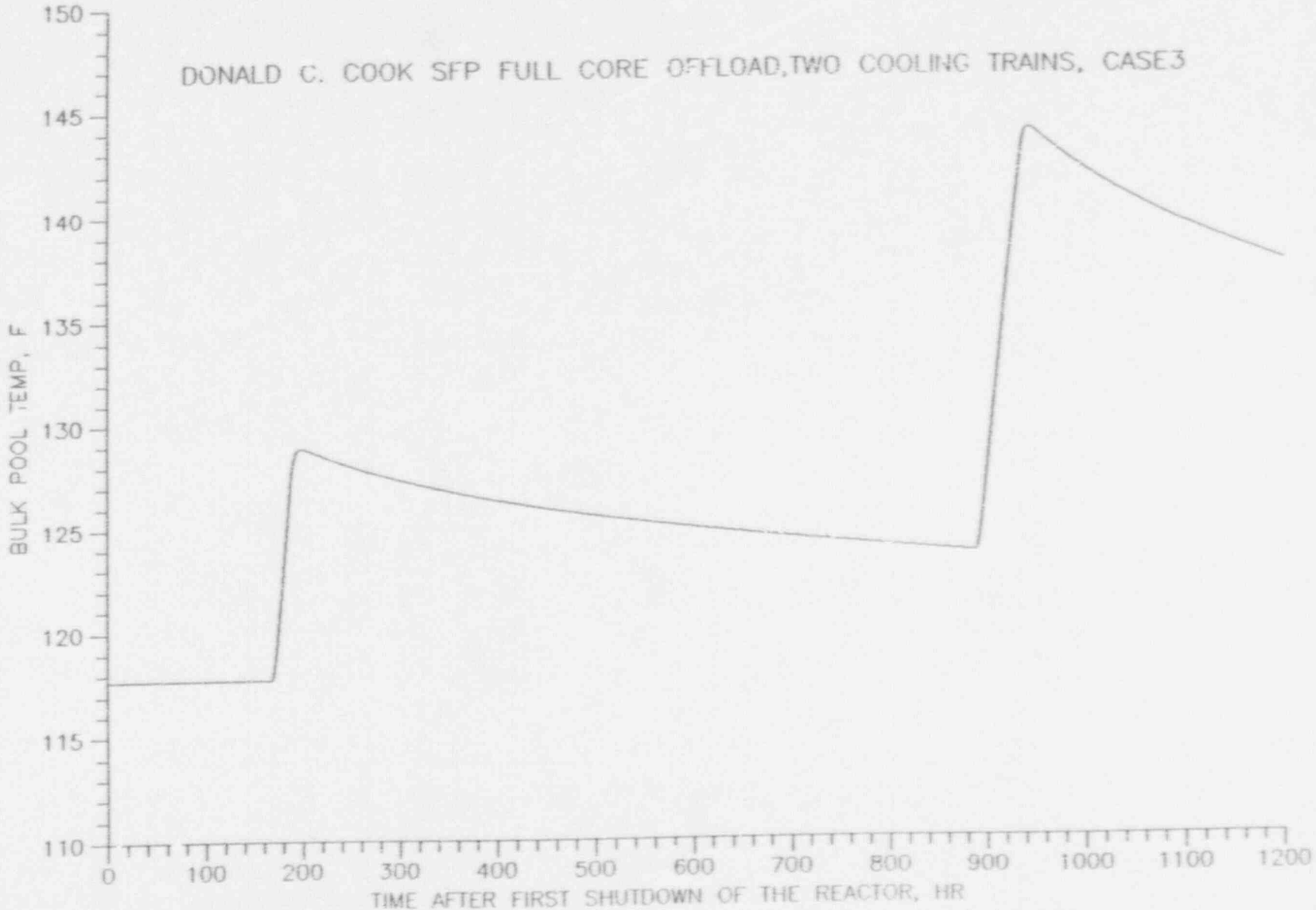
DONALD C. COOK SFP FULL CORE OFFLOAD,TWO COOLING TRAINS, CASE3
BULK POOL TEMP, F
150
145
140
135
130
125
120
115
110
0
100
200
300
400
500
600
700
800
900
1000
1100
1200
TIME AFTER FIRST SHUTDOWN OF THE REACTOR, HR

FIGURE 5.5.5

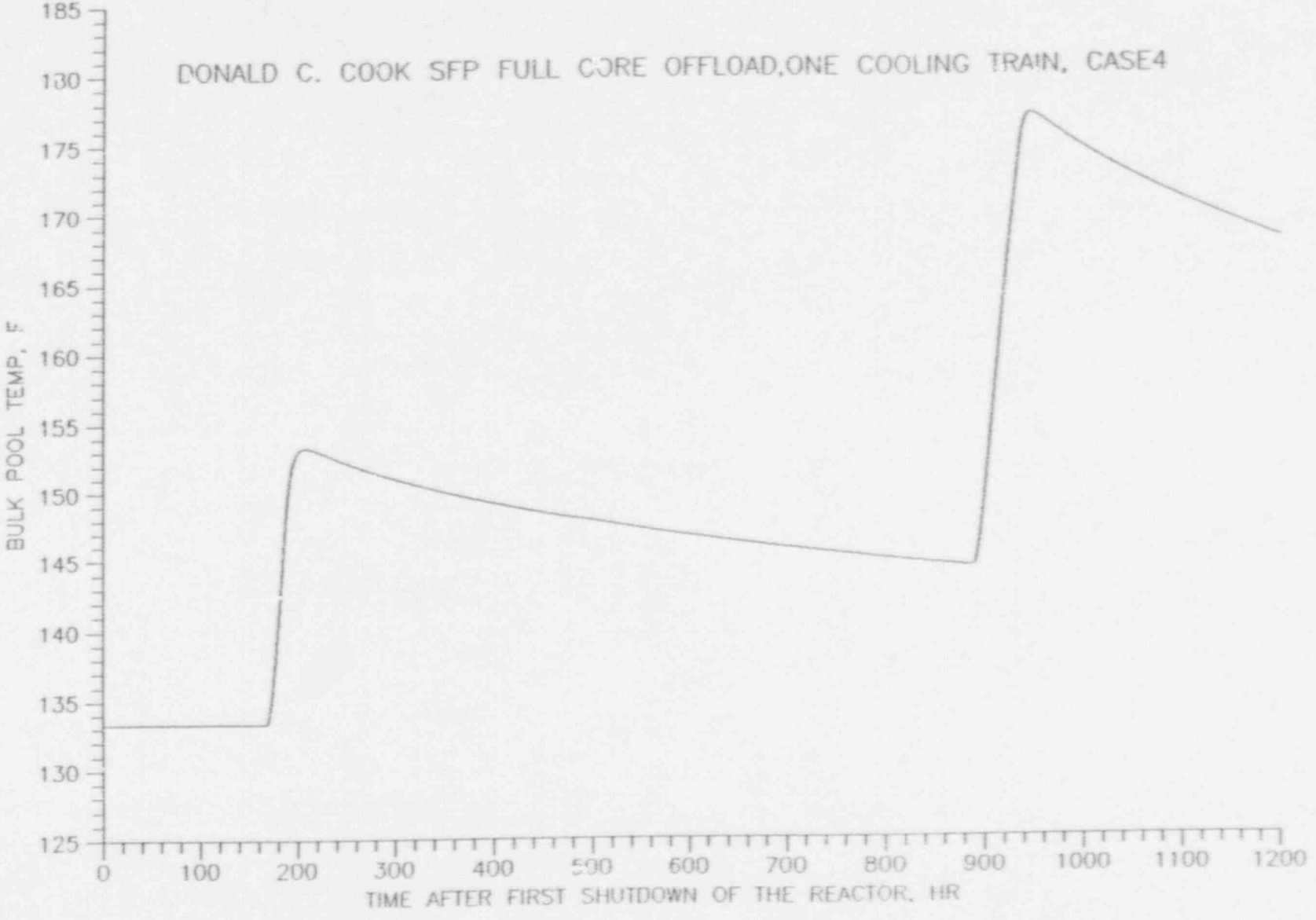
DONALD C. COOK SFP FULL CORE OFFLOAD,ONE COOLING TRAIN, CASE4
BULK POOL TEMP, F
185
180
175
170
165
160
155
150
145
140
135
130
125
0
100
200
300
400
500
600
700
800
900
1000
1100
1200
TIME AFTER FIRST SHUTDOWN OF THE REACTOR, HR

FIGURE 5.5.6

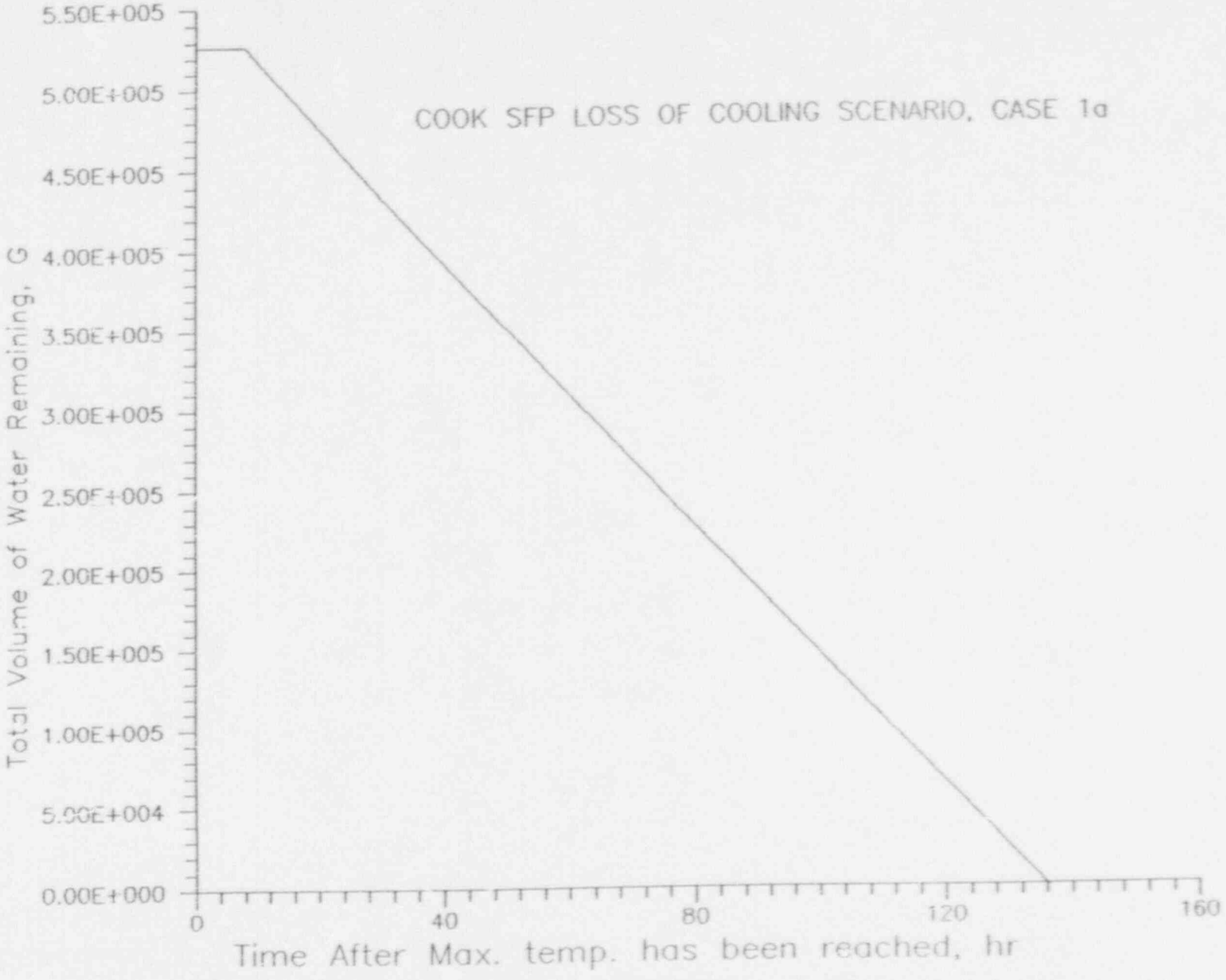
COOK SFP LOSS OF COOLING SCENARIO, CASE 1a
Total Volume of Water Remaining, G
5.50E+005
5.00E+005
4.50E+005
4.00E+005
3.50E+005
3.00E+005
2.50E+005
2.00E+005
1.50E+005
1.00E+005
5.00E+004
0.00E+000
0
40
80
120
160
Time After Max. temp. has been reached, hr

FIGURE 5.5.7

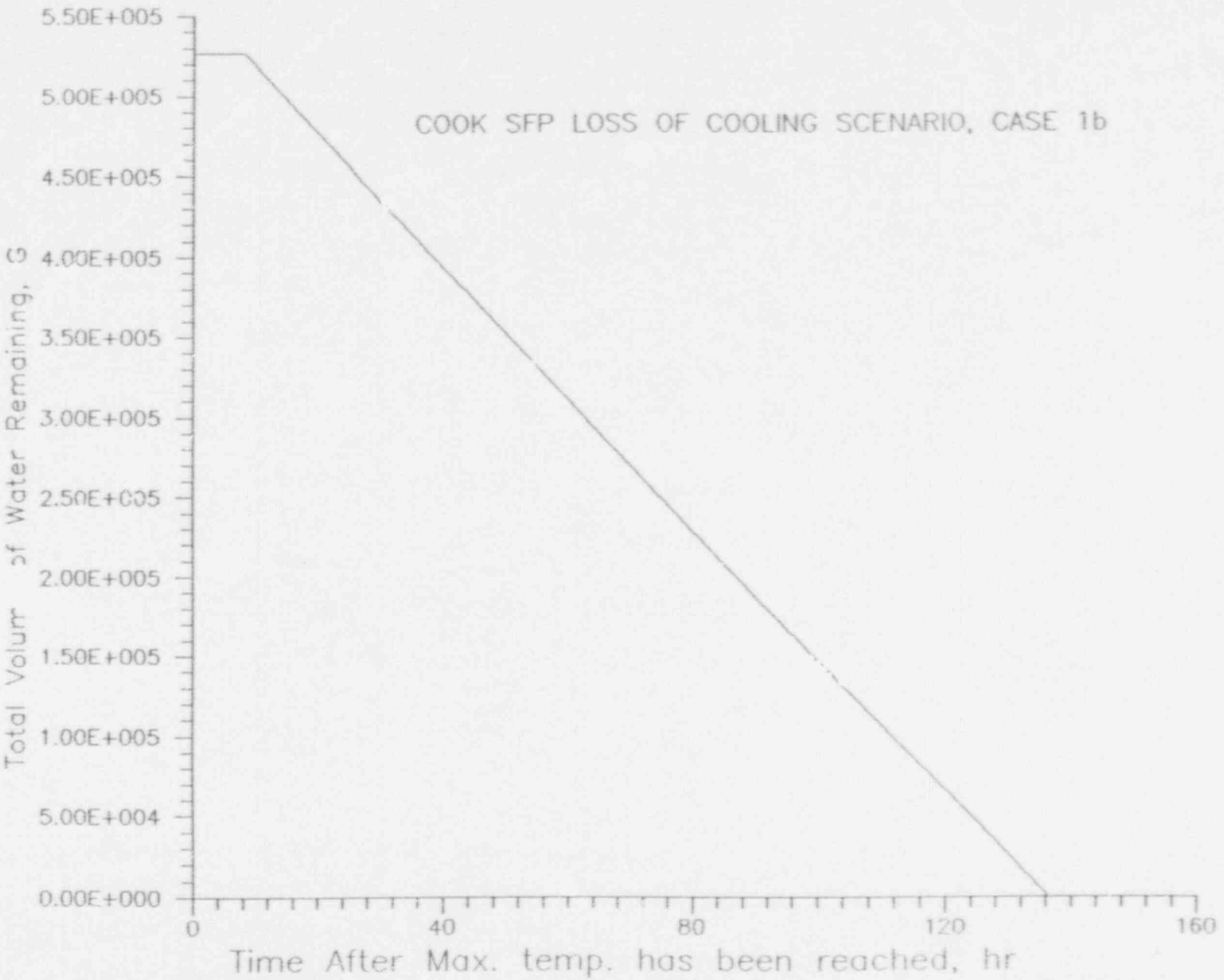
COOK SFP LOSS OF COOLING SCENARIO, CASE 1b
Total Volume of Water Remaining, G
5.50E+005
5.00E+005
4.50E+005
4.00E+005
3.50E+005
3.00E+005
2.50E+005
2.00E+005
1.50E+005
1.00E+005
5.00E+004
0.00E+000
0
40
80
120
160
Time After Max. temp. has been reached, hr

FIGURE 5.5.8

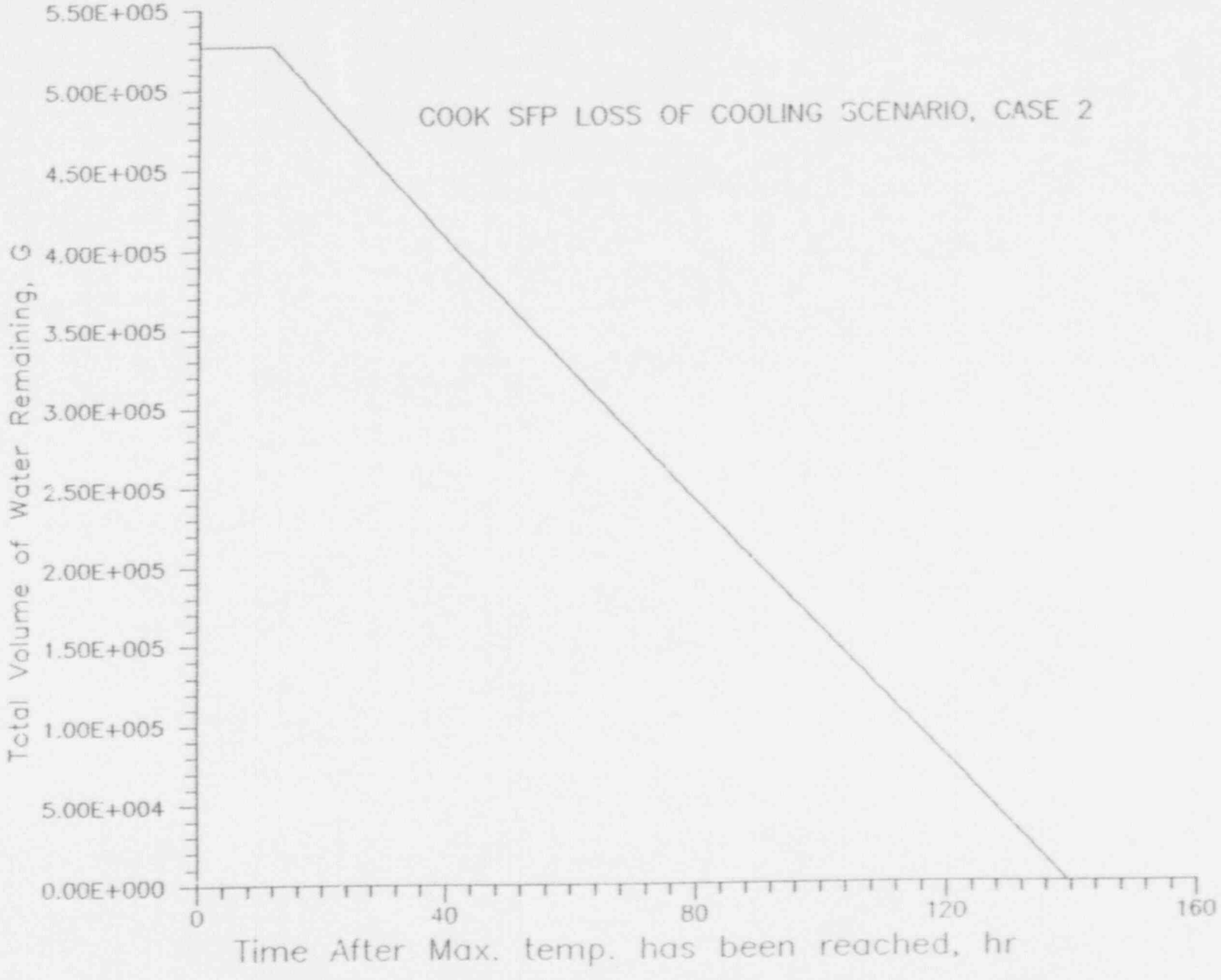
COOK SFP LOSS OF COOLING SCENARIO, CASE 2
Total Volume of Water Remaining, G
5.50E+005
5.00E+005
4.50E+005
4.00E+005
3.50E+005
3.00E+005
2.50E+005
2.00E+005
1.50E+005
1.00E+005
5.00E+004
0.00E+000
0
40
80
120
160
Time After Max. temp. has been reached, hr

FIGURE 5.5.9

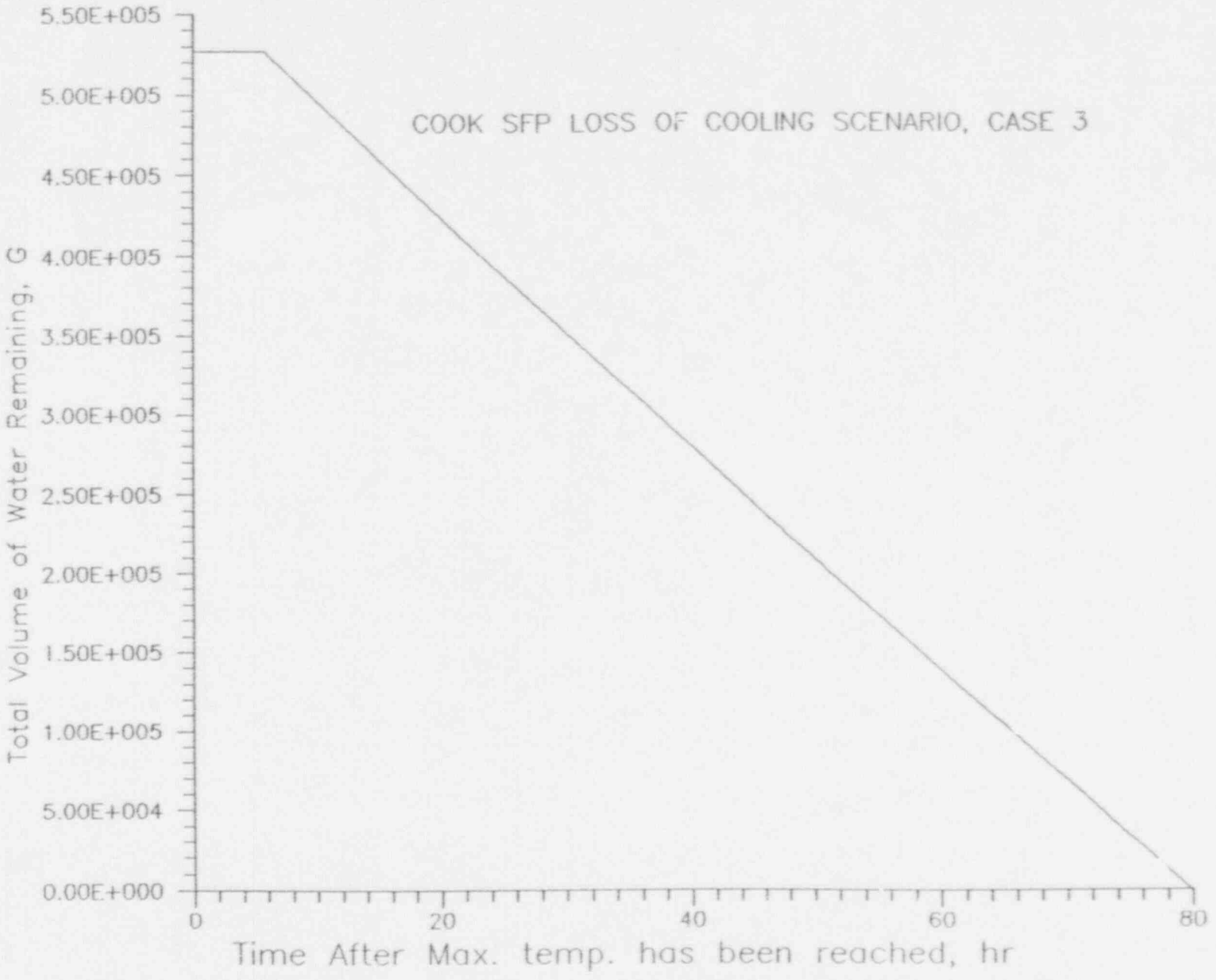
COOK SFP LOSS OF COOLING SCENARIO, CASE 3
Total Volume of Water Remaining, G
5.50E+005
5.00E+005
4.50E+005
4.00E+005
3.50E+005
3.00E+005
2.50E+005
2.00E+005
1.50E+005
1.00E+005
5.00E+004
0.00E+000
0
20
40
60
80
Time After Max. temp. has been reached, hr

FIGURE 5.5.10

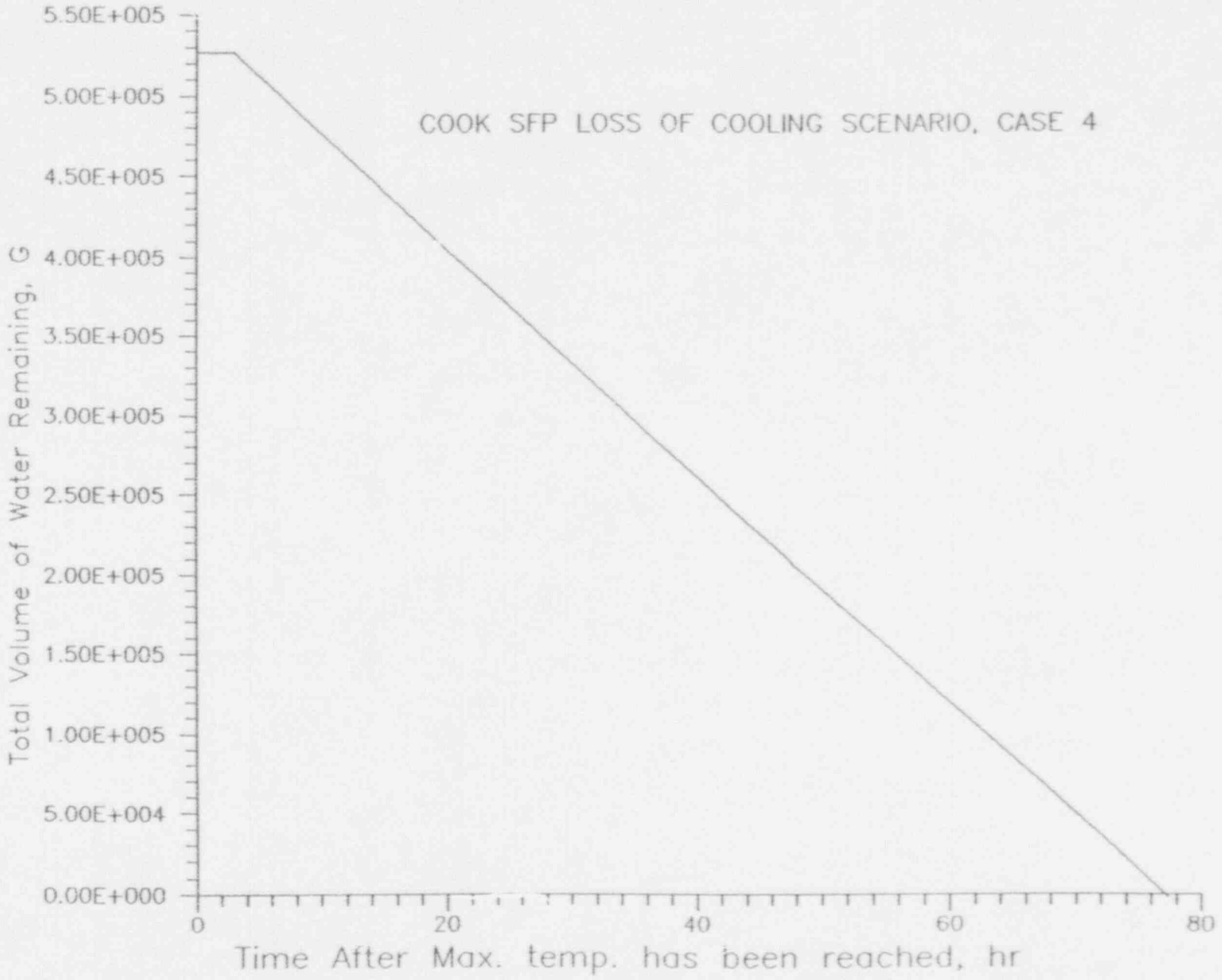
COOK SFP LOSS OF COOLING SCENARIO, CASE 4
Total Volume of Water Remaining, G
5.50E+005
5.00E+005
4.50E+005
4.00E+005
3.50E+005
3.00E+005
2.50E+005
2.00E+005
1.50E+005
1.00E+005
5.00E+004
0.00E+000
0
20
40
60
80
Time After Max. temp. has been reached, hr

FIGURE 5.5.11

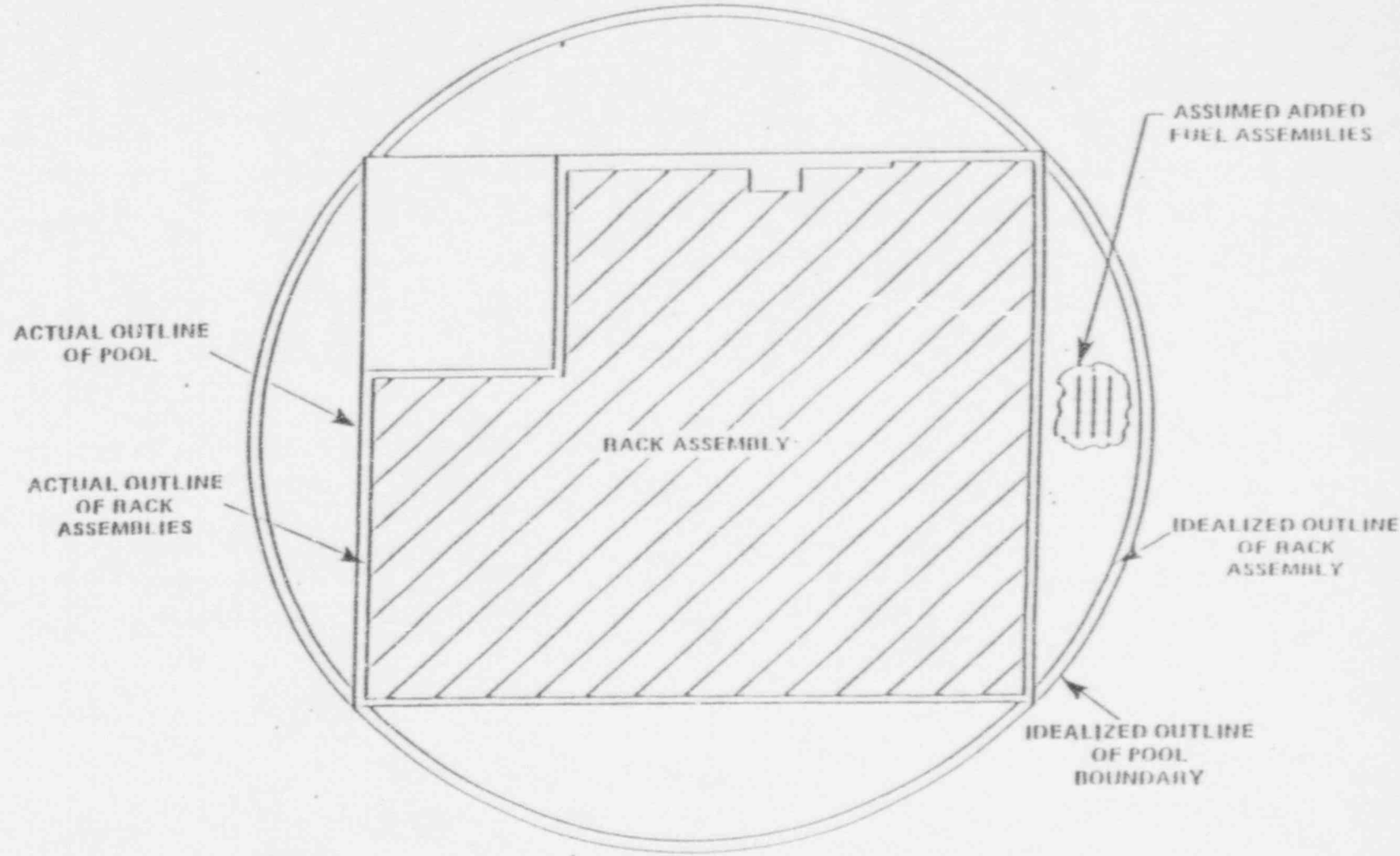

FIGURE 5.6.1 IDEALIZATION OF RACK ASSEMBLY

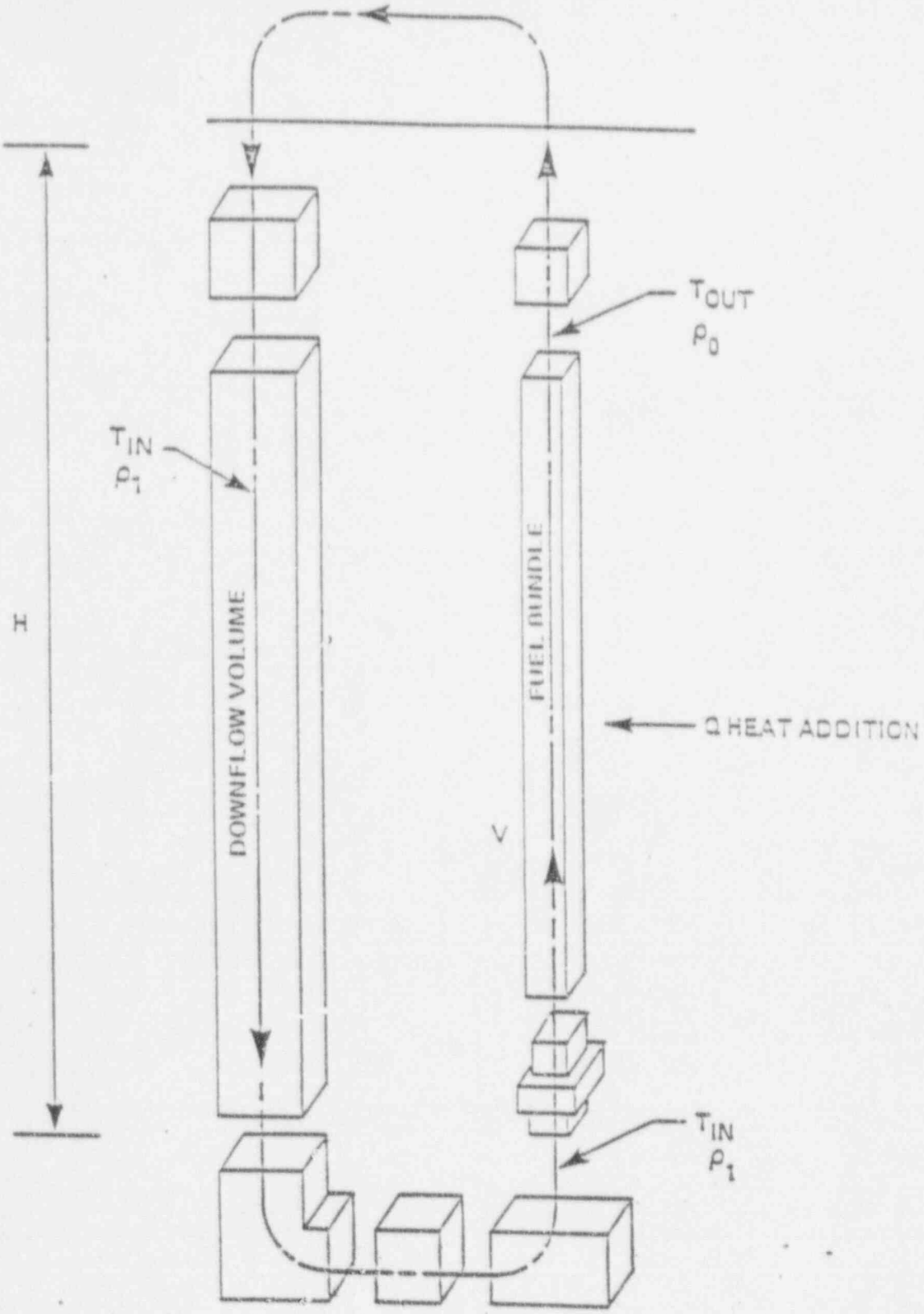

THERMAL CHIMNEY FLOW MODEL

FIGURE 5.6.2

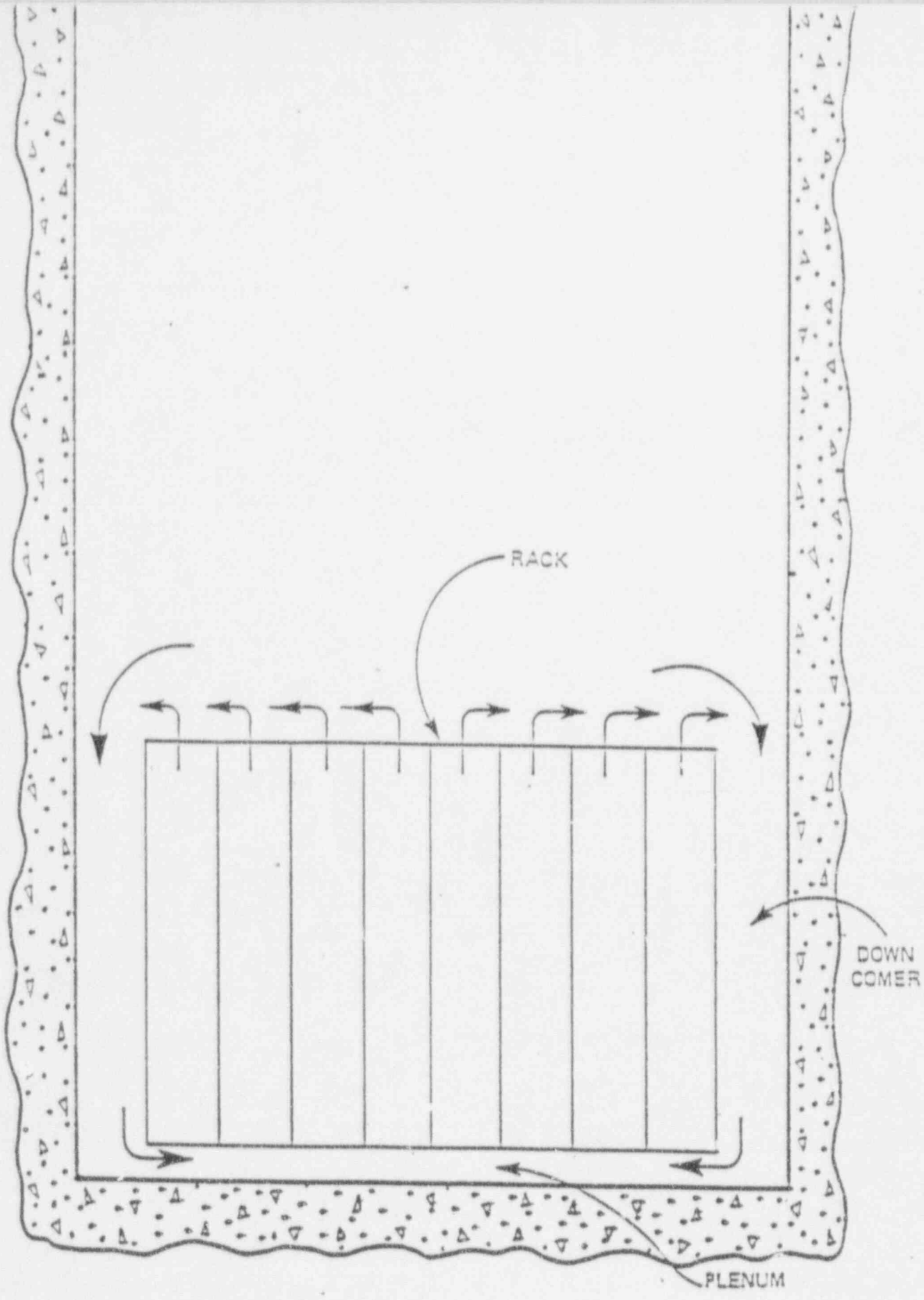

CONVECTION CURRENTS
IN THE POOL
FIGURE 5.6.3

6.0 STATIC AND DYNAMIC ANALYSIS OF RACK STRUCTURE

6.1 Introduction

The purpose of this section is to present analyses which demonstrate the structural adequacy of the Donald C. Cook spent fuel high density rack design under normal storage and the postulated accident loading conditions as defined by and following the guidelines of the USNRC Standard Review Plan (Ref. 6.1.1). The method of analysis presented uses a time-history integration method similar to that previously used in the licensing reports on high density spent fuel racks for Enrico Fermi Unit 2 (USNRC Docket No. 50-341), Quad Cities 1 and 2 (USNRC Docket Nos. 50-254 and 50-265), Rancho Seco (USNRC Docket No. 50-312), Grand Gulf Unit 1 (USNRC Docket No. 50-416), Oyster Creek (USNRC Docket No. 50-219), V.C. Summer (USNRC Docket No. 50-395), Diablo Canyon Units 1 and 2 (USNRC Docket Nos. 50-275 and 50-323), Vogtle Unit 2 (USNRC Docket No. 50-425) and Millstone Point Unit 1 (USNRC Docket No. 50-245). The analyses carried out for the Donald C. Cook racks are considerably more elaborate and exhaustive in scope and substance than those performed in the aforementioned dockets, and reflect advances in 3-D fuel rack simulation technology in the past two years. The details are presented later in this section, after the essential elements of the dynamic model are fully explained.

The results show that the high density spent fuel racks are structurally adequate to resist the postulated stress combinations associated with level A, B, C, and D conditions as defined in Refs. 6.1.1, 6.1.2, and 6.1.3.

6.2 Analysis Outline

The principal steps in performing the seismic analysis of Donald C. Cook racks are summarized below:

a. Develop statistically independent synthetic time histories for three orthogonal directions which satisfy USNRC SRP3.8.4. Two time histories are considered to be statistically independent if their normalized correlation coefficient is less than 0.15.

b. Prepare a three-dimensional dynamic model of the fuel rack which embodies all elastostatic characteristics and structural nonlinearities of the Donald C. Cook rack modules.

c. Perform a series of 3-D dynamic analyses on a limiting module geometry type from those listed in Tables 2.1.1 and 2.1.3 and for varying physical conditions (such as coefficient of friction, extent of cells containing fuel assemblies, and proximity of other racks).

d. Perform stress analysis for the critical case from the dynamic analysis runs made in the foregoing steps. Demonstrate compliance with ASME Code Section III, subsection NF (Ref. 6.1.2) limits.

e. Carry out a degree-of-freedom (DOF) reduction procedure on the single rack 3-D model such that the kinematic responses calculated by the reduced DOF (model RDOFM) are in agreement with the baseline model of step (b) above. This reduced DOF model is also truly three-dimensional.

f. Prepare a whole pool multi-rack dynamic model by compiling the RDOFM's of <u>all</u> rack modules in the pool, and by including all fluid coupling interactions among them, as well as those between the racks and pool walls. This 3-D multi-module simulation is referred to as a Whole Pool Multi-Rack (WPMR) model.

g. Perform a 3-D Whole Pool Multi-Rack (WPMR) analysis to demonstrate that all kinematic criteria for Donald C. Cook rack modules are satisfied (see Section 6.8), and that pedestal compressive loads are comparable to the loads used for structural qualification per item d above. Section 6.8 gives the criteria which need to be checked.

   For the Donald C. Cook racks, the principal kinematic criteria are (i) no rack to pool wall impact, and (ii) no rack-to-rack impact in the cellular region of the racks.

Figure 6.2.1 shows a pictorial view of the rack module. It is noted that the baseplate extends beyond the cellular region envelope, thus ensuring that the inter-rack impact, if any, would first occur at the baseplate elevation. The baseplate of the rack modules is structurally qualifiable to withstand large in-plane impact loads.

We describe each of the above analysis steps in some detail in the following sub-sections with special emphasis on the baseline 3-D dynamic model which is the building block for all subsequent analyses. We also present the results of the analysis in the concluding sub-section.

6.3 Artificial Slab Motions

The UFSAR provides a single response spectrum in the horizontal direction and a single response spectrum in the vertical direction (2/3 of the horizontal) for the Design Basis Earthquake (DBE). A corresponding pair of spectra are provided for the Operating Basis Earthquake (OBE).

Holtec's Q.A. validated time history generation code GENEQ [6.3.1] was used to generate three synthetic statistically independent time histories for the North-South, East-West and vertical directions, respectively, from the two response spectra. 5% damping is used for the DBE condition. Figures 6.3.1 - 6.3.3 show the DBE time history plots. Response spectra corresponding to these time histories were also generated and are shown overlaid on the design spectra in Figures 6.3.4 - 6.3.6.

The normalized correlation coefficients p_{ij} between time histories i and j (1 ≡ N-S, 2 = E-W, 3 ≡ vertical) are provided in Table 6.3.1.

The above analyses were repeated for the OBE spectra using 2% damping. Figures 6.3.7 - 6.3.9 present the time history plots, and Figures 6.3.10 -6.3.12 show the comparison between the design spectra and the derived spectra. Table 6.3.1 also provides p_{ij} for the OBE time histories. It is noted that the enveloping requirement on the derived spectra and statistical non-coherence of artificial motions are unconditionally satisfied.

6.4 Outline of Single Rack 3-D Analysis

The spent fuel storage racks are Seismic Class I equipment. They are required to remain functional during and after a Design Basis Earthquake (Ref. 6.1.3). These racks are neither anchored to the pool floor nor attached to the sidewalls. The individual rack modules are not interconnected. Furthermore, a particular rack may be completely loaded with fuel assemblies (which corresponds to greatest rack inertia), or it may be completely empty. The coefficient of friction, μ, between the supports and pool floor is another indeterminate factor. According to Rabinowicz (Ref. 6.4.1), the results of 199 tests performed on austenitic stainless steel plates submerged in water show a mean value of μ to be 0.503 with a standard deviation of 0.125. The upper and lower bounds (based on twice the standard deviation) are thus 0.753 and 0.253, respectively. Analyses are therefore performed for single rack simulations using values of the coefficient of friction equal to 0.2 (lower limit) and 0.8 (upper limit), respectively. The bounding values of μ = 0.2 and 0.8 have been found to bracket the upper limit of the module response in previous rerack projects.

A single rack 3-D analysis requires another key modelling assumption. This relates to the location and relative motion of neighboring racks. The gap between a peripheral rack and an adjacent pool wall is known, and the motion of the pool wall is prescribed without any ambiguity. However, another rack adjacent to the rack being analyzed is also free-standing and subject to motion during a seismic event. To conduct the seismic analysis of a given rack its physical interface with neighboring modules must be specified. The standard procedure in the single rack analysis is to specify that the neighboring racks move 180° out-of-phase in

relation to the subject rack. Thus, the available gap before inter-rack impact occurs is one half of the physical gap. This "opposed phase motion" assumption increases the likelihood of predicting intra-rack impacts and is thus a conservative assumption. However, it also increases the relative contribution of fluid coupling terms, which depend on fluid gaps and relative movements of bodies, making the outright conservatism a less certain assertion. In fact, 3-D Whole Pool Multi-rack analyses carried out for Taiwan Power Company's Chin Shan Station, and for GPU Nuclear's Oyster Creek Nuclear Station show that the single rack simulations predict smaller rack displacement during seismic responses. Nevertheless, single rack analyses permit detailed evaluation of stress fields, and serve as a benchmark check for the much more involved, WPMR analysis results. In order to predict the limiting conditions of rack module seismic response within the framework of single rack analysis, module A4 (13x14) is analyzed. This is typical of the largest module, and is also a corner module. The corner module has larger rack-to-wall gaps which will minimize the fluid coupling.

The rack is considered fully loaded or half loaded, with limiting coefficients of friction; these simulations identify the worst case response for rack movement and for rack structural integrity. After completion of reracking, the gaps between the rack modules and those between the racks and walls will be in the manner of Figure 2.1.1. We show in this report that all single rack 3-D simulations predict that no rack-to-rack or rack-to-wall impacts will occur in the cellular region of the racks.

The seismic analyses were performed utilizing the time-history method. Pool slab acceleration data presented in the preceding sub-section was used.

The objective of the seismic analysis of single racks is to determine the structural response (stresses, deformation, rigid body motion, etc.) due to simultaneous application of the three statistically independent, orthogonal seismic excitations. Thus, recourse to approximate statistical summation techniques such as the "Square-Root-of-the-Sum-of-the-Squares" method (Ref. 6.4.2) is avoided. For nonlinear analysis, the only practical method is simultaneous application of the seismic loading to a nonlinear model of the structure.

The seismic analysis of a single rack is performed in three steps, namely:

1. Development of a nonlinear dynamic model consisting of inertial mass elements, spring, gap, and friction elements.

2. Generation of the equations of motion and inertial coupling and solution of the equations using the "component element method" (Refs. 6.4.3 and 6.4.4) to determine nodal forces and displacements. The Holtec computer code DYNARACK is used to solve the system of equations [6.4.5].

3. Computation of the detailed stress field in the rack just above the baseplate and in the support legs is made using the nodal forces calculated in the previous step. These stresses are checked against the design limits given in a later sub-section.

A brief description of the dynamic model follows.

6.5 Dynamic Model for The Single Rack Analysis

Since the racks are not anchored to the pool slab or attached to the pool walls or to each other, they can execute a wide variety of motions. For example, the rack may slide on the pool floor

(so-called "sliding condition"); one or more legs may momentarily lose contact with the liner ("tipping condition"); or the rack may experience a combination of sliding and tipping conditions. The structural model should permit simulation of these kinematic events with inherent built-in conservatisms. Since the modules are designed to preclude the incidence of inter-rack impact in the cellular region, it is also necessary to include the potential for inter-rack impact phenomena in the analysis to demonstrate that such impacts do not occur. Lift-off of the support legs and subsequent liner impacts must be modelled using appropriate impact (gap) elements, and Coulomb friction between the rack and the pool liner must be simulated by appropriate piecewise linear springs. The elasticity of the rack structure, relative to the base, must also be included in the model even though the rack may be nearly rigid. These special attributes of rack dynamics require a strong emphasis on the modeling of the linear and nonlinear springs, dampers, and compression only stop elements. The term non-linear spring is the generic term to denote the mathematical element representing the situation where the restoring force exerted by the element is not linearly proportional to the displacement. In the fuel rack simulation the Coulomb friction interface between the rack support leg and the liner is a typical example of a non-linear spring. The model outline in the remainder of this sub-section, and the model description in the following sub-section, describe the detailed modeling technique to simulate these effects, with considerable emphasis placed on the nonlinearity of the rack seismic response.

6.5.1 Assumptions

a. The fuel rack structure is a folded metal plate assemblage welded to a baseplate and supported on four legs. An odd-shaped module may have more than four legs. The rack structure itself is a very rigid structure. Dynamic analysis of typical multi-cell racks has shown that the motion of the structure is captured almost completely by modelling the rack as a twelve degree-of-freedom structure, where the movement of the rack cross-section at any height is described in terms of six degrees-of-freedom of the rack base and six degrees of freedom defined at the rack top. The rattling fuel is modelled by five lumped masses located at H, .75H, .5H, .25H, and at the rack base, where H is the rack height as measured from the base.

b. The seismic motion of a fuel rack is characterized by random rattling of fuel assemblies in their individual storage locations. Assuming a certain statistical coherence (i.e. assuming that all fuel elements move in-phase within a rack) in the vibration of the fuel assemblies exaggerates the computed dynamic loading on the rack structure. This assumption, however, greatly reduces the required degrees-of-freedom needed to model the fuel assemblies which are represented by five lumped masses located at different levels of the rack. The centroid of each fuel assembly mass can be located, relative to the rack structure centroid at that level, so as to simulate a partially loaded rack.

c. The local flexibility of the pedestal is modelled so as to account for floor elasticity, and local rack elasticity just above the pedestal.

d. The rack base support may slide or lift-off the pool floor.

e. The pool floor has a specified time-history of seismic accelerations along the three orthogonal directions.

f. Fluid coupling between rack and fuel assemblies, and between rack and wall, is simulated by introducing appropriate inertial coupling into the system kinetic energy. Inclusion of these effects uses the methods of Refs. 6.5.1 and 6.5.2 for rack/assembly coupling and for rack/rack coupling.

g. Potential impacts between rack and fuel assemblies are accounted for by appropriate "compression only" gap elements between masses involved.

h. Fluid damping due to viscous effects between rack a assemblies, and between rack and adjacent rack, conservatively neglected.

i. The supports are modeled as "compression only" elements for the vertical direction and as "rigid links" for transferring horizontal stress. The bottom of a support leg is attached to a frictional spring as described in sub-section 6.6. The cross-section inertial properties of the support legs are computed and used in the final computations to determine support leg stresses.

j. The effect of sloshing is negligible at the level of the top of the rack and is hence neglected.

k. The possible incidence of rack-to-wall or rack-to-rack impact is simulated by gap elements at the top and bottom of the rack in the two horizontal directions. The bottom elements are located at the baseplate elevation.

l. Rattling of fuel assemblies inside the storage locations causes the "gap" between the fuel assemblies and the cell wall to change from a maximum of twice the nominal gap to a theoretical zero gap. Fluid coupling coefficients are based on the nominal gap.

m. The form drag due to motion of the fuel assembly in the storage cell, or that due to movement of a rack in the pool, has been neglected in this analysis for added conservatism.

n. The fluid coupling terms are based on opposed phase motion of adjacent modules.

Figure 6.5.1 shows a schematic of the model. Twelve degrees of freedom are used to track the motion of the rack structure. Figures 6.5.2 and 6.5.3, respectively, show the inter-rack impact springs (to track the potential for impact between racks or between rack and wall) and fuel assembly/storage cell impact

springs at a particular level. S_i (i = 1,..4) represent support locations, p_i represent absolute degrees-of-freedom, and q_i represent degrees-of-freedom relative to the slab. a is the height of the rack above the baseplate.

As shown in Figure 6.5.1, the model for simulating fuel assembly motion incorporates five rattling lumped masses. The five rattling masses are located at the baseplate, at quarter height, at half height, at three quarter height, and at the top of the rack. Two degrees-of-freedom are used to track the motion of each rattling mass in the horizontal plane. The vertical motion of each rattling mass is assumed to be the same as the rack base. Figures 6.5.4, 6.5.5, and 6.5.6 show the modelling scheme for including rack elasticity and the degrees of freedom associated with rack elasticity. In each plane of bending a shear and a bending spring are used to simulate elastic effects in accordance with Ref. 6.5.1. Table 6.6.2 gives spring constants for these bending springs as well as corresponding constants for extensional and torsional rack elasticity.

6.5.2 Model Description

The absolute degrees-of-freedom associated with each of the mass locations are identified in Figure 6.5.1 and in Table 6.5.1. The rattling masses (nodes 1^*, 2^*, 3^*, 4^*, 5^*) are described by translational degrees-of-freedom q_7-q_{16}.

$U_i(t)$ is the pool floor slab displacement seismic time-history. Thus, there are twenty-two degrees of freedom in the system. Not shown in Fig. 6.5.1 are the gap elements used to model the support legs and the impacts with adjacent racks.

6.5.3 Fluid Coupling

An effect of some significance requiring careful modeling is the "fluid coupling effect" (Refs. 6.5.1 and 6.5.2). If one body of mass (m_1) vibrates adjacent to another body (mass m_2), and both bodies are submerged in a frictionless fluid medium, then Newton's equations of motion for the two bodies have the form:

$$(m_1 + M_{11})\ddot{X}_1 + M_{12}\ddot{X}_2 = \text{applied forces on mass } m_1 + O(\dot{x}_1^2)$$

$$M_{21}\ddot{X}_1 + (m_2 + M_{22})\ddot{X}_2 = \text{applied forces on mass } m_2 + O(\dot{x}_2^2)$$

$\ddot{X}_1$, $\ddot{X}_2$ denote absolute accelerations of masses m_1 and m_2, respectively and the notation $O(\dot{x}^2)$ denotes non-linear terms which arise in the derivation.

M_{11}, M_{12}, M_{21}, and M_{22} are fluid coupling coefficients which depend on the shape of the two bodies, their relative disposition, etc. Fritz (Ref. 6.5.2) gives data for M_{ij} for various body shapes and arrangements. The above equations indicate that the effect of the fluid is to add a certain amount of mass to the body (M_{11} to body 1), and an external force which is proportional to the acceleration of the adjacent body (mass m_2). Thus, the acceleration of one body affects the force field on another. This force is a strong function of the interbody gap, reaching large values for very small gaps. This inertial coupling is called fluid coupling. It has an important effect in rack dynamics. The lateral motion of a fuel assembly inside the storage location will encounter this effect. So will the motion of a rack adjacent to another rack if the racks are closely spaced. These effects are included in the equations of motion. For example, the fluid

coupling is between nodes 2 and 2* in Figure 6.5.1. Furthermore, the rack equations contain coupling terms which model the effect of fluid in the gaps between adjacent racks. The coupling terms modeling the effects of fluid flowing between adjacent racks are computed assuming that all adjacent racks are vibrating 180^0 out of phase from the rack being analyzed. Therefore, only one rack is considered surrounded by a hydrodynamic mass computed as if there were a plane of symmetry located in the middle of the gap region.

Finally, fluid virtual mass is included in the vertical direction vibration equations of the rack; virtual inertia is also added to the governing equation corresponding to the rotational degree of freedom, $q_6(t)$ and $q_{22}(t)$.

6.5.4 Damping

In reality, damping (Ref. 6.5.3) of the rack motion arises from material hysteresis (material damping), relative intercomponent motion in structures (structural damping), and fluid viscous effects (fluid damping). In the analysis, a maximum of 1% structural damping is imposed on elements of the rack structure during OBE and DBE simulations. Material and fluid damping due to fluid viscosity are conservatively neglected. The dynamic model has the provision to incorporate form drag effects; however, no form drag has been used for this analysis.

6.5.5 Impact

Any fuel assembly node (e.g., 2*) may impact the corresponding structural mass node 2. To simulate this impact, four compression-only gap elements around each rattling fuel assembly

node are provided (see Figure 6.5.3). The compressive loads developed in these springs provide the necessary data to evaluate the integrity of the cell wall structure and stored array during the seismic event. Figure 6.5.2 shows the location of the impact springs used to simulate any potential for inter-rack or rack-to-wall impacts. Sub-section 6.6 gives more details on these additional impact springs. Since there are five rattling masses, a total of 20 impact springs are used to model fuel assembly-cell wall impact.

6.6 Assembly of the Dynamic Model

The cartesian coordinate system associated with the rack has the following nomenclature:

- x = Horizontal coordinate along the short direction of rack rectangular planform
- y = Horizontal coordinate along the long direction of the rack rectangular planform
- z = Vertical coordinate upward from the rack base

Table 6.6.1 lists all spring elements used in the 3-D single rack analysis.

If the simulation model is restricted to two dimensions (one horizontal motion plus vertical motion, for example) for the purposes of model clarification only, then a descriptive model of the simulated structure which includes gap and friction elements is shown in Figure 6.6.1.

The impacts between fuel assemblies and rack show up in the gap elements, having local stiffness K_I, in Figure 6.6.1. In Table 6.6.1, gap elements 5 through 8 are for the vibrating mass at the

top of the rack. The support leg spring rates K_S are modeled by elements 1 through 4 in Table 6.6.1. Note that the local compliance of the concrete floor is included in K_S. To simulate sliding potential, friction elements 2 plus 8 and 4 plus 6 (Table 6.6.1) are shown in Figure 6.6.1. The friction of the support/liner interface is modeled by a piecewise linear spring with a suitably large stiffness K_f up to the limiting lateral load, μN, where N is the current compression load at the interface between support and liner. At every time step during the transient analysis, the current value of N (either zero for lift-off condition, or a compressive finite value) is computed. Finally, the support rotational friction springs K_R reflect any rotational restraint that may be offered by the foundation. This spring rate is calculated using a modified Bousinesq equation and is included to simulate the resistive moment of the support to counteract rotation of the rack leg in a vertical plane. This rotation spring is also nonlinear, with a zero spring constant value assigned after a certain limiting condition of slab moment loading is reached.

The nonlinearity of these springs (friction elements 9, 11, 13, and 15 in Table 6.6.1) reflects the edging limitation imposed on the base of the rack support legs and the shifts in the centroid of load application as the rack rotates. If this effect is neglected, any support leg bending, induced by liner/baseplate friction forces, is resisted by the leg acting as a beam cantilevered from the rack baseplate. This leads to higher predicted loads at the support leg - baseplate junction than if the moment resisting capacity due to floor elasticity at the floor is included in the model.

The spring rate K_S, modeling the effective compression stiffness of the structure in the vicinity of the support, is computed from the equation:

The spring rate K_S, modeling the effective compression stiffness of the structure in the vicinity of the support, is computed from the equation:

$$\frac{1}{K_S} = \frac{1}{K_1} + \frac{1}{K_2} + \frac{1}{K_3}$$

where:

K_1 = spring rate of the support leg treated as a tension-compression member

K_2 = local spring rate of pool slab

K_3 = spring rate of folded plate cell structure above support leg

As described in the preceding section, the rack, along with the base, supports, and stored fuel assemblies, is modeled for the general three-dimensional (3-D) motion simulation by a twenty-two degree of freedom model. To simulate the impact and sliding phenomena expected, up to 64 nonlinear gap elements and 16 nonlinear friction elements are used. Gap and friction elements, with their connectivity and purpose, are also presented in Table 6.6.1. Table 6.6.2 lists representative values for a module used in the single rack dynamic simulations.

For the 3-D simulation of a single rack, all support elements (described in Table 6.6.1) are included in the model. Coupling between the two horizontal seismic motions is provided both by any offset of the fuel assembly group centroid which causes the rotation of the entire rack and/or by the possibility of lift-off of one or more support legs. The potential exists for the rack to be supported on one or more support legs during any instant of a complex 3-D seismic event. All of these potential events may be

simul ed during a 3-D motion so that a mechanism exists in the model to simulate the real behavior.

6.7 Time Integration of the Equations of Motion

6.7.1 Time-History Analysis Using Multi-Degree of Freedom Rack Model

Having assembled the structural model, the dynamic equations of motion corresponding to each degree of freedom are written by using Lagrange's Formulation. The system kinetic energy can be constructed including contributions from the solid structures and from the trapped and surrounding fluid. A single rack is modelled in detail. The system of equations can be represented in matrix notation as:

$$[M] \{q''\} = \{Q\} + \{G\}$$

where:

- $[M]$ - total mass matrix;
- $\{q\}$ - the nodal displacement vector relative to the pool slab displacement; double prime stands for secondary derivations;
- $\{G\}$ - a vector dependent on the given ground acceleration;
- $\{Q\}$ - a vector dependent on the spring forces (linear and non-linear) and the coupling between masses.

The equation can be rewritten as

$$\{q''\} = [M]^{-1} \{Q\} + [M]^{-1} \{G\}$$

As noted earlier, in the numerical simulations run to verify structural integrity during a seismic event, the rattling fuel assemblies are assumed to move in phase. This will provide maximum impact force level, and induce additional conservatism in the time-history analysis.

This equation set is mass uncoupled, displacement coupled at each instant in time, and is ideally suited for numerical solution using a central difference scheme. The proprietary, USNRC accepted, computer program "DYNARACK"* is utilized for this purpose.

Stresses in various portions of the structure are computed from known element forces at each instant of time and the maximum value of critical stresses over the entire simulation is reported in summary form at the end of each run.

In summary, dynamic analysis of typical multi-cell racks has shown that the motion of the structure is captured almost completely by the behavior of a twenty-two degree of freedom structure; therefore, in this analysis model, the movement of the rack cross-section at any height is described in terms of the rack degrees of freedom ($q_1(t),...q_6(t)$ and q_{17}-$q_{22}(t)$). The remaining degrees of freedom are associated with horizontal movements of the fuel assembly masses. In this dynamic model, five rattling masses are used to represent fuel assembly movement in the horizontal

---

* This code has been previously utilized in licensing of similar racks for Enrico Fermi Unit 2 (USNRC Docket No. 50-341), Quad Cities 1 and 2 (USNRC Docket Nos. 50-254 and 265), Rancho Seco (USNRC Docket No. 50-312), Oyster Creek (USNRC Docket No. 50-219), V.C. Summer (USNRC Docket No. 50-395), and Diablo Canyon 1 and 2 (USNRC Docket Nos. 50-275 and 50-323), St. Lucie Unit I (USNRC Docket No. 50-335), Byron Units I and II (USNRC Docket Nos. 50-454, 50-455), Vogtle 2 (USNRC Docket 50-425), and Millstone Unit 1 (USNRC Docket 50-245), Indian Point Unit 2 (USNRC Docket No. 50-247), among others.

plane. Therefore, the final dynamic model consists of twelve degrees of freedom for the rack plus ten additional mass degrees of freedom for the five rattling masses. The totality of fuel mass is included in the simulation and is distributed among the five rattling masses.

6.7.2 Evaluation of Potential for Inter-Rack Impact

Since racks are usually closely spaced, the simulation includes impact springs to model the potential for inter-rack impact. To account for this potential, yet still retain the simplicity of simulating only a single rack, gap elements are located on the rack at the top and at the baseplate level. Fig. 6.5.2 shows the location of these gap elements. The baseplate location is a designated potential impact region, and the impact springs located in this region are expected to register impact loads. However, the impact is disallowed in the cellular region of the racks. Therefore, the impact springs located at the top must not indicate any loads at any time during the seismic event.

6.8 Structural Acceptance Criteria

There are two sets of criteria to be satisfied by the rack modules:

a. Kinematic Criterion

This criterion seeks to ensure that the rack is a physically stable structure. The racks are designed to preclude inter-rack impacts in the cellular region. Therefore, physical stability of the rack is considered along with the criterion that inter-rack impact or rack-to-wall impacts in the cellular region do not occur.

b. Stress Limits

The stress limits of the ASME Code, Section III, Subsection NF, 1989 Edition are used. The following loading combinations are applicable (Ref. 6.1.2) and are consistent with the plant UFSAR commitments.

Loading Combination	Stress Limit
$D + L$ $D + L + T_o$ $D + L + T_o + E$	Level A service limits
$D + L + T_a + E$ $D + L + T_o + P_f$	Level B service limits
$D + L + T_a + E'$ $D + L + F_d$	Level D service limits The functional capability of the fuel racks should be demonstrated.

The abbreviations in the table are those used in Section 3.8.4 of the Standard Review Plan and the "Review and Acceptance of Spent Fuel Storage and Handling Applications":

D = Dead weight-induced internal moments (including fuel assembly weight)

L = Live Load (not applicable for the fuel rack, since there are no moving objects in the rack load path).

F_d = Force caused by the accidental drop of the heaviest load from the maximum possible height.

P_f = Upward force on the racks caused by postulated stuck fuel assembly

E = Operating Basis Earthquake (OBE)

E' = Design Basis Earthquake (DBE)

T_o = Differential temperature induced loads (normal operating or shutdown condition based on the most critical transient or steady state condition).

T_a = Differential temperature induced loads (the highest temperature associated with the postulated abnormal design conditions).

The conditions T_a and T_o cause local thermal stresses to be produced. For fuel rack analysis, only one scenario need be examined. The worst situation will be obtained when an isolated storage location has a fuel assembly which is generating heat at the maximum postulated rate. The surrounding storage locations are assumed to contain no fuel. The heated water makes unobstructed contact with the inside of the storage walls, thereby producing the maximum possible temperature difference between the adjacent cells. The secondary stresses thus produced are limited to the body of the rack; that is, the support legs do not experience the secondary (thermal) stresses. For rack qualification, T_o, T_a are the same.

6.9 Material Properties

The data on the physical properties of the rack and support materials, obtained from the ASME Boiler & Pressure Vessel Code, Section III, appendices, are listed in Table 6.9.1. Since the maximum pool bulk temperature is less than 200°F, this is used as the reference design temperature for evaluation of material properties.

6.10 Stress Limits for Various Conditions

The following stress limits are derived from the guidelines of the ASME Code, Section III, Subsection NF [6.1.2], in conjunction with the material properties data of the preceding section. All parameters and terminology are in accordance with the Code.

6.10.1 Normal and Upset Conditions (Level A or Level B)

a. Allowable stress in tension on a net section = $F_t = 0.6\ S_y$ (S_y = yield stress at temperature)

$F_t = (0.6)\ (25,000) = 15,000$ psi (rack material)

F_t = is equivalent to primary membrane stresses
$F_t = (.6)\ (25,000) = 15,000$ psi (upper part of support feet)

$= (.6)\ (106,300) = 63,780$ psi (lower part of support feet)

b. On the gross section, allowable stress in shear is:

$F_v = .4\ S_y$
$(.4)\ (25,000) = 10,000$ psi (main rack body)

$F_t = (.4)\ (25,000) = 10,000$ psi (upper part of support feet)

$= (.4)\ (106,300) = 42,520$ psi (lower part of support feet)

c. Allowable stress in compression, F_a:

$$F_a = \frac{\left[1 - \frac{(kl)^2}{r^2} / 2C_c^2\right] S_y}{\left\{\left(\frac{5}{3}\right) + \left[3\left(\frac{kl}{r}\right) / 8C_c\right] - \left[\left(\frac{kl}{r}\right)^3 / 8C_c^3\right]\right\}}$$

where:

$$C_c = \left[\frac{(2\pi^2 E)}{S_y}\right]^{1/2}$$

l = unsupported length of component

k = length coefficient which gives influence of boundary conditions; e.g.

k = 1 (simple support both ends)
= 1/2 (cantilever beam)
= 2 (clamped at both ends)

E = Young's Modulus

r = radius of gyration of component

kl/r for the main rack body is based on the full height and cross section of the honeycomb region. Substituting numbers, we obtain, for both support leg and honeycomb region:

F_a = 15,000 psi (main rack body)
F_a = 15,000 psi (upper part of support feet)
= 63,780 psi (lower part of support feet)

d. Maximum allowable bending stress at the outermost fiber due to flexure about one plane of symmetry:

$F_b = 0.60\ S_y$ = 15,000 psi (rack body)
F_b = 15,000 psi (upper part of support feet)
= 63,780 psi (lower part of support feet)

e. Combined flexure and compression:

$$\frac{f_a}{F_a} + \frac{C_{mx}\, f_{bx}}{D_x F_{bx}} + \frac{C_{my} f_{by}}{D_y F_{by}} < 1$$

where:

f_a = Direct compressive stress in the section

f_{bx} = Maximum flexural stress along x-axis

f_{by} = Maximum flexural stress along y-axis

$C_{mx} = C_{my} = 0.85$

$$D_x = 1 - \frac{f_a}{F'_{ex}}$$

$$D_y = 1 - \frac{f_a}{F'_{ey}}$$

$$F'_{ex,ey} = \frac{12\ \pi^2 E}{23 \left(\frac{kl}{r}\right)_{x,y}}$$

and the subscripts x,y reflect the particular bending plane of interest.

f. Combined flexure and compression (or tension):

$$\frac{f_a}{0.6S_y} + \frac{f_{bx}}{F_{bx}} + \frac{f_{by}}{F_{by}} < 1.0$$

The above requirement should be met for both the direct tension or compression case.

6.10.2 Level D Service Limits

Section F-1370 (ASME Section III, Appendix F), states that the limits for the Level D condition are the minimum of 1.2 (S_y/F_t) or ($0.7S_u/F_t$) times the corresponding limits for Level A condition. S_u is the ultimate tensile stress at 200°F per Table 6.9.1. Since 1.2 S_y is greater than 0.7 S_u for the lower part of the support feet, the limit is 1.54 for the lower section under DBE conditions. The limit for the upper portion of the support foot is 2.0 under DBE conditions.

Instead of tabulating the results of the different stresses as dimensioned values, they are presented in a dimensionless form. These dimensionless stress factors are defined as the ratio of the actual developed stress to its specified limiting value. With this definition, the limiting value of each stress factor is 1.0 for the OBE and 2.0 (or 1.54) for the DBE condition.

6.11 Results for the Analysis of Spent Fuel Racks Using a Single Rack Model and 3-D Seismic Motion

A complete synopsis of the analysis of the single rack, subject to the postulated earthquake motions, is presented in a summary Table 6.11.1 which gives the bounding values of stress factors R_i (i = 1... 7). The stress factors are defined as:

R_1 = Ratio of direct tensile or compressive stress on a net section to its allowable value (note support feet only support compression)

R_2 = Ratio of gross shear on a net section in the x-direction to its allowable value

R_3 = Ratio of maximum bending stress due to bending about the x-axis to its allowable value for the section

R_4 = Ratio of maximum bending stress due to bending about the y-axis to its allowable value

R_5 = Combined flexure and compressive factor (as defined in 6.10.1e above)

R_6 = Combined flexure and tension (or compression) factor (as defined in 6.10.1f)

R_7 = Ratio of gross shear on a net section in the y-direction to its allowable value.

As stated before, the allowable value of R_i (i =1,2,3,4,5,6,7) is 1 for the OBE condition and 2 for the DBE (except for the lower section of the support where the factor is 1.54)

The dynamic analysis gives the maximax (maximum in time and in space) values of the stress factors at critical locations in the rack module. Values are also obtained for maximum rack displacements and for critical impact loads. Table 6.11.1 presents critical results for the stress factors, and for rack-to-fuel impact load. Table 6.11.2 presents maximum results for horizontal displacements at the top and bottom of the rack in the x and y direction. For single rack simulations "x" is always the short direction of the rack. In Table 6.11.2, for each run, both the maximum value of the sum of all support foot loadings (4 supports) as well as the maximum value on any single foot is reported. The table also gives values for the maximum vertical load and the corresponding net shear force at the liner at essentially the same time instant, and for the maximum net shear load and the corresponding vertical force at a support foot at essentially the same time instant.

The results presented in Tables 6.11.1 and 6.11.2 represent the totality of single rack runs carried out. The critical case for structural integrity calculations is included. Displacements at the baseplate level are minimal.

The single rack analysis for run A04 gave the highest stress factors for subsequent structural integrity calculations. Subsequent to the detailed analysis, pedestals adjacent to the pool walls were relocated from the corner cell to new locations 2 cells inboard from the edge. Since this relocation could affect the conclusions concerning rack structural integrity, the critical case of run A04 was re-considered using the new pedestal locations. The results of that re-analysis are presented in the tables as run A94. The detailed structural integrity computations reported herein are based on the critical case for the loading scenario investigated. Subsequent Whole Pool Multi-Rack analyses are also based on the final pedestal locations.

The results corresponding to DBE give the highest load factors. The critical load factors reported for the support feet are all for the upper segment of the foot for DBE simulations and are to be compared with the limiting value of 2.0. Results for the lower portion of the support foot are not critical and are not reported in the tables.

Analyses show that significant margins of safety exist against local deformation of the fuel storage cell due to rattling impact of fuel assemblies.

Overturning has also been considered. This has been done by assuming a multiplier of 1.5 on the DBE horizontal earthquakes (more conservative than required by the USNRC Standard Review Plan) and checking predicted displacements. The horizontal displacements do not grow to such an extent as to imply any possibility for overturning.

It is noted that the analyses of the Donald C. Cook plant fuel racks have included some asymetrically loaded racks. The results of these studies can be used as bounding analyses for the case when a rack module is picked up and relocated when loaded asymmetrically with fuel assemblies. The results presented herein indicate that twisting or deformation that would cause loss of function or violation of safety margins will not occur during a planned rack relocation.

6.12 Impact Analyses

6.12.1 Impact Loading Between Fuel Assembly and Cell Wall

The local stress in a cell wall is conservatively estimated from the peak impact loads obtained from the dynamic simulations. Plastic analysis is used to obtain the limiting impact load. The limit load is calculated as 3125 lbs. per cell which is much greater than the loads obtained from any of the simulations.

6.12.2 Impacts Between Adjacent Racks

All of the dynamic analyses assume, conservatively, that the racks are isolated. However, the displacements obtained from the dynamic analyses are less than 50% of the rack-to-rack spacing or rack-to-wall spacing if the pool is assumed fully populated.

Therefore, we conclude that no impacts between racks or between racks and walls occur during the DBE event. This has been further proven by the Whole Pool Multi-Rack Analysis discussed in Section 6.14.

6.13 Weld Stresses

Critical weld locations under seismic loading are at the bottom of the rack at the baseplate connection and at the welds on the support legs. Results from the dynamic analysis using the simulation codes are surveyed and the maximum loading is used to qualify the welds on these locations.

6.13.1 Baseplate to Rack Welds and Cell-to-Cell Welds

Ref. [6.1.2] (ASME Code Section III, Subsection NF) permits, for the DBE condition, an allowable weld stress $\tau = .42\ S_u = 29,820$ psi. Based on the worst case of all runs reported, the maximum weld stress for the baseplate to rack welds is 7605 psi for DBE conditions.

The weld between baseplate and support leg is checked using limit analysis techniques. The structural weld at that location is considered safe if the interaction curve between net force and moment is such that a derived function of F/F_y and M/M_y is below a limiting value of 1.0.

Fy, My are the limit load and moment under direct load only and direct moment only. F, M are the absolute values of the actual force and moments applied to the weld section. The calculated value is .637 < 1.0 based on the instantaneous peak loading. This value conservatively neglects any gussets in place to increase pedestal area and inertia.

The critical area that must be considered for cell-to-cell welds is the weld between the cells. This weld is discontinuous as we proceed along the cell length.

Stresses in the storage cell to storage cell welds develop along the length of each storage cell due to fuel assembly impact with the cell wall. This occurs if fuel assemblies in adjacent cells are moving out of phase with one another so that impact loads in two adjacent cells are in opposite directions which would tend to separate the channel from the cell at the weld. The critical load that can be transferred in this weld region for the DBE condition is calculated as 5273 lbs. at every fuel cell connection to adjacent cells. An upper bound to the load required to be transferred is 593 lbs. Where we have used a maximum impact load of 210 lbs. (obtained from Table 6.11.1), we have assumed two impact locations are supported by each weld region, and we have increased the load by $\sqrt{2}$ to account for 3-D effects.

6.13.2 Heating of an Isolated Cell

Weld stresses due to heating of an isolated hot cell are also computed. The assumption used is that a single cell is heated, over its entire length, to a temperature above the value associated with all surrounding cells. No thermal gradient in the

vertical direction is assumed so that the results are conservative. Using the temperatures associated with this unit, analysis shows that the weld stresses along the entire cell length do not exceed the allowable value for a thermal loading condition. Section 7 reports the value for this thermal stress.

6.14 Whole Pool Multi-Rack (WPMR) Analysis

The single rack 3-D simulations presented in the preceding sections demonstrate the structural integrity, physical stability, and kinematic compliance (no rack-to-rack impact in the cellular region) of the rack modules. However, as noted before, prescribing the motion of the racks adjacent to the module being analyzed introduces an assumption of unpredictable import in the single rack modules. For closely spaced racks, it is possible to demonstrate kinematic compliance only by modelling all rack modules in one comprehensive simulation which is referred to as Whole Pool Multi-Rack (WPMR) model. In the WPMR analysis, DBE seismic load is applied (Ref. 6.1.3) and all racks are assumed fully loaded with fuel assemblies. The primary intent of the analysis is to confirm structural integrity conclusions from 3-D single rack analysis and to ensure that hydrodynamic effects not able to be modelled in a single rack analysis do not cause unanticipated structural impacts.

The cross coupling effects due to the movement of fluid from one interstitial (inter-rack) space to the adjacent one is modelled using classical potential flow theory and Kelvin's circulation theorem. This formulation has been reviewed and approved by the Nuclear Regulatory Commission, during the post-licensing multi-rack analysis for Diablo Canyon Unit I and II reracking project. The coupling coefficients are based on a consistent modelling of

the fluid flow. While updating of the fluid flow coefficients, based on the current gap, is permitted in the algorithm, the analyses here are conservatively carried out using the constant nominal gaps that exist at the start of the seismic event.

Such a comprehensive WPMR model was prepared for the racks shown in the module layout drawing (Fig. 6.4.1). Computer code DYNARACK was used to perform the simulations.

In order to eliminate the last significant element of uncertainty in rack dynamic analyses, the friction coefficient was also ascribed to the support leg/pool bearing pad interface in a manner consistent with Rabinowicz's experimental data [6.4.1]. A set of friction coefficients were developed by a random number generator with Gaussian normal distribution characteristics. These random derived coefficients are imposed on each pedestal of each rack in the pool. The assigned values are then held constant during the entire simulation in order that the results are reproducible.

6.14.1 Multi-Rack Model

Figure 6.14.1 shows a planform view of the Donald C. Cook spent fuel pool. A rack and pedestal numbering scheme is set up in the figure. We set up a global x axis towards the East. Table 6.14.1 gives information on the number of cells per rack, and on the rack and fuel weights. All racks are assumed loaded with regular fuel. There are twenty-three racks in the pool. The cask area in the pool is modelled as a fictitious rack (Rack #24 in Figure 6.14.1). As noted previously, the presence of a fluid moving in the narrow gaps between racks and between racks and pool walls causes fluid coupling effects which cannot be modelled with a simulation using

only a single rack. Very simply, a single rack simulation can effectively include only the hydrodynamic effects due to contiguous racks when a certain set of assumptions is used for the motion of contiguous racks. In a multi-rack analysis the far field fluid coupling effects of all racks is accounted for using an appropriate model of the pool-rack fluid mechanics. For Donald C. Cook, the cask area was modelled assuming very large fluid gaps between racks 18 and 24 and between racks 23 and 24.

In the Whole Pool Multi-Rack analysis, used to investigate the interaction effects of all racks, we employ a reduced degree-of-freedom (RDOF) set for each rack plus its contained fuel. The purpose of the whole pool dynamic analysis, including the complete set of racks in the pool, is to determine whether effects, not able to be considered in a single rack analysis, alter any of the conclusions that are based on the results of the 22 DOF single rack analysis. In particular, the multi-rack analysis focusses on displacement excursions of each rack and on pedestal compressive loads. The Whole Pool Multi-Rack analysis is also utilized to investigate the possibility of impacts between racks or between racks and pool walls.

The reduced degree-of-freedom structural model for each rack is developed in a systematic way so that the important kinematic results from a dynamic analysis are in agreement with similar results from a solution obtained using the 22 DOF single rack model. The external hydrodynamic mass due to the presence of walls or adjacent racks is computed in a manner consistent with fundamental fluid mechanics principles and the use of a reduced

DOF fuel rack model [6.14.1]. The fluid flow model, used to obtain the whole pool hydrodynamic effect is site specific and reflects actual gaps and rack locations.

The whole pool multi-rack model includes many non-linear compression only gap elements. There are gap elements representing compression only pedestals (normally four pedestals are assumed for each rack), gap elements describing the impact potential of the fuel assembly-fuel rack interface, and gap elements tracking rack-to-rack or rack-to-wall impact potential at the top and bottom corners of the rack cell structure. In addition to the compression only gap elements, each pedestal has two friction springs associated with the compression spring. As noted previously, a random number generator is used to establish a friction coefficient for each pedestal at each instant when the pedestal is in contact with the liner.

The seismic excitation directions X and Y are shown in Figure 6.14.1. The critical DBE event that governs the behavior of the single rack analysis is applied to the 3-D multi-rack model in the appropriate directions. Three simulations have been carried out using coefficients of friction assumed to be 0.2, to be random with a mean of 0.5 at all pedestals, and to be 0.8, respectively.

6.14.2 Results of Multi-Rack Analysis

Tables 6.14.2 - 6.14.4 show the maximum corner absolute displacements at both the top and bottom of each rack in x and y directions from three multi-rack runs. In Table 6.14.5, the maximum displacements obtained from the three multi-rack simulations are compared with a single rack analysis. In all of

these tables, the results for fuel rack 24 can be ignored since there is no real rack at that location.

The absolute displacement values are higher than those obtained from single rack analysis. Thus, it appears essential to perform Whole Pool Multi-Rack analyses to verify that racks do not impact or hit the wall. Figures 6.14.2 - 6.14.5 show the time history of rack-to-rack gaps for the critical racks. It is shown that the rack-to-rack dynamic gaps are greater than 1.65" during a 15 second earthquake. Detailed examination of the rack-to-rack dynamic gaps show that the racks primarily move in-phase in all three simulations. That is, the entire assemblage of racks tends to move and minimize changes in rack-to-rack gaps.

Table 6.14.5 also presents peak pedestal compressive loads of all pedestals on the twenty-three real racks. In addition to a report of maximum pedestal loads, the time history of each pedestal load for each rack is archived for use in the structural evaluation of the fuel pool slab and the enveloping walls of the fuel pool.

It is noted that predicted maximum pedestal force from the multi-rack simulation giving the largest pedestal load (Run MP3 in Table 6.14.5) is lower than the result obtained from single rack analysis. The maximum instantaneous vertical foot load obtained from single rack analysis is 183300 lbs. From the Whole Pool Multi-Rack Run MP3, we find a peak single pedestal load of 180900 lbs. Because, detailed rack stress calculations are based on the single rack analysis results, no new structure concerns are identified by the scoping Whole Pool analysis and the overall structural integrity conclusions are confirmed.

6.15 Bearing Pad Analysis

To protect the slab from high localized dynamic loadings, bearing pads are placed between the pedestal base and the slab. Fuel rack pedestals impact on these bearing pads during a seismic event and the vertical pedestal loading is transferred to the liner. The bearing pad dimensions are set to ensure that the average pressure impacted to the slab surface due to a static load plus a dynamic impact load does not exceed the American Concrete Institute [6.15.1] limit on bearing pressures.

The time history results from the dynamic simulations for each pedestal are used to generate appropriate static and dynamic pedestal loads which are used to develop the bearing pad size.

From the whole pool multi-rack analysis, the worst case loading on a pedestal (instantaneous peak load) is 183,300 lbs. (see Table 6.14.5). For a 12" x 12" pad, this gives an average instanteous pressure p_a = 1273 psi.

Section 10.15 of [6.15.1] gives the design bearing strength as

$$f_b = \phi\ (.85\ f_c')\ \epsilon$$

where ϕ = .7 and f_c' = 3500 psi for Donald C. Cook. ϵ = 1 except when the supporting surface is wider on all sides than the loaded area. In that case, $\epsilon = (A_2/A_1)^{.5}$, but not more than 2. A_1 is the actual loaded area, and A_2 is an area greater than A_1 which is defined pictorially in the ACI commentary on Section 10.15. For Donald C. Cook, $1 \leq \epsilon \leq 2$; if we conservatively use ϵ = 1, then f_b = 2083 psi which is in excess of the calculated pressure p_a. Thus, significant margin is provided by the bearing pads.

6.16 References for Section 6

6.1.1 USNRC Standard Review Plan, NUREG-0800 (1981).

6.1.2 ASME Boiler & Pressure Vessel Code, Section III, Subsection NF, appendices (1989).

6.1.3 USNRC Regulatory Guide 1.29, "Seismic Design Classification," Rev. 3, 1978.

6.3.1 Holtec Proprietary Report - Verification and User's Manual, Report HI-89364, January, 1990.

6.4.1 "Friction Coefficients of Water Lubricated Stainless Steels for a Spent Fuel Rack Facility," Prof. Ernest Rabinowicz, MIT, a report for Boston Edison Company, 1976.

6.4.2 USNRC Regulatory Guide 1.92, "Combining Modal Responses and Spatial Components in Seismic Response Analysis," Rev. 1, February, 1976.

6.4.3 "The Component Element Method in Dynamics with Application to Earthquake and Vehicle Engineering," S. Levy and J.P.D. Wilkinson, McGraw Hill, 1976.

6.4.4 "Dynamics of Structures," R.W. Clough and J. Penzien, McGraw Hill (1975).

6.4.5 Holtec Proprietary Reports: User's Manual, Report HI-89343, Revision 0; Theory, Reports HI-87162, Revision 1, and HI-90439, Revision 0; Verification, Report HI-87161, Revision 2.

6.5.1 "Dynamic Coupling in a Closely Spaced Two-Body System Vibrating in Liquid Medium: The Case of Fuel Racks," K.P. Singh and A.I. Soler, 3rd International Conference on Nuclear Power Safety, Keswick, England, May 1982.

6.5.2 R.J. Fritz, "The Effects of Liquids on the Dynamic Motions of Immersed Solids," Journal of Engineering for Industry, Trans. of the ASME, February 1972, pp 167-172.

6.5.3 USNRC Regulatory Guide 1.61, "Damping Values for Seismic Design of Nuclear Power Plants," 1973.

6.14.1 "Fluid Coupling in Fuel Racks: Correlation of Theory and Experiment", by B. Paul, Holtec Report HI-88243.

6.15.1 ACI 318-89, ACI 318R-89, Building Code Requirements for Reinforced Concrete, American Concrete Institute, Detroit, Michigan, 1989.

Table 6.3.1

CORRELATION COEFFICIENT

	Value of ρ_{ij}	
Time History Group	DBE	OBE
N-S and E-W (1,2)	0.0146	0.1056
N-S to Vertical (1,3)	0.1269	0.0956
E-W to Vertical (2,3)	0.01016	0.1060

Table 6.5.1

DEGREES OF FREEDOM

Location (Node)	Displacement U_x	U_y	U_z	Rotation θ_x	θ_y	θ_z
1	P1	P2	P3	q4	q5	q6
2	P17	P18	P19	q20	q21	q22
	Point 2 is assumed attached to rigid rack at the top most point.					
2*	P7	P8				
3*	P9	P10				
4*	P11	P12				
5*	P13	P14				
1*	P15	P16				

where:

$p_i = q_i(t) + U_1(t)$ $\quad i = 1,7,9,11,13,15,17$

$= q_i(t) + U_2(t)$ $\quad i = 2,8,10,12,14,16,18$

$= q_i(t) + U_3(t)$ $\quad i = 3,19$

$U_i(t)$ are the 3 known earthquake displacements.

Table 6.6.1
NUMBERING SYSTEM FOR .P ELEMENTS AND FRICTION ELEMENTS

I. Nonlinear Springs (Gap Elements) (64 Total)

Number	Node Location	Description
1	Support S1	Z compression only element
2	Support S2	Z compression only element
3	Support S3	Z compression only element
4	Support S4	Z compression only element
5	2,2*	X rack/fuel assembly impact element
6	2,2*	X rack/fuel assembly impact element
7	2,2*	Y rack/fuel assembly impact element
8	2,2*	Y rack/fuel assembly impact element
9-24	Other rattling masses for nodes 1*, 3*, 4* and 5*	
25	Bottom cross-section of rack (around edge)	Inter-rack impact elements
.		Inter-rack impact elements
.		Inter-rack impact elements
.		Inter-rack impact elements
.		Inter-rack impact elements
.		Inter-rack impact elements
44		Inter-rack impact elements
45	Top cross-section of rack (around edge)	Inter-rack impact elements
.		Inter-rack impact elements
.		Inter-rack impact elements
.		Inter-rack impact elements
.		Inter-rack impact elements
.		Inter-rack impact elements
.		Inter-rack impact elements
64		Inter-rack impact elements

Table 6.6.1 (continued)

NUMBERING SYSTEM FOR GAP ELEMENTS AND FRICTION ELEMENTS

II. Friction Elements (16 total)

Number	Node Location	Description
1	Support S1	X direction friction
2	Support S1	Y direction friction
3	Support S2	X direction friction
4	Support S2	Y direction friction
5	Support S3	X direction friction
6	Support S3	Y direction friction
7	Support S4	X direction friction
8	Support S4	Y direction friction
9	S1	X Slab moment
10	S1	Y Slab moment
11	S2	X Slab moment
12	S2	Y Slab moment
13	S3	X Slab moment
14	S3	Y Slab moment
15	S4	X Slab moment
16	S4	Y Slab moment

Table 6.6.2

TYPICAL INPUT DATA FOR RACK ANALYSES (lb-inch units)

Support Foot Spring Constant K_s (#/in.)	4.91×10^6
Frictional Spring Constant K_f (#/in.)	1.837×10^9
Rack to Fuel Assembly Impact Spring Constant (#/in.)	1.38×10^5 (x-direction) 1.61×10^5 (y-direction)
Elastic Shear Spring for Rack (#/in.)	5.986×10^6 (x-direction) 4.866×10^6 (y-direction)
Elastic Bending Spring for Rack (#-in/in.)	5.458×10^{10} (x-z plane) 4.71×10^{10} (y-z plane)
Elastic Extensional Spring (#/in.)	4.074×10^7
Elastic Torsional Spring (#-in./in.)	1.322×10^9
Gaps (in.) (for hydrodynamic calculations)	

Table 6.9.1

RACK MATERIAL DATA (200°F)

Material	Young's Modulus E (psi)	Yield Strength S_y (psi)	Ultimate Strength S_u (psi)
304 S.S.	27.9×10^6	25000	71000
Section III Reference	Table I-6.0	Table I-2.2	Table I-3.2

SUPPORT MATERIAL DATA (200°F)

	Material			
1	SA-240, Type 304 (upper part of support feet)	27.9×10^6 psi	25,000 psi	71000 psi
2	SA-564-630 (age hardened at 1100°F)	27.9×10^6 psi	106,300 psi	140,000 psi

Table 6.11.1
STRESS FACTORS AND RACK-TO-FUEL IMPACT LOAD

Run	Remarks	Rack/Fuel Impact Load Per Cell at Worst Location Along Height Critical Location (lbs)	R_1	R_2	R_3	R_4	R_5	R_6	R_7
a03	DBE μ = .2 182 cells loaded with reg. fuel	180.2	.018 .274	.023 .074	.159 .167	.166 .161	.198 .417	.231 .442	.027* .078**
a04	DBE μ = .8 182 cells loaded with reg. fuel	179.6	.018 .284	.025 .079	.172 .214	.178 .172	.204 .431	.239 .460	.033 .095
a30	μ = 0.2 91 cells loaded with reg. fuel	190	.012 .181	.012 .046	.090 .118	.073 .106	.109 .281	.127 .299	.013 .052
a32	μ = 0.2 91 cells loaded with reg. fuel	209.8	.012 .176	.011 .045	.094 .112	.090 .110	.109 .271	.127 .289	.015 .049
a94	Same as a04 with relocated pedestals	174.8	.018 .325	.018 .056	.168 .250	.121 .118	.187 .483	.219 .522	.032 .113

* Upper values are for rack cell cross-section just above baseplate.
** Lower values are for support foot female cross-section just below attachment to baseplate.

Table 6.11.2
Rack Displacements and Support Loads
(all loads are in lbs.)

RUN		FLOOR LOAD (sum of all support feet) in a rack (lbs.)	MAXIMUM VERTICAL LOAD (1 foot) (lbs.)	MAXIMUM SHEAR* LOAD AND COINCIDENT VERTICAL LOAD	DX (in.)	DY** (in.)
a03	Full load μ = 0.2 DBE, Reg. Fuel	3.510×10^5	1.549×10^5	30212 (1.511×10^5)	.0609 .0084	.0562 .0105
a04	Full load μ = 0.8 DBE, Reg. Fuel	3.510×10^5	1.605×10^5	35832(9.791×10^4)	.0679 .0015	.0583 .0012
a30	Half load in Pos. x μ = 0.2 DBE, Reg. Fuel	1.883×10^5	1.021×10^5	20108(1.005×10^5)	.0520 .0019	.0450 .0008
a32	Half load in Pos. y μ = 0.2 DBE, Reg. Fuel	1.883×10^5	9.973×10^4	19389(9.71×10^4)	.0482 .0055	.0515 .0080
a94	Same as a04 with reloca-pedestals	3.508×10^5	1.833×10^5	44406 (1.4829×10^5)	.0678 .0014	.0778 .0018

* The value in parenthesis is the vertical load at the instant when the shear load is maximum. The maximum vertical and shear loads generally do not occur at the same instant.

** Upper values are top movements; lower values are baseplate movements (not necessarily at the same time).

Table 6.14.1

RACK NUMBERING AND WEIGHT INFORMATION

Rack No.	No. of Cells	Weight of Rack, lb.	Weight of Fuel Assembly, lb.
1	182	25700	1550
2	168	23700	1550
3	168	23700	1550
4	182	25700	1550
5	182	25700	1550
6	182	25700	1550
7	156	22500	1550
8	144	20900	1550
9	144	20900	1550
10	156	22500	1550
11	156	22500	1550
12	156	22500	1550
13	143	20800	1550
14	132	19300	1550
15	132	19300	1550
16	143	20800	1550
17	143	20800	1550
18	143	20800	1550
19	182	25700	1550
20	168	23700	1550
21	168	23700	1550
22	166	23900	1550
23	120	17700	1550
24*	0	0	0

* fictitious

Table 6.14.2

MAXIMUM DISPLACEMENTS FROM WPMR RUN MP1
(Friction Coefficient = 0.2)

rack	uxt	uyt	uxb	uyb
1	.7004E-01	.7756E-01	.6235E-01	.7303E-01
2	.7506E-01	.5227E-01	.6494E-01	.3936E-01
3	.8464E-01	.7521E-01	.6897E-01	.6619E-01
4	.5943E-01	.5218E-01	.4960E-01	.3597E-01
5	.5131E-01	.5306E-01	.4290E-01	.4496E-01
6	.6793E-01	.9512E-01	.5135E-01	.9095E-01
7	.4783E-01	.8928E-01	.3978E-01	.7830E-01
8	.4856E-01	.7065E-01	.3607E-01	.5917E-01
9	.4533E-01	.6377E-01	.3196E-01	.5192E-01
10	.3830E-01	.5754E-01	.2848E-01	.4354E-01
11	.4224E-01	.5336E-01	.3659E-01	.4329E-01
12	.6411E-01	.9620E-01	.4885E-01	.8429E-01
13	.7253E-01	.1079E+00	.6568E-01	.9505E-01
14	.4602E-01	.1114E+00	.3650E-01	.9847E-01
15	.3557E-01	.1079E+00	.2634E-01	.9325E-01
16	.3467E-01	.9211E-01	.2817E-01	.8608E-01
17	.5755E-01	.4429E-01	.5326E-01	.3140E-01
18	.1011E+00	.1301E+00	.8596E-01	.9693E-01
19	.6980E-01	.1125E+00	.6341E-01	.8575E-01
20	.8202E-01	.8680E-01	.6878E-01	.6048E-01
21	.8404E-01	.1455E+00	.6800E-01	.1229E+00
22	.8173E-01	.1057E+00	.7111E-01	.9050E-01
23	.5647E-01	.6598E-01	.4812E-01	.6156E-01

---

uxt=absolute value of maximum rack corner displacement in x-direction at rack top;
uyt=absolute value of maximum rack corner displacement in y-direction at rack top;
uxb=absolute value of maximum rack corner displacement in x-direction at rack baseplate;
uyb=absolute value of maximum rack corner displacement in y-direction at rack baseplate.

Table 6.14.3

MAXIMUM DI. LACEMENTS FROM WPMR RUN MP2
(Random Friction Coefficient)

rack	uxt	uyt	uxb	uyb
1	.6524E-01	.4772E-01	.3373E-01	.2303E-01
2	.1423E+00	.5829E-01	.1442E+00	.4598E-01
3	.1247E+00	.4122E-01	.1161E+00	.2566E-01
4	.1860E+00	.6628E-01	.1859E+00	.3161E-01
5	.1106E+00	.6379E-01	.1091E+00	.2673E-01
6	.9642E-01	.7250E-01	.8330E-01	.6348E-01
7	.4742E-01	.6267E-01	.3334E-01	.5443E-01
8	.1801E+00	.5755E-01	.1819E+00	.4534E-01
9	.1275E+00	.3974E-01	.1207E+00	.2115E-01
10	.2336E+00	.7640E-01	.2336E+00	.5527E-01
11	.1710E+00	.8644E-01	.1712E+00	.6245E-01
12	.4015E-01	.4740E-01	.2869E-01	.2678E-01
13	.1088E+00	.1034E+00	.1030E+00	.1040E+00
14	.1439E+00	.4029E-01	.1282E+00	.1865E-01
15	.6218E-01	.5620E-01	.6029E-01	.3386E-01
16	.3322E+00	.5413E-01	.3374E+00	.3677E-01
17	.1727E+00	.5385E-01	.1727E+00	.4896E-01
18	.1269E+00	.1958E+00	.1223E+00	.1913E+00
19	.8411E-01	.8106E-01	.6365E-01	.7508E-01
20	.8402E-01	.6480E-01	.5976E-01	.4419E-01
21	.1280E+00	.4742E-01	.1281E+00	.3530E-01
22	.8427E-01	.4951E-01	.7430E-01	.2335E-01
23	.2389E+00	.6471E-01	.2388E+00	.5758E-01

uxt=absolute value of maximum rack corner displacement in x-direction at rack top;
uyt=absolute value of maximum rack corner displacement in y-direction at rack top;
uxb=absolute value of maximum rack corner displacement in x-direction at rack baseplate;
uyb=absolute value of maximum rack corner displacement in y-direction at rack baseplate.

Table 6.14.4

MAXIMUM DISPLACEMENTS FROM WPMR RUN MP3
(Friction Coefficient=0.8)

rack	uxt	uyt	uxb	uyb
1	.2035E+00	.1702E+00	.1987E+00	.1774E+00
2	.2751E+00	.5173E-01	.2732E+00	.1658E-01
3	.2637E+00	.5740E-01	.2638E+00	.4010E-01
4	.1363E+00	.5449E-01	.1321E+00	.2788E-01
5	.1333E+00	.8237E-01	.1273E+00	.6876E-01
6	.1720E+00	.1514E+00	.1609E+00	.1617E+00
7	.2425E+00	.8747E-01	.2461E+00	.8782E-01
8	.1785E+00	.6039E-01	.1784E+00	.4260E-01
9	.1519E+00	.4434E-01	.1506E+00	.3129E-01
10	.8112E-01	.5007E-01	.7887E-01	.2883E-01
11	.1146E+00	.7975E-01	.1117E+00	.5071E-01
12	.1005E+00	.1602E+00	.9143E-01	.1601E+00
13	.1604E+00	.1310E+00	.1633E+00	.1073E+00
14	.7786E-01	.7618E-01	.7823E-01	.5953E-01
15	.8616E-01	.5521E-01	.8214E-01	.3148E-01
16	.9843E-01	.4780E-01	.1024E+00	.2903E-01
17	.8975E-01	.7115E-01	.9063E-01	.7056E-01
18	.1418E+00	.4416E+00	.1089E+00	.4526E+00
19	.1959E+00	.1720E+00	.1922E+00	.1806E+00
20	.2741E+00	.5563E-01	.2727E+00	.3118E-01
21	.2117E+00	.5159E-01	.2120E+00	.2287E-01
22	.2361E+00	.6081E-01	.2242E+00	.3986E-01
23	.1016E+00	.7703E-01	.1033E+00	.7364E-01

uxt=absolute value of maximum rack corner displacement in x-direction at rack top;
uyt=absolute value of maximum rack corner displacement in y-direction at rack top;
uxb=absolute value of maximum rack corner displacement in x-direction at rack baseplate;
uyb=absolute value of maximum rack corner displacement in y-direction at rack baseplate.

Table 6.14.5

MAXIMUM RACK DISPLACEMENT AND FOOT LOAD

Run	Remarks	Maximum Rack Corner Displacement inch	Maximum Foot Pedestal Force, lbs.
a94	Single Rack Analysis	0.0778	183,300
MP1	WPMR, μ = 0.2	0.1455 (Rack #21 in y)	157,400 (Rack #19, Foot 4)
MP2	WPMR, Random μ	0.3322 (Rack #16 in x)	170,900 (Rack #19, Foot 4)
MP3	WPMR, μ = 0.8	0.4416 (Rack #18 in y)	180,900 (Rack #5, Foot 2)

μ = friction coefficient

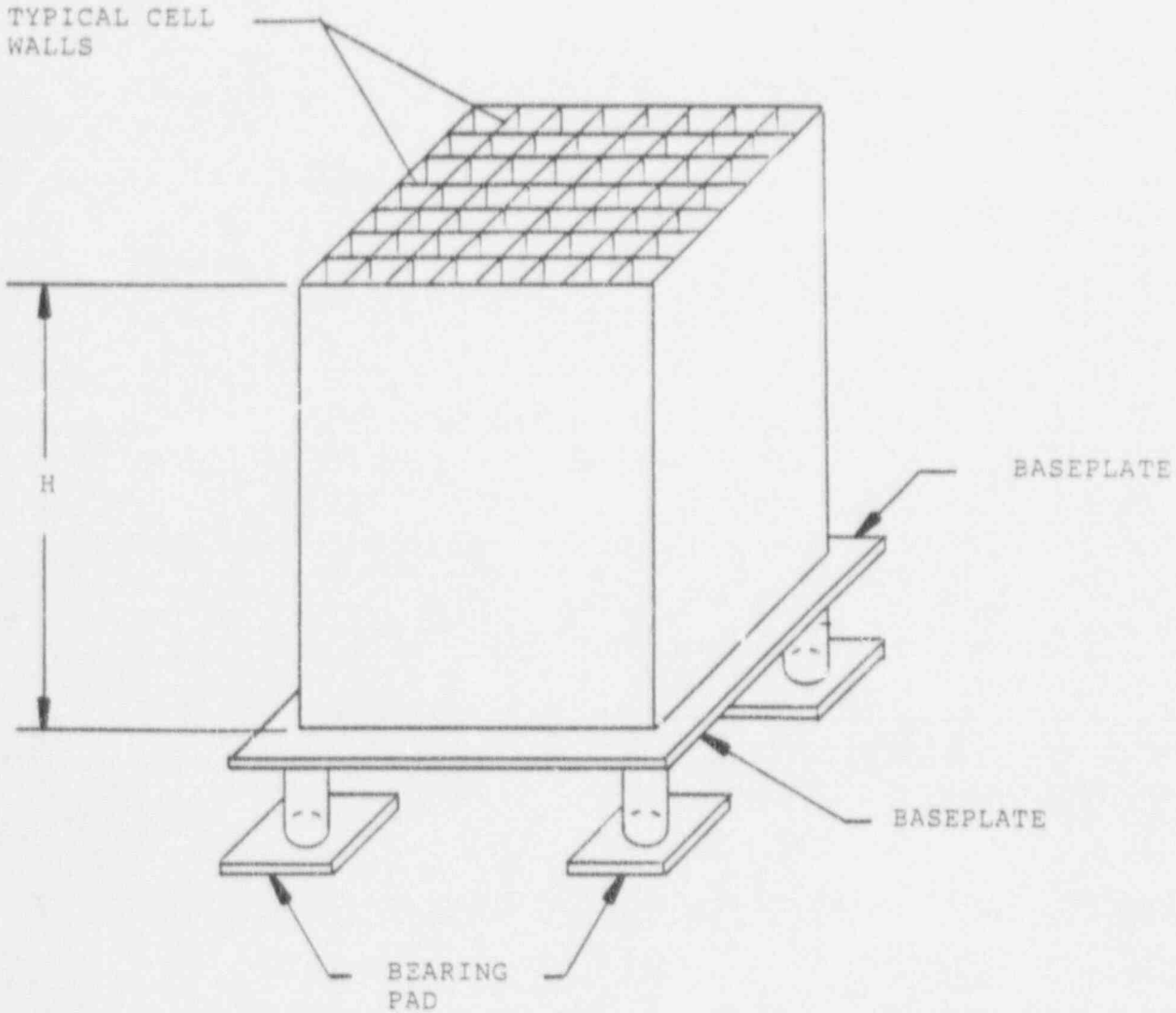

Figure 6.2.1 Pictorial View of Rack Structure

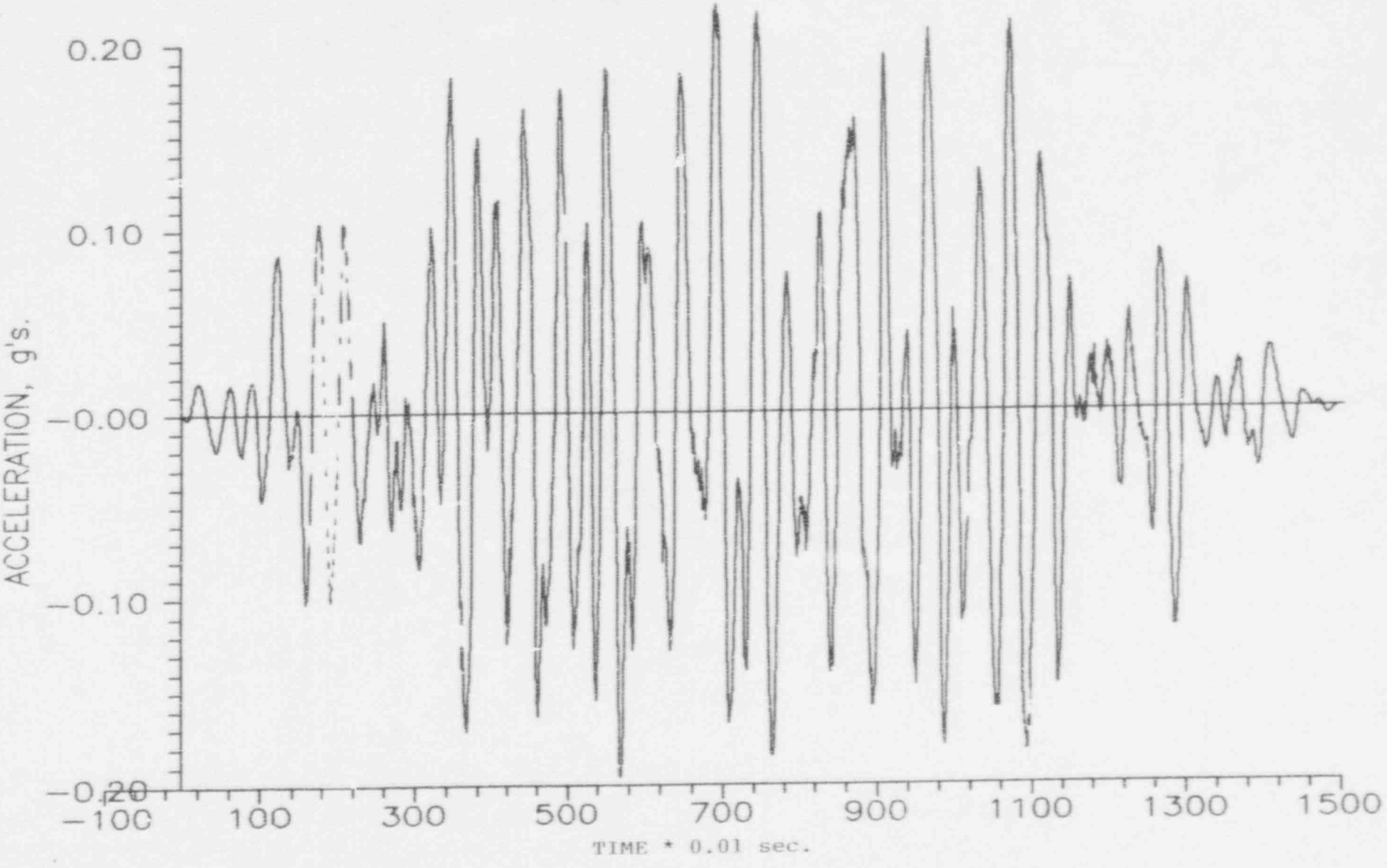

FIGURE 6.3.1 DBE - N-S ACCELERATION TIME-HISTORY

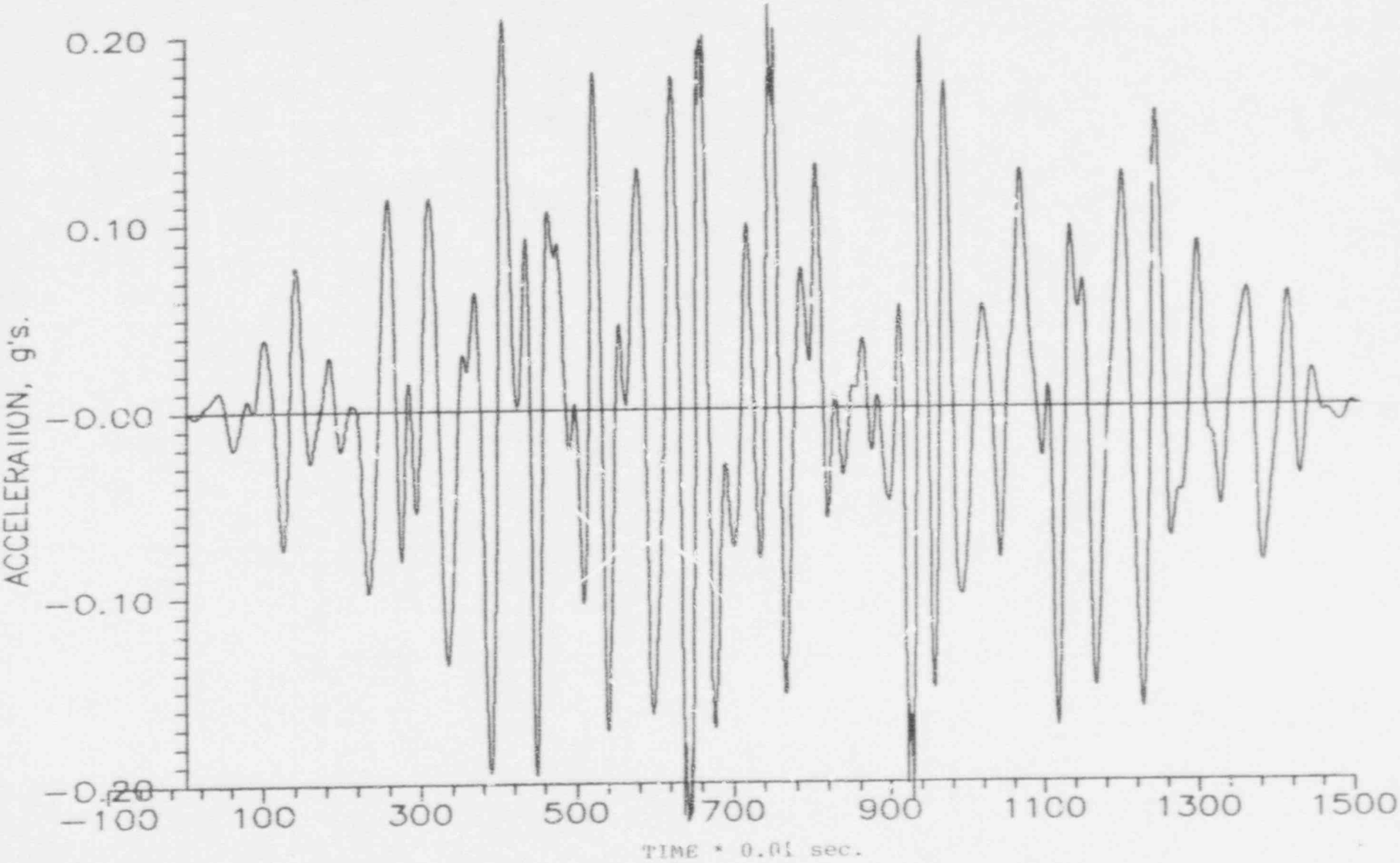

FIGURE 6.3.2 DBE E-W ACCELERATION TIME HISTORY

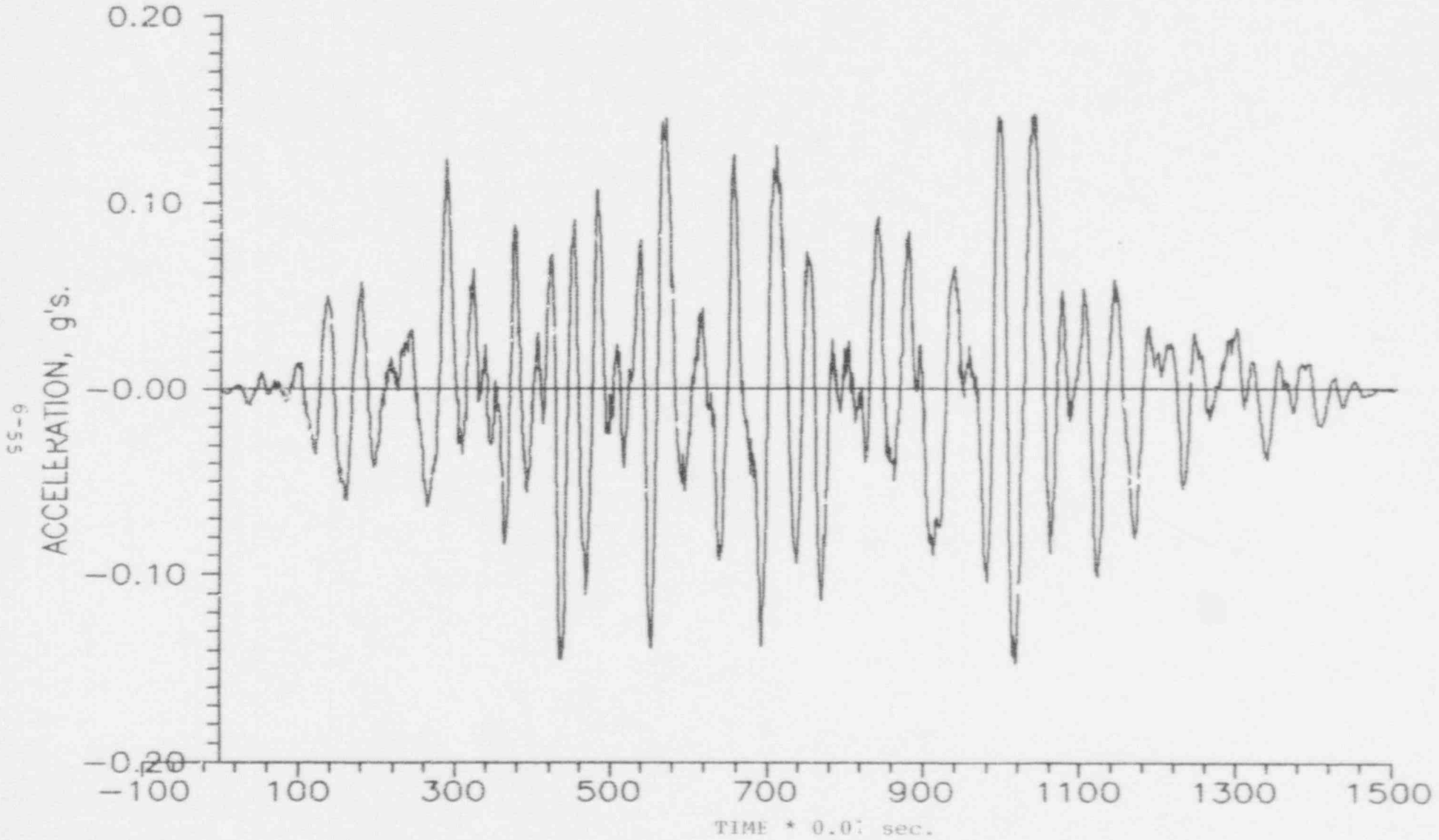

FIGURE 6.3.3 DBE - VERTICAL ACCELERATION TIME HISTORY

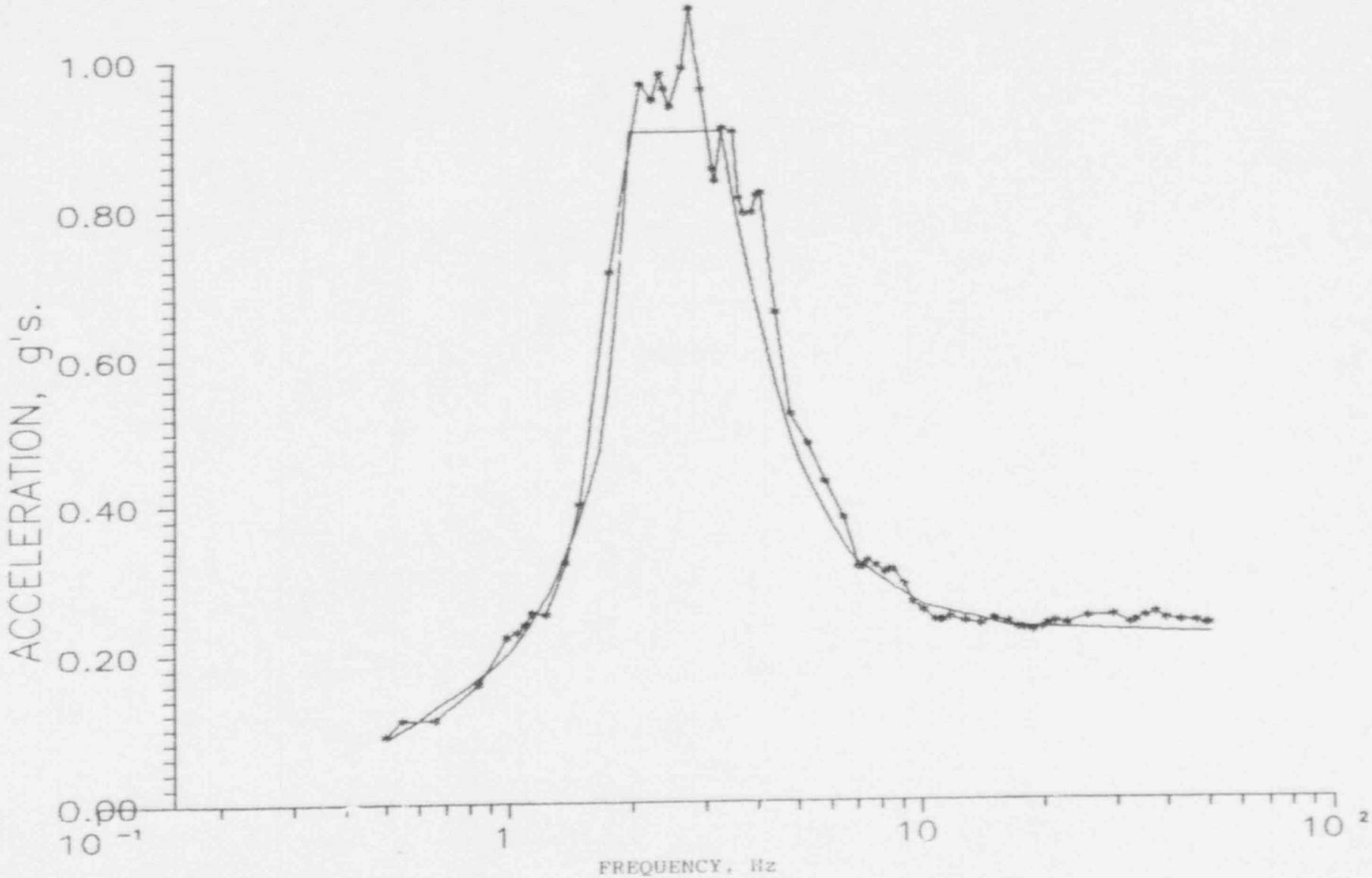

FIGURE 6.3.4 HORIZONTAL DESIGN SPECTRUM AND
N-S TIME HISTORY SPECTRUM (5% damping)

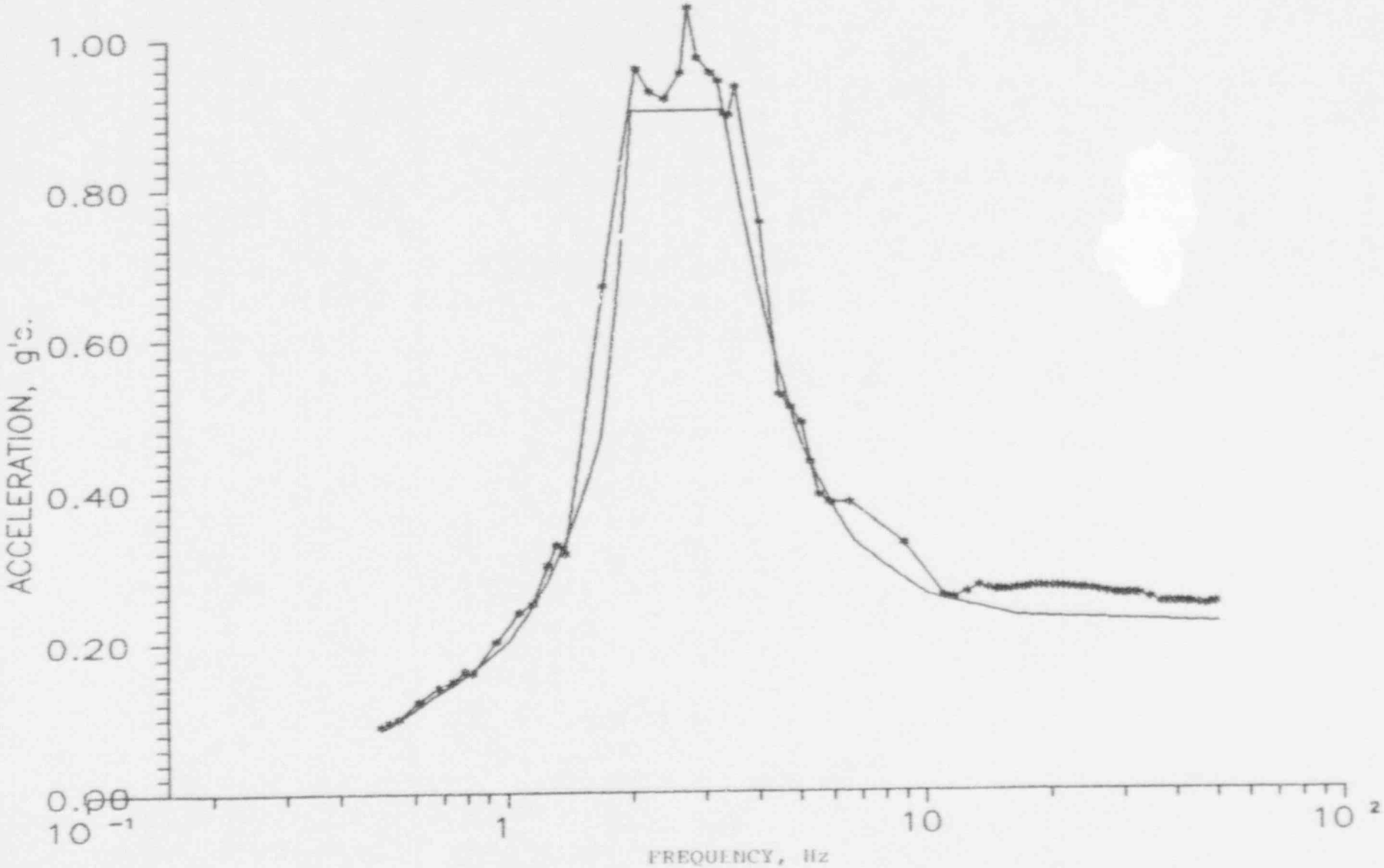

FIGURE 6.3.5 HORIZONTAL DESIGN SPECTRUM AND E-W TIME HISTORY SPECTRUM (5% damping)

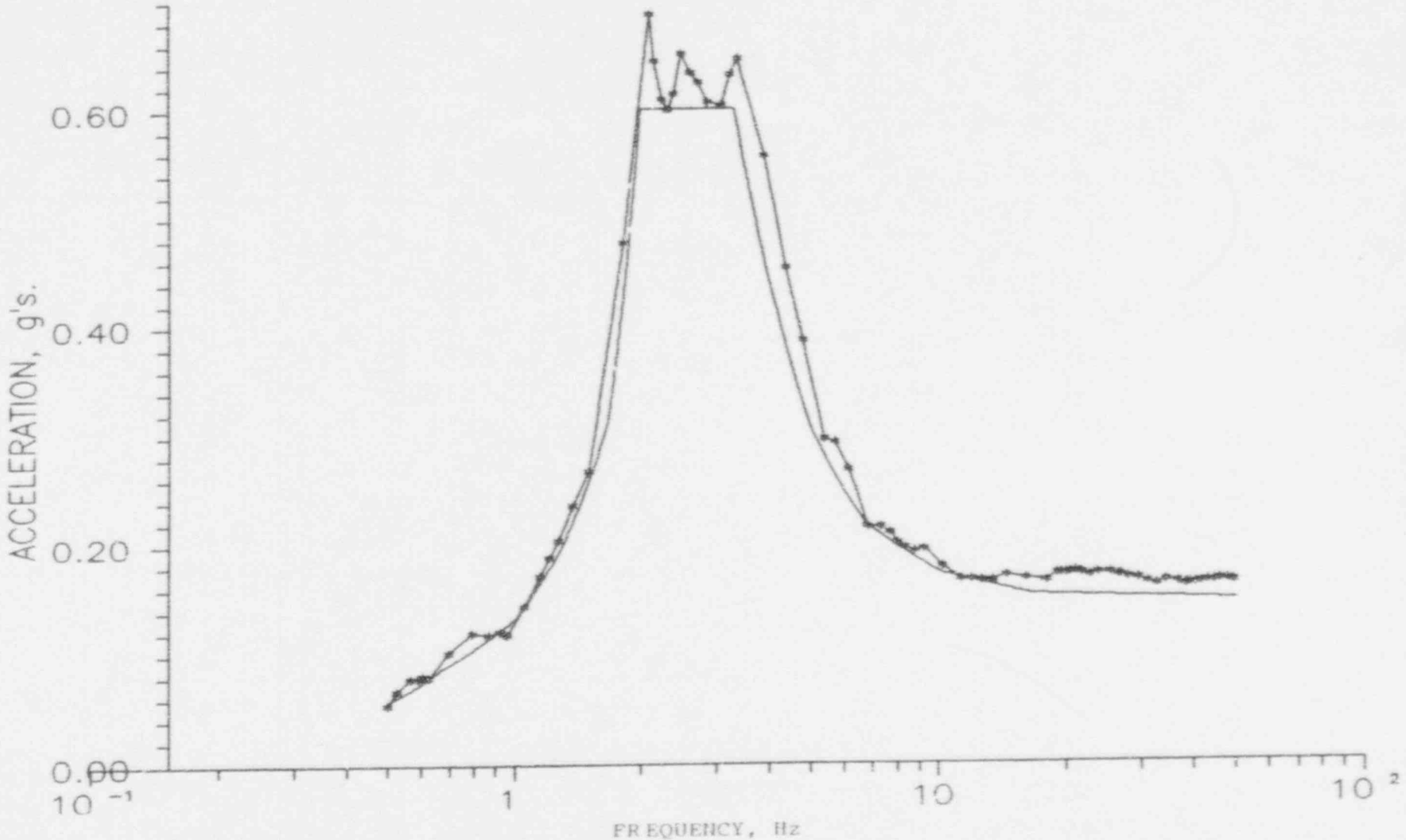

Figure 6.3.6 VERTICAL DESIGN AND TIME HISTORY DERIVED SPECTRA
(5% damping)

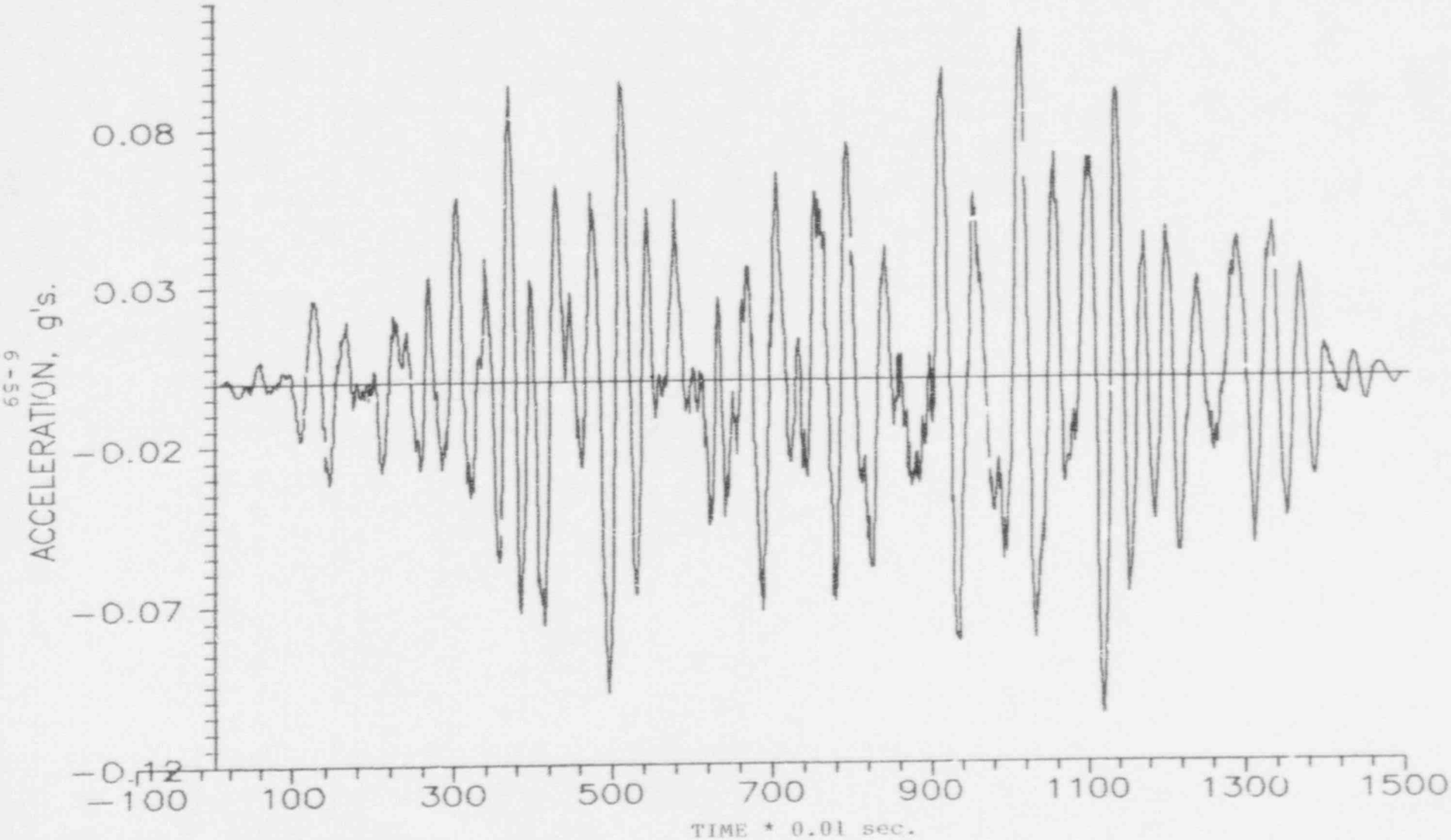

FIGURE 6.3.7 OBE - N-S ACCELERATION TIME HISTORY

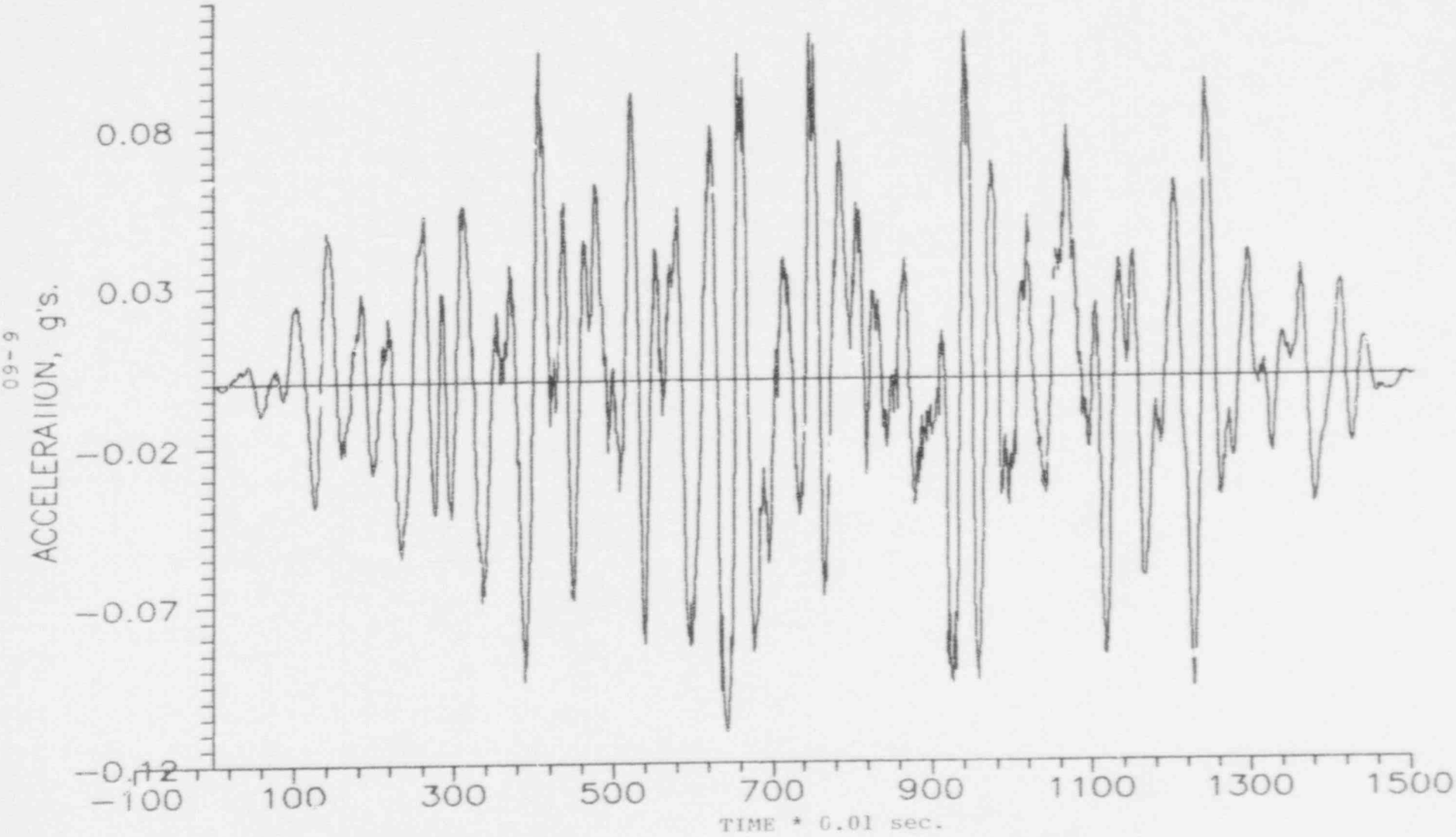

FIGURE 6.3.8 OBE - E-W ACCELERATION TIME HISTORY

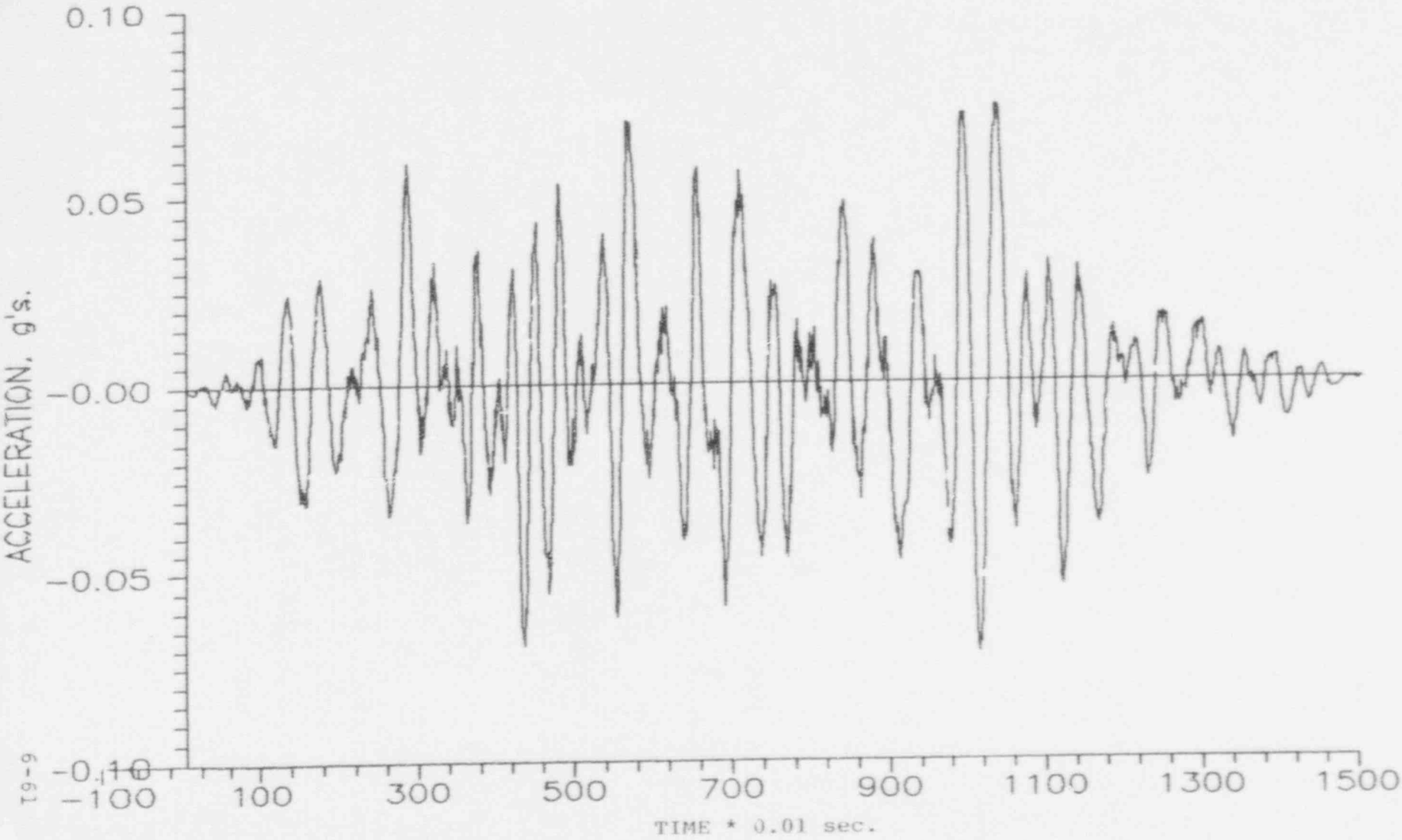

FIGURE 6.3.9 OBE - VERTICAL ACCELERATION TIME HISTORY

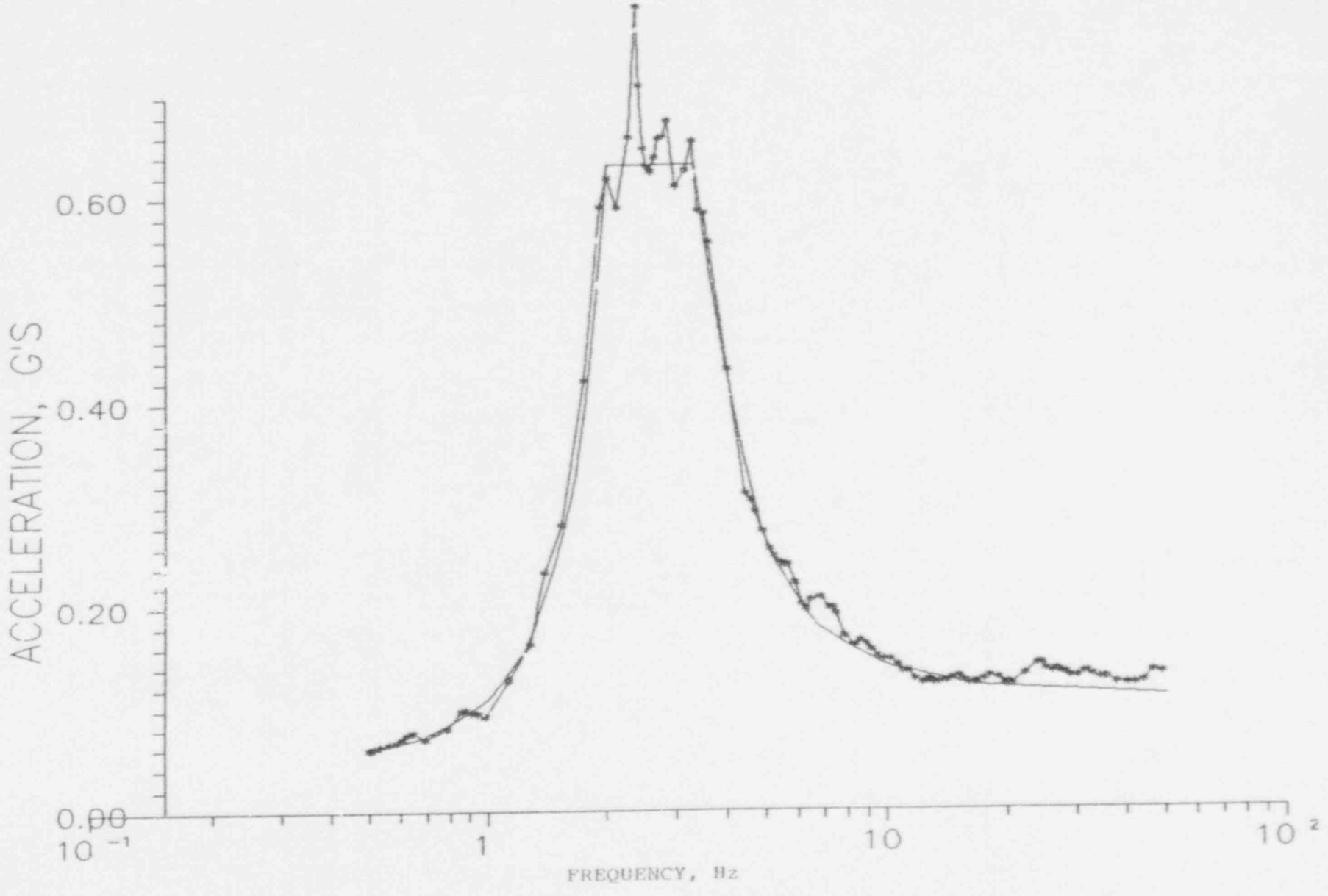

Figure 6.3.10 HORIZONTAL DESIGN SPECTRUM AND TIME HISTORY DERIVED N-S SPECTRUM (2% damping)

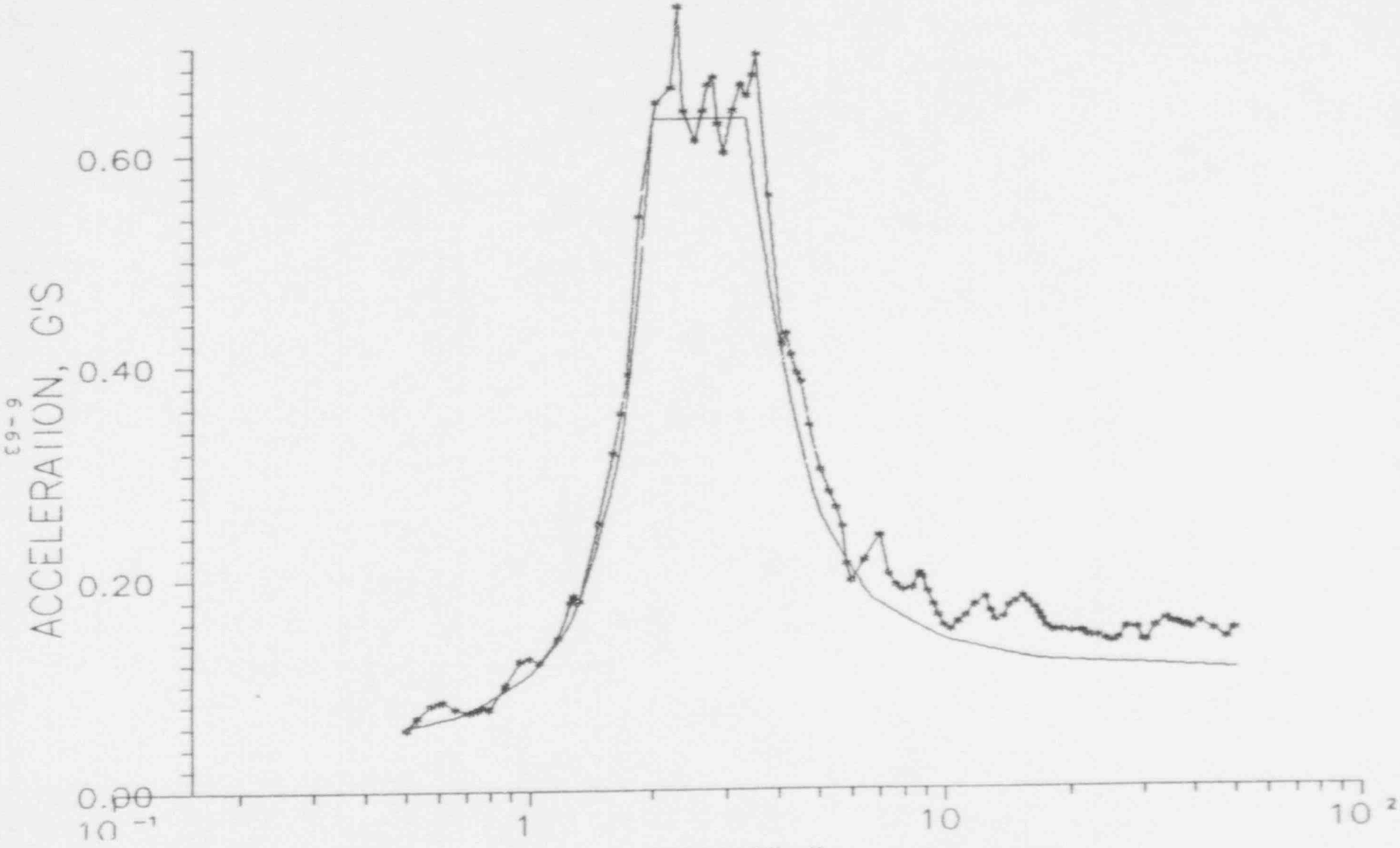

Figure 6.3.11 HORIZONTAL DESIGN SPECTRUM AND E-W TIME HISTORY'S DERIVED SPECTRUM (2% damping)

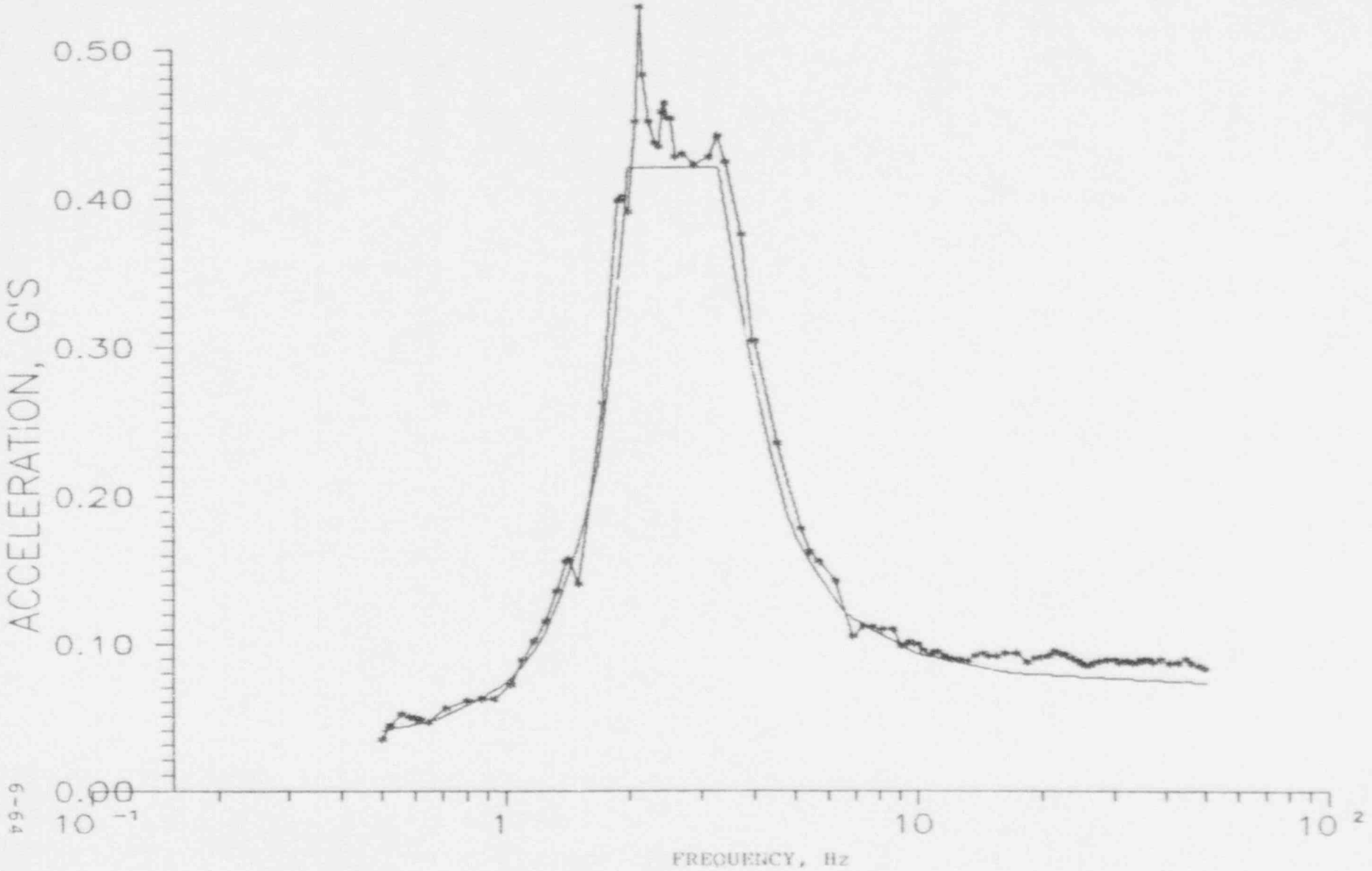

Figure 6.3.12 VERTICAL DESIGN AND TIME HISTORY DERIVED SPECTRA (2% damping)

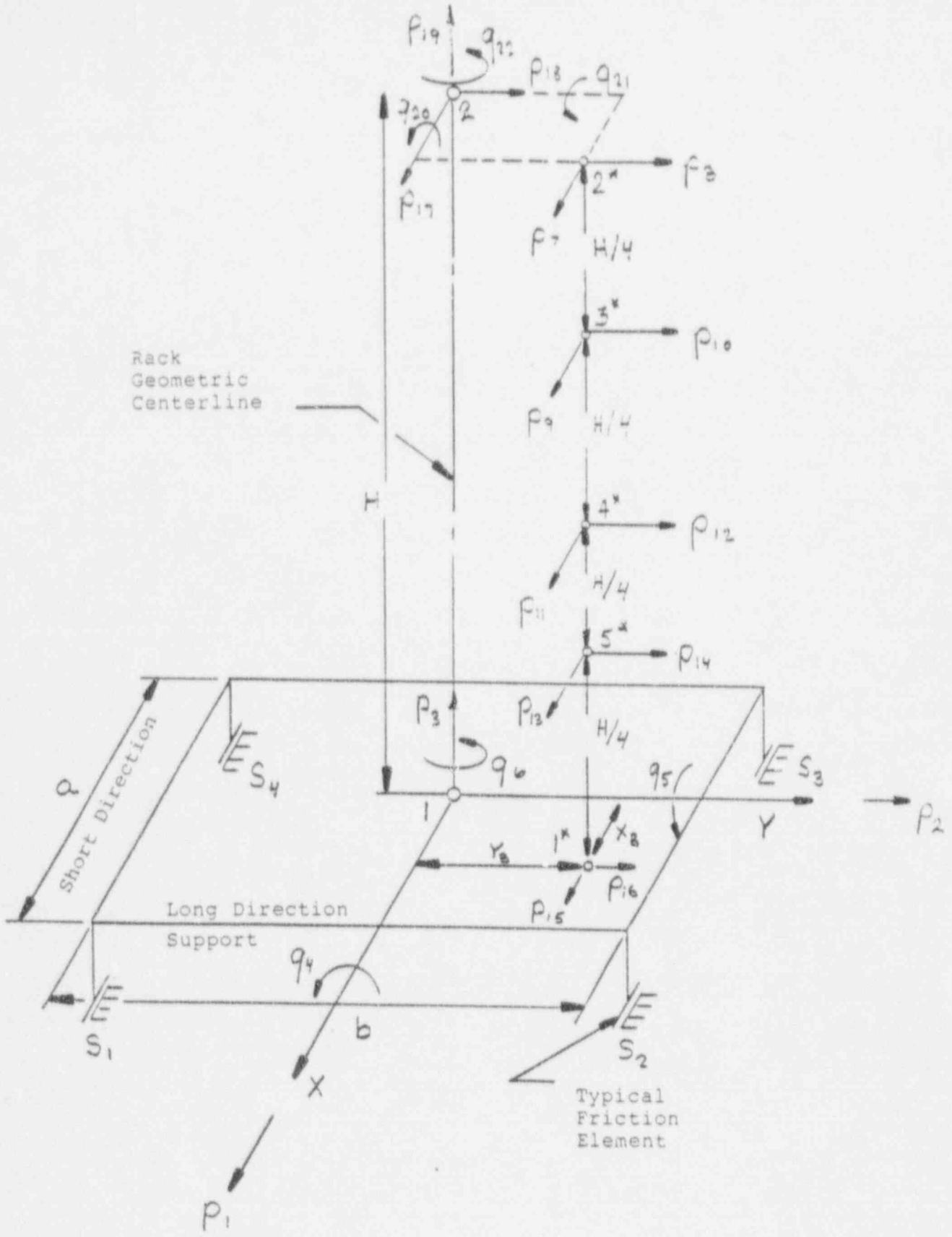

Figure 6.5.1 SCHEMATIC MODEL FOR DYNARACK

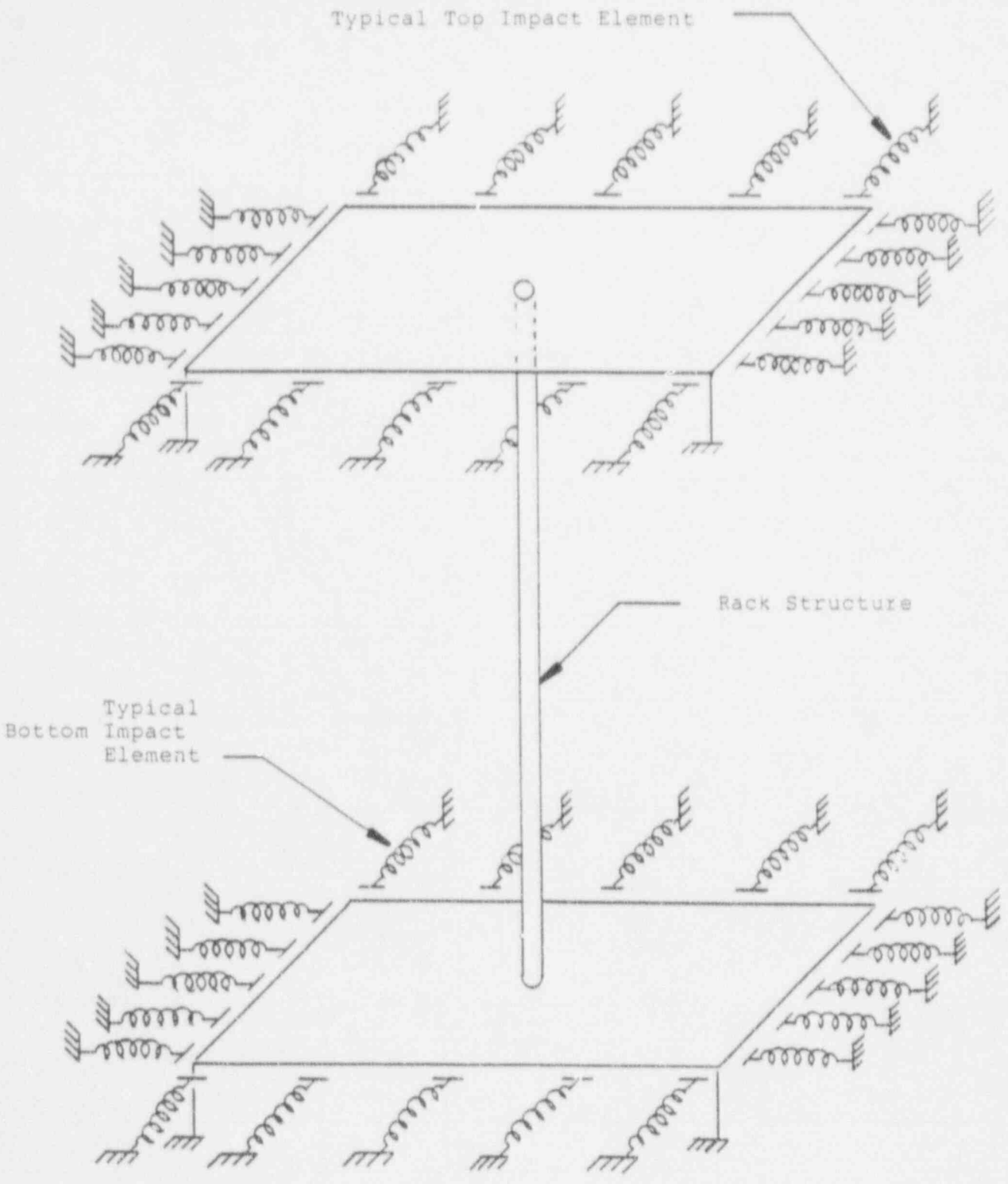

Figure 6.5.2 RACK-TO-RACK IMPACT SPRINGS

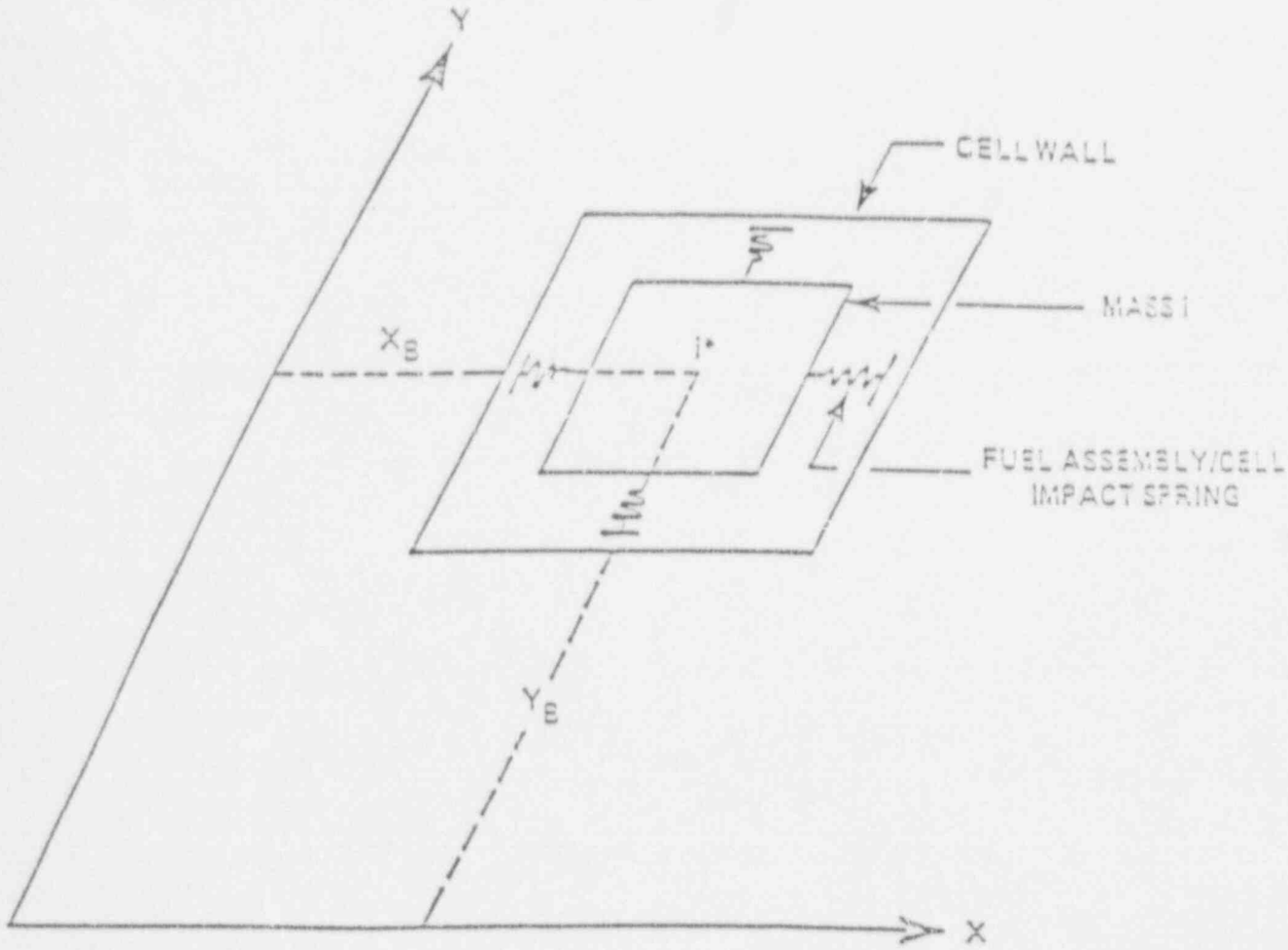

FIGURE 6.5.3 IMPACT SPRING ARRANGEMENT AT NODE i

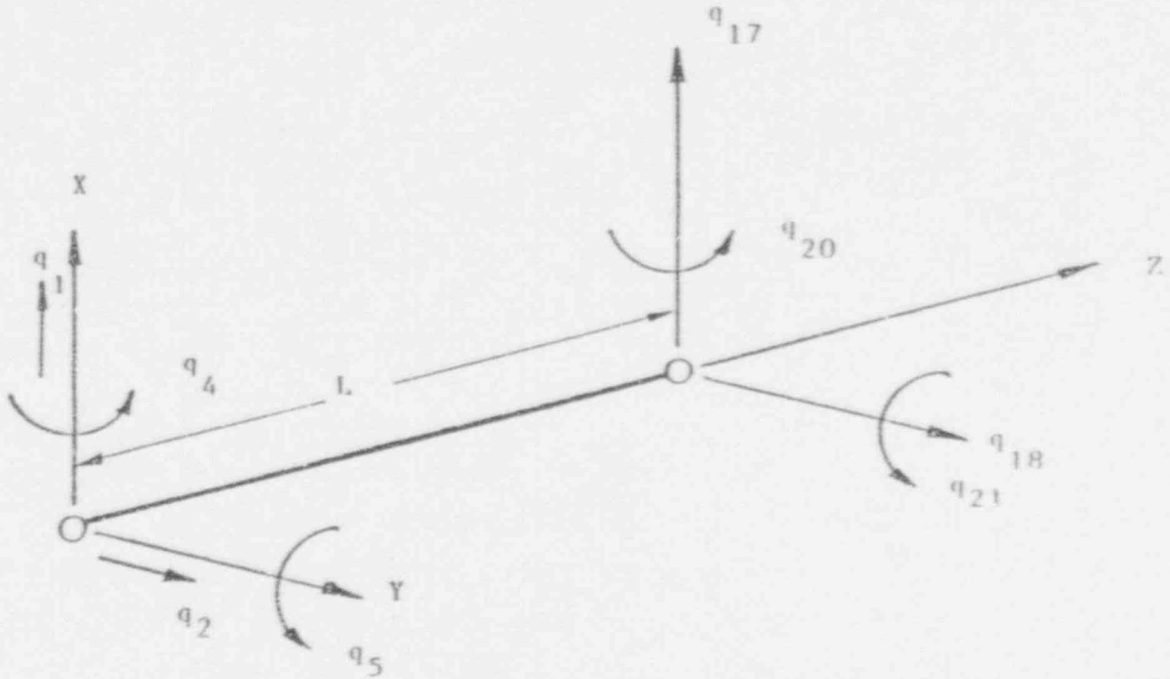

Figure 6.5.4

DEGREES OF FREEDOM MODELLING RACK MOTION

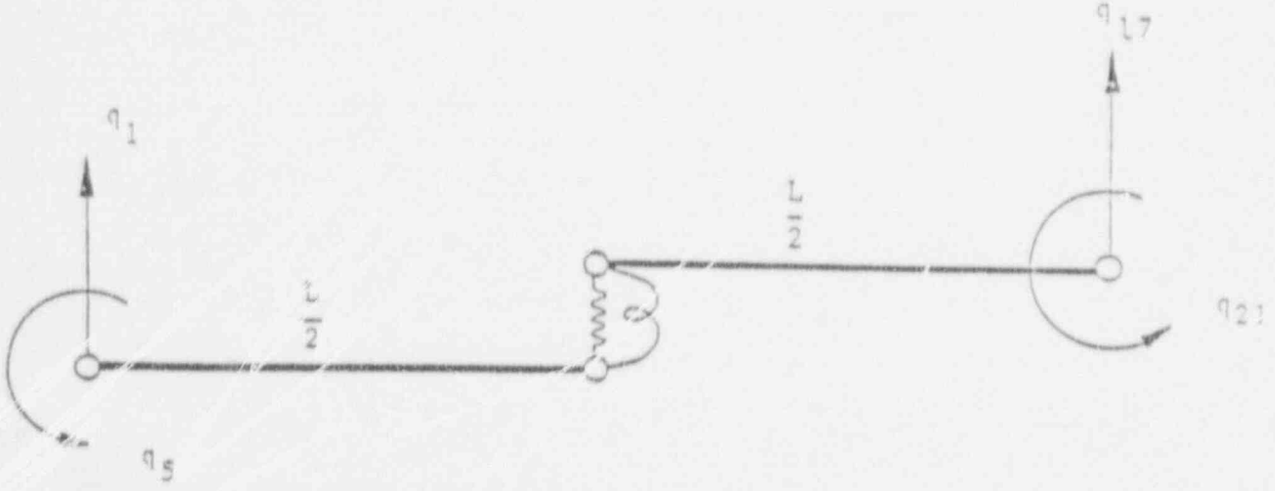

FIGURE 6.5.5 RACK DEGREES OF FREEDOM FOR X-Z PLANE BENDING

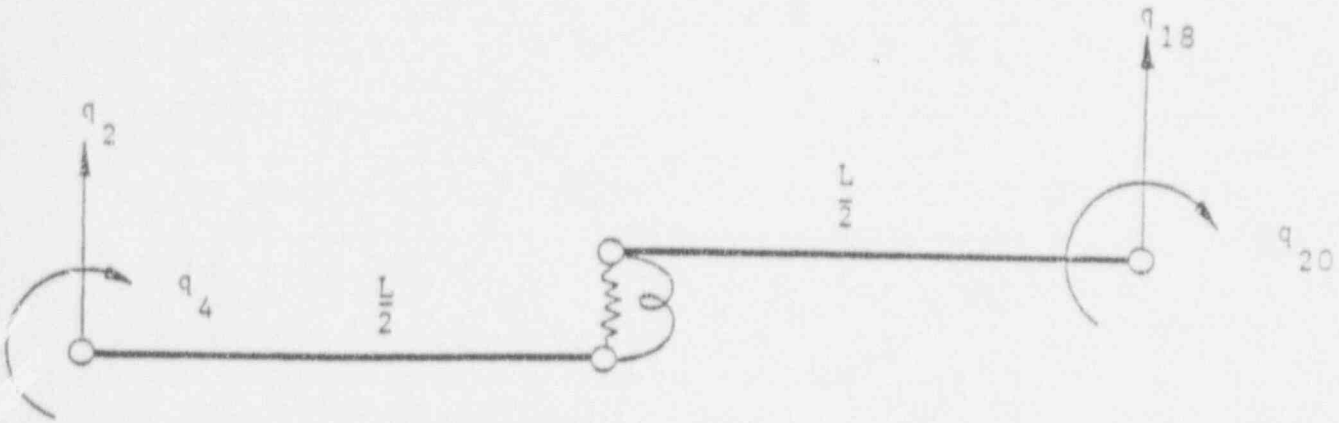

FIGURE 6.5.6 RACK DEGREES OF FREEDOM FOR Y-Z PLANE BENDING

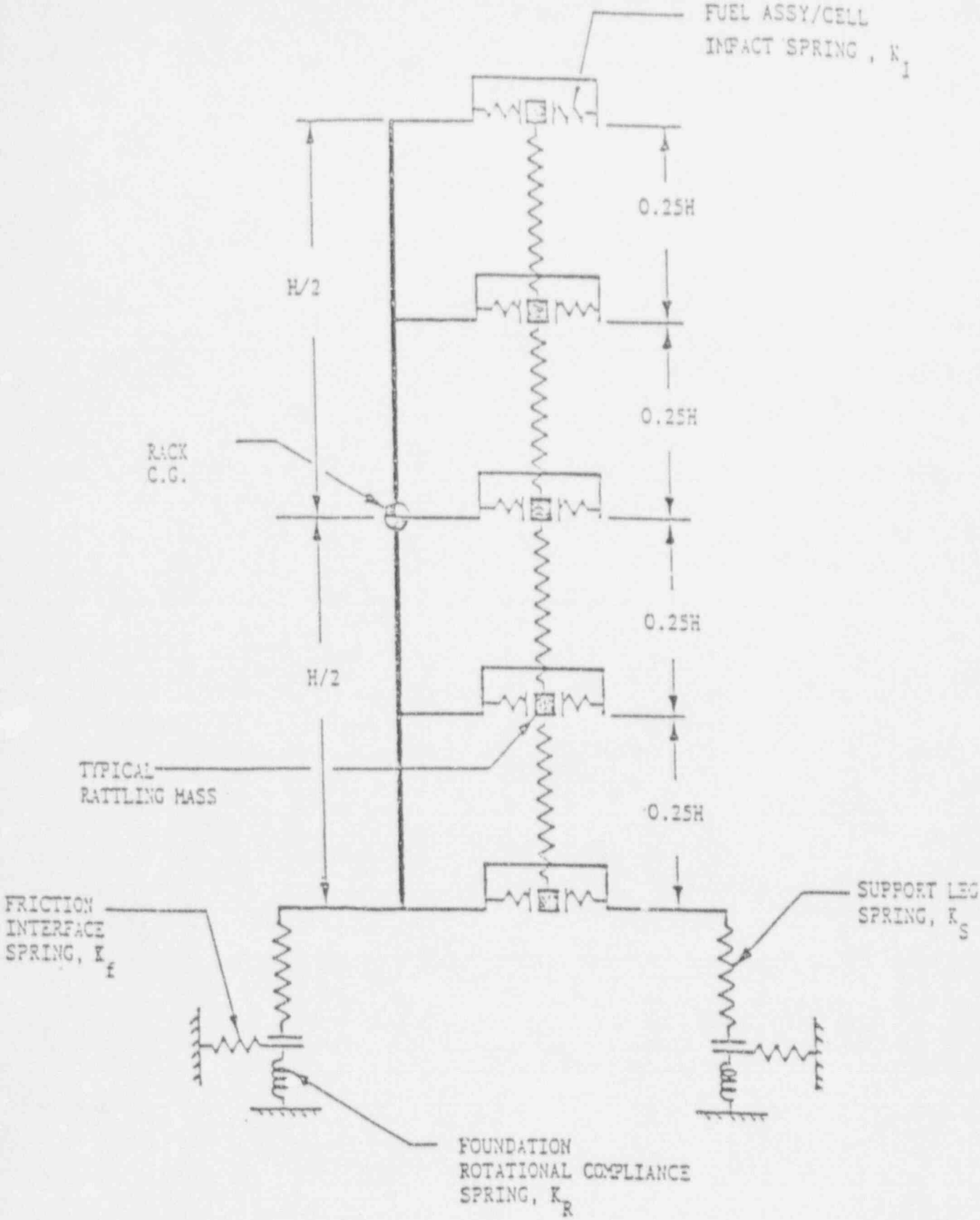

FIGURE 6.6.1 2-D VIEW OF RACK MODULE

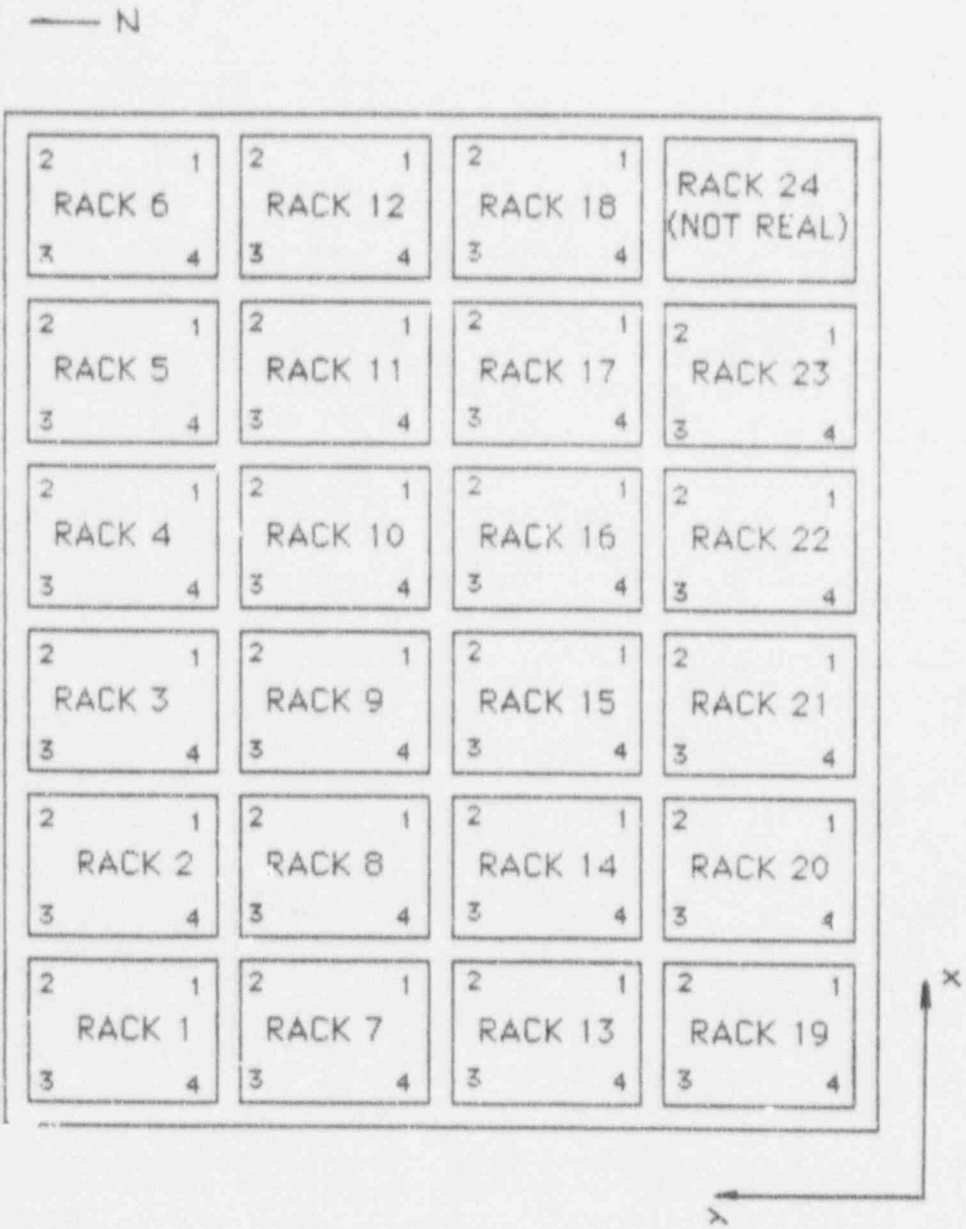

FIGURE 6.14.1 RACK AND FOOT PEDESDAL NUMBERING FOR D. C. COOK MULTI-RACK MODEL

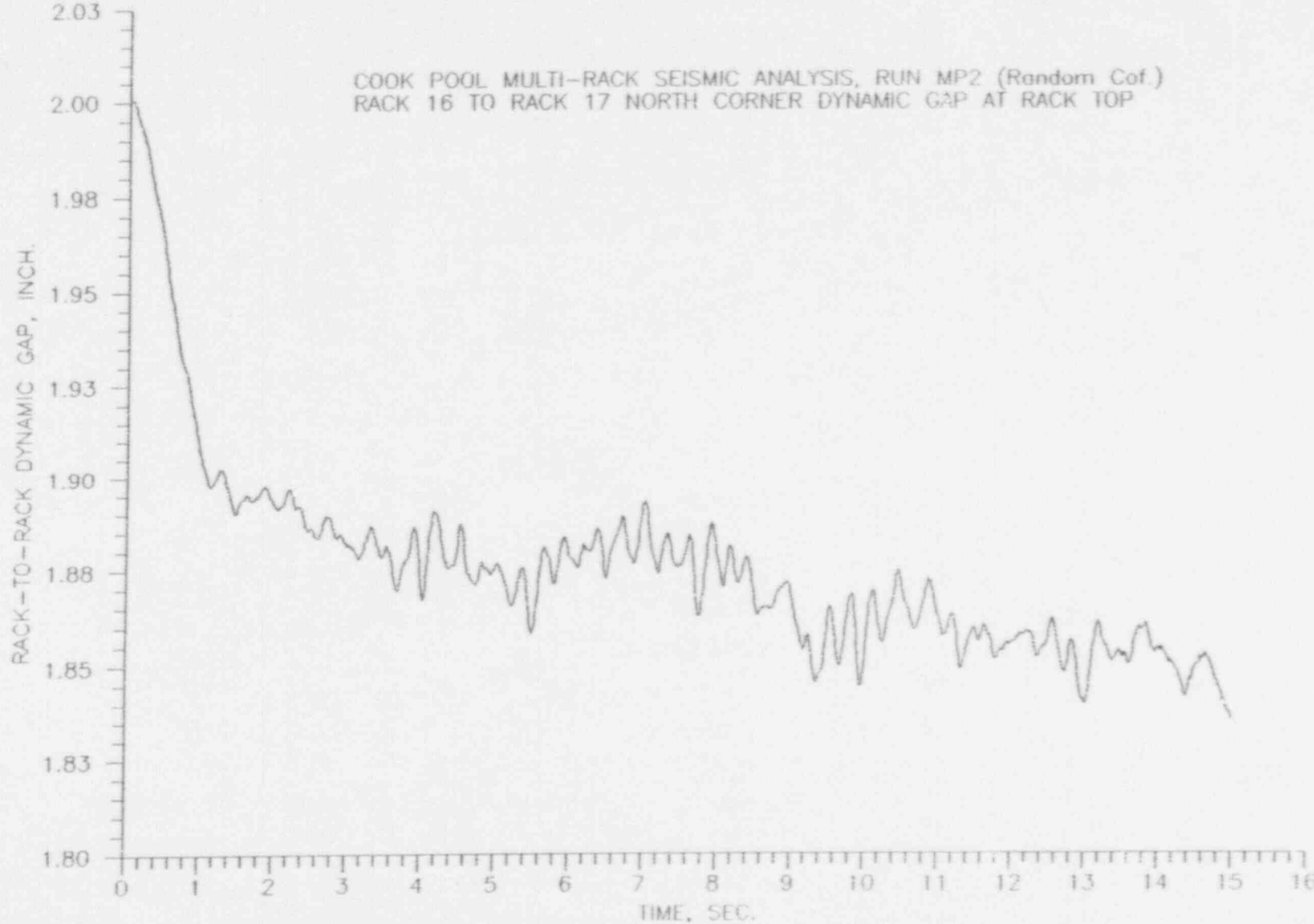
COOK POOL MULTI-RACK SEISMIC ANALYSIS, RUN MP2 (Random Cof.)
RACK 16 TO RACK 17 NORTH CORNER DYNAMIC GAP AT RACK TOP
RACK-TO-RACK DYNAMIC GAP, INCH.
2.03
2.00
1.98
1.95
1.93
1.90
1.88
1.85
1.83
1.80
0
1
2
3
4
5
6
7
8
9
10
11
12
13
14
15
16
TIME, SEC.

FIGURE 6.14.2

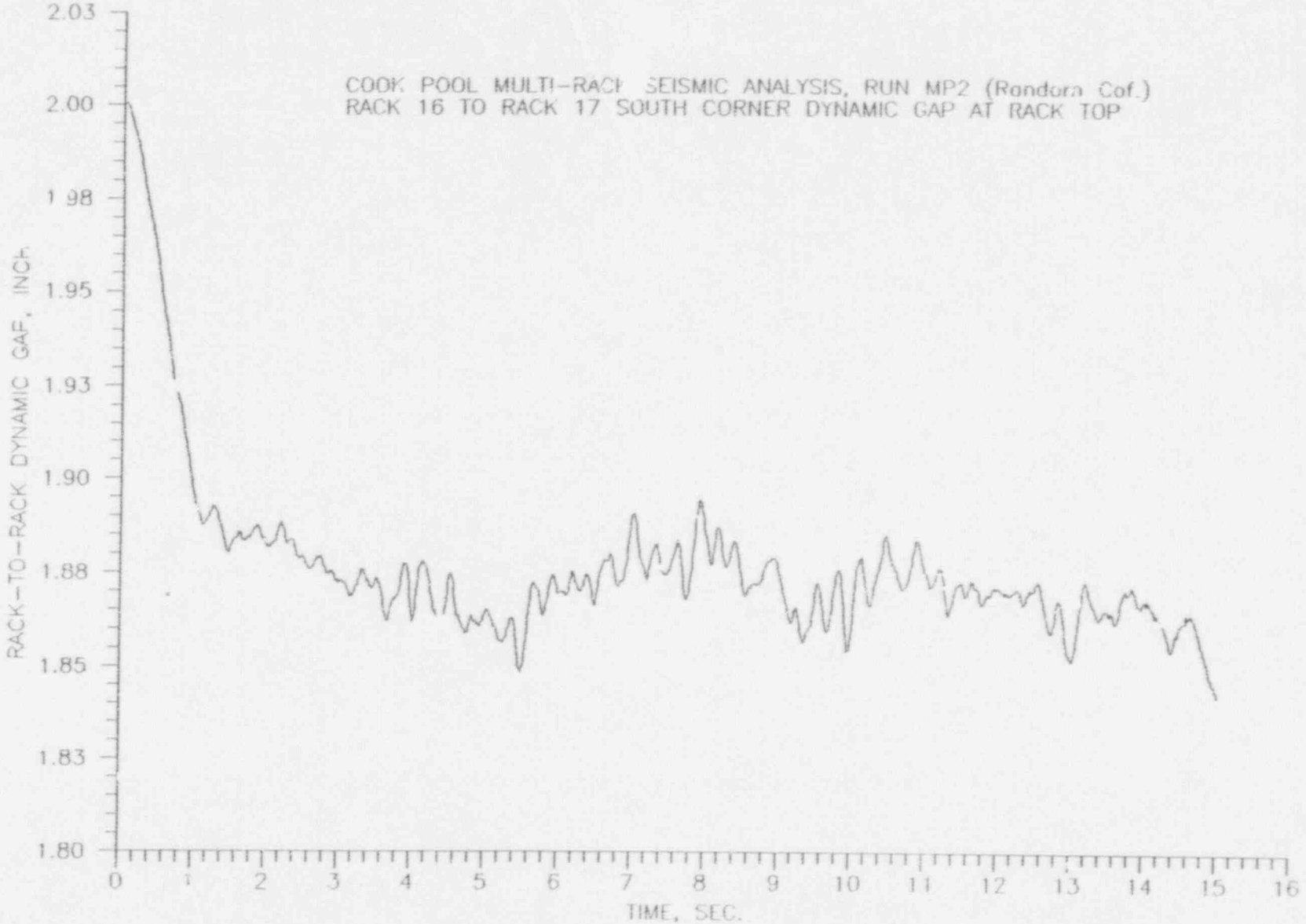
COOK POOL MULTI-RACK SEISMIC ANALYSIS, RUN MP2 (Rondorn Cof.)
RACK 16 TO RACK 17 SOUTH CORNER DYNAMIC GAP AT RACK TOP
RACK-TO-RACK DYNAMIC GAP, INCH
2.03
2.00
1.98
1.95
1.93
1.90
1.88
1.85
1.83
1.80
0
1
2
3
4
5
6
7
8
9
10
11
12
13
14
15
16
TIME, SEC.

FIGURE 6.14.3

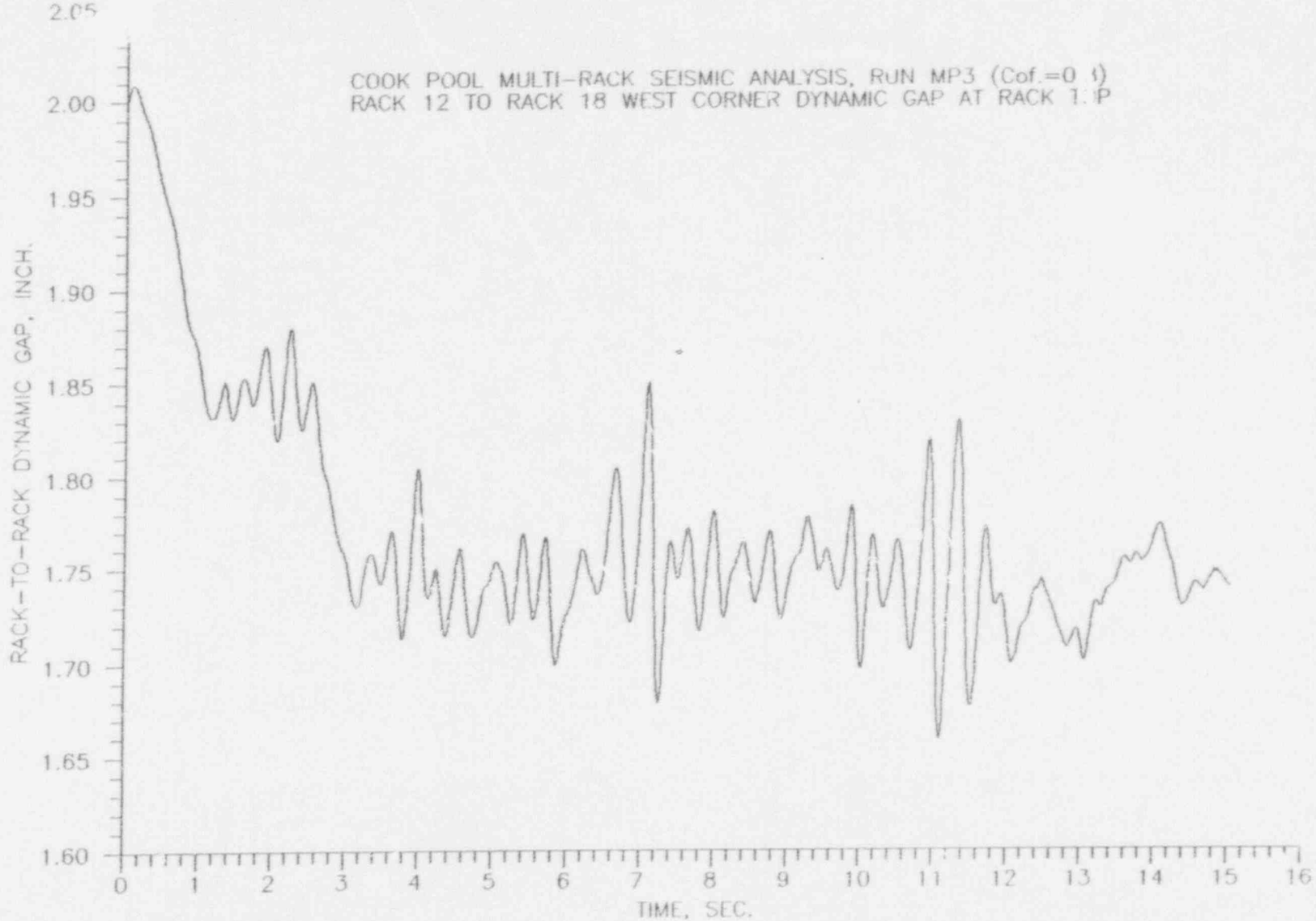
COOK POOL MULTI-RACK SEISMIC ANALYSIS, RUN MP3 (Cof.=0.1)
RACK 12 TO RACK 18 WEST CORNER DYNAMIC GAP AT RACK 1: P
RACK-TO-RACK DYNAMIC GAP, INCH.
2.05
2.00
1.95
1.90
1.85
1.80
1.75
1.70
1.65
1.60
0
1
2
3
4
5
6
7
8
9
10
11
12
13
14
15
16
TIME, SEC.

FIGURE 6.14.4

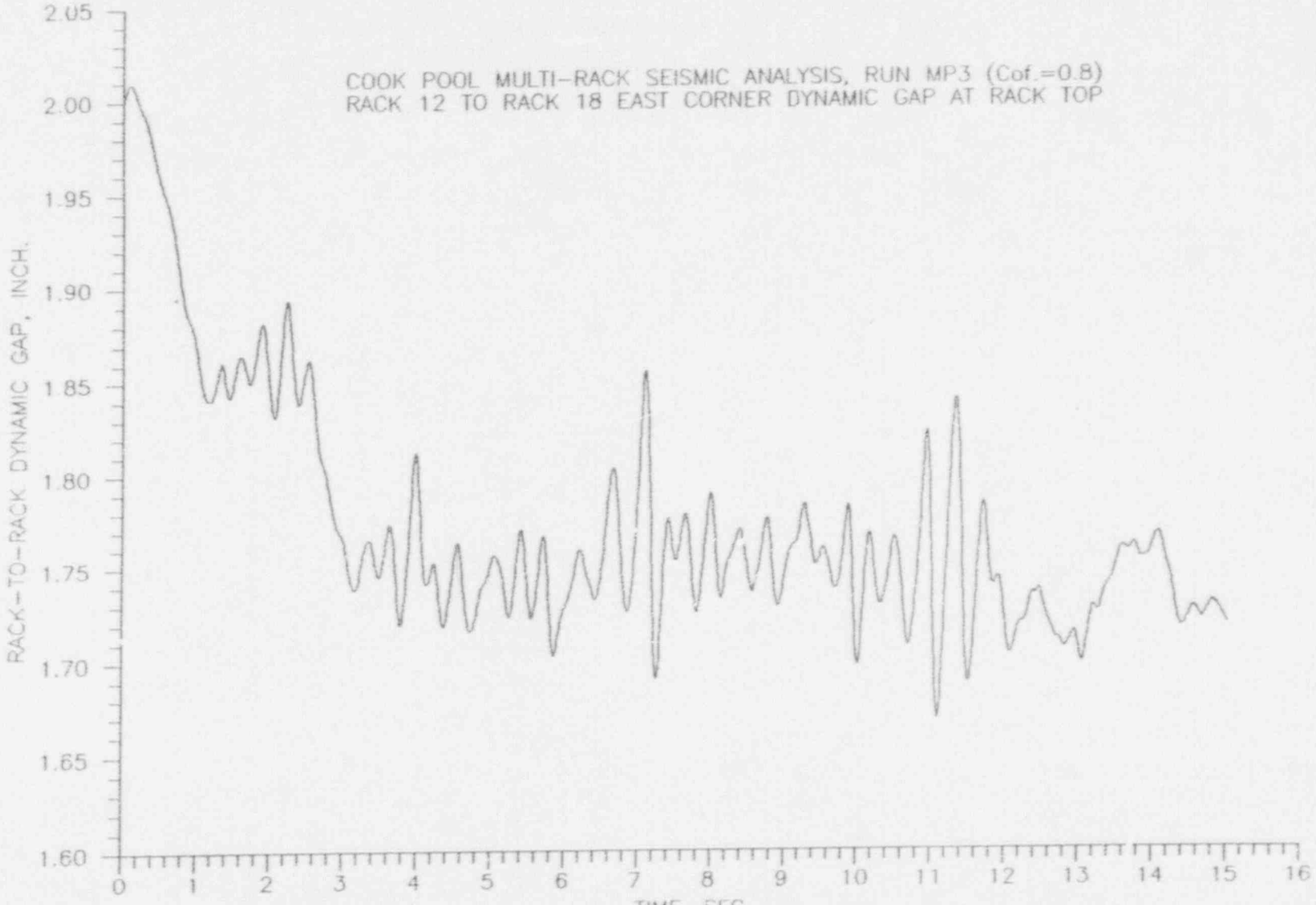
COOK POOL MULTI-RACK SEISMIC ANALYSIS, RUN MP3 (Cof.=0.8)
RACK 12 TO RACK 18 EAST CORNER DYNAMIC GAP AT RACK TOP
RACK-TO-RACK DYNAMIC GAP, INCH.
2.05
2.00
1.95
1.90
1.85
1.80
1.75
1.70
1.65
1.60
0
1
2
3
4
5
6
7
8
9
10
11
12
13
14
15
16
TIME, SEC.

FIGURE 6.14.5

7.0 ACCIDENT ANALYSIS AND MISCELLANEOUS STRUCTURAL EVALUATIONS

7.1 Introduction

This section provides results of accident analyses performed to demonstrate regulatory compliance of the new fuel racks.

There are several types of accidents which could potentially affect the spent fuel storage pool. Installation of the proposed high density racks will enable the storage of increased amounts of spent fuel in the Donald C. Cook spent fuel pool. Accordingly, accidents involving the spent fuel pool have been evaluated to ensure that the proposed spent fuel pool modification does not change the present degree of assurance to public health and safety. The following accidents and miscellaneous structural evaluations have been considered:

- Refueling accident - Dropped Fuel
- Local Cell Wall Buckling
- Analysis of Welded Joints due to Isolated Hot Cell
- Crane Uplift Load

7.2 Refueling Accidents

This section considers three (3) accidents associated with the handling of fuel assemblies.

7.2.1 Dropped Fuel Assembly

The consequences of dropping a new or spent fuel assembly as it is being moved over stored fuel is discussed below.

a. Dropped Fuel Assembly Accident I

A fuel assembly is dropped from 36" above the top of a storage location and impacts the base of the module. Local failure of the baseplate is acceptable; however, the rack design should ensure that gross structural failure does not occur and the subcriticality of the adjacent fuel assemblies is not violated. Calculated

results show that there will be no change in the spacing between cells. Local deformation of the baseplate in the neighborhood of the impact will occur, but the dropped assembly will be contained and not impact the liner. We show that the maximum movement of the baseplate toward the liner after the impact is less than 1.52". The load transmitted to the liner through the support by such an accident is well below that caused by seismic loads.

b. Dropped Fuel Assembly Accident II

One fuel assembly is (assumed dry weight = 1550 lbs.) dropped from 36" above the top of the rack and impacts the top of the rack. This is a more severe condition than the currently postulated drop of 1616 lbs. from a height of 15" above the top of the rack. Permanent deformation of the rack is acceptable, but is required to be limited to the top region such that the rack cross-sectional geometry at the level of the top of the active fuel (and below) is not altered. Analysis shows that although local deformation occurs, it is confined to a region above the active fuel area. The region of permanent deformation is to a depth 5.34" below the top of the rack.

c. Dropped Fuel Assembly Accident III

This postulated accident is identical to (b) above except that the fuel assembly is assumed to drop in an inclined manner on top of the rack. Analyses show that the straight drop case (case b above) bounds the results.

7.3 Local Buckling of Fuel Cell Walls

This subsection and the next one presents details on the secondary stresses produced by buckling and by temperature effects.

The allowable local buckling stresses in the fuel cell walls are obtained by using classical plate buckling analysis. The following formula for the critical stress has been used based on a width of cell "b": (See Figure 7.3.1.)

$$\sigma_{cr} = \frac{\beta \pi^2 E t^2}{12 b^2 (1 - \mu^2)}$$

where E = 27.9 x 10^6 psi, μ = 0.3, (Poison's ratio), t = .075", b = 8.75". The factor β is suggested in (Ref. 7.3.1) to be 4.0 for a long panel.

For the given data

$$\sigma_{cr} = 7411 \text{ psi}$$

It should be noted that this stability calculation is based on the applied stress being uniform along the entire length of the cell wall. In the actual fuel rack, the compressive stress comes from consideration of overall bending of the rack structures during a seismic event and as such is negligible at the rack top and maximum at the rack bottom. It is conservative to apply the above equation to the rack cell wall if we compare σ_{cr} with the maximum compressive stress anywhere in the cell wall. As shown in Section 6, the local buckling stress limit of 7411 psi is not violated anywhere in the body of the rack modules, since the maximum compressive stress in the outermost cell is σ = 3585 psi. (From Table 6.11.1 for R6 = .239, the stress at the base of the rack under combined direct plus bending loads is σ = R6 x allowable stress).

7.4 Analysis of Welded Joints in Rack due to Isolated Hot Cell

In this subsection, in-rack welded joints are examined under the loading conditions arising from thermal effects due to an isolated hot cell.

A thermal gradient between cells will develop when an isolated storage location contains a fuel assembly emitting maximum postulated heat, while the surrounding locations are empty. We can obtain a conservative estimate of weld stresses along the length of an isolated hot cell by considering a beam strip (a cell wall) uniformly heated and restrained from growth along one long

edge. The strip is subject to a uniform temperature rise ΔT = 59.66°F. The temperature rise has been calculated from the difference of the maximum local water temperature and bulk water temperature in the spent fuel pool. (see Tables 5.5.1 and 5.7.1). Then, using a shear beam theory, we can calculate an estimate of the maximum value of the average shear stress in the strip (see Figure 7.4.1).

The final result for wall maximum shear stress, under conservative restraint assumptions is given as

$$\tau_{max} = \frac{E\ \alpha\ T}{.931}$$

where α = 9.5 x 10⁻6 in/in °F

Therefore, we obtain an estimate of maximum weld shear stress in an isolated hot cell as

$$\tau_{max} = 16984.8$$

Since this is a secondary thermal stress, it is appropriate to compare this to the allowable weld shear stress for a faulted event $\tau < .42S_u$ = 29820 psi. In the fuel rack, this maximum stress occurs near the top of the rack and does not interact with any other critical stress.

7.5 Crane Uplift Load of 3000 lb.

A local uplift load of 3000 lb. (UFSAR limit is 2950 lb.) will not induce any uplift stresses in the rack which are more severe than the limiting conditions discussed in the foregoing. This choice of load should be an upper bound load on the maximum load that can be applied to a struck fuel assembly during removal.

7.6 References for Section 7

7.3.1 "Strength of Materials", S.P. Timoshenko, 3rd Edition, Part II, pp 194-197 (1956).

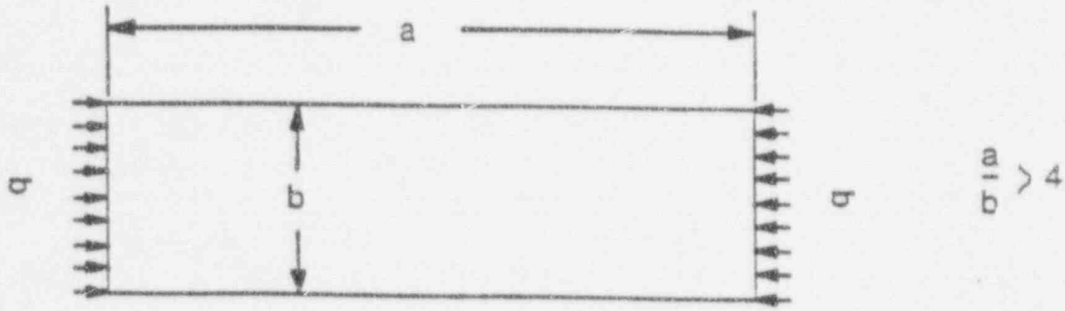

FIGURE 7.3.1

LOADING ON RACK WALL

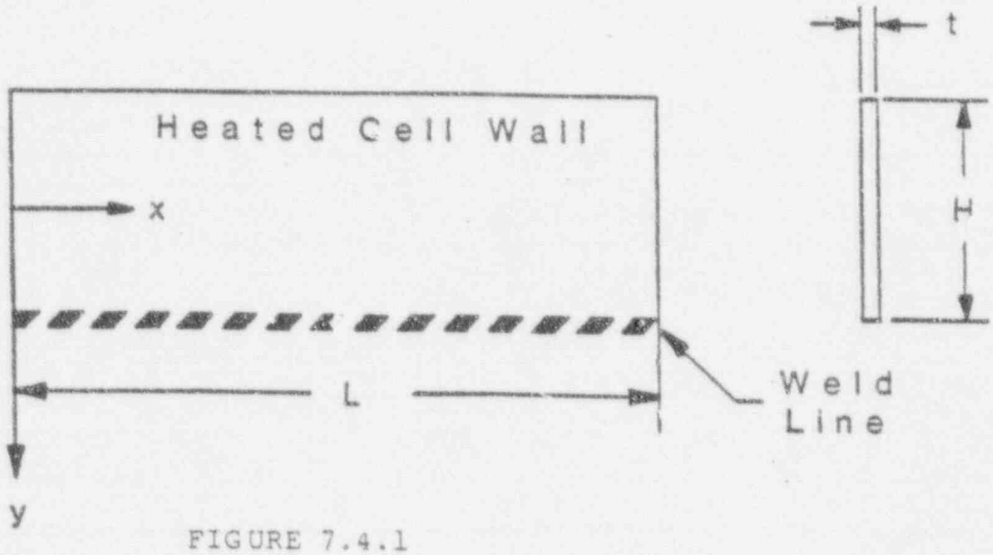

FIGURE 7.4.1

WELDED JOINT IN RACK

8.0 STATIC AND DYNAMIC ANALYSIS OF FUEL POOL STRUCTURE

8.1 Introduction

The Donald C. Cook spent fuel pool is a safety related, seismic category I, reinforced concrete structure. In this section an abstract of the analysis to demonstrate the structural adequacy of the pool structure is presented. The object of the analysis is to demonstrate the compliance of the pool slab and confining walls to the applicable design codes and to NRC regulations for the condition of increased loadings due to high density fuel storage. The loading on the pool structure is produced by the following discrete components:

a) Static Loading

1) Dead weight of pool structure plus pool water (including hydraulic pressure on the pool walls).

2) Dead weight of the rack modules and fuel assemblies stored therein.

b) Dynamic Loading

1) Vertical loads transmitted by the rack support pedestals to the slab during a DBE or OBE event.

2) Inertia loads due to the slab, pool walls and contained water mass which arise during a DBE or OBE event.

c) Thermal Loading

1) Mean temperature rise and temperature gradient across the pool slab and the pool walls due to temperature differential between the pool water and the atmosphere external to the slab and walls.

The spent fuel pool is analyzed using the finite element method. The results for the above load components are combined using factored load combinations mandated by NUREG-0800, the Standard Review Plan (SRP), Section 3.8.4 (Ref. 8.1.1). It is demonstrated that for the critical factored load combinations, structural integrity is maintained when the fuel pool is assumed to be fully loaded with high density fuel racks with all storage locations occupied by fuel assemblies. The general purpose finite element code ANSYS (Ref. 8.1.2) is utilized to perform the analysis.

The critical regions examined are the fuel pool slab and the most critical wall sections adjoining the pool slab. Both moment and shear capacities of the critical regions are checked for structural integrity. Also evaluated is local punching integrity in the vicinity of a fuel rack bearing pad. Structural capacity evaluations are carried out in accordance with the requirements of the American Concrete Institute (ACI) (Refs. 8.1.3 and 8.1.4). In this analysis, the load factors of SRP Section 3.8.4 have been used together with the allowable concrete and reinforcement loads as called for by the American Concrete Institute. This constitutes the most conservative approach to the structural qualification of the pool structure based on a static load qualification method.

8.2 General Features of the Model

The fuel pool model is constructed using information from design basis Donald C. Cook auxiliary building structural drawings. A description of the portion of the pool modelled for analysis is given in the following.

The fuel pool slab is a 5'-2 1/2" thick reinforced concrete slab with inside dimensions 39'-1 9/16" wide and 58'-3 1/8" long. The slab is located at elevation 600'-605'-2 1/2" and its long direction is aligned along the plant East-West direction. The East edge of the slab has a 5'-2" thick vertical reinforced wall which extends above the slab and is modeled to level 650'. The West edge of the slab has a 6' thick wall from level 605'-2 1/2" to level 650'. The West wall separates the fuel pool from the fuel transfer canal which is not modelled; however, the discontinuity in the wall structure in the center of the West wall is included. All wall modeling is done to level 650', and we assume free edges at this level. The North wall is a 6' thick wall extending from the slab to level 650'. The South edge of the slab has a 5' thick wall extending up to level 650'. It is clear from the above description that the South wall has the largest length to thickness ratio, and therefore, may represent a limiting condition of structural strength. The foundation mat is at elevation 584' and the pool slab and upper walls are supported on the foundation mat by walls and columns around the periphery. The North edge of the slab is supported by a continuous 3'-0" thick wall, while the East edge is partially supported along its length by a 2'-6" thick wall. There are three vertical columns located at the Southeast and Southwest corner of the slab, and intermediate along the South edge. There is also a portion of a wall below the South edge at one location. The floor slab has interior vertical support provided by a 2'-0" thick vertical wall providing vertical restraint in both the North-South and East-West direction over a substantial length of slab. In addition, there is a 25' span standard W14 x 158 wide flange beam from the slab North edge supporting wall to give additional pool slab support. This propped beam is skewed toward the East 16' from the North edge.

The entire beam (the straight part plus the skewed part) is supported vertically by four TS10" x 10" square tubes. Each tubular column has also been stiffened by four 8" x 3/8" plates. Figure 8.2.1 shows a schematic of the above geometry.

The pool slab is assumed to be loaded with 23 high density fuel racks having a total of 3616 cells. For analysis purposes, each cell is assumed to contain a 1550 lb. weight fuel assembly. As noted previously, all fuel pool walls above the pool slab are assumed to have a free edge at level 650'. Lateral restraint is provided to the vertical walls at certain locations above the 605' level. This restraint simulates the effect of adjacent structure which is not included in the modelled envelope. Figures 8.2.2 and 8.2.3 show layouts of the entire 3-D finite element model. The gridwork in different regions shows the totality of elements used. Shell elements are used to model the slab and walls, while beam elements are used to model the columns.

The finite element model is constructed using the ANSYS classical shell element STIF63 and the beam element STIF44 of the ANSYS finite element code. The shell element thickness in the various regions of the structure is the actual thickness of the structure at the location. The finite element model is prepared for the analysis of both mechanical load and thermal load. The effects of the reinforced concrete (cracked or uncracked) are accounted for in the finite element model by establishing an appropriate effective modulus for each shell element and effective inertias for the column elements. Effective moduli are defined for each local in-plane axis for the shell elements. The different moduli reflect the fact that different reinforcement geometries may be used in perpendicular directions of the plate-like sections when

the different concrete section assumptions (cracked or uncracked) are applied to the slab and walls. Only major reinforcement which affects the plate and shell-like behavior of the structure is incorporated into the definition of the effective moduli; additional local reinforcement in various areas of the pool structure are neglected in the defining of the effective moduli. However, such local reinforcement is accounted for in the strength evaluation after results are obtained. The non-homogeneous nature of the reinforcement is taken into account by defining different material types as necessary to reflect the varying values of effective moduli in different regions. The concrete section assumptions (cracked or uncracked) are fully in accordance with the requirements of American Concrete Institute (Refs. 8.1.3 and 8.1.4). In accordance with Ref. 8.1.4, we assume uncracked section properties for the mechanical load analyses (including load factors). For the thermal analyses, it is shown that the thermal gradients will always yield a cracked section if the uncracked stiffness is used; therefore, an iterative solution is used to show that cracked section properties should be used for the thermal analyses.

The effective properties for the elements used in the finite element model are calculated using standard procedures for reinforced concrete sections to define equivalent effective homogeneous materials having the appropriate stiffness and strength.

8.3 Loading Conditions

In order to evaluate the response due to the different load mechanisms outlined in Section 8.1, the following finite element analyses are carried out. Six loading cases are defined below which enable us to obtain the moments and shears for factored loadings by linear combination.

1. Dead loading from concrete, reinforcement and 40' of hydrostatic head. The loading is applied as a 1.0g vertical gravitational load for the structure and a surface pressure on the slab and walls for the hydrostatic head.

2. Dead loading due to weights of rack plus full fuel load. These loads are applied as a uniform static pressure applied to the slab.

3. Seismic vertical loading due to racks plus fuel load applied as an effective sustained pressure on the floor slab pedestals. The loading applied is obtained from the 3-D whole pool multi-rack analysis described in Section 6 of this report. From the results of that analysis, we take the stored time history of each pedestal load and define an effective sustained pool pressure load which yields the same total impulse over the time duration of the seismic event. The details of developing this effective sustained pressure load are presented later. We develop effective sustained vertical pressure loads for both OBE and DBE events and then perform appropriate finite element analyses.

4. Seismic horizontal loading due to structure weight (including reinforcement). The loading is applied as a 1g horizontal and vertical acceleration applied to the structure plus a hydrodynamic pressure equivalent to an acceleration of all of the water mass against the weakest wall. The acceleration level is obtained from the applicable response spectra and is taken as the peak g level on the spectra at frequencies above the lowest natural frequency for the structure. A separate ANSYS frequency analysis simulation is carried out to establish the dynamic characteristics of the structure.

5. Seismic horizontal load due to shear loads from each of the pedestals. This loading is obtained by using the static + effective dynamic loads developed for case 3 above and assuming a coefficient of friction = .8. The direction of these loads is set so as to develop stresses that maximize the load combinations necessary to satisfy structural integrity requirements discussed below. In this load case we also impose a lateral pressure on the weakest pool wall to simulate hydrodynamic effects from fluid coupling due to rack motion relative to the wall.

6. A mean temperature rise plus a thermal gradient is applied across the walls and floor slab to simulate the heating effect of the water in the pool. This gradient is calculated based on the maximum wall temperature deduced from the pool bulk temperature calculations for the licensing basis scenarios presented in Section 5 of this report.

For subsequent discussion of structural integrity checks using various mandated load combinations, we refer to the above individual finite element load cases as "case 1-6", respectively. As noted above, in addition to the static analyses using the developed finite element model, we also perform a frequency analysis of the pool structure assuming that all contained fluid is attached to the pool slab. Uncracked section properties are used here. This frequency analysis is used to determine the lowest pool structural frequencies so as to establish appropriate seismic amplifiers to apply to load cases 1 and 4. These seismic

amplifiers are obtained from the response spectra of the seismic event and multiply the results of load cases 1 and 4 when forming the mandated load combinations.

As noted above, the case 3 loading involves the determination of an effective pressure load to represent the seismic load on the slab due to the racks plus fuel. The method of determination of this effective pressure is described below.

As noted previously, the Holtec 3-D dynamic simulation code DYNARACK is used to simulate the seismic response of the entire fuel pool containing multiple racks. The vertical load time history from each pedestal on each rack is saved in an archival file. For the pool slab structural analysis, which is based on static analyses, we compute an effective static load increment based on averaging of the time history. Figure 8.3.1 is used to illustrate the concept where the total pedestal load is considered as the static load (F_s in Figure 8.3.1 plus a time varying component). Note that in Figure 8.3.1 a zero load during a portion of the time means that the pedestal has lifted off. We define an effective static load for the purposes of pool static analysis and structural qualification as follows:

a. From the archival pedestal load time history we may, at each point in time, determine the total pool load F_T by summing the total loads for each pedestal.

b. At each point in time i, we can define the dynamic load increment for the pool as $F_T - F_S = DF_i$ where F_S now represents the total static load on the slab. We keep track of the number of time points i where $DF_i > 0$.

c. An equivalent static pool load (seismic adder to the static pool load) is defined as

$$\text{SEISMIC ADDER} = \text{SUMDF}_I/\text{SUMNI}_i$$

where $SUMDF_I$ is the sum of all of the non zero DF_I and $SUMN_i$ is the total number of points in the time history where the dynamic pool load increment is greater than zero.

d. In forming the appropriate load combinations mandated for structural integrity checks, the calculated "seismic adder" divided by the pool area, is used as the effective seismic pressure on the slab.

Of all loading conditions mandated in Ref. 8.1.1, the factored loads which apply to this structure and are deemed critical are:

A. $1.4D + 1.9E$
B. $.75\ (1.4D + 1.9E + 1.7T_o)$
C. $D + E' + T_o$

where:

D = Dead load
E' = Design Basis Earthquake (DBE)
E = Operating Basis Earthquake (OBE)
T_o = Steady State Thermal Load

The appropriate load cases are formed from the individual finite element analyses as follows:

D = case 1 + case 2

E' = DBE amplifier x case 1 + DBE amplifier x case 4 + case 3 (for DBE) + case 5 (for DBE)

E = OBE amplifier x case 1 + OBE amplifier + case 4 + case 3 (for OBE) + case 5 (for OBE)

T_o = case 6

Load combinations are formed using absolute values where necessary so as to maximize critical stress resultants.

As noted above, for analysis of fuel pool structural integrity, the seismic amplifiers are based on the peak g level responses at the lowest resonant frequency that are obtained from the plant acceleration response spectrum. We show that this is conservative.

8.4 Results of Analyses

The ANSYS postprocessing capability is used to form the appropriate load combinations identified above and to establish the critical bending moments in various sections of the pool structure. The ultimate moments for each section are computed using allowable limit strength levels as described in Ref. 8.1.3. For Donald C. Cook, the following limit strengths for concrete and for reinforcement are used in the computation of limit (ultimate) moments.

concrete σ_c = 3500 psi (compression)
reinforcement = σ_y = 40000 psi (tension/compression)

In each section, we define the safety margin for bending as the ultimate bending moment divided by the calculated bending moment (from the ANSYS postprocessing of the required load cases). Table 8.4.1 summarizes the results obtained from the finite element analyses and shows minimum safety margins on each section of the structure. Note that these are safety margins based on the factored load conditions as mandated in Ref. 8.1.1 and need only satisfy a limit ≥ 1.0.

The floor slab perimeter is also checked against gross shear failure under factored load conditions. Local bearing strength and punching shear calculations are performed in accordance with (Ref. 8.1.3).

8.5 Pool Liner

The pool liner is subject to in-plane strains due to movement of the rack support feet during the seismic event. Calculations are made to establish that the liner will not fail due to cyclic straining caused by the rack foot loading. An ANSYS analysis of a liner plate section subjected to vertical and horizontal static pedestal loading is carried out. The time history result for the pedestal loading is then used to evaluate the number of stress cycles to be expected in the liner for each event. The cumulative damage factor (CDF) is computed and shown to be less than 1.0 in critical regions of the liner and attachment locations. The number of stress cycles used in the CDF evaluation is based on 1 DBE and 20 OBE events.

8.6 Conclusions

Critical regions affected by loading the fuel pool completely with high density racks are examined for structural integrity under bending and shearing action. It is determined that adequate safety factors exist assuming that all racks are fully loaded with normal (unconsolidated) fuel and that the factored load combinations are checked against the appropriate structural design strengths. It is also shown that local frictional loading on the liner results in in-plane stresses that are low enough so that liner fatigue is not a concern.

8.7 References for Section 8

8.1.1 NUREG-0800, SRP for Review of Safety Analysis Reports for Nuclear Power Plants, Section 3.8.4, July 1981.

8.1.2 ANSYS User's Manual, Swanson Analysis Rev. 4.3, 1987.

8.1.3 ACI 318-89, ACI 318R-89, Building Code Requirements for Reinforced Concrete, American Concrete Institute, Detroit, Michigan.

8.1.4 ACI349.1R-80, Reinforced Concrete Design for Thermal Effects on Nuclear Power Plant Structures, 1981.

Table 8.4.1

SAFETY FACTORS FOR BENDING OF POOL STRUCTURE REGIONS

REGION	FACTOR OF SAFETY*
Slab	1.23
North Wall	1.00
East Wall	1.08
South Wall	1.26
West Wall	1.05

* The factors of safety have been obtained using conservative assumptions on mechanical and thermal load distribution. They represent factors of safety over the values required by NUREG-0800.

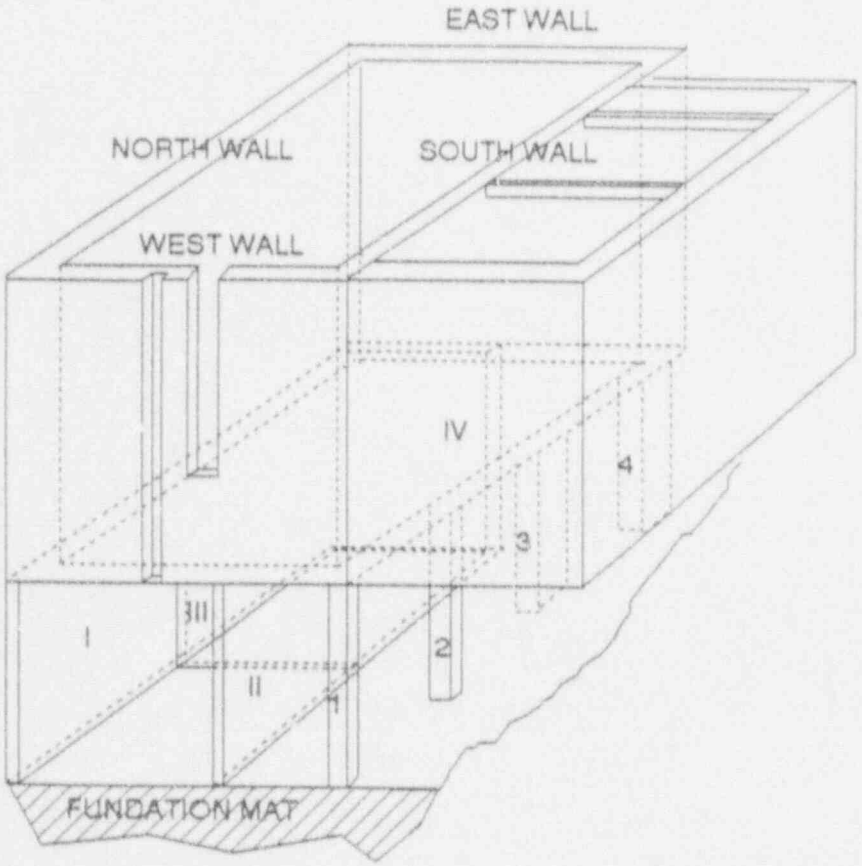

FIGURE 8.2.1 ISOMETRIC VIEW OF COOK SPENT FUEL POOL

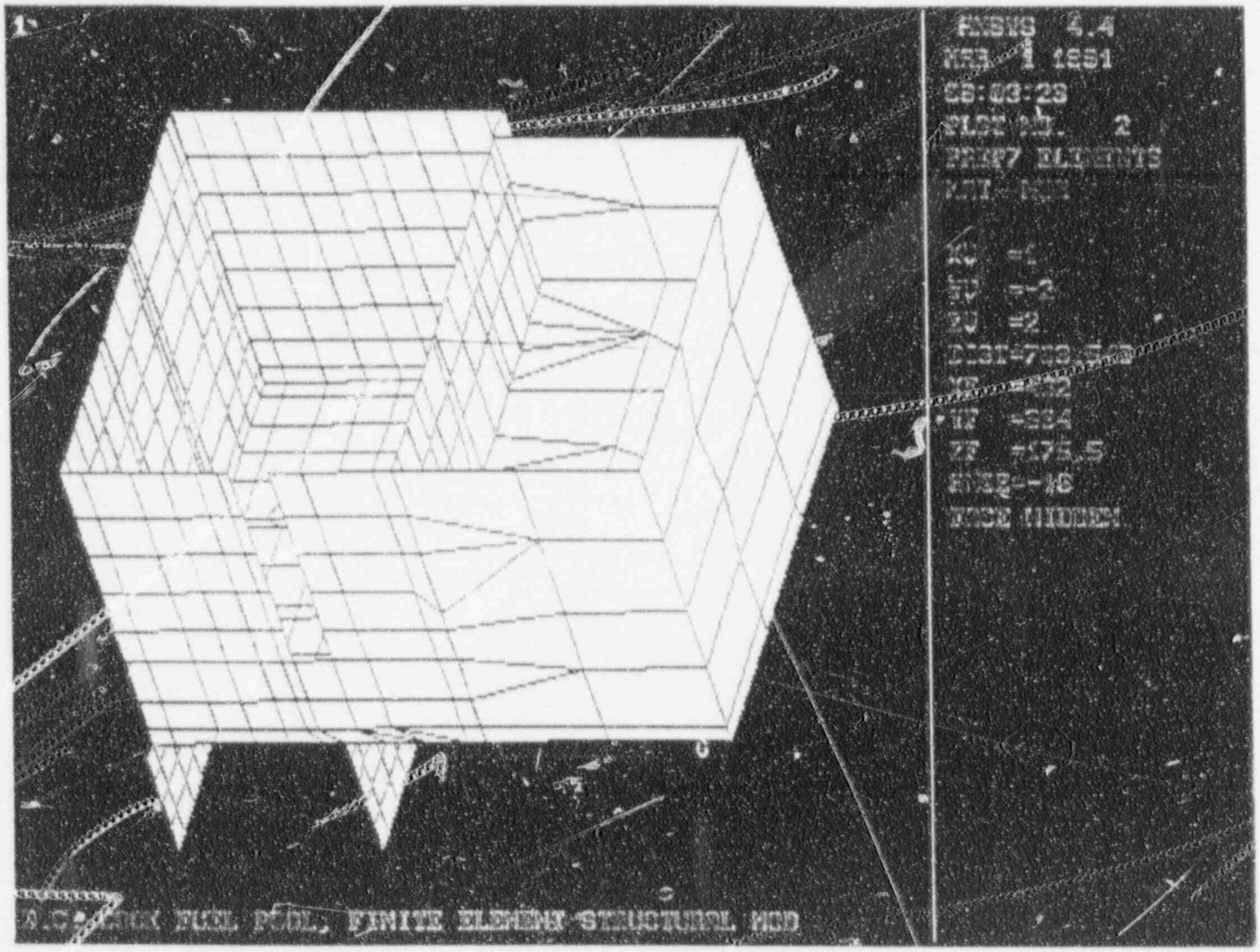

FIGURE 8.2.2 OVERALL FINITE MODEL OF COOK POOL
TOP VIEW

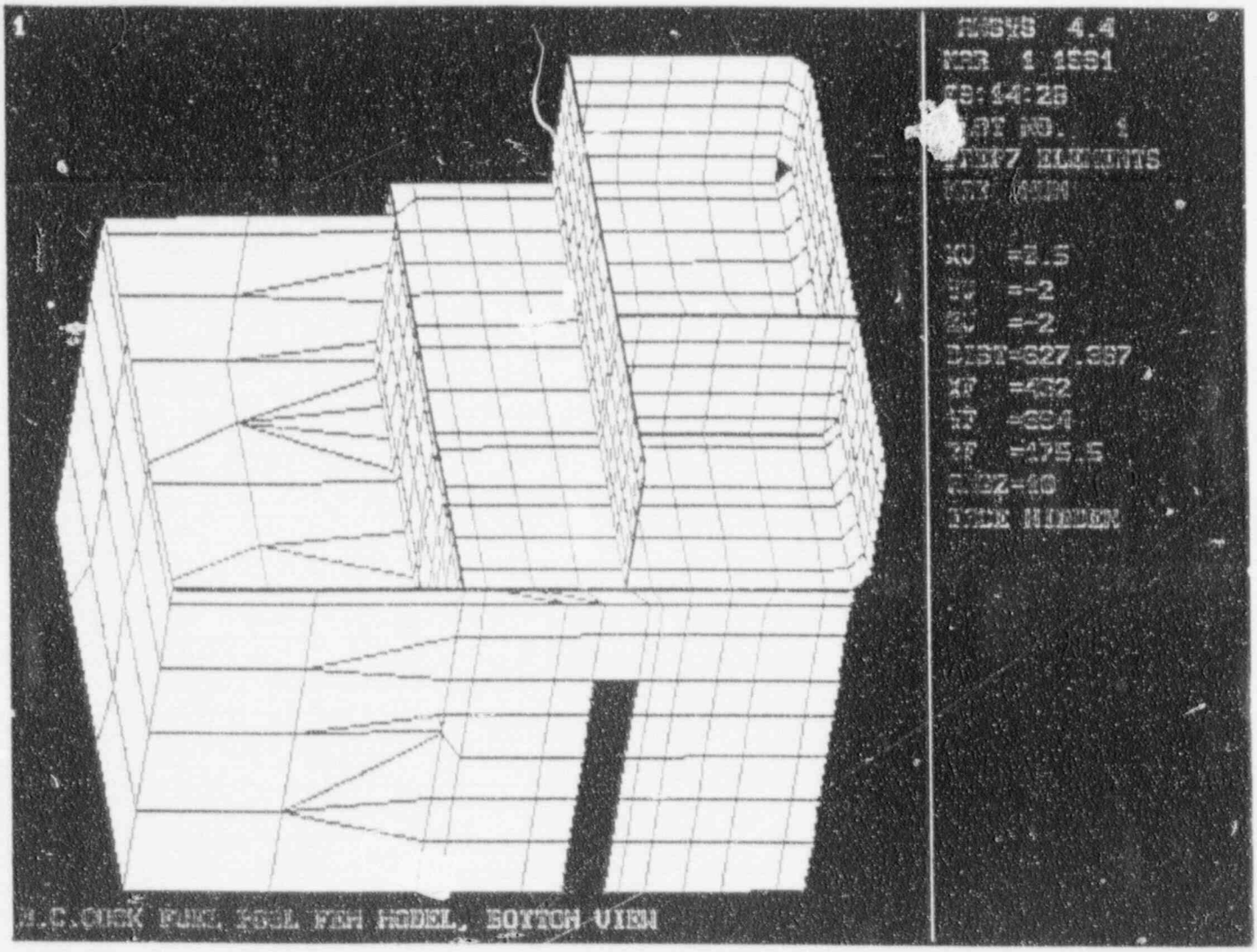

FIGURE 8.2.3 OVERALL FINITE MODEL OF COOK POOL BOTTOM VIEW

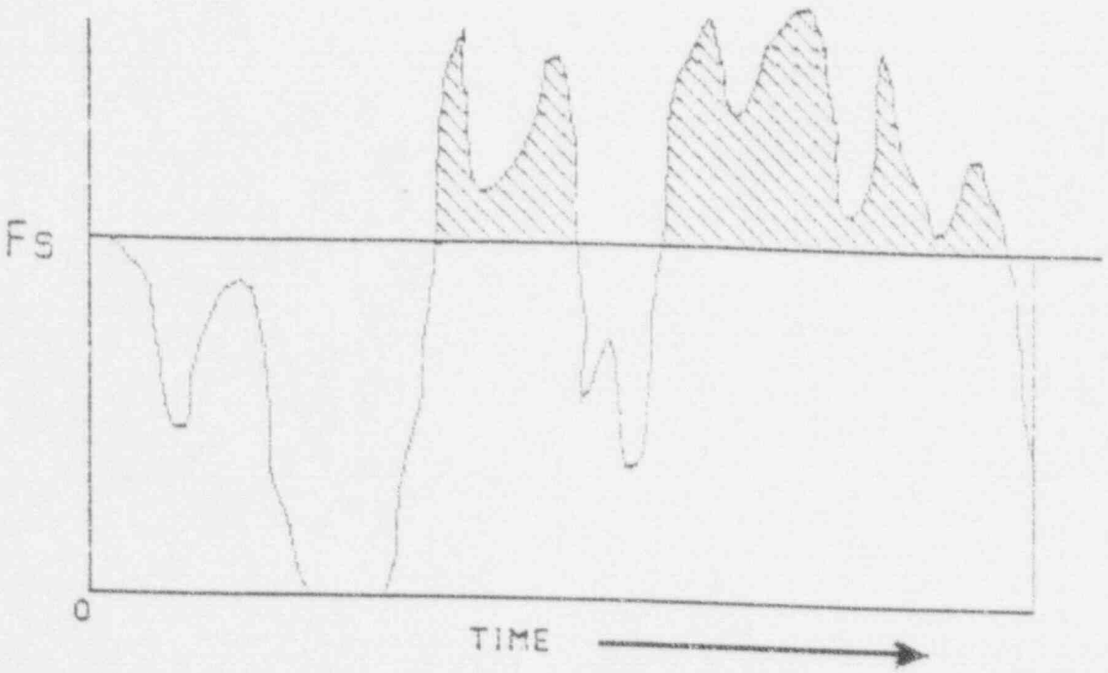

FIGURE 8.3.1 PEDESTAL LOAD VS. TIME
(Positive Load Means Pedestal in Contact with Liner)

9.0 RADIOLOGICAL EVALUATION

9.1 Fuel Handling Accident

9.1.1 Assumptions and Source Term Calculations

An evaluation of the consequences of a fuel handling accident has been made for fuel of 5.0 wt% initial enrichment burned to 60,000 MWD/MTU, with the reactor conservatively assumed to have been operating at 3411 MW thermal power (38.8 MWD/KgU specific power) prior to reactor shutdown. Except for the fuel enrichment and discharge burnup, the assumptions used in the evaluation are the same as those previously reviewed and accepted by the USNRC. As in the previous evaluation, the fuel handling accident was conservatively assumed to result in the release of the gaseous fission products contained in the fuel-rod gaps of all the rods in the peak-power fuel assembly at the time of the accident. Gap inventories of fission products available for release were estimated using both the assumptions identified in Regulatory Guide 1.25[1] and those in NUREG/CR-5009[2]. NUREG/CR-5009 has confirmed that the Reg Guide 1.25 assumptions remain conservative for extended burnup except for I-131, for which the release fraction was reported to be 20% higher.

Most of the gaseous fission products having a significant impact on the off-site doses are the short-lived nuclides of Iodine and Xenon which reach saturation inventories during in-core operation. These inventories depend primarily on the fuel specific power over the few months immediately preceding reactor shutdown. In the highest power assembly, the specific power and hence the inventory of Iodine and Xenon will be directly related to the peaking factor (assumed to be 1.65 per Reg. Guide 1.25).

The inventory of long-lived Kr-85 (10.73 year half-life), however, is nearly proportional to the accumulated fuel discharge burnup and hence is independent of the peaking factor. Because Kr-85 is a weak beta emitter, it has only a minor impact on off-site doses, primarily affecting the whole-body beta dose. The off-site radiological consequences are dominated by the short-lived radionuclides (which are at saturation concentration independent of fuel burnup). In the present analysis, the calculated doses are higher and more coservative than those of the previous evaluation because (1) the analyses reported here use higher gap inventories based on Reg Guide 1.25 assumptions and (2) the use of the up-dated ORIGEN-2 code[3] for calculating the fission product inventories. Results of the evaluation confirm that the off-site doses remain within the regulatory limits.

The present evaluation uses values for the 2-hour atmospheric dispersion factor (X/Q) and filter efficiencies that have previously been reviewed and accepted. Core inventories of fission products were estimated with the ORIGEN-2 code based upon a reactor power of 3411 MWt and fuel with an initial enrichment of 5.0% U-235 burned to 60,000 MWD/MTU. Calculations were made for 100 hours cooling time as the source term for the fuel handling accident. The release fraction of the core inventories assumed to be in the gap by both the Reg Guide 1.25 and NUREG/CR5009 assumptions are listed in Table 9.1.

The following equation, from Reg Guide 1.25, was used to calculate the thyroid dose (D) from the inhalation of radioiodine,

$$D = \sum_i \frac{F_g\ I_i\ F\ P\ B\ R_i\ (x/Q)}{DF_p\ \ DF_f} \quad \text{Rads}$$

summed over all Iodine radionuclides.

F_g = fraction of fuel rod Iodine inventory in gap space

I_i = core Iodine radio-nuclide inventory at time of the accident (curies)

F = fraction of core damaged sc . to release Iod:.e in the rod gap (1,193)

P = Core peaking factor (1.65)

DF_f = effective Iodine decontamination factor for filters (= 10)

B = Breathing rate = 3.47×10^{-4} cubic meters per second

R_i = Dose conversion factor (rads/curie) from Reg. Guide 1.25

(X/Q) = atmospheric diffusion factor (3.15×10^{-4} sec/m^3)

DF_p = effective Iodine decontamination factor for pool water (= 150)

The gap inventories listed in Table 9-1 are the product of I_i (core inventory) and F_g (the fraction existing in the gap).

The function used to calculate the external whole body dose from beta (D_β) or gamma (D_Γ) radiation in the cloud uses many of the terms defined above and is given by:

$$D_\beta = \sum_i 0.23\ (X/Q)\ F\ P\ G_i\ E_{\beta\ i} \quad \text{and}$$

$$D_\Gamma = \sum_i 0.25\ (X/Q)\ F\ P\ G_i\ E_{\Gamma\ i}$$

where G_i is the gap inventory of the gaseous radionuclides of Xe and K: and the functions above are summed over all the noble gases. E_β and E_Γ are the average energies of decay (beta and gamma radiation respectively) for the various radionuclides. These functions assume the noble gas decontamination factors in water and the charcoal filters are 1.0. The gap inventories of radioiodine

make a negligible contribution to the whole body doses, D_β or D_γ, because of the large decontamination factors appropriate to the iodines.

9.1.2 Results

A summary of the assumptions used to evaluate the fuel handling accident is given in Table 9-2. The minimum time after shutdown when fuel assemblies would be moved was conservatively assumed to be 100 hours as identified in the Technical Specifications. At 100 hours after shutdown, the two-hour dose at the site boundary, for a fuel handling accident releasing all of the gaseous fission product radioactivity in the gaps of all rods in the highest power assembly, are as follows:

Two-Hour Site Boundary Dose

	NUREG/CR-5009 Method	Reg. Guide 1.25	Previous Analysis
Inhalation thyroid dose =	7.07 Rads	5.97 Rads	2.15
Whole body beta dose, D_β =	0.36 Rads	0.70 Rads	-
Whole body gamma dose, D_γ =	0.31 Rads	0.58 Rads	0.51

These doses are well within the limits of 10 CFR Part 100 in conformance with the acceptance criteria of SPP 15.7.4. (Rev.1, July 1981)[4].

9.2 Solid Radwaste

The necessity for resin replacement is determined primarily by the requirement for water clarity and the resin is normally changed about once a year. No significant increase in the volume of solid radioactive wastes is expected with the expanded storage capacity. During reracking operations, a certain amount of additional resins may be generated by the pool cleanup system on a one-time basis (perhaps 10 to 30 cubic feet).

9.3 Gaseous Releases

Gaseous releases from the fuel storage area of the auxiliary building are combined with other plant exhausts. Normally, the contribution from the fuel storage area of the auxiliary building is negligible compared to the other releases and no significant increases are expected as a result of the expanded storage capacity.

9.4 Personnel Exposures

During normal operations, personnel working in the fuel storage area may be exposed to radiation from the spent fuel pool. Operating experience has shown that the area radiation dose rates, which originate primarily from radionuclides in the pool water, are generally less than 1 mrem/hr but may temporarily increase to 2.5 - 5 mrem/hr during refueling operations. No evidence has been observed of any crud deposition around the edges of the pool that might cause local areas of high radiation.

Radiation levels in zones surrounding the pool are not expected to be significantly affected. Existing shielding around the pool (water depth and concrete walls) provide more than adequate protection, despite the slightly closer approach to the walls of the pool.

Typical concentrations of radionuclides in the pool water are shown in Table 9.3. During fuel reload operations, the concentrations will increase due to crud deposits spalling from spent fuel assemblies and to activities carried into the pool from the primary system. While these effects may increase the concentrations (as much as a factor of 10), the pool cleanup system soon reduces the concentrations to the normal operating range. No evidence has been seen of any significantly higher radiation doses near the edge of the pool that might suggest the accumulation of crud deposits.

Operating experience has shown that there have been negligible concentrations of airborne radioactivity and no increases are expected as a result of the expanded storage capacity. Area monitors for airborne activities are available in the immediate vicinity of the spent fuel pool.

No increase in radiation exposure to operating personnel is expected and therefore neither the current health physics program nor the area monitoring systems need to be modified.

9.5 Anticipated Exposure During Reracking

Total occupational exposure for the reracking operation is estimated to be between 6 and 11 person-rem, as indicated in Table 9.4. While individual task efforts and exposures may differ from those in Table 9.4, the total is believed to be a reasonable estimate for planning purposes. Divers will be necessary to remove

certain underwater appurtenances. These appurtenances are well removed for the stored fuel which minimizes the radiation dose rate to the divers. Carefu monitoring and adherence to pre-prepared procedures will assur hat the radiation dose to the divers will be maintained ALARA. All of the reracking operation will utilize detailed procedures prepared with full consideration of ALARA principles. Similar operations have been performed in a number of facilities in the past and there is every reason to believe that reracking can be safely and efficiently accomplished at the Donald C. Cook Nuclear Plant, with minimum radiation exposure to personnel.

The existing radiation protection program at the Cook Nuclear Plant is adequate for the reracking operations. Where there is a potential for significant airborne activity, continuous air samplers will be in operation. Personnel wear protective clothing and, if necessary, respiratory protective equipment. Activities are governed by a Radiation Work Permit and personnel monitoring equipment will be assigned to each individual. As a minimum, this includes thermoluminescent dosimeters and pocket dosimeters. Additional personnel monitoring equipment (i.e., extremity badges or alarming dosimeters may be utilized as required. Work, personnel traffic and the movement of equipment will be monitored and controlled to minimize contamination and to assure that exposures are maintained ALARA.

In reracking, the existing storage racks will be removed, decontaminated as much as possible by washing and wipe-downs, packaged and shipped to a licensed processing/disposal facility. Shipping containers and procedures will conform to Federal DOT regulations and the requirements of any State DOT office through which the shipment may pass.

9.6 References for Section 9

1. Reg. Guide 1.25 (AEC Safety Guide 25), "Assumptions used for evaluating the potential radiological consequences of a fuel handling accident in the fuel handling and storage facility for boiling and pressurized water reactors".

2. C.E. Beyer, et al., "Assessment of the Use of Extended Burnup Fuel in Light Water Power Reactors", NUREG/CR-5009, Pacific Northwest Laboratory (PNL-6258).

3. A.G. Croff, "A User's Manual for the ORIGEN2 Computer Code", ORNL/TM-7175, July 1980 (ORIGEN = ORNL Isotope Generation and Depletion)

4. Section 15.7.4, "Radiological Consequences of Fuel Handling Accidents" NUREG-0800, Section 15.7.4, Rev. 1 July 1981

Table 9-1 INVENTORIES AND CONSTANTS OF SIGNIFICANT FISSION PRODUCT RADIONUCLIDES

NUCLIDE	SHUTDOWN CORE INVENTORY CURIES	DECAY CONST. λ, 1/HRS	TOTAL GAP INVENTORY, CURIES		DOSE CONVERSION Ri	E_β (MEV)	E_γ (MEV)
			NUREG/CR-5009	Reg. Guide 1.25			
			100 hrs	100 hrs			
I-131	9.0 E+7	3.591E-3	7.5 E+6	6.3 E+6	1.48E+6	0.186	0.389
I-132	1.3 E+8	3.013E-1	Negligible*	Negligible	5.35E+4	–	–
I-133	1.8 E+8	3.332E-2	6.3 E+5*	6.3 E+5	4.0 E+5	0.419	0.597
I-134	1.9 E+8	7.905E-1	Negligible*	Negligible	2.5 E+4	–	–
I-135	1.7 E+8	1.048E-1	Negligible*	Negligible	1.24E+5	0.394	1.456
Kr-85M	1.9 E+7	1.547E-1	Negligible*	Negligible		–	–
Kr-85	1.4 E+6	7.376E-6	2.0 E+5	4.2 E+5		0.251	0.002
Kr-87	3.6 E+7	5.451E-1	Negligible	Negligible		–	–
Kr-88	5.0 E+7	2.442E-1	Negligible	Negligible		–	–
Xe-131M	1.0 E+6	2.427E-3	7.9 E+4*	7.9 E+4		–	0.163
Xe-133M	5.6 E+6	1.319E-2	1.5 E+5*	1.5 E+5		–	0.233
Xe-133	1.8 E+8	5.506E-3	5.1 E+6	1.0 E+7		0.102	0.081
Xe-135	3.9 E+7	7.626E-2	Negligible	Negligible		0.309	0.262

* NO RELEASE FRACTION GIVEN – ASSUMED SAME AS REG. GUIDE 1.25

Table 9.2

DATA AND ASSUMPTIONS FOR THE EVALUATION
OF THE FUEL HANDLING ACCIDENT

1. Source Term Assumptions	VALUES
Core power level, MWT	3411
Fuel burnup, MWD/MTU	60,000
Analytical method	ORIGEN
2. Release Assumptions	
Number of failed fuel rods	all rods in 1 of 193 assemblies
Fraction of core inventory released to gap (NUREG/CR-5009 % release of Iodine-131 is reported to be 20% higher)	Reg. Guide 1.25 % of the Iodine - 10 % of the Xenon - 10 % of Kr-85 - 30
Assumed power peaking factor	1.65
Inventory in gap available for release	Table 9.1
Pool decontamination factors	
For Iodines	150
For noble gases	1
Filter decontamination factors	
For Iodines	10
For noble gases	1
Atmospheric Dispersion, (x/Q)	3.15×10^{-4} sec/m^3
Breathing rate	3.47×10^{-4} m^3/sec

Table 9.3 Typical Concentrations of Radionuclides in the Spent Fuel Pool Water

Nuclide	Concentration $\mu C_i/ml$
Ag-110M	4.6×10^{-5}
Co-58	1.5×10^{-5}
Co-60	4.4×10^{-5}
Cs-134	3.2×10^{-4}
Cs-137	6.4×10^{-4}

Table 9.4

PRELIMINARY ESTIMATE OF PERSON-REM EXPOSURES
DURING RERACKING

Step	Number of Personnel	Hours	Estimated Exposure[1]
Remove empty racks	5	40	0.5 to 1.0
Wash and Decon racks	3	10	0.08 to 0.2
Clean and Vacuum Pool	3	25	0.3 to 0.6
Remove underwater appurtences	4	5	0.4 to 0.8
Partial installation of new rack modules	5	20	0.25 to 0.5
Move fuel to new racks	2	150	0.8 to 1.5
Remove remaining racks	5	120	1.5 to 3.0
Wash and Decon racks	3	30	0.2 to 0.4
Install remaining new rack modules	5	35	0.4 to 0.8
Prepare old racks for shipment	4	80	1.0 to 2.0[2]
Total Exposure, person-rem			6 to 12

(1) Assumes minimum dose rate of 2 1/2 mR/hr (expected) to a maximum of 5 mR/nr, except for pool vacuuming operations which assumes 4 to 8 mR/hr and diving operations which assume 20 to 40 mR/hr.

(2) Maximum expected exposure, although details of preparation and packaging of old racks for shipment have not yet been determined.

10.0 IN-SERVICE SURVEILLANCE PROGRAM

10.1 Purpose

This section describes the programmatic commitments made by Indiana Michigan Power Company (I&M) for in-service surveillance of the Boral neutron absorption material to comply with the provisions of Section IV (8) of the OT Position Paper (Ref. 10.1.1).

All material used within a storage system for spent nuclear fuel are qualified to a level of performance predicated upon calculated worst case environmental conditions and are based on accelerated testing of the materials to levels of service life corresponding to that environment. Because such environmental compatibility testing in the laboratory conditions is accelerated, it is prudent that each of the system components be monitored to some extent throughout the service life to assure that the actual in-service performance remains within acceptable parameters as defined by the accelerated testing. For many of the materials, monitoring throughout the service life is relatively easy, however, the neutron absorbing material is encased in a stainless steel jacket precluding a direct visual or physical examination during the in-service condition.

The coupon surveillance program presented herein is intended to provide a definitive assessment of the present physical integrity of the neutron absorber, as well as inferential information to detect future degradation.

The coupon surveillance procedure consists of preparing twelve neutron absorber coupons carefully encased in a stainless steel metal jacket, and suspending them from a "coupon tree".

The coupon tree is placed in the center of a group of freshly discharged fuel assemblies each time a new batch is discharged to the pool. The group of assemblies surrounding the coupon tree shall be those which have the above-average values of radial peaking factor. The object, of course, is to subject this "tree" to the maximum radiation exposure in the fuel pool in the minimum amount of time.

Further details are provided in the following.

10.2 Coupon Surveillance

10.2.1 Description of Test Coupons

The neutron absorber used in the surveillance program shall be representative of the material used within the storage system. It shall be of the same composition, produced by the same method, and certified to the same criteria as the production lot neutron absorber. The sample coupon shall be the same thickness as the neutron absorber used within the storage system and shall meet the referenced Holtec drawing dimensional requirements. Each neutron absorber specimen shall be encased in a stainless steel jacket of an alloy identical to that used in the storage system, formed so as to encase the neutron absorbing material and fix it in a position and with tolerances similar to that for the storage racks. The jacket would be similar to that for the storage racks.

The jacket would be closed by quick disconnect clamps or screws with lock nuts in such a manner as to retain its form throughout the use period and also allow rapid and easy opening without contributing mechanical damage to the neutron absorber specimen contained therein.

Consistent with the USNRC OT Position Paper [reference 10.1.1], requirements of a statistically acceptable sample size, a total of twelve jacketed neutron absorber specimens, shall be used.

10.2.2 Benchmark Data

The following benchmark tests shall be performed on test coupons derived from the same production run as the actual neutron absorber panels.

(i) Length, width, thickness and weight measurements
(ii) Wet chemistry
(iii) Neutron attenuation measurement (optional)

10.2.3 Coupon Reference Data

Prior to encasing the coupons, each coupon shall be carefully calibrated. Their width, thickness, length and weight shall be carefully measured and recorded. The wet chemistry will be performed on a strip taken from the same Boral plates from which the coupons are made to provide a benchmark B-10 loading data.

Three points on each coupon will be designated for neutron attenuation measurement. Neutron attenuation measurements at those three points will be made and recorded.

10.2.4 Accelerated Surveillance

At the time of the first off-load of spent fuel, the coupon tree is surrounded by storage cells containing fuel assemblies from the peak power region of the reactor core. At the time of the second off-load of the fuel assemblies, the tree is withdrawn from the fuel pool and one coupon is taken for evaluation. The specimen strip is replaced in the fuel pool in a new location, where it is again surrounded by peak power region fuel assemblies. The storage cell that was vacated may now be used to store a fuel assembly. This arrangement is repeated at the first two off-loads of fuel and after that, every third outage. By evaluation of the specimens, an accelerated monitor of environmental effects on the neutron absorber will be obtained.

10.2.5 Post-Irradiation Tests

Coupons removed from the pool will be tested for dimensional, neutron attenuation, and wet chemistry changes using the same procedures which were used in initial benchmarking to minimize the potential for instrument errors.

10.2.6 Acceptance Criteria

A plant procedure will be developed to execute the commitments made in this licensing submittal. Equipment requirements, step-by-step instructions for executing inspections and acceptance criteria will be described in that procedure for use by plant personnel.

10.3 References for Section 10

10.1.1 OT Position for Review and Acceptance of Spent Fuel Storage and Handling Applications", by Brian K. Grimes, USNRC, April 14, 1978, and Revision dated January 18, 1979.

11.0 ENVIRONMENTAL COST/BENEFIT ASSESSMENT

11.1 Introduction

The specific need to increase the existing storage capacity of the spent fuel pool at the Donald C. Cook Nuclear Plant is based on the continually-increasing inventory in the pool, the prudent requirement to maintain full-core offload capability, and a lack of viable economic alternatives.

The inventory increase can be inferred from the fuel assembly discharge schedule contained in Table 11.1.

The proposed project contemplates the reracking of spent fuel pool with free-standing, high density, poisoned spent fuel racks. The engineering design and licensing will be completed for a full reracking of the pool, which is currently only partially racked. Engineering and design will also be completed to accommodate consolidated fuel. The licensing effort for consolidated fuel will, however, be pursued at a later date if consolidation is chosen to accommodate future storage needs.

11.2 Project Cost Assessment

The total capital cost for the rerack project is estimated to be approximately $14.1 million.

Many alternatives were considered prior to proceeding with reracking, which is not the only technical option available to increase on-site storage capacity. Reracking does, however, enjoy a cost advantage over other technologies, as shown:

Type of Storage	Capital Costs $/KgU
Rerack	$20[1]
Fuel consolidation	$20 - 34[2]
Dry cask storage	$45 - 110[2]
Storage vault	$40 - 90[2]
New pool	$115[3]

There are no acceptable alternatives to develop off-site spent fuel storage capacity for the Cook Nuclear Plant. First, there are no commercial independent spent fuel storage facilities operating in the U.S. Second, the adoption of the Nuclear Waste Policy Act (NWPA) created a de facto throw-away nuclear fuel cycle. Since the cost of spent fuel reprocessing is not offset by the salvage value of the residual uranium, reprocessing represents an added cost for the nuclear fuel cycle which already includes the NWPA Nuclear Waste Fund fees. In any event, there are no domestic reprocessing facilities. Third, I&M has no other operating power plant; therefore, shipment of spent fuel from the Cook Nuclear Plant to other system nuclear power plants is not possible. Fourth, at $600,000 per day replacement power cost, shutting down the Cook Nuclear Plant is many times more expensive than simply reracking the existing spent fuel pools.

---

(1) From EPRI NF-3580, May 1984

(2) From DOE RW-0220, "Final Version Dry Cask Storage Study," February 1989

(3) Actual estimated cost per KgU of storage space gained for this project

11.3 Resource Commitment

The expansion of the spent fuel pool capacity is expected to require the following primary resources:

Stainless steel 360 tons.

Boral Neutron Absorber 30 tons, of which 30 tons are Boron Carbide Powder and 20 tons are aluminum.

The requirements for stainless steel and aluminum represent a small fraction of total world output of these metals (less than .0001%). Although the fraction of world production of Boron Carbide required for the fabrication is somewhat higher than that of stainless steel or aluminum, it is unlikely that the commitment of Boron Carbide to this project will affect other alternatives. Experience has shown that the production of Boron Carbide is highly variable and depends upon need, and can easily be expanded to accommodate worldwide needs.

11.4 Environment Assessment

Due to the additional heat-load arising from increased spent fuel pool inventory, the anticipated maximum bulk pool temperature increases from a previously-licensed 140°F to approximately 160°F, as detailed in the calculations described in Section 5.0 of this report. The resultant total heat-load (worst case) is 35.5 million BTU/HR, which is less than 0.5% of the total plant heat loss to the environment.

The net result of the increased heat loss and water vapor emission (due to increased evaporation) to the environment is negligible.

Table 11.1

DONALD C. COOK NUCLEAR PLANT
WORST CASE SPENT FUEL INVENTORY

YEAR	ASSEMBLIES IN STORAGE	
1991	1362	
1992	1518	
1993	1678	
1994	1838	
1995	1918	Lose full core discharge capability with current capacity
1996	1998	
1997	2158	Lose normal discharge capability with current capacity
1998	2318	
1999	2318	
2000	2478	
2001	2638	
2002	2798	
2003	2798	
2004	2958	
2005	3118	
2006	3198	
2007	3278	
2008	3438	Lose full core discharge capability with proposed rerack
2009	3598	
2010	3678	Lose normal discharge capability with proposed rerack
2011	3758	
2012	3918	
2013	4078	
2014	4158	
2015	4351	
2016	4431	
2017	4624	